

Lecture Notes for Physics 110B

Daniel Arovas
Department of Physics
University of California, San Diego

June 21, 2020

Contents

Contents	i
List of Figures	vii
12 Noninertial Reference Frames	1
12.1 Accelerated Coordinate Systems	1
12.1.1 Translations	3
12.1.2 Motion on the surface of the earth	3
12.2 Spherical Polar Coordinates	5
12.3 Centrifugal Force	5
12.3.1 Rotating tube of fluid	6
12.4 The Coriolis Force	7
12.4.1 Projectile motion	7
12.4.2 Foucault's pendulum	10
13 Rigid Body Motion and Rotational Dynamics	13
13.1 Rigid Bodies	13
13.1.1 Examples of rigid bodies	13
13.2 The Inertia Tensor	14
13.2.1 Coordinate transformations	15
13.2.2 The case of no fixed point	16
13.3 Parallel Axis Theorem	16

13.3.1 Example	17
13.3.2 General planar mass distribution	19
13.4 Principal Axes of Inertia	19
13.5 Euler's Equations	21
13.5.1 Example	23
13.6 Euler's Angles	25
13.6.1 Torque-free symmetric top	27
13.6.2 Symmetric top with one point fixed	27
13.7 Rolling and Skidding Motion of Real Tops	30
13.7.1 Rolling tops	31
13.7.2 Skidding tops	32
13.7.3 Tippie-top	33
14 Dynamical Systems	35
14.1 Introduction	35
14.1.1 Phase space and phase curves	35
14.1.2 Vector fields	35
14.1.3 Autonomous <i>vs.</i> non-autonomous ODEs	36
14.1.4 Existence / uniqueness / extension theorems	37
14.1.5 Linear differential equations	37
14.1.6 Lyapunov functions	38
14.2 $N = 1$ Systems	38
14.2.1 Classification of fixed points ($N = 1$)	39
14.2.2 Logistic equation	40
14.2.3 Recommended exercises	41
14.2.4 Nongeneric cases with singular $f(u)$	41
14.2.5 Non-autonomous ODEs	42
14.3 Flows on the Circle	43
14.3.1 Nonuniform oscillator	43

14.4 Appendix I : Evolution of Phase Space Volumes	45
14.5 Appendix II : Lyapunov Characteristic Exponents	46
15 Bifurcations	49
15.1 Types of Bifurcations	49
15.1.1 Saddle-node bifurcation	49
15.1.2 Transcritical bifurcation	50
15.1.3 Pitchfork bifurcation	52
15.1.4 Imperfect bifurcation	53
15.2 Examples	55
15.2.1 Population dynamics	55
15.2.2 The Bletch	58
15.3 Appendix : Landau Theory of Phase Transitions	61
15.3.1 Landau coefficients from mean field theory	62
15.3.2 Magnetization dynamics	63
15.3.3 Cubic terms in Landau theory : first order transitions	66
15.3.4 Magnetization dynamics	68
15.3.5 Sixth order Landau theory : tricritical point	70
15.3.6 Hysteresis for the sextic potential	71
16 Two-Dimensional Phase Flows	75
16.1 Harmonic Oscillator and Pendulum	75
16.1.1 Simple harmonic oscillator	75
16.1.2 Pendulum	77
16.2 General $N = 2$ Systems	78
16.2.1 The damped driven pendulum	78
16.2.2 Classification of $N = 2$ fixed points	81
16.2.3 The fixed point zoo	83
16.2.4 Limit cycles	84

16.2.5 Andronov-Hopf bifurcation	84
16.2.6 Fixed points for $N = 3$ systems	85
16.3 Population Biology : Lotka-Volterra Models	87
16.3.1 Rabbits and foxes	87
16.3.2 Rabbits and sheep	88
16.4 Poincaré-Bendixson Theorem	90
16.5 Index Theory	92
16.5.1 Gauss-Bonnet Theorem	95
16.5.2 Singularities and topology	97
16.6 Appendix : Example Problem	99
17 Maps, Strange Attractors, and Chaos	103
17.1 One-dimensional Maps	103
17.1.1 Lyapunov Exponents	105
17.1.2 Chaos in the logistic map	106
17.1.3 Intermittency	107
17.2 Maps from Time-Dependent Hamiltonian Systems	108
17.2.1 Parametric Oscillator	108
17.2.2 Kicked dynamics	111
17.3 Local Stability and Lyapunov Exponents	114
17.3.1 The fate of nearly separated initial conditions under iteration	114
17.3.2 Kolmogorov-Sinai entropy	115
17.4 The Lorenz Model and Chaos	117
17.4.1 Attractors	117
17.4.2 The Lorenz equations	117
17.4.3 Fixed point analysis	118
17.4.4 Poincaré section	120
17.4.5 Rössler System	121

18 Continuum Mechanics	123
18.1 Continuum Mechanics of the String	123
18.1.1 Lagrangian formulation	123
18.1.2 d'Alembert's Solution to the Wave Equation	125
18.1.3 Energy density and energy current	126
18.1.4 Reflection at an interface	129
18.1.5 Mass point on a string	129
18.1.6 Interface between strings of different mass density	133
18.1.7 Finite Strings : Bernoulli's Solution	135
18.2 Sturm-Liouville Theory	137
18.2.1 Mathematical formalism	137
18.2.2 Variational method	138
18.3 Continua in Higher Dimensions	141
18.3.1 General formalism	141
18.3.2 Membranes	142
18.3.3 Helmholtz equation	143
18.3.4 Rectangles	144
18.3.5 Circles	144
18.3.6 Sound in fluids	145
18.4 Dispersion	147
18.4.1 Helmholtz <i>versus</i> Klein-Gordon equations	147
18.4.2 Schrödinger's equation	148
18.5 General Field Theoretic Formulation	150
18.5.1 Euler-Lagrange equations for classical field theories	150
18.5.2 Conserved currents in field theory	151
18.5.3 Gross-Pitaevskii model	152
18.6 Appendix : Three Strings	153
18.7 Appendix : Green's Functions for Strings	156

18.7.1 Inhomogeneous Sturm-Liouville problem	156
18.7.2 Perturbation theory	159
18.7.3 Perturbation theory for eigenvalues and eigenfunctions	160
19 Special Relativity	163
19.1 Introduction	163
19.1.1 Michelson-Morley experiment	163
19.1.2 Einsteinian and Galilean relativity	166
19.2 Intervals	168
19.2.1 Proper time	168
19.2.2 Irreverent problem from Spring 2002 final exam	170
19.3 Four-Vectors and Lorentz Transformations	171
19.3.1 Covariance and contravariance	175
19.3.2 What to do if you hate raised and lowered indices	176
19.3.3 Comparing frames	176
19.3.4 Example I	177
19.3.5 Example II	177
19.3.6 Deformation of a rectangular plate	178
19.3.7 Transformation of velocities	179
19.3.8 Four-velocity and four-acceleration	180
19.4 Three Kinds of Relativistic Rockets	181
19.4.1 Constant acceleration model	181
19.4.2 Constant force with decreasing mass	182
19.4.3 Constant <i>ejecta</i> velocity	183
19.5 Relativistic Mechanics	184
19.5.1 Relativistic harmonic oscillator	185
19.5.2 Energy-momentum 4-vector	186
19.5.3 4-momentum for massless particles	187
19.6 Relativistic Doppler Effect	187

19.6.1 Romantic example	188
19.7 Relativistic Kinematics of Particle Collisions	190
19.7.1 Spontaneous particle decay into two products	191
19.7.2 Miscellaneous examples of particle decays	193
19.7.3 Threshold particle production with a stationary target	193
19.7.4 Transformation between frames	195
19.7.5 Compton scattering	196
19.8 Covariant Electrodynamics	197
19.8.1 Lorentz force law	199
19.8.2 Gauge invariance	200
19.8.3 Transformations of fields	200
19.8.4 Invariance <i>versus</i> covariance	202
19.9 Appendix I : The Pole, the Barn, and <i>Rashoman</i>	204
19.10 Appendix II : Photographing a Moving Pole	206

List of Figures

12.1 Reference frames related by both translation and rotation.	2
12.2 The locally orthonormal triad $\{\hat{r}, \hat{\theta}, \hat{\phi}\}$	4
12.3 A rotating cylinder of fluid.	7
12.4 Foucault's pendulum.	12
13.1 A wheel rolling to the right without slipping.	14
13.2 Precession of a spinning bicycle wheel.	15
13.3 Application of the parallel axis theorem.	17
13.4 A planar mass distribution in the shape of a triangle.	19

13.5 Wobbling of a torque-free symmetric top.	22
13.6 A general rotation, defined in terms of the Euler angles $\{\phi, \theta, \psi\}$.	26
13.7 The <i>dreidl</i> : a symmetric top.	28
13.8 The effective potential of eq. 13.82.	29
13.9 Precession and nutation of the symmetry axis of a symmetric top.	30
13.10A top with a peg end.	31
13.11 Circular rolling motion of the peg top.	32
13.12 The tippie-top.	34
14.1 An example of a phase curve.	36
14.2 Phase flow for an $N = 1$ system.	39
14.3 Flow diagram for the logistic equation.	41
14.4 $f(u) = A u - u^* ^\alpha$, for $\alpha > 1$ and $\alpha < 1$.	42
14.5 Solutions to $\dot{e} = \mp A e^\alpha$.	42
14.6 Flow for the nonuniform oscillator $\dot{\theta} = \omega - \sin \theta$.	44
15.1 Evolution of $F(x, \alpha)$ as a function of the control parameter α .	50
15.2 Flow diagrams for $\dot{u} = r + u^2$ and $\dot{u} = ru - u^2$.	51
15.3 Extended phase space flow for the saddle-node and transcritical bifurcations.	51
15.4 Supercritical and subcritical pitchfork bifurcations.	52
15.5 Extended phase space flow for supercritical and subcritical pitchfork bifurcations.	53
15.6 Scaled free energy and phase diagram.	54
15.7 Imperfect pitchfork bifurcation.	55
15.8 Phase flow for the constantly harvested population.	56
15.9 Plot of $h(n) = n/(n^2 + 1)$.	57
15.10 Phase diagram for the equation $\dot{n} = \gamma(1 - n/c)n - n^2/(n^2 + 1)$.	58
15.11 Phase flow for the scaled bletch population, $\dot{n} = n^2 - n^3$.	59
15.12 Phase flow for the harvested bletch population, $\dot{n} = -\nu n + n^2 - n^3$.	60
15.13 Scaled bletch harvest r versus scaled harvesting rate ν .	60
15.14 Phase diagram for the quartic mean field theory $f = f_0 + \frac{1}{2}am^2 + \frac{1}{4}bm^4 - hm$.	63

15.15 Mean field free energy $f(m)$ at $h = 0.1$.	64
15.16 Dissipative magnetization dynamics $\dot{m} = -f'(m)$.	65
15.17 Hysteretic dynamics.	66
15.18 Behavior of the quartic free energy $f(m) = \frac{1}{2}am^2 - \frac{1}{3}ym^3 + \frac{1}{4}bm^4$.	67
15.19 Fixed points for $\varphi(u) = \frac{1}{2}\bar{r}u^2 - \frac{1}{3}u^3 + \frac{1}{4}u^4$.	69
15.20 Behavior of the sextic free energy $f(m) = \frac{1}{2}am^2 + \frac{1}{4}bm^4 + \frac{1}{6}cm^6$.	70
15.21 Free energy $\varphi(u) = \frac{1}{2}\bar{r}u^2 - \frac{1}{4}u^4 + \frac{1}{6}u^6$.	72
15.22 Fixed points $\varphi'(u^*) = 0$ for the sextic potential.	73
16.1 Phase curves for the harmonic oscillator.	76
16.2 Phase curves for the simple pendulum.	77
16.3 The resistively and capacitively shunted Josephson junction.	79
16.4 Phase flows for the equation $\ddot{\phi} + \gamma^{-1}\dot{\phi} + \sin\phi = j$.	80
16.5 Complete classification of fixed points for the $N = 2$ system.	81
16.6 Fixed point zoo for $N = 2$ systems.	82
16.7 Phase portrait for an $N = 2$ flow.	83
16.8 Stable, unstable, and half-stable limit cycles.	84
16.9 Limit cycle of the Van der Pol oscillator for $\mu \gg 1$.	85
16.10 The Hopf bifurcation.	86
16.11 Rabbits <i>vs.</i> foxes.	89
16.12 Two possible phase flows for the rabbits <i>vs.</i> sheep.	90
16.13 Two singularities with index +1.	91
16.14 Two singularities with index -1.	93
16.15 Singularities with net index +2.	94
16.16 A vector field with index -2.	95
16.17 Two smooth vector fields on the sphere \mathbb{S}^2 .	96
16.18 Smooth vector fields on the torus.	97
16.19 Composition of two circles.	98
16.20 Sketch of phase flow for $\dot{x} = \frac{1}{2}x + xy - 2x^3$, $\dot{y} = \frac{5}{2}y + xy - y^2$.	100

17.1 Cobweb diagram showing iterations of the logistic map $f(x) = rx(1 - x)$.	104
17.2 Iterates of the logistic map $f(x) = rx(1 - x)$.	105
17.3 Lyapunov exponent (in red) for the logistic map.	106
17.4 Iterates of the sine map $f(x) = r \sin(\pi x)$.	107
17.5 Intermittency in the logistic map in the vicinity of the 3-cycle.	108
17.6 Phase diagram for the parametric oscillator.	110
17.7 The standard map.	112
17.8 The kicked Harper map.	113
17.9 The baker's transformation involves cutting and restacking.	116
17.10 The Lorenz map.	118
17.11 Evolution of the Lorenz equations.	119
17.12 $X(t)$ for the Lorenz equations with $\sigma = 10$, $b = \frac{8}{3}$, and $r = 28$.	120
17.13 The Lorenz attractor.	121
17.14 Period doubling bifurcations of the Rössler attractor with $a = b = \frac{1}{10}$.	122
17.15 Period doubling bifurcations of the Rössler attractor with $a = b = \frac{1}{5}$.	122
18.1 A string is described by the vertical displacement field $y(x, t)$.	124
18.2 Reflection of a pulse at an interface at $x = 0$, with $y(0, t) = 0$.	129
18.3 Reflection of a pulse at an interface at $x = 0$, with $y'(0, t) = 0$.	130
18.4 Reflection and transmission at an impurity.	131
18.5 Reflection and transmission of a square wave pulse by a point mass.	133
18.6 A string formed from two semi-infinite regions of different densities.	134
18.7 Evolution of a string with fixed ends starting from an isosceles triangle shape.	136
18.8 One-parameter variational solution for a string with a point mass m at $x = \frac{1}{2}L$.	140
18.9 Wavepacket spreading for $k_0 \ell_0 = 2$ with $t/\tau = 0, 2, 4, 6$, and 8 .	149
18.10 Three identical strings arranged symmetrically in a plane, attached to a common end.	154
18.11 Diagrammatic representation of the perturbation expansion in eqn. 18.247.	159
19.1 The Michelson-Morley experiment.	164
19.2 Experiment to test source velocity dependence of c .	166

19.3 Two reference frames.	167
19.4 A $(1 + 1)$ -dimensional light cone.	169
19.5 A rectangular plate moving at velocity $\mathbf{V} = V \hat{\mathbf{x}}$	178
19.6 Relativistic deformation of the rectangular plate.	179
19.7 Alice's big adventure.	189
19.8 Spontaneous decay of a single reactant into two products.	192
19.9 A two-particle initial state and an N' -particle final state.	194
19.10 Compton scattering of a photon and an electron.	196
19.11 Homer celebrates the manifest gauge invariance of classical electromagnetic theory.	201
19.12 The pole and the barn.	204
19.13 Relativity and photography.	206

Chapter 12

Noninertial Reference Frames

12.1 Accelerated Coordinate Systems

A reference frame which is fixed with respect to a rotating rigid body is not inertial. The paradigm example of this is an observer fixed on the surface of the earth. Due to the rotation of the earth, such an observer is in a noninertial frame, and there are corresponding corrections to Newton's laws of motion which must be accounted for in order to correctly describe mechanical motion in the observer's frame. As is well known, these corrections involve fictitious centrifugal and Coriolis forces.

Consider an inertial frame with a fixed set of coordinate axes $\hat{\mathbf{e}}_\mu$, where μ runs from 1 to d , the dimension of space, and a noninertial frame with axes $\hat{\mathbf{e}}'_\mu$. Any vector \mathbf{A} may be written in either basis:

$$\mathbf{A} = \sum_{\mu} A_{\mu} \hat{\mathbf{e}}_{\mu} = \sum_{\mu} A'_{\mu} \hat{\mathbf{e}}'_{\mu}, \quad (12.1)$$

where $A_{\mu} = \mathbf{A} \cdot \hat{\mathbf{e}}_{\mu}$ and $A'_{\mu} = \mathbf{A} \cdot \hat{\mathbf{e}}'_{\mu}$ are projections onto the different coordinate axes. We may now write

$$\begin{aligned} \left(\frac{d\mathbf{A}}{dt} \right)_{\text{inertial}} &= \sum_{\mu} \frac{dA_{\mu}}{dt} \hat{\mathbf{e}}_{\mu} \\ &= \sum_i \frac{dA'_{\mu}}{dt} \hat{\mathbf{e}}'_{\mu} + \sum_{\mu} A'_{\mu} \frac{d\hat{\mathbf{e}}'_{\mu}}{dt}. \end{aligned}$$

The first term on the RHS is $(d\mathbf{A}/dt)_{\text{body}}$, the time derivative of \mathbf{A} along body-fixed axes, *i.e.* as seen by an observer rotating with the body. But what is $d\hat{\mathbf{e}}'_{\mu}/dt$? Well, we can always expand it in the $\{\hat{\mathbf{e}}'_i\}$ basis:

$$d\hat{\mathbf{e}}'_{\mu} = \sum_{\nu} d\Omega_{\mu\nu} \hat{\mathbf{e}}'_{\nu} \iff d\Omega_{\mu\nu} \equiv d\hat{\mathbf{e}}'_{\mu} \cdot \hat{\mathbf{e}}'_{\nu}. \quad (12.2)$$

Note that $d\Omega_{\mu\nu} = -d\Omega_{\nu\mu}$ is antisymmetric, because

$$0 = d(\hat{\mathbf{e}}'_{\mu} \cdot \hat{\mathbf{e}}'_{\nu}) = d\Omega_{\nu\mu} + d\Omega_{\mu\nu}, \quad (12.3)$$

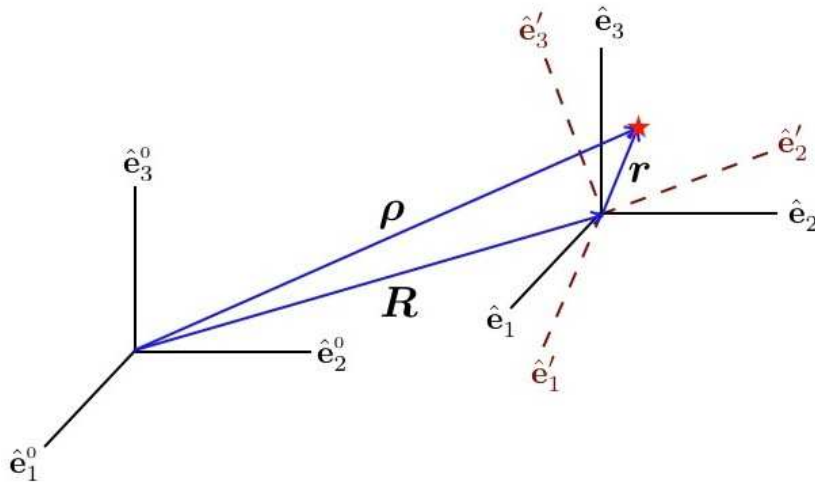


Figure 12.1: Reference frames related by both translation and rotation. Note $\hat{\mathbf{e}}_\mu = \hat{\mathbf{e}}_\mu^0$.

because $\hat{\mathbf{e}}'_\mu \cdot \hat{\mathbf{e}}'_\nu = \delta_{\mu\nu}$ is a constant. Now we may define $d\Omega_{12} \equiv d\Omega_3$, *et cyc.*, so that

$$d\Omega_{\mu\nu} = \sum_{\sigma} \epsilon_{\mu\nu\sigma} d\Omega_{\sigma} \quad , \quad \omega_{\sigma} \equiv \frac{d\Omega_{\sigma}}{dt} \quad , \quad (12.4)$$

which yields

$$\frac{d\hat{\mathbf{e}}'_\mu}{dt} = \boldsymbol{\omega} \times \hat{\mathbf{e}}'_\mu \quad . \quad (12.5)$$

Finally, we obtain the important result

$$\left(\frac{d\mathbf{A}}{dt} \right)_{\text{inertial}} = \left(\frac{d\mathbf{A}}{dt} \right)_{\text{body}} + \boldsymbol{\omega} \times \mathbf{A} \quad (12.6)$$

which is valid for any vector \mathbf{A} .

Applying this result to the position vector \mathbf{r} , we have

$$\left(\frac{d\mathbf{r}}{dt} \right)_{\text{inertial}} = \left(\frac{d\mathbf{r}}{dt} \right)_{\text{body}} + \boldsymbol{\omega} \times \mathbf{r} \quad . \quad (12.7)$$

Applying it twice,

$$\begin{aligned} \left(\frac{d^2\mathbf{r}}{dt^2} \right)_{\text{inertial}} &= \left(\frac{d}{dt} \Big|_{\text{body}} + \boldsymbol{\omega} \times \right) \left(\frac{d}{dt} \Big|_{\text{body}} + \boldsymbol{\omega} \times \right) \mathbf{r} \\ &= \left(\frac{d^2\mathbf{r}}{dt^2} \right)_{\text{body}} + \frac{d\boldsymbol{\omega}}{dt} \times \mathbf{r} + 2\boldsymbol{\omega} \times \left(\frac{d\mathbf{r}}{dt} \right)_{\text{body}} + \boldsymbol{\omega} \times (\boldsymbol{\omega} \times \mathbf{r}) \quad . \end{aligned}$$

Note that $d\boldsymbol{\omega}/dt$ appears with no “inertial” or “body” label. This is because, upon invoking eq. 12.6,

$$\left(\frac{d\boldsymbol{\omega}}{dt} \right)_{\text{inertial}} = \left(\frac{d\boldsymbol{\omega}}{dt} \right)_{\text{body}} + \boldsymbol{\omega} \times \boldsymbol{\omega} \quad , \quad (12.8)$$

and since $\boldsymbol{\omega} \times \boldsymbol{\omega} = 0$, inertial and body-fixed observers will agree on the value of $\dot{\boldsymbol{\omega}}_{\text{inertial}} = \dot{\boldsymbol{\omega}}_{\text{body}} \equiv \dot{\boldsymbol{\omega}}$.

12.1.1 Translations

Suppose that frame K moves with respect to an inertial frame K^0 , such that the origin of K lies at $\mathbf{R}(t)$. Suppose further that frame K' rotates with respect to K , but shares the same origin (see Fig. 12.1). Consider the motion of an object lying at position ρ relative to the origin of K^0 , and \mathbf{r} relative to the origin of K/K' . Thus,

$$\rho = \mathbf{R} + \mathbf{r} , \quad (12.9)$$

and

$$\begin{aligned} \left(\frac{d\rho}{dt} \right)_{\text{inertial}} &= \left(\frac{d\mathbf{R}}{dt} \right)_{\text{inertial}} + \left(\frac{d\mathbf{r}}{dt} \right)_{\text{body}} + \boldsymbol{\omega} \times \mathbf{r} \\ \left(\frac{d^2\rho}{dt^2} \right)_{\text{inertial}} &= \left(\frac{d^2\mathbf{R}}{dt^2} \right)_{\text{inertial}} + \left(\frac{d^2\mathbf{r}}{dt^2} \right)_{\text{body}} + \frac{d\boldsymbol{\omega}}{dt} \times \mathbf{r} + 2\boldsymbol{\omega} \times \left(\frac{d\mathbf{r}}{dt} \right)_{\text{body}} + \boldsymbol{\omega} \times (\boldsymbol{\omega} \times \mathbf{r}) . \end{aligned} \quad (12.10)$$

Here, $\boldsymbol{\omega}$ is the angular velocity in the frame K or K' .

12.1.2 Motion on the surface of the earth

The earth both rotates about its axis and orbits the Sun. If we add the infinitesimal effects of the two rotations,

$$\begin{aligned} d\mathbf{r}_1 &= \boldsymbol{\omega}_1 \times \mathbf{r} dt \\ d\mathbf{r}_2 &= \boldsymbol{\omega}_2 \times (\mathbf{r} + d\mathbf{r}_1) dt \\ d\mathbf{r} &= d\mathbf{r}_1 + d\mathbf{r}_2 = (\boldsymbol{\omega}_1 + \boldsymbol{\omega}_2) dt \times \mathbf{r} + \mathcal{O}((dt)^2) . \end{aligned} \quad (12.11)$$

Thus, *infinitesimal rotations add*. Dividing by dt , this means that

$$\boldsymbol{\omega} = \sum_i \boldsymbol{\omega}_i , \quad (12.12)$$

where the sum is over all the rotations. For the earth, $\boldsymbol{\omega} = \boldsymbol{\omega}_{\text{rot}} + \boldsymbol{\omega}_{\text{orb}}$.

- The rotation about earth's axis, $\boldsymbol{\omega}_{\text{rot}}$ has magnitude $\omega_{\text{rot}} = 2\pi/(1 \text{ day}) = 7.29 \times 10^{-5} \text{ s}^{-1}$. The radius of the earth is $R_e = 6.37 \times 10^3 \text{ km}$.
- The orbital rotation about the Sun, $\boldsymbol{\omega}_{\text{orb}}$ has magnitude $\omega_{\text{orb}} = 2\pi/(1 \text{ yr}) = 1.99 \times 10^{-7} \text{ s}^{-1}$. The radius of the earth's orbit is $a_e = 1.50 \times 10^8 \text{ km}$.

Thus, $\omega_{\text{rot}}/\omega_{\text{orb}} = T_{\text{orb}}/T_{\text{rot}} = 365.25$, which is of course the number of days (*i.e.* rotational periods) in a year (*i.e.* orbital period). There is also a very slow precession of the earth's axis of rotation, the period of which is about 25,000 years, which we will ignore. Note $\dot{\boldsymbol{\omega}} = 0$ for the earth. Thus, applying Newton's second law and then invoking eq. 12.10, we arrive at

$$m \left(\frac{d^2\mathbf{r}}{dt^2} \right)_{\text{earth}} = \mathbf{F}^{(\text{tot})} - m \left(\frac{d^2\mathbf{R}}{dt^2} \right)_{\text{Sun}} - 2m\boldsymbol{\omega} \times \left(\frac{d\mathbf{r}}{dt} \right)_{\text{earth}} - m\boldsymbol{\omega} \times (\boldsymbol{\omega} \times \mathbf{r}) , \quad (12.13)$$

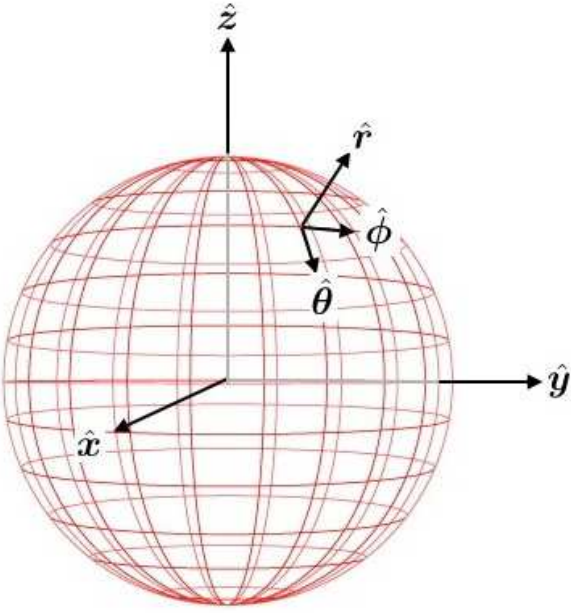


Figure 12.2: The locally orthonormal triad $\{\hat{r}, \hat{\theta}, \hat{\phi}\}$.

where $\boldsymbol{\omega} = \boldsymbol{\omega}_{\text{rot}} + \boldsymbol{\omega}_{\text{orb}}$, and where $\ddot{\mathbf{R}}_{\text{Sun}}$ is the acceleration of the center of the earth around the Sun, assuming the Sun-fixed frame to be inertial. The force $\mathbf{F}_{(\text{tot})}$ is the total force on the object, and arises from three parts: (i) gravitational pull of the Sun, (ii) gravitational pull of the earth, and (iii) other earthly forces, such as springs, rods, surfaces, electric fields, *etc.*

On the earth's surface, the ratio of the Sun's gravity to the earth's is

$$\frac{F_{\odot}}{F_e} = \frac{GM_{\odot}m}{a_e^2} / \frac{GM_e m}{R_e^2} = \frac{M_{\odot}}{M_e} \left(\frac{R_e}{a_e} \right)^2 \approx 6.02 \times 10^{-4}. \quad (12.14)$$

In fact, it is clear that the Sun's field precisely cancels with the term $m \ddot{\mathbf{R}}_{\text{Sun}}$ at the earth's center, leaving only gradient contributions of even lower order, *i.e.* multiplied by another factor of $R_e/a_e \approx 4.25 \times 10^{-5}$. Thus, to an excellent approximation, we may neglect the Sun entirely and write

$$\frac{d^2 \mathbf{r}}{dt^2} = \frac{\mathbf{F}'}{m} + \mathbf{g} - 2\boldsymbol{\omega} \times \frac{d\mathbf{r}}{dt} - \boldsymbol{\omega} \times (\boldsymbol{\omega} \times \mathbf{r})$$

(12.15)

Note that we've dropped the 'earth' label here and henceforth. We define $\mathbf{g} = -GM_e \hat{r}/r^2$, the acceleration due to gravity; \mathbf{F}' is the sum of all earthly forces other than the earth's gravity. The last two terms on the RHS are corrections to $m\ddot{\mathbf{r}} = \mathbf{F}$ due to the noninertial frame of the earth, and are recognized as the Coriolis and centrifugal acceleration terms, respectively.

12.2 Spherical Polar Coordinates

The locally orthonormal triad $\{\hat{r}, \hat{\theta}, \hat{\phi}\}$ varies with position. In terms of the body-fixed triad $\{\hat{x}, \hat{y}, \hat{z}\}$, we have

$$\begin{aligned}\hat{r} &= \sin \theta \cos \phi \hat{x} + \sin \theta \sin \phi \hat{y} + \cos \theta \hat{z} \\ \hat{\theta} &= \cos \theta \cos \phi \hat{x} + \cos \theta \sin \phi \hat{y} - \sin \theta \hat{z} \\ \hat{\phi} &= -\sin \phi \hat{x} + \cos \phi \hat{y}\end{aligned}\tag{12.16}$$

where $\theta = \frac{\pi}{2} - \lambda$ is the *colatitude* (*i.e.* $\lambda \in [-\frac{\pi}{2}, +\frac{\pi}{2}]$ is the latitude). Inverting the relation between the triads $\{\hat{r}, \hat{\theta}, \hat{\phi}\}$ and $\{\hat{x}, \hat{y}, \hat{z}\}$, we obtain

$$\begin{aligned}\hat{x} &= \sin \theta \cos \phi \hat{r} + \cos \theta \cos \phi \hat{\theta} - \sin \phi \hat{\phi} \\ \hat{y} &= \sin \theta \sin \phi \hat{r} + \cos \theta \sin \phi \hat{\theta} + \cos \phi \hat{\phi} \\ \hat{z} &= \cos \theta \hat{r} - \sin \theta \hat{\theta}.\end{aligned}\tag{12.17}$$

The differentials of these unit vectors are

$$\begin{aligned}d\hat{r} &= \hat{\theta} d\theta + \sin \theta \hat{\phi} d\phi \\ d\hat{\theta} &= -\hat{r} d\theta + \cos \theta \hat{\phi} d\phi \\ d\hat{\phi} &= -\sin \theta \hat{r} d\phi - \cos \theta \hat{\theta} d\phi.\end{aligned}\tag{12.18}$$

Thus,

$$\begin{aligned}\dot{\hat{r}} &= \frac{d}{dt}(r \hat{r}) = \dot{r} \hat{r} + r \dot{\hat{r}} \\ &= \dot{r} \hat{r} + r \dot{\theta} \hat{\theta} + r \sin \theta \dot{\phi} \hat{\phi}.\end{aligned}\tag{12.19}$$

If we differentiate a second time, we find, after some tedious accounting,

$$\begin{aligned}\ddot{\hat{r}} &= (\ddot{r} - r \dot{\theta}^2 - r \sin^2 \theta \dot{\phi}^2) \hat{r} + (2 \dot{r} \dot{\theta} + r \ddot{\theta} - r \sin \theta \cos \theta \dot{\phi}^2) \hat{\theta} \\ &\quad + (2 \dot{r} \dot{\phi} \sin \theta + 2 r \dot{\theta} \dot{\phi} \cos \theta + r \sin \theta \ddot{\phi}) \hat{\phi}.\end{aligned}\tag{12.20}$$

12.3 Centrifugal Force

One major distinction between the Coriolis and centrifugal forces is that the Coriolis force acts only on moving particles, whereas the centrifugal force is present even when $\dot{\mathbf{r}} = 0$. Thus, the equation for stationary equilibrium on the earth's surface is

$$m\mathbf{g} + \mathbf{F}' - m\boldsymbol{\omega} \times (\boldsymbol{\omega} \times \mathbf{r}) = 0,\tag{12.21}$$

involves the centrifugal term. We can write this as $\mathbf{F}' + m\tilde{\mathbf{g}} = 0$, where

$$\begin{aligned}\tilde{\mathbf{g}} &= -\frac{GM_e \hat{r}}{r^2} - \boldsymbol{\omega} \times (\boldsymbol{\omega} \times \mathbf{r}) \\ &= -(g_0 - \omega^2 R_e \sin^2 \theta) \hat{r} + \omega^2 R_e \sin \theta \cos \theta \hat{\theta},\end{aligned}\tag{12.22}$$

where $g_0 = GM_e/R_e^2 = 980 \text{ cm/s}^2$. Thus, on the equator, where $\theta = \frac{\pi}{2}$, we have $\tilde{\mathbf{g}} = -(g_0 - \omega^2 R_e) \hat{\mathbf{r}}$, with $\omega^2 R_e \approx 3.39 \text{ cm/s}^2$, a small but significant correction. You therefore weigh less on the equator. Note also that $\tilde{\mathbf{g}}$ has a component along $\hat{\theta}$. This means that a plumb bob suspended from a general point above the earth's surface won't point exactly toward the earth's center. Moreover, if the earth were replaced by an equivalent mass of fluid, the fluid would rearrange itself so as to make its surface locally perpendicular to $\tilde{\mathbf{g}}$. Indeed, the earth (and Sun) do exhibit quadrupolar distortions in their mass distributions – both are oblate spheroids. In fact, the observed difference $\tilde{g}(\theta = 0) - \tilde{g}(\theta = \frac{\pi}{2}) \approx 5.2 \text{ cm/s}^2$, which is 53% greater than the naively expected value of 3.39 cm/s^2 . The earth's oblateness enhances the effect.

12.3.1 Rotating tube of fluid

Consider a cylinder filled with a liquid, rotating with angular frequency ω about its symmetry axis $\hat{\mathbf{z}}$. In steady state, the fluid is stationary in the rotating frame, and we may write, for any given element of fluid

$$0 = \mathbf{f}' + \mathbf{g} - \omega^2 \hat{\mathbf{z}} \times (\hat{\mathbf{z}} \times \mathbf{r}) , \quad (12.23)$$

where \mathbf{f}' is the force per unit mass on the fluid element. Now consider a fluid element on the surface. Since there is no static friction to the fluid, any component of \mathbf{f}' parallel to the fluid's surface will cause the fluid to flow in that direction. This contradicts the steady state assumption. Therefore, we must have $\mathbf{f}' = f' \hat{\mathbf{n}}$, where $\hat{\mathbf{n}}$ is the local unit normal to the fluid surface. We write the equation for the fluid's surface as $z = z(\rho)$. Thus, with $\mathbf{r} = \rho \hat{\rho} + z(\rho) \hat{\mathbf{z}}$, Newton's second law yields

$$f' \hat{\mathbf{n}} = g \hat{\mathbf{z}} - \omega^2 \rho \hat{\rho} , \quad (12.24)$$

where $\mathbf{g} = -g \hat{\mathbf{z}}$ is assumed. From this, we conclude that the unit normal to the fluid surface and the force per unit mass are given by

$$\hat{\mathbf{n}}(\rho) = \frac{g \hat{\mathbf{z}} - \omega^2 \rho \hat{\rho}}{\sqrt{g^2 + \omega^4 \rho^2}} , \quad f'(\rho) = \sqrt{g^2 + \omega^4 \rho^2} . \quad (12.25)$$

Now suppose $\mathbf{r}(\rho, \phi) = \rho \hat{\rho} + z(\rho) \hat{\mathbf{z}}$ is a point on the surface of the fluid. We have that

$$d\mathbf{r} = \hat{\rho} d\rho + z'(\rho) \hat{\mathbf{z}} d\rho + \rho \hat{\phi} d\phi , \quad (12.26)$$

where $z' = dz/d\rho$, and where we have used $d\hat{\rho} = \hat{\phi} d\phi$, which follows from the first of eqn. 12.18 after setting $\theta = \frac{\pi}{2}$. Now $d\mathbf{r}$ must lie along the surface, therefore $\hat{\mathbf{n}} \cdot d\mathbf{r} = 0$, which says

$$g \frac{dz}{d\rho} = \omega^2 \rho . \quad (12.27)$$

Integrating this equation, we obtain the shape of the surface:

$$z(\rho) = z_0 + \frac{\omega^2 \rho^2}{2g} . \quad (12.28)$$

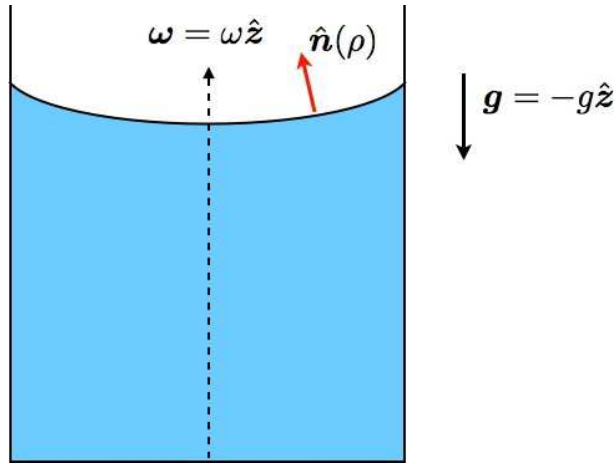


Figure 12.3: A rotating cylinder of fluid.

12.4 The Coriolis Force

12.4.1 Projectile motion

The Coriolis force is given by $\mathbf{F}_{\text{Cor}} = -2m\boldsymbol{\omega} \times \dot{\mathbf{r}}$. According to (12.15), the acceleration of a free particle ($\mathbf{F}' = 0$) isn't along $\tilde{\mathbf{g}}$ – an orthogonal component is generated by the Coriolis force. To actually solve the coupled equations of motion is difficult because the unit vectors $\{\hat{\mathbf{r}}, \hat{\theta}, \hat{\phi}\}$ change with position, and hence with time. The following standard problem highlights some of the effects of the Coriolis and centrifugal forces.

PROBLEM: A cannonball is dropped from the top of a tower of height h located at a northerly latitude of λ . Assuming the cannonball is initially at rest with respect to the tower, and neglecting air resistance, calculate its deflection (magnitude and direction) due to (a) centrifugal and (b) Coriolis forces by the time it hits the ground. Evaluate for the case $h = 100$ m, $\lambda = 45^\circ$. The radius of the earth is $R_e = 6.4 \times 10^6$ m.

SOLUTION: The equation of motion for a particle near the earth's surface is

$$\ddot{\mathbf{r}} = -2\boldsymbol{\omega} \times \dot{\mathbf{r}} - g_0 \hat{\mathbf{r}} - \boldsymbol{\omega} \times (\boldsymbol{\omega} \times \mathbf{r}) , \quad (12.29)$$

where $\boldsymbol{\omega} = \omega \hat{z}$, with $\omega = 2\pi/(24 \text{ hrs}) = 7.3 \times 10^{-5} \text{ rad/s}$. Here, $g_0 = GM_e/R_e^2 = 980 \text{ cm/s}^2$. We use a locally orthonormal coordinate system $\{\hat{\mathbf{r}}, \hat{\theta}, \hat{\phi}\}$ and write

$$\mathbf{r} = x \hat{\theta} + y \hat{\phi} + (R_e + z) \hat{\mathbf{r}} , \quad (12.30)$$

where $R_e = 6.4 \times 10^6$ m is the radius of the earth. Expressing \hat{z} in terms of our chosen orthonormal triad,

$$\hat{z} = \cos \theta \hat{\mathbf{r}} - \sin \theta \hat{\theta} , \quad (12.31)$$

where $\theta = \frac{\pi}{2} - \lambda$ is the polar angle, or ‘colatitude’. Since the height of the tower and the deflections are all very small on the scale of R_e , we may regard the orthonormal triad as fixed and time-independent,

although, in general, these unit vectors change as a function of \mathbf{r} . Thus, we have $\dot{\mathbf{r}} \simeq \dot{x}\hat{\theta} + \dot{y}\hat{\phi} + \dot{z}\hat{\mathbf{r}}$, and we find

$$\begin{aligned}\hat{z} \times \dot{\mathbf{r}} &= (\cos \theta \hat{\mathbf{r}} - \sin \theta \hat{\theta}) \times (\dot{x}\hat{\theta} + \dot{y}\hat{\phi} + \dot{z}\hat{\mathbf{r}}) \\ &= -\dot{y} \cos \theta \hat{\theta} + (\dot{x} \cos \theta + \dot{z} \sin \theta) \hat{\phi} - \dot{y} \sin \theta \hat{\mathbf{r}}\end{aligned}\quad (12.32)$$

and

$$\begin{aligned}\boldsymbol{\omega} \times (\boldsymbol{\omega} \times \mathbf{r}) &= \omega^2 (\cos \theta \hat{\mathbf{r}} - \sin \theta \hat{\theta}) \times \left((\cos \theta \hat{\mathbf{r}} - \sin \theta \hat{\theta}) \times \underbrace{(R_e \hat{\mathbf{r}} + x\hat{\theta} + y\hat{\phi} + z\hat{\mathbf{r}})}_{\text{negligible}} \right) \\ &\approx \omega^2 (\cos \theta \hat{\mathbf{r}} - \sin \theta \hat{\theta}) \times R_e \sin \theta \hat{\phi} \\ &= -\omega^2 R_e \sin \theta \cos \theta \hat{\theta} - \omega^2 R_e \sin^2 \theta \hat{\mathbf{r}}.\end{aligned}\quad (12.33)$$

Note that the distances x , y , and z are all extremely small in magnitude compared with R_e .

The equations of motion, written in components, are then

$$\begin{aligned}\dot{v}_x &= g_1 \sin \theta \cos \theta + 2\omega \cos \theta v_y \\ \dot{v}_y &= -2\omega \cos \theta v_x - 2\omega \sin \theta v_z \\ \dot{v}_z &= -g_0 + g_1 \sin^2 \theta + 2\omega \sin \theta v_y,\end{aligned}\quad (12.34)$$

with $g_1 \equiv \omega^2 R_e$. While these (inhomogeneous) equations are linear, they also are coupled, so an exact analytical solution is not trivial to obtain (but see below). Fortunately, the deflections are small, so we can solve this perturbatively. To do so, let us write $\mathbf{v}(t)$ as a power series in t . For each component, we write

$$v_\alpha(t) = \sum_{n=0}^{\infty} v_{\alpha,n} t^n, \quad (12.35)$$

with $v_{\alpha,0} = v_\alpha(t=0) \equiv v_\alpha^0$. Eqns. 12.34 then may be written as the coupled hierarchy

$$\begin{aligned}nv_{x,n} &= g_1 \sin \theta \cos \theta \delta_{n,1} + 2\omega \cos \theta v_{y,n-1} \\ nv_{y,n} &= -2\omega \cos \theta v_{x,n-1} - 2\omega \sin \theta v_{z,n-1} \\ nv_{z,n} &= -(g_0 - g_1 \sin^2 \theta) \delta_{n,1} + 2\omega \sin \theta v_{y,n-1}.\end{aligned}\quad (12.36)$$

Integrating $\mathbf{v}(t)$, we obtain the displacements,

$$x_\alpha(t) = x_\alpha^0 + \sum_{n=0}^{\infty} \frac{v_{\alpha,n}}{n+1} t^{n+1}. \quad (12.37)$$

Now let's roll up our sleeves and solve for the coefficients $v_{\alpha,n}$ for $n = 0, 1, 2$. This will give us the displacements up to terms of order t^3 . For $n = 0$ we already have $v_{\alpha,0} = v_\alpha^0$. For $n = 1$, we use Eqns. 12.36 with $n = 1$ to obtain

$$\begin{aligned}v_{x,1} &= 2\omega \cos \theta v_y^0 + g_1 \sin \theta \cos \theta \\ v_{y,1} &= -2\omega \cos \theta v_x^0 - 2\omega \sin \theta v_z^0 \\ v_{z,1} &= 2\omega \sin \theta v_y^0 - g_0 + g_1 \sin^2 \theta.\end{aligned}\quad (12.38)$$

Finally, at level $n = 2$, we have

$$\begin{aligned} v_{x,2} &= \omega \cos \theta v_{y,1} = -2\omega^2 \cos \theta (\cos \theta v_x^0 + \sin \theta v_z^0) \\ v_{y,2} &= -2\omega \cos \theta v_{x,1} - 2\omega \sin \theta v_{z,1} = -2\omega^2 v_y^0 + \omega \sin \theta (g_0 - g_1) \\ v_{z,2} &= \omega \sin \theta v_{y,1} = -2\omega^2 \sin \theta (\cos \theta v_x^0 + \sin \theta v_z^0) . \end{aligned} \quad (12.39)$$

Thus, the displacements are given by

$$\begin{aligned} x(t) &= x(0) + v_x^0 t + \frac{1}{2}(2\omega \cos \theta v_y^0 + g_1 \sin \theta \cos \theta) t^2 - \frac{2}{3}\omega^2 \cos \theta (\cos \theta v_x^0 + \sin \theta v_z^0) t^3 + \mathcal{O}(t^4) \\ y(t) &= y(0) + v_y^0 t - \omega (\cos \theta v_x^0 + \sin \theta v_z^0) t^2 - \frac{2}{3}\omega^2 v_y^0 t^3 + \frac{1}{3}\omega \sin \theta (g_0 - g_1) t^3 + \mathcal{O}(t^4) \\ z(t) &= z(0) + v_z^0 t + \frac{1}{2}(2\omega \sin \theta v_y^0 - g_0 + g_1 \sin^2 \theta) t^2 - \frac{2}{3}\omega^2 \sin \theta (\cos \theta v_x^0 + \sin \theta v_z^0) t^3 + \mathcal{O}(t^4) . \end{aligned} \quad (12.40)$$

When dropped from rest, with $x(0) = y(0) = 0$ and $z(0) = h_0$, we have

$$\begin{aligned} x(t) &= \frac{1}{2}g_1 \sin \theta \cos \theta t^2 + \mathcal{O}(t^4) \\ y(t) &= \frac{1}{3}\omega \sin \theta (g_0 - g_1) t^3 + \mathcal{O}(t^4) \\ z(t) &= h_0 - \frac{1}{2}(g_0 - g_1 \sin^2 \theta) t^2 + \mathcal{O}(t^4) . \end{aligned} \quad (12.41)$$

Recall $g_1 = \omega^2 R_e$, so if we neglect the rotation of the earth and set $\omega = 0$, we have $\omega = g_1 = 0$, and $z(t) = h_0 - \frac{1}{2}g_0 t^2$ with $x(t) = y(t) = 0$. This is the familiar high school physics result. As we see, in the noninertial reference frame of the rotating earth, there are deflections along $\hat{\theta}$ given by $x(t)$, along $\hat{\phi}$ given by $y(t)$, and also a correction $\Delta z(t) = \frac{1}{2}g_1 \sin^2 \theta t^2 + \mathcal{O}(t^4)$ to the motion along \hat{r} . To find the deflection of an object dropped from a height h_0 , solve $z(t^*) = 0$ to obtain $t^* = \sqrt{2h/(g_0 - g_1 \sin^2 \theta)}$ for the drop time, and substitute. For $h_0 = 100$ m and $\lambda = \frac{\pi}{2}$, find $\delta x(t^*) = 17$ cm south (centrifugal) and $\delta y(t^*) = 1.6$ cm east (Coriolis). Note that the centrifugal term dominates the deflection in this example. Why is the Coriolis deflection always to the east? The earth rotates eastward, and an object starting from rest in the earth's frame has initial angular velocity equal to that of the earth. To conserve angular momentum, the object must speed up as it falls.

Exact solution for velocities

In fact, an exact solution to (12.34) is readily obtained, via the following analysis. The equations of motion may be written $\dot{\mathbf{v}} = 2i\omega \mathcal{J} \mathbf{v} + \mathbf{b}$, or

$$\begin{pmatrix} \dot{v}_x \\ \dot{v}_y \\ \dot{v}_z \end{pmatrix} = 2i\omega \underbrace{\begin{pmatrix} 0 & -i \cos \theta & 0 \\ i \cos \theta & 0 & i \sin \theta \\ 0 & -i \sin \theta & 0 \end{pmatrix}}_{\mathcal{J}} \begin{pmatrix} v_x \\ v_y \\ v_z \end{pmatrix} + \underbrace{\begin{pmatrix} g_1 \sin \theta \cos \theta \\ 0 \\ -g_0 + g_1 \sin^2 \theta \end{pmatrix}}_{\mathbf{b}} . \quad (12.42)$$

Note that $\mathcal{J}^\dagger = \mathcal{J}$, *i.e.* \mathcal{J} is a Hermitian matrix. The formal solution is

$$\mathbf{v}(t) = e^{2i\omega \mathcal{J} t} \mathbf{v}(0) + \left(\frac{e^{2i\omega \mathcal{J} t} - 1}{2i\omega} \right) \mathcal{J}^{-1} \mathbf{b} . \quad (12.43)$$

When working with matrices, it is convenient to work in an eigenbasis. The characteristic polynomial for \mathcal{J} is $P(\lambda) = \det(\lambda \cdot 1 - \mathcal{J}) = \lambda(\lambda^2 - 1)$, hence the eigenvalues are $\lambda_1 = 0$, $\lambda_2 = +1$, and $\lambda_3 = -1$. The corresponding eigenvectors are easily found to be

$$\psi_1 = \begin{pmatrix} \sin \theta \\ 0 \\ -\cos \theta \end{pmatrix}, \quad \psi_2 = \frac{1}{\sqrt{2}} \begin{pmatrix} \cos \theta \\ i \\ \sin \theta \end{pmatrix}, \quad \psi_3 = \frac{1}{\sqrt{2}} \begin{pmatrix} \cos \theta \\ -i \\ \sin \theta \end{pmatrix}. \quad (12.44)$$

Note that $\psi_a^\dagger \cdot \psi_{a'} = \delta_{aa'}$.

Expanding \mathbf{v} and \mathbf{b} in this eigenbasis, we have $\dot{u}_a = 2i\omega\lambda_a u_a + b_a$, where $u_a = \psi_{ia}^* v_i$ and $b_a = \psi_{ia}^* b_i$. The solution is

$$u_a(t) = u_a(0) e^{2i\lambda_a \omega t} + \left(\frac{e^{2i\lambda_a \omega t} - 1}{2i\lambda_a \omega} \right) b_a. \quad (12.45)$$

Since the eigenvectors of \mathcal{J} are orthonormal, $u_a = \psi_{ia}^* v_i$ entails $v_i = \psi_{ia} u_a$, hence

$$v_i(t) = \sum_j \left(\sum_a \psi_{ia} e^{2i\lambda_a \omega t} \psi_{ja}^* \right) v_j(0) + \sum_j \left(\sum_a \psi_{ia} \left(\frac{e^{2i\lambda_a \omega t} - 1}{2i\lambda_a \omega} \right) \psi_{ja}^* \right) b_j. \quad (12.46)$$

Doing the requisite matrix multiplications, and assuming $\mathbf{v}(0) = 0$, we obtain

$$\begin{pmatrix} v_x(t) \\ v_y(t) \\ v_z(t) \end{pmatrix} = \begin{pmatrix} t \sin^2 \theta + \frac{\sin 2\omega t}{2\omega} \cos^2 \theta & \frac{\sin^2 \omega t}{\omega} \cos \theta & -\frac{1}{2}t \sin 2\theta + \frac{\sin 2\omega t}{4\omega} \sin 2\theta \\ -\frac{\sin^2 \omega t}{\omega} \cos \theta & \frac{\sin 2\omega t}{2\omega} & -\frac{\sin^2 \omega t}{\omega} \sin \theta \\ -\frac{1}{2}t \sin 2\theta + \frac{\sin 2\omega t}{4\omega} \sin 2\theta & \frac{\sin^2 \omega t}{\omega} \sin \theta & t \cos^2 \theta + \frac{\sin 2\omega t}{2\omega} \sin^2 \theta \end{pmatrix} \begin{pmatrix} g_1 \sin \theta \cos \theta \\ 0 \\ -g_0 + g_1 \sin^2 \theta \end{pmatrix}, \quad (12.47)$$

which says

$$\begin{aligned} v_x(t) &= \left(\frac{\sin 2\omega t}{2\omega t} - 1 \right) g_0 t \sin \theta \cos \theta + \frac{\sin 2\omega t}{2\omega t} g_1 t \sin \theta \cos \theta \\ v_y(t) &= \frac{\sin^2 \omega t}{\omega t} (g_0 - g_1) t \sin \theta \\ v_z(t) &= -\left(\cos^2 \theta + \frac{\sin 2\omega t}{2\omega t} \sin^2 \theta \right) g_0 t + \frac{\sin^2 \omega t}{2\omega t} g_1 t \sin^2 \theta. \end{aligned} \quad (12.48)$$

One can check that by expanding in a power series in t we recover the results of the previous section.

12.4.2 Foucault's pendulum

A pendulum swinging over one of the poles moves in a fixed inertial plane while the earth rotates underneath. Relative to the earth, the plane of motion of the pendulum makes one revolution every day. What happens at a general latitude? Assume the pendulum is located at colatitude θ and longitude ϕ . Assuming the length scale of the pendulum is small compared to R_e , we can regard the local triad $\{\hat{\theta}, \hat{\phi}, \hat{r}\}$ as fixed. The situation is depicted in Fig. 12.4. We write

$$\mathbf{r} = x \hat{\theta} + y \hat{\phi} + z \hat{r}, \quad (12.49)$$

with

$$x = \ell \sin \psi \cos \alpha, \quad y = \ell \sin \psi \sin \alpha, \quad z = \ell (1 - \cos \psi). \quad (12.50)$$

In our analysis we will ignore centrifugal effects, which are of higher order in ω , and we take $\mathbf{g} = -g \hat{\mathbf{r}}$. We also idealize the pendulum, and consider the suspension rod to be of negligible mass.

The total force on the mass m is due to gravity and tension:

$$\begin{aligned}\mathbf{F} &= m\mathbf{g} + \mathbf{T} \\ &= (-T \sin \psi \cos \alpha, -T \sin \psi \sin \alpha, T \cos \psi - mg) \\ &= (-Tx/\ell, -Ty/\ell, T - Mg - Tz/\ell).\end{aligned}\tag{12.51}$$

The Coriolis term is

$$\begin{aligned}\mathbf{F}_{\text{Cor}} &= -2m\boldsymbol{\omega} \times \dot{\mathbf{r}} \\ &= -2m\omega(\cos \theta \hat{\mathbf{r}} - \sin \theta \hat{\boldsymbol{\theta}}) \times (\dot{x} \hat{\boldsymbol{\theta}} + \dot{y} \hat{\boldsymbol{\phi}} + \dot{z} \hat{\mathbf{r}}) \\ &= 2m\omega(\dot{y} \cos \theta, -\dot{x} \cos \theta - \dot{z} \sin \theta, \dot{y} \sin \theta).\end{aligned}\tag{12.52}$$

The equations of motion are $m\ddot{\mathbf{r}} = \mathbf{F} + \mathbf{F}_{\text{Cor}}$:

$$\begin{aligned}m\ddot{x} &= -Tx/\ell + 2m\omega \cos \theta \dot{y} \\ m\ddot{y} &= -Ty/\ell - 2m\omega \cos \theta \dot{x} - 2m\omega \sin \theta \dot{z} \\ m\ddot{z} &= T - mg - Tz/\ell + 2m\omega \sin \theta \dot{y}.\end{aligned}\tag{12.53}$$

These three equations are to be solved for the three unknowns x , y , and T . Note that

$$x^2 + y^2 + (\ell - z)^2 = \ell^2,\tag{12.54}$$

so $z = z(x, y)$ is not an independent degree of freedom. This equation may be recast in the form $z = (x^2 + y^2 + z^2)/2\ell$ which shows that if x and y are both small, then z is at least of second order in smallness. Therefore, we will approximate $z \approx 0$, in which case \dot{z} may be neglected from the second equation of motion. The third equation is used to solve for T :

$$T \approx mg - 2m\omega \sin \theta \dot{y}.\tag{12.55}$$

Adding the first plus i times the second then gives the complexified equation

$$\begin{aligned}\ddot{\xi} &= -\frac{T}{m\ell} \xi - 2i\omega \cos \theta \dot{\xi} \\ &\approx -\omega_0^2 \xi - 2i\omega \cos \theta \dot{\xi}\end{aligned}\tag{12.56}$$

where $\xi \equiv x + iy$, and where $\omega_0 = \sqrt{g/\ell}$. Note that we have approximated $T \approx mg$ in deriving the second line.

It is now a trivial matter to solve the homogeneous linear ODE of eq. 12.56. Writing

$$\xi = \xi_0 e^{-i\Omega t}\tag{12.57}$$

and plugging in to find Ω , we obtain

$$\Omega^2 - 2\omega_{\perp} \Omega - \omega_0^2 = 0,\tag{12.58}$$

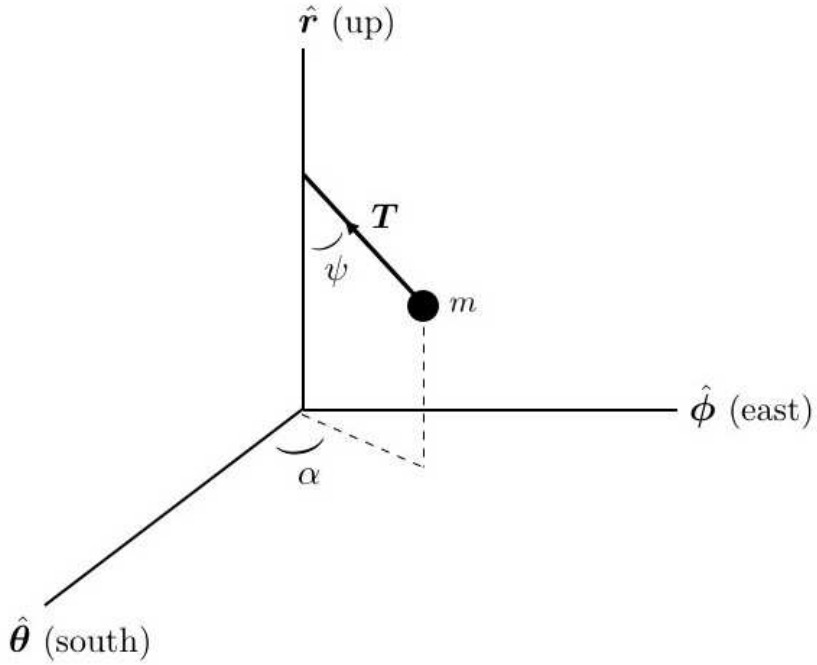


Figure 12.4: Foucault's pendulum.

with $\omega_{\perp} \equiv \omega \cos \theta$. The roots are

$$\Omega_{\pm} = \omega_{\perp} \pm \sqrt{\omega_0^2 + \omega_{\perp}^2}, \quad (12.59)$$

hence the most general solution is

$$\xi(t) = A_+ e^{-i\Omega_+ t} + A_- e^{-i\Omega_- t}. \quad (12.60)$$

Finally, if we take as initial conditions $x(0) = a$, $y(0) = 0$, $\dot{x}(0) = 0$, and $\dot{y}(0) = 0$, we obtain

$$\begin{aligned} x(t) &= \left(\frac{a}{\nu}\right) \cdot \left\{ \omega_{\perp} \sin(\omega_{\perp} t) \sin(\nu t) + \nu \cos(\omega_{\perp} t) \cos(\nu t) \right\} \\ y(t) &= \left(\frac{a}{\nu}\right) \cdot \left\{ \omega_{\perp} \cos(\omega_{\perp} t) \sin(\nu t) - \nu \sin(\omega_{\perp} t) \cos(\nu t) \right\}, \end{aligned} \quad (12.61)$$

with $\nu = \sqrt{\omega_0^2 + \omega_{\perp}^2}$. Typically $\omega_0 \gg \omega_{\perp}$, since $\omega = 7.3 \times 10^{-5} \text{ s}^{-1}$. In the limit $\omega_{\perp} \ll \omega_0$, then, we have $\nu \approx \omega_0$ and

$$x(t) \simeq a \cos(\omega_{\perp} t) \cos(\omega_0 t), \quad y(t) \simeq -a \sin(\omega_{\perp} t) \cos(\omega_0 t), \quad (12.62)$$

and the plane of motion rotates with angular frequency $-\omega_{\perp}$, i.e. the period is $|\sec \theta|$ days. Viewed from above, the rotation is clockwise in the northern hemisphere, where $\cos \theta > 0$ and counterclockwise in the southern hemisphere, where $\cos \theta < 0$.

Chapter 13

Rigid Body Motion and Rotational Dynamics

13.1 Rigid Bodies

A rigid body consists of a group of particles whose separations are all fixed in magnitude. Six independent coordinates are required to completely specify the position and orientation of a rigid body. For example, the location of the first particle is specified by three coordinates. A second particle requires only two coordinates since the distance to the first is fixed. Finally, a third particle requires only one coordinate, since its distance to the first two particles is fixed (think about the intersection of two spheres). The positions of all the remaining particles are then determined by their distances from the first three. Usually, one takes these six coordinates to be the center-of-mass position $\mathbf{R} = (X, Y, Z)$ and three angles specifying the orientation of the body (*e.g.* the Euler angles).

As derived previously, the equations of motion are

$$\begin{aligned}\mathbf{P} &= \sum_i m_i \dot{\mathbf{r}}_i \quad , \quad \dot{\mathbf{P}} = \mathbf{F}^{(\text{ext})} \\ \mathbf{L} &= \sum_i m_i \mathbf{r}_i \times \dot{\mathbf{r}}_i \quad , \quad \dot{\mathbf{L}} = \mathbf{N}^{(\text{ext})} .\end{aligned}\tag{13.1}$$

These equations determine the motion of a rigid body.

13.1.1 Examples of rigid bodies

Our first example of a rigid body is of a wheel rolling with constant angular velocity $\dot{\phi} = \omega$, and without slipping. This is shown in Fig. 13.1. The no-slip condition is $dx = R d\phi$, so $\dot{x} = V_{\text{CM}} = R\omega$. The velocity of a point within the wheel is

$$\mathbf{v} = \mathbf{V}_{\text{CM}} + \boldsymbol{\omega} \times \mathbf{r} ,\tag{13.2}$$

where \mathbf{r} is measured from the center of the disk. The velocity of a point on the surface is then given by $\mathbf{v} = \omega R (\hat{\mathbf{x}} + \hat{\boldsymbol{\omega}} \times \hat{\mathbf{r}})$.

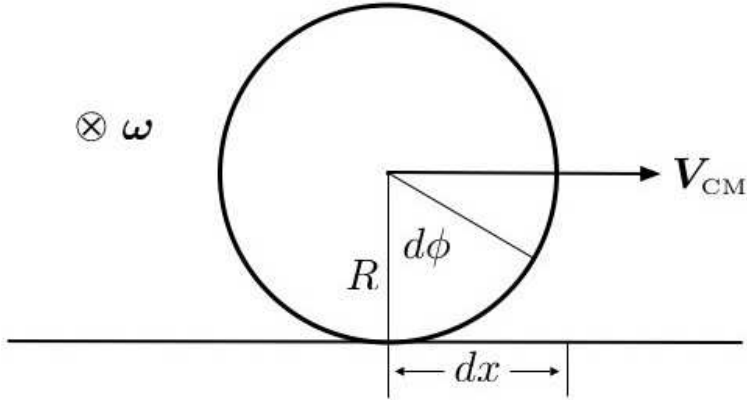


Figure 13.1: A wheel rolling to the right without slipping.

As a second example, consider a bicycle wheel of mass M and radius R affixed to a light, firm rod of length d , as shown in Fig. 13.2. Assuming \mathbf{L} lies in the (x, y) plane, one computes the gravitational torque $\mathbf{N} = \mathbf{r} \times (M\mathbf{g}) = Mgd\hat{\phi}$. The angular momentum vector then rotates with angular frequency $\dot{\phi}$. Thus,

$$d\phi = \frac{dL}{L} \implies \dot{\phi} = \frac{Mgd}{L} . \quad (13.3)$$

But $L = MR^2\omega$, so the precession frequency is

$$\omega_p = \dot{\phi} = \frac{gd}{\omega R^2} . \quad (13.4)$$

For $R = d = 30$ cm and $\omega/2\pi = 200$ rpm, find $\omega_p/2\pi \approx 15$ rpm. Note that we have here ignored the contribution to \mathbf{L} from the precession itself, which lies along \hat{z} , resulting in the *nutation* of the wheel. This is justified if $L_p/L = (d^2/R^2) \cdot (\omega_p/\omega) \ll 1$.

13.2 The Inertia Tensor

Suppose first that a point within the body itself is fixed. This eliminates the translational degrees of freedom from consideration. We now have

$$\left(\frac{d\mathbf{r}}{dt} \right)_{\text{inertial}} = \boldsymbol{\omega} \times \mathbf{r} , \quad (13.5)$$

since $\dot{\mathbf{r}}_{\text{body}} = 0$. The kinetic energy is then

$$\begin{aligned} T &= \frac{1}{2} \sum_i m_i \left(\frac{d\mathbf{r}_i}{dt} \right)_{\text{inertial}}^2 = \frac{1}{2} \sum_i m_i (\boldsymbol{\omega} \times \mathbf{r}_i) \cdot (\boldsymbol{\omega} \times \mathbf{r}_i) \\ &= \frac{1}{2} \sum_i m_i [\omega^2 \mathbf{r}_i^2 - (\boldsymbol{\omega} \cdot \mathbf{r}_i)^2] \equiv \frac{1}{2} I_{\alpha\beta} \omega_\alpha \omega_\beta , \end{aligned} \quad (13.6)$$

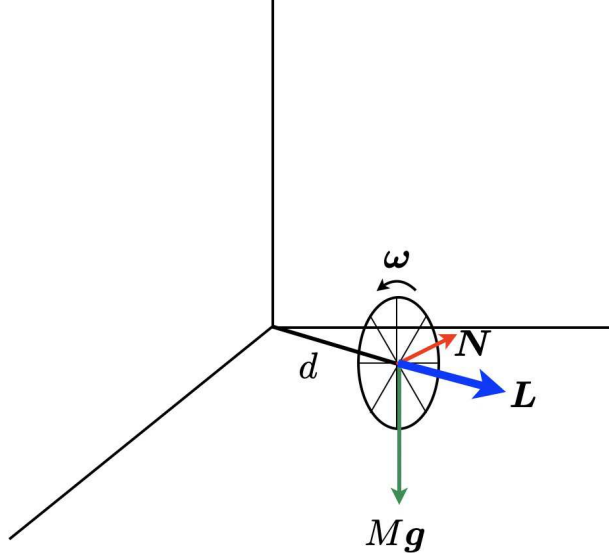


Figure 13.2: Precession of a spinning bicycle wheel.

where ω_α is the component of $\boldsymbol{\omega}$ along the body-fixed axis \mathbf{e}_α . The quantity $I_{\alpha\beta}$ is the *inertia tensor*,

$$\begin{aligned} I_{\alpha\beta} &= \sum_i m_i (\mathbf{r}_i^2 \delta_{\alpha\beta} - r_{i,\alpha} r_{i,\beta}) \\ &= \int d^d r \varrho(\mathbf{r}) (\mathbf{r}^2 \delta_{\alpha\beta} - r_\alpha r_\beta) \quad (\text{continuous media}) . \end{aligned} \quad (13.7)$$

The angular momentum is

$$\begin{aligned} \mathbf{L} &= \sum_i m_i \mathbf{r}_i \times \left(\frac{d\mathbf{r}_i}{dt} \right)_{\text{inertial}} \\ &= \sum_i m_i \mathbf{r}_i \times (\boldsymbol{\omega} \times \mathbf{r}_i) = I_{\alpha\beta} \omega_\beta . \end{aligned} \quad (13.8)$$

The diagonal elements of $I_{\alpha\beta}$ are called the *moments of inertia*, while the off-diagonal elements are called the *products of inertia*.

13.2.1 Coordinate transformations

Consider the basis transformation

$$\hat{\mathbf{e}}'_\alpha = \mathcal{R}_{\alpha\beta} \hat{\mathbf{e}}_\beta . \quad (13.9)$$

We demand $\hat{\mathbf{e}}'_\alpha \cdot \hat{\mathbf{e}}'_\beta = \delta_{\alpha\beta}$, which means $\mathcal{R} \in O(d)$ is an orthogonal matrix, i.e. $\mathcal{R}^t = \mathcal{R}^{-1}$. Thus the inverse transformation is $\mathbf{e}_\alpha = \mathcal{R}_{\alpha\beta}^t \mathbf{e}'_\beta$. Consider next a general vector $\mathbf{A} = A_\beta \hat{\mathbf{e}}_\beta$. Expressed in terms of the new basis $\{\hat{\mathbf{e}}'_\alpha\}$, we have

$$\mathbf{A} = A_\beta \overbrace{\mathcal{R}_{\beta\alpha}^t \hat{\mathbf{e}}'_\alpha}^{\hat{\mathbf{e}}_\beta} = \overbrace{\mathcal{R}_{\alpha\beta} A_\beta}^{A'_\alpha} \hat{\mathbf{e}}'_\alpha \quad (13.10)$$

Thus, the components of \mathbf{A} transform as $A'_\alpha = \mathcal{R}_{\alpha\beta} A_\beta$. This is true for any vector.

Under a rotation, the density $\rho(\mathbf{r})$ must satisfy $\rho'(\mathbf{r}') = \rho(\mathbf{r})$. This is the transformation rule for scalars. The inertia tensor therefore obeys

$$\begin{aligned} I'_{\alpha\beta} &= \int d^3r' \rho'(\mathbf{r}') \left[\mathbf{r}'^2 \delta_{\alpha\beta} - r'_\alpha r'_\beta \right] \\ &= \int d^3r \rho(\mathbf{r}) \left[\mathbf{r}^2 \delta_{\alpha\beta} - (\mathcal{R}_{\alpha\mu} r_\mu)(\mathcal{R}_{\beta\nu} r_\nu) \right] \\ &= \mathcal{R}_{\alpha\mu} I_{\mu\nu} \mathcal{R}_{\nu\beta}^t . \end{aligned} \quad (13.11)$$

I.e. $I' = \mathcal{R} I \mathcal{R}^t$, the transformation rule for tensors. The angular frequency $\boldsymbol{\omega}$ is a vector, so $\omega'_\alpha = \mathcal{R}_{\alpha\mu} \omega_\mu$. The angular momentum \mathbf{L} also transforms as a vector. The kinetic energy is $T = \frac{1}{2} \boldsymbol{\omega}^t \cdot \mathbf{I} \cdot \boldsymbol{\omega}$, which transforms as a scalar.

13.2.2 The case of no fixed point

If there is no fixed point, we can let \mathbf{r}' denote the distance from the center-of-mass (CM), which will serve as the instantaneous origin in the body-fixed frame. We then adopt the notation where \mathbf{R} is the CM position of the rotating body, as observed in an inertial frame, and is computed from the expression

$$\mathbf{R} = \frac{1}{M} \sum_i m_i \mathbf{r}_i = \frac{1}{M} \int d^3r \rho(\mathbf{r}) \mathbf{r} , \quad (13.12)$$

where the total mass is of course

$$M = \sum_i m_i = \int d^3r \rho(\mathbf{r}) . \quad (13.13)$$

The kinetic energy and angular momentum are then

$$\begin{aligned} T &= \frac{1}{2} M \dot{\mathbf{R}}^2 + \frac{1}{2} I_{\alpha\beta} \omega_\alpha \omega_\beta \\ L_\alpha &= \epsilon_{\alpha\beta\gamma} M R_\beta \dot{R}_\gamma + I_{\alpha\beta} \omega_\beta , \end{aligned} \quad (13.14)$$

where $I_{\alpha\beta}$ is given in eqs. 13.7, where the origin is the CM.

13.3 Parallel Axis Theorem

Suppose $I_{\alpha\beta}$ is given in a body-fixed frame. If we displace the origin in the body-fixed frame by \mathbf{d} , then let $I_{\alpha\beta}(\mathbf{d})$ be the inertial tensor with respect to the new origin. If, relative to the origin at $\mathbf{0}$ a mass element lies at position \mathbf{r} , then relative to an origin at \mathbf{d} it will lie at $\mathbf{r} - \mathbf{d}$. We then have

$$I_{\alpha\beta}(\mathbf{d}) = \sum_i m_i \left\{ (\mathbf{r}_i^2 - 2\mathbf{d} \cdot \mathbf{r}_i + \mathbf{d}^2) \delta_{\alpha\beta} - (r_{i,\alpha} - d_\alpha)(r_{i,\beta} - d_\beta) \right\} . \quad (13.15)$$

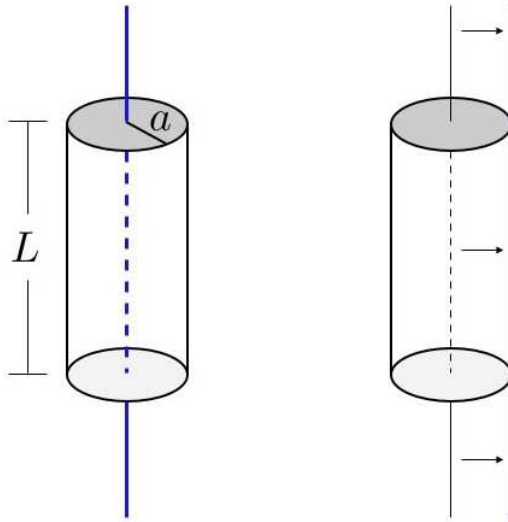


Figure 13.3: Application of the parallel axis theorem to a cylindrically symmetric mass distribution.

If \mathbf{r}_i is measured with respect to the CM, then

$$\sum_i m_i \mathbf{r}_i = 0 \quad (13.16)$$

and

$$I_{\alpha\beta}(\mathbf{d}) = I_{\alpha\beta}(0) + M(d^2 \delta_{\alpha\beta} - d_\alpha d_\beta) , \quad (13.17)$$

a result known as the *parallel axis theorem*.

As an example of the theorem, consider the situation depicted in Fig. 13.3, where a cylindrically symmetric mass distribution is rotated about its symmetry axis, and about an axis tangent to its side. The component I_{zz} of the inertia tensor is easily computed when the origin lies along the symmetry axis:

$$\begin{aligned} I_{zz} &= \int d^3 r \rho(\mathbf{r}) (\mathbf{r}^2 - z^2) = \rho L \cdot 2\pi \int_0^a dr_\perp r_\perp^3 \\ &= \frac{\pi}{2} \rho L a^4 = \frac{1}{2} M a^2 , \end{aligned} \quad (13.18)$$

where $M = \pi a^2 L \rho$ is the total mass. If we compute I_{zz} about a vertical axis which is tangent to the cylinder, the parallel axis theorem tells us that

$$I'_{zz} = I_{zz} + Ma^2 = \frac{3}{2} Ma^2 . \quad (13.19)$$

Doing this calculation by explicit integration of $\int dm r_\perp^2$ would be tedious!

13.3.1 Example

Problem: Compute the CM and the inertia tensor for the planar right triangle of Fig. 13.4, assuming it to be of uniform two-dimensional mass density ρ .

Solution: The total mass is $M = \frac{1}{2}\rho ab$. The x -coordinate of the CM is then

$$\begin{aligned} X &= \frac{1}{M} \int_0^a dx \int_0^{b(1-\frac{x}{a})} dy \rho x = \frac{\rho}{M} \int_0^a dx b\left(1 - \frac{x}{a}\right) x \\ &= \frac{\rho a^2 b}{M} \int_0^1 du u(1-u) = \frac{\rho a^2 b}{6M} = \frac{1}{3} a . \end{aligned} \quad (13.20)$$

Clearly we must then have $Y = \frac{1}{3}b$, which may be verified by explicit integration.

We now compute the inertia tensor, with the origin at $(0,0,0)$. Since the figure is planar, $z = 0$ everywhere, hence $I_{xz} = I_{zx} = 0$, $I_{yz} = I_{zy} = 0$, and also $I_{zz} = I_{xx} + I_{yy}$. We now compute the remaining independent elements:

$$\begin{aligned} I_{xx} &= \rho \int_0^a dx \int_0^{b(1-\frac{x}{a})} dy y^2 = \rho \int_0^a dx \frac{1}{3} b^3 \left(1 - \frac{x}{a}\right)^3 \\ &= \frac{1}{3} \rho ab^3 \int_0^1 du (1-u)^3 = \frac{1}{12} \rho ab^3 = \frac{1}{6} Mb^2 \end{aligned} \quad (13.21)$$

and

$$\begin{aligned} I_{xy} &= -\rho \int_0^a dx \int_0^{b(1-\frac{x}{a})} dy xy = -\frac{1}{2} \rho b^2 \int_0^a dx x \left(1 - \frac{x}{a}\right)^2 \\ &= -\frac{1}{2} \rho a^2 b^2 \int_0^1 du u (1-u)^2 = -\frac{1}{24} \rho a^2 b^2 = -\frac{1}{12} Mab . \end{aligned} \quad (13.22)$$

Thus,

$$I = \frac{M}{6} \begin{pmatrix} b^2 & -\frac{1}{2}ab & 0 \\ -\frac{1}{2}ab & a^2 & 0 \\ 0 & 0 & a^2 + b^2 \end{pmatrix} . \quad (13.23)$$

Suppose we wanted the inertia tensor relative in a coordinate system where the CM lies at the origin. What we computed in eqn. 13.23 is $I(\mathbf{d})$, with $\mathbf{d} = -\frac{a}{3}\hat{\mathbf{x}} - \frac{b}{3}\hat{\mathbf{y}}$. Thus,

$$\mathbf{d}^2 \delta_{\alpha\beta} - d_\alpha d_\beta = \frac{1}{9} \begin{pmatrix} b^2 & -ab & 0 \\ -ab & a^2 & 0 \\ 0 & 0 & a^2 + b^2 \end{pmatrix} . \quad (13.24)$$

Since

$$I(\mathbf{d}) = I^{\text{CM}} + M \left(\mathbf{d}^2 \delta_{\alpha\beta} - d_\alpha d_\beta \right) , \quad (13.25)$$

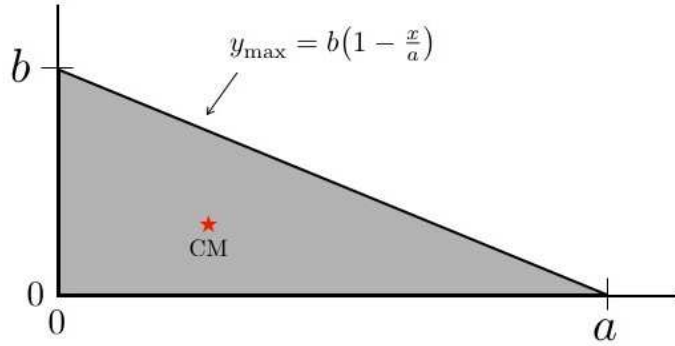


Figure 13.4: A planar mass distribution in the shape of a triangle.

we have that

$$\begin{aligned} I^{\text{CM}} &= I(\mathbf{d}) - M \left(\mathbf{d}^2 \delta_{\alpha\beta} - d_\alpha d_\beta \right) \\ &= \frac{M}{18} \begin{pmatrix} b^2 & \frac{1}{2}ab & 0 \\ \frac{1}{2}ab & a^2 & 0 \\ 0 & 0 & a^2 + b^2 \end{pmatrix}. \end{aligned} \quad (13.26)$$

13.3.2 General planar mass distribution

For a general planar mass distribution,

$$\rho(x, y, z) = \sigma(x, y) \delta(z) , \quad (13.27)$$

which is confined to the plane $z = 0$, we have $I_{xz} = I_{yz} = 0$, and

$$\begin{aligned} I_{xx} &= \int dx \int dy \sigma(x, y) y^2 \\ I_{yy} &= \int dx \int dy \sigma(x, y) x^2 \\ I_{xy} &= - \int dx \int dy \sigma(x, y) xy . \end{aligned} \quad (13.28)$$

Furthermore, $I_{zz} = I_{xx} + I_{yy}$, regardless of the two-dimensional mass distribution $\sigma(x, y)$.

13.4 Principal Axes of Inertia

We found that an orthogonal transformation to a new set of axes $\hat{\mathbf{e}}'_\alpha = \mathcal{R}_{\alpha\beta} \hat{\mathbf{e}}_\beta$ entails $I' = \mathcal{R} I \mathcal{R}^t$ for the inertia tensor. Since $I = I^t$ is manifestly a symmetric matrix, it can be brought to diagonal form by such an orthogonal transformation. To find \mathcal{R} , follow this recipe:

- Find the diagonal elements of I' by setting $P(\lambda) = 0$, where

$$P(\lambda) = \det(\lambda \cdot 1 - I) , \quad (13.29)$$

is the characteristic polynomial for I , and 1 is the unit matrix.

- For each eigenvalue λ_a , solve the d equations

$$\sum_{\nu} I_{\mu\nu} \psi_{\nu}^a = \lambda_a \psi_{\mu}^a . \quad (13.30)$$

Here, ψ_{μ}^a is the μ^{th} component of the a^{th} eigenvector. Since $(\lambda \cdot 1 - I)$ is degenerate, these equations are linearly dependent, which means that the first $d - 1$ components may be determined in terms of the d^{th} component.

- Because $I = I^t$, eigenvectors corresponding to different eigenvalues are orthogonal. In cases of degeneracy, the eigenvectors may be chosen to be orthogonal, *e.g.* via the Gram-Schmidt procedure.
- Due to the underdetermined aspect to step 2, we may choose an arbitrary normalization for each eigenvector. It is conventional to choose the eigenvectors to be orthonormal: $\sum_{\mu} \psi_{\mu}^a \psi_{\mu}^b = \delta^{ab}$.
- The matrix \mathcal{R} is explicitly given by $\mathcal{R}_{a\mu} = \psi_{\mu}^a$, the matrix whose row vectors are the eigenvectors ψ^a . Of course \mathcal{R}^t is then the corresponding matrix of column vectors.
- The eigenvectors form a complete basis. The resolution of unity may be expressed as

$$\sum_a \psi_{\mu}^a \psi_{\nu}^a = \delta_{\mu\nu} . \quad (13.31)$$

As an example, consider the inertia tensor for a general planar mass distribution, which is of the form

$$I = \begin{pmatrix} I_{xx} & I_{xy} & 0 \\ I_{yx} & I_{yy} & 0 \\ 0 & 0 & I_{zz} \end{pmatrix} , \quad (13.32)$$

where $I_{yx} = I_{xy}$ and $I_{zz} = I_{xx} + I_{yy}$. Define

$$\begin{aligned} A &= \frac{1}{2}(I_{xx} + I_{yy}) \\ B &= \sqrt{\frac{1}{4}(I_{xx} - I_{yy})^2 + I_{xy}^2} \\ \vartheta &= \tan^{-1} \left(\frac{2I_{xy}}{I_{xx} - I_{yy}} \right) , \end{aligned} \quad (13.33)$$

so that

$$I = \begin{pmatrix} A + B \cos \vartheta & B \sin \vartheta & 0 \\ B \sin \vartheta & A - B \cos \vartheta & 0 \\ 0 & 0 & 2A \end{pmatrix} , \quad (13.34)$$

The characteristic polynomial is found to be

$$P(\lambda) = (\lambda - 2A) \left[(\lambda - A)^2 - B^2 \right] , \quad (13.35)$$

which gives $\lambda_1 = A + B$, $\lambda_2 = A - B$, and $\lambda_3 = 2A$. The corresponding normalized eigenvectors are

$$\psi^1 = \begin{pmatrix} \cos \frac{1}{2}\vartheta \\ \sin \frac{1}{2}\vartheta \\ 0 \end{pmatrix}, \quad \psi^2 = \begin{pmatrix} -\sin \frac{1}{2}\vartheta \\ \cos \frac{1}{2}\vartheta \\ 0 \end{pmatrix}, \quad \psi^3 = \begin{pmatrix} 0 \\ 0 \\ 1 \end{pmatrix} \quad (13.36)$$

and therefore

$$\mathcal{R} = \begin{pmatrix} \cos \frac{1}{2}\vartheta & \sin \frac{1}{2}\vartheta & 0 \\ -\sin \frac{1}{2}\vartheta & \cos \frac{1}{2}\vartheta & 0 \\ 0 & 0 & 1 \end{pmatrix}. \quad (13.37)$$

We then have

$$I' = \mathcal{R} I \mathcal{R}^t = \begin{pmatrix} A + B & 0 & 0 \\ 0 & A - B & 0 \\ 0 & 0 & 2A \end{pmatrix}. \quad (13.38)$$

13.5 Euler's Equations

Let us now choose our coordinate axes to be the principal axes of inertia, with the CM at the origin. We may then write

$$\boldsymbol{\omega} = \begin{pmatrix} \omega_1 \\ \omega_2 \\ \omega_3 \end{pmatrix}, \quad I = \begin{pmatrix} I_1 & 0 & 0 \\ 0 & I_2 & 0 \\ 0 & 0 & I_3 \end{pmatrix} \implies \mathbf{L} = \begin{pmatrix} I_1 \omega_1 \\ I_2 \omega_2 \\ I_3 \omega_3 \end{pmatrix}. \quad (13.39)$$

The equations of motion are

$$\begin{aligned} \mathbf{N}^{\text{ext}} &= \left(\frac{d\mathbf{L}}{dt} \right)_{\text{inertial}} \\ &= \left(\frac{d\mathbf{L}}{dt} \right)_{\text{body}} + \boldsymbol{\omega} \times \mathbf{L} \\ &= I \dot{\boldsymbol{\omega}} + \boldsymbol{\omega} \times (I \boldsymbol{\omega}). \end{aligned}$$

Thus, we arrive at *Euler's equations*:

$$\begin{aligned} I_1 \dot{\omega}_1 &= (I_2 - I_3) \omega_2 \omega_3 + N_1^{\text{ext}} \\ I_2 \dot{\omega}_2 &= (I_3 - I_1) \omega_3 \omega_1 + N_2^{\text{ext}} \\ I_3 \dot{\omega}_3 &= (I_1 - I_2) \omega_1 \omega_2 + N_3^{\text{ext}}. \end{aligned} \quad (13.40)$$

These are coupled and nonlinear. Also note the fact that the external torque must be evaluated along body-fixed principal axes. We can however make progress in the case where $\mathbf{N}^{\text{ext}} = 0$, *i.e.* when there are no external torques. This is true for a body in free space, or in a uniform gravitational field. In the latter case,

$$\mathbf{N}^{\text{ext}} = \sum_i \mathbf{r}_i \times (m_i \mathbf{g}) = \left(\sum_i m_i \mathbf{r}_i \right) \times \mathbf{g}, \quad (13.41)$$

where \mathbf{g} is the uniform gravitational acceleration. In a body-fixed frame whose origin is the CM, we have $\sum_i m_i \mathbf{r}_i = 0$, and the external torque vanishes!

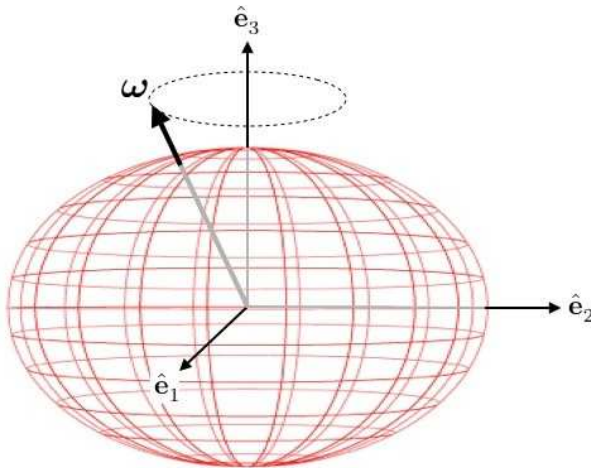


Figure 13.5: Wobbling of a torque-free symmetric top.

Precession of torque-free symmetric tops: Consider a body which has a symmetry axis $\hat{\mathbf{e}}_3$. This guarantees $I_1 = I_2$, but in general we still have $I_1 \neq I_3$. In the absence of external torques, the last of Euler's equations says $\dot{\omega}_3 = 0$, so ω_3 is a constant. The remaining two equations are then

$$\dot{\omega}_1 = \left(\frac{I_1 - I_3}{I_1} \right) \omega_3 \omega_2 \quad , \quad \dot{\omega}_2 = \left(\frac{I_3 - I_1}{I_1} \right) \omega_3 \omega_1 . \quad (13.42)$$

I.e. $\dot{\omega}_1 = -\Omega \omega_2$ and $\dot{\omega}_2 = +\Omega \omega_1$, with

$$\Omega = \left(\frac{I_3 - I_1}{I_1} \right) \omega_3 , \quad (13.43)$$

which are the equations of a harmonic oscillator. The solution is easily obtained:

$$\omega_1(t) = \omega_{\perp} \cos(\Omega t + \delta) \quad , \quad \omega_2(t) = \omega_{\perp} \sin(\Omega t + \delta) \quad , \quad \omega_3(t) = \omega_3 , \quad (13.44)$$

where ω_{\perp} and δ are constants of integration, and where $|\boldsymbol{\omega}| = (\omega_{\perp}^2 + \omega_3^2)^{1/2}$. This motion is sketched in Fig. 13.5. Note that the perpendicular components of $\boldsymbol{\omega}$ oscillate harmonically, and that the angle ω makes with respect to $\hat{\mathbf{e}}_3$ is $\lambda = \tan^{-1}(\omega_{\perp}/\omega_3)$.

For the earth, $(I_3 - I_1)/I_1 \approx \frac{1}{305}$, so $\omega_3 \approx \omega$, and $\Omega \approx \omega/305$, yielding a precession period of 305 days, or roughly 10 months. Astronomical observations reveal such a precession, known as the *Chandler wobble*. For the earth, the precession angle is $\lambda_{\text{Chandler}} \simeq 6 \times 10^{-7}$ rad, which means that the North Pole moves by about 4 meters during the wobble. The Chandler wobble has a period of about 14 months, so the naïve prediction of 305 days is off by a substantial amount. This discrepancy is attributed to the mechanical properties of the earth: elasticity and fluidity. The earth is not solid!¹

Asymmetric tops: Next, consider the torque-free motion of an asymmetric top, where $I_1 \neq I_2 \neq I_3 \neq I_1$. Unlike the symmetric case, there is no conserved component of $\boldsymbol{\omega}$. True, we can invoke conservation

¹The earth is a layered like a *Mozartkugel*, with a solid outer shell, an inner fluid shell, and a solid (iron) core.

of energy and angular momentum,

$$\begin{aligned} E &= \frac{1}{2}I_1\omega_1^2 + \frac{1}{2}I_2\omega_2^2 + \frac{1}{2}I_3\omega_3^2 \\ \mathbf{L}^2 &= I_1^2\omega_1^2 + I_2^2\omega_2^2 + I_3^2\omega_3^2, \end{aligned} \quad (13.45)$$

and, in principle, solve for ω_1 and ω_2 in terms of ω_3 , and then invoke Euler's equations (which must honor these conservation laws). However, the nonlinearity greatly complicates matters and in general this approach is a dead end.

We can, however, find a *particular* solution quite easily – one in which the rotation is about a single axis. Thus, $\omega_1 = \omega_2 = 0$ and $\omega_3 = \omega_0$ is indeed a solution for all time, according to Euler's equations. Let us now perturb about this solution, to explore its stability. We write

$$\boldsymbol{\omega} = \omega_0 \hat{\mathbf{e}}_3 + \delta\boldsymbol{\omega}, \quad (13.46)$$

and we invoke Euler's equations, linearizing by dropping terms quadratic in $\delta\boldsymbol{\omega}$. This yield

$$\begin{aligned} I_1\delta\dot{\omega}_1 &= (I_2 - I_3)\omega_0\delta\omega_2 + \mathcal{O}(\delta\omega_2\delta\omega_3) \\ I_2\delta\dot{\omega}_2 &= (I_3 - I_1)\omega_0\delta\omega_1 + \mathcal{O}(\delta\omega_3\delta\omega_1) \\ I_3\delta\dot{\omega}_3 &= 0 + \mathcal{O}(\delta\omega_1\delta\omega_2). \end{aligned} \quad (13.47)$$

Taking the time derivative of the first equation and invoking the second, and *vice versa*, yields

$$\delta\ddot{\omega}_1 = -\Omega^2\delta\omega_1, \quad \delta\ddot{\omega}_2 = -\Omega^2\delta\omega_2, \quad (13.48)$$

with

$$\Omega^2 = \frac{(I_3 - I_2)(I_3 - I_1)}{I_1 I_2} \cdot \omega_0^2. \quad (13.49)$$

The solution is then $\delta\omega_1(t) = C \cos(\Omega t + \delta)$.

If $\Omega^2 > 0$, then Ω is real, and the deviation results in a harmonic precession. This occurs if I_3 is either the largest or the smallest of the moments of inertia. If, however, I_3 is the middle moment, then $\Omega^2 < 0$, and Ω is purely imaginary. The perturbation will in general increase exponentially with time, which means that the initial solution to Euler's equations is *unstable* with respect to small perturbations. This result can be vividly realized using a tennis racket, and sometimes goes by the name of the “tennis racket theorem.”

13.5.1 Example

PROBLEM: A unsuspecting solid spherical planet of mass M_0 rotates with angular velocity ω_0 . Suddenly, a giant asteroid of mass αM_0 smashes into and sticks to the planet at a location which is at polar angle θ relative to the initial rotational axis. The new mass distribution is no longer spherically symmetric, and the rotational axis will precess. Recall Euler's equation

$$\frac{d\mathbf{L}}{dt} + \boldsymbol{\omega} \times \mathbf{L} = \mathbf{N}^{\text{ext}} \quad (13.50)$$

for rotations in a body-fixed frame.

(a) What is the new inertia tensor $I_{\alpha\beta}$ along principal center-of-mass frame axes? Don't forget that the CM is no longer at the center of the sphere! Recall $I = \frac{2}{5}MR^2$ for a solid sphere.

(b) What is the period of precession of the rotational axis in terms of the original length of the day $2\pi/\omega_0$?

SOLUTION: Let's choose body-fixed axes with \hat{z} pointing from the center of the planet to the smoldering asteroid. The CM lies a distance

$$d = \frac{\alpha M_0 \cdot R + M_0 \cdot 0}{(1 + \alpha)M_0} = \frac{\alpha}{1 + \alpha} R \quad (13.51)$$

from the center of the sphere. Thus, relative to the center of the sphere, we have

$$I = \frac{2}{5}M_0R^2 \begin{pmatrix} 1 & 0 & 0 \\ 0 & 1 & 0 \\ 0 & 0 & 1 \end{pmatrix} + \alpha M_0R^2 \begin{pmatrix} 1 & 0 & 0 \\ 0 & 1 & 0 \\ 0 & 0 & 0 \end{pmatrix}. \quad (13.52)$$

Now we shift to a frame with the CM at the origin, using the parallel axis theorem,

$$I_{\alpha\beta}(\mathbf{d}) = I_{\alpha\beta}^{\text{CM}} + M(\mathbf{d}^2 \delta_{\alpha\beta} - d_\alpha d_\beta). \quad (13.53)$$

Thus, with $\mathbf{d} = d\hat{z}$,

$$\begin{aligned} I_{\alpha\beta}^{\text{CM}} &= \frac{2}{5}M_0R^2 \begin{pmatrix} 1 & 0 & 0 \\ 0 & 1 & 0 \\ 0 & 0 & 1 \end{pmatrix} + \alpha M_0R^2 \begin{pmatrix} 1 & 0 & 0 \\ 0 & 1 & 0 \\ 0 & 0 & 0 \end{pmatrix} - (1 + \alpha)M_0d^2 \begin{pmatrix} 1 & 0 & 0 \\ 0 & 1 & 0 \\ 0 & 0 & 0 \end{pmatrix} \\ &= M_0R^2 \begin{pmatrix} \frac{2}{5} + \frac{\alpha}{1+\alpha} & 0 & 0 \\ 0 & \frac{2}{5} + \frac{\alpha}{1+\alpha} & 0 \\ 0 & 0 & \frac{2}{5} \end{pmatrix}. \end{aligned} \quad (13.54)$$

In the absence of external torques, Euler's equations along principal axes read

$$\begin{aligned} I_1 \frac{d\omega_1}{dt} &= (I_2 - I_3)\omega_2\omega_3 \\ I_2 \frac{d\omega_2}{dt} &= (I_3 - I_1)\omega_3\omega_1 \\ I_3 \frac{d\omega_3}{dt} &= (I_1 - I_2)\omega_1\omega_2 \end{aligned} \quad (13.55)$$

Since $I_1 = I_2$, $\omega_3(t) = \omega_3(0) = \omega_0 \cos \theta$ is a constant. We then obtain $\dot{\omega}_1 = \Omega\omega_2$, and $\dot{\omega}_2 = -\Omega\omega_1$, with

$$\Omega = \frac{I_2 - I_3}{I_1} \omega_3 = \frac{5\alpha}{7\alpha + 2} \omega_3. \quad (13.56)$$

The period of precession τ in units of the pre-cataclysmic day is

$$\frac{\tau}{T} = \frac{\omega}{\Omega} = \frac{7\alpha + 2}{5\alpha \cos \theta}. \quad (13.57)$$

13.6 Euler's Angles

In d dimensions, an orthogonal matrix $\mathcal{R} \in O(d)$ has $\frac{1}{2}d(d - 1)$ independent parameters. To see this, consider the constraint $\mathcal{R}^t \mathcal{R} = 1$. The matrix $\mathcal{R}^t \mathcal{R}$ is manifestly symmetric, so it has $\frac{1}{2}d(d+1)$ independent entries (*e.g.* on the diagonal and above the diagonal). This amounts to $\frac{1}{2}d(d + 1)$ constraints on the d^2 components of \mathcal{R} , resulting in $\frac{1}{2}d(d - 1)$ freedoms. Thus, in $d = 3$ rotations are specified by three parameters. The *Euler angles* $\{\phi, \theta, \psi\}$ provide one such convenient parameterization.

A general rotation $\mathcal{R}(\phi, \theta, \psi)$ is built up in three steps. We start with an orthonormal triad $\hat{\mathbf{e}}_\mu^0$ of body-fixed axes. The first step is a rotation by an angle ϕ about $\hat{\mathbf{e}}_3^0$:

$$\hat{\mathbf{e}}'_\mu = \mathcal{R}_{\mu\nu}(\hat{\mathbf{e}}_3^0, \phi) \hat{\mathbf{e}}_\nu^0 \quad , \quad \mathcal{R}(\hat{\mathbf{e}}_3^0, \phi) = \begin{pmatrix} \cos \phi & \sin \phi & 0 \\ -\sin \phi & \cos \phi & 0 \\ 0 & 0 & 1 \end{pmatrix} \quad (13.58)$$

This step is shown in panel (a) of Fig. 13.6. The second step is a rotation by θ about the new axis $\hat{\mathbf{e}}'_1$:

$$\hat{\mathbf{e}}''_\mu = \mathcal{R}_{\mu\nu}(\hat{\mathbf{e}}'_1, \theta) \hat{\mathbf{e}}'_\nu \quad , \quad \mathcal{R}(\hat{\mathbf{e}}'_1, \theta) = \begin{pmatrix} 1 & 0 & 0 \\ 0 & \cos \theta & \sin \theta \\ 0 & -\sin \theta & \cos \theta \end{pmatrix} \quad (13.59)$$

This step is shown in panel (b) of Fig. 13.6. The third and final step is a rotation by ψ about the new axis $\hat{\mathbf{e}}''_3$:

$$\hat{\mathbf{e}}'''_\mu = \mathcal{R}_{\mu\nu}(\hat{\mathbf{e}}''_3, \psi) \hat{\mathbf{e}}''_\nu \quad , \quad \mathcal{R}(\hat{\mathbf{e}}''_3, \psi) = \begin{pmatrix} \cos \psi & \sin \psi & 0 \\ -\sin \psi & \cos \psi & 0 \\ 0 & 0 & 1 \end{pmatrix} \quad (13.60)$$

This step is shown in panel (c) of Fig. 13.6. Putting this all together,

$$\begin{aligned} \mathcal{R}(\phi, \theta, \psi) &= \mathcal{R}(\hat{\mathbf{e}}''_3, \psi) \mathcal{R}(\hat{\mathbf{e}}'_1, \theta) \mathcal{R}(\hat{\mathbf{e}}_3^0, \phi) \\ &= \begin{pmatrix} \cos \psi & \sin \psi & 0 \\ -\sin \psi & \cos \psi & 0 \\ 0 & 0 & 1 \end{pmatrix} \begin{pmatrix} 1 & 0 & 0 \\ 0 & \cos \theta & \sin \theta \\ 0 & -\sin \theta & \cos \theta \end{pmatrix} \begin{pmatrix} \cos \phi & \sin \phi & 0 \\ -\sin \phi & \cos \phi & 0 \\ 0 & 0 & 1 \end{pmatrix} \\ &= \begin{pmatrix} \cos \psi \cos \phi - \sin \psi \cos \theta \sin \phi & \cos \psi \sin \phi + \sin \psi \cos \theta \cos \phi & \sin \psi \sin \theta \\ -\sin \psi \cos \phi - \cos \psi \cos \theta \sin \phi & -\sin \psi \sin \phi + \cos \psi \cos \theta \cos \phi & \cos \psi \sin \theta \\ \sin \theta \sin \phi & -\sin \theta \cos \phi & \cos \theta \end{pmatrix}. \end{aligned} \quad (13.61)$$

Next, we'd like to relate the components $\omega_\mu = \boldsymbol{\omega} \cdot \hat{\mathbf{e}}_\mu$ (with $\hat{\mathbf{e}}_\mu \equiv \hat{\mathbf{e}}_\mu'''$) of the rotation in the body-fixed frame to the derivatives $\dot{\phi}$, $\dot{\theta}$, and $\dot{\psi}$. To do this, we write

$$\boldsymbol{\omega} = \dot{\phi} \hat{\mathbf{e}}_\phi + \dot{\theta} \hat{\mathbf{e}}_\theta + \dot{\psi} \hat{\mathbf{e}}_\psi, \quad (13.62)$$

where

$$\begin{aligned} \hat{\mathbf{e}}_3^0 &= \hat{\mathbf{e}}_\phi = \sin \theta \sin \psi \hat{\mathbf{e}}_1 + \sin \theta \cos \psi \hat{\mathbf{e}}_2 + \cos \theta \hat{\mathbf{e}}_3 \\ \hat{\mathbf{e}}_\theta &= \cos \psi \hat{\mathbf{e}}_1 - \sin \psi \hat{\mathbf{e}}_2 \quad (\text{"line of nodes"}) \\ \hat{\mathbf{e}}_\psi &= \hat{\mathbf{e}}_3. \end{aligned} \quad (13.63)$$

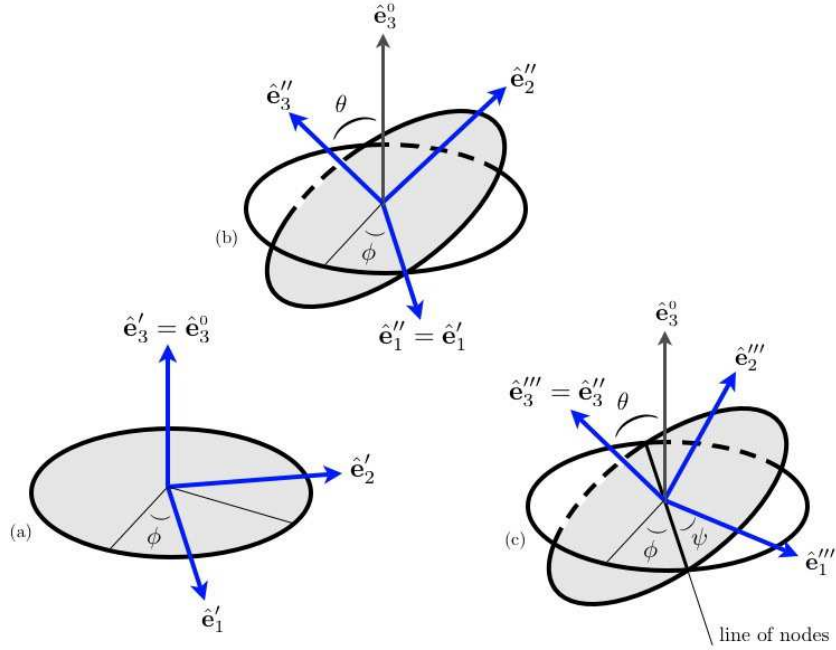


Figure 13.6: A general rotation, defined in terms of the Euler angles $\{\phi, \theta, \psi\}$. Three successive steps of the transformation are shown.

The first of these follows from the relation $\hat{\mathbf{e}}_\mu = \mathcal{R}_{\mu\nu}(\phi, \theta, \psi) \hat{\mathbf{e}}_\nu^0$, whose inverse is $\hat{\mathbf{e}}_\mu^0 = \mathcal{R}_{\mu\nu}^t(\phi, \theta, \psi) \hat{\mathbf{e}}_\nu$, since $\mathcal{R}^{-1} = \mathcal{R}^t$. Thus the coefficients of $\hat{\mathbf{e}}_{1,2,3}$ in $\hat{\mathbf{e}}_3^0$ are the elements of the rightmost ($\nu = 3$) column of $\mathcal{R}(\phi, \theta, \psi)$. We may now read off

$$\begin{aligned}\omega_1 &= \boldsymbol{\omega} \cdot \hat{\mathbf{e}}_1 = \dot{\phi} \sin \theta \sin \psi + \dot{\theta} \cos \psi \\ \omega_2 &= \boldsymbol{\omega} \cdot \hat{\mathbf{e}}_2 = \dot{\phi} \sin \theta \cos \psi - \dot{\theta} \sin \psi \\ \omega_3 &= \boldsymbol{\omega} \cdot \hat{\mathbf{e}}_3 = \dot{\phi} \cos \theta + \dot{\psi}.\end{aligned}\tag{13.64}$$

Note that

$$\dot{\phi} \leftrightarrow \text{precession}, \quad \dot{\theta} \leftrightarrow \text{nutation}, \quad \dot{\psi} \leftrightarrow \text{axial rotation}.\tag{13.65}$$

The general form of the kinetic energy is then

$$\begin{aligned}T &= \frac{1}{2} I_1 (\dot{\phi} \sin \theta \sin \psi + \dot{\theta} \cos \psi)^2 \\ &\quad + \frac{1}{2} I_2 (\dot{\phi} \sin \theta \cos \psi - \dot{\theta} \sin \psi)^2 + \frac{1}{2} I_3 (\dot{\phi} \cos \theta + \dot{\psi})^2.\end{aligned}$$

Note that

$$\boldsymbol{L} = p_\phi \hat{\mathbf{e}}_\phi + p_\theta \hat{\mathbf{e}}_\theta + p_\psi \hat{\mathbf{e}}_\psi,\tag{13.66}$$

which may be verified by explicit computation.

13.6.1 Torque-free symmetric top

A body falling in a gravitational field experiences no net torque about its CM:

$$\mathbf{N}^{\text{ext}} = \sum_i \mathbf{r}_i \times (-m_i \mathbf{g}) = \mathbf{g} \times \sum_i m_i \mathbf{r}_i = 0 . \quad (13.67)$$

For a symmetric top with $I_1 = I_2$, we have

$$T = \frac{1}{2}I_1(\dot{\theta}^2 + \dot{\phi}^2 \sin^2\theta) + \frac{1}{2}I_3(\dot{\phi} \cos\theta + \dot{\psi})^2 . \quad (13.68)$$

The potential is cyclic in the Euler angles, hence the equations of motion are

$$\frac{d}{dt} \frac{\partial T}{\partial(\dot{\phi}, \dot{\theta}, \dot{\psi})} = \frac{\partial T}{\partial(\phi, \theta, \psi)} . \quad (13.69)$$

Since ϕ and ψ are cyclic in T , their conjugate momenta are conserved:

$$\begin{aligned} p_\phi &= \frac{\partial L}{\partial \dot{\phi}} = I_1 \dot{\phi} \sin^2\theta + I_3 (\dot{\phi} \cos\theta + \dot{\psi}) \cos\theta \\ p_\psi &= \frac{\partial L}{\partial \dot{\psi}} = I_3 (\dot{\phi} \cos\theta + \dot{\psi}) . \end{aligned} \quad (13.70)$$

Note that $p_\psi = I_3 \omega_3$, hence ω_3 is constant, as we have already seen.

To solve for the motion, we first note that \mathbf{L} is conserved in the inertial frame. We are therefore permitted to define $\hat{\mathbf{L}} = \hat{\mathbf{e}}_3^0 = \hat{\mathbf{e}}_\phi$. Thus, $p_\phi = L$. Since $\hat{\mathbf{e}}_\phi \cdot \hat{\mathbf{e}}_\psi = \cos\theta$, we have that $p_\psi = \mathbf{L} \cdot \hat{\mathbf{e}}_\psi = L \cos\theta$. Finally, $\hat{\mathbf{e}}_\phi \cdot \hat{\mathbf{e}}_\theta = 0$, which means $p_\theta = \mathbf{L} \cdot \hat{\mathbf{e}}_\theta = 0$. From the equations of motion,

$$\dot{p}_\theta = I_1 \ddot{\theta} = (I_1 \dot{\phi} \cos\theta - p_\psi) \dot{\phi} \sin\theta , \quad (13.71)$$

hence we must have

$$\dot{\theta} = 0 \quad , \quad \dot{\phi} = \frac{p_\psi}{I_1 \cos\theta} . \quad (13.72)$$

Note that $\dot{\theta} = 0$ follows from conservation of $p_\psi = L \cos\theta$. From the equation for p_ψ , we may now conclude

$$\dot{\psi} = \frac{p_\psi}{I_3} - \frac{p_\psi}{I_1} = \left(\frac{I_3 - I_1}{I_3} \right) \omega_3 , \quad (13.73)$$

which recapitulates (13.43), with $\dot{\psi} = \Omega$.

13.6.2 Symmetric top with one point fixed

Consider the case of a symmetric top with one point fixed, as depicted in Fig. 13.7. The Lagrangian is

$$L = \frac{1}{2}I_1(\dot{\theta}^2 + \dot{\phi}^2 \sin^2\theta) + \frac{1}{2}I_3(\dot{\phi} \cos\theta + \dot{\psi})^2 - M g \ell \cos\theta . \quad (13.74)$$

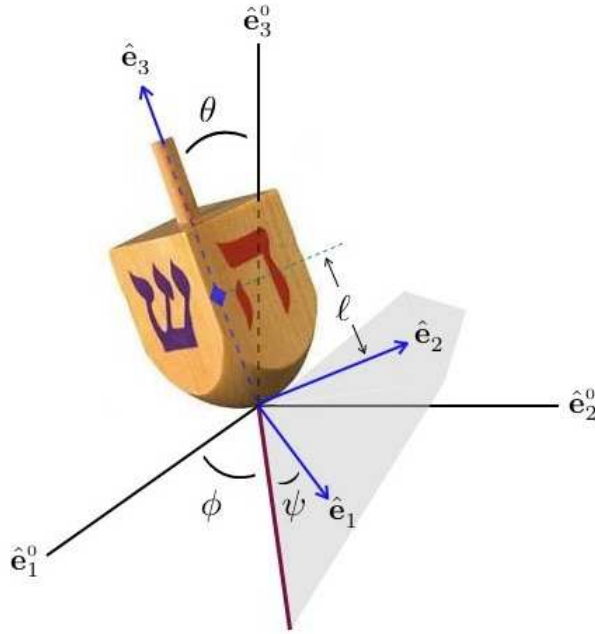


Figure 13.7: A *dreidl* is a symmetric top. The four-fold symmetry axis guarantees $I_1 = I_2$. The blue diamond represents the center-of-mass.

Here, ℓ is the distance from the fixed point to the CM, and the inertia tensor is defined along principal axes whose origin lies at the fixed point (not the CM!). Gravity now supplies a torque, but as in the torque-free case, the Lagrangian is still cyclic in ϕ and ψ , so

$$\begin{aligned} p_\phi &= (I_1 \sin^2\theta + I_3 \cos^2\theta) \dot{\phi} + I_3 \cos\theta \dot{\psi} \\ p_\psi &= I_3 \cos\theta \dot{\phi} + I_3 \dot{\psi} \end{aligned} \quad (13.75)$$

are each conserved. We can invert these relations to obtain $\dot{\phi}$ and $\dot{\psi}$ in terms of $\{p_\phi, p_\psi, \theta\}$:

$$\dot{\phi} = \frac{p_\phi - p_\psi \cos\theta}{I_1 \sin^2\theta} \quad , \quad \dot{\psi} = \frac{p_\psi}{I_3} - \frac{(p_\phi - p_\psi \cos\theta) \cos\theta}{I_1 \sin^2\theta} . \quad (13.76)$$

In addition, since $\partial L/\partial t = 0$, the total energy is conserved:

$$E = T + U = \frac{1}{2} I_1 \dot{\theta}^2 + \underbrace{\frac{(p_\phi - p_\psi \cos\theta)^2}{2I_1 \sin^2\theta} + \frac{p_\psi^2}{2I_3}}_{U_{\text{eff}}(\theta)} + M g \ell \cos\theta , \quad (13.77)$$

where the term under the brace is the effective potential $U_{\text{eff}}(\theta)$.

The problem thus reduces to the one-dimensional dynamics of $\theta(t)$, i.e.

$$I_1 \ddot{\theta} = -\frac{\partial U_{\text{eff}}}{\partial \theta} , \quad (13.78)$$

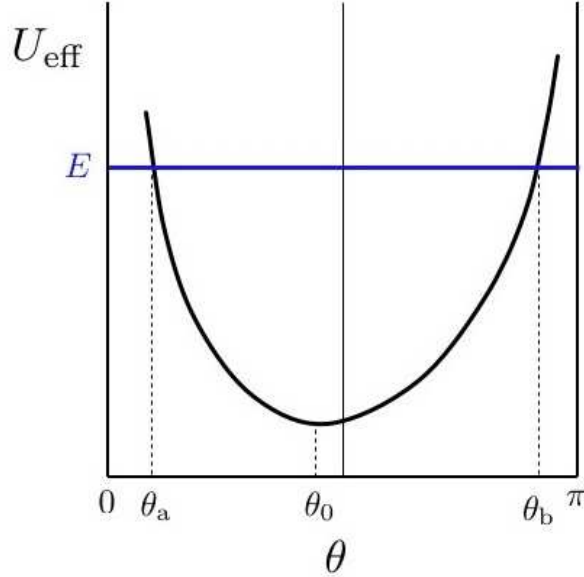


Figure 13.8: The effective potential of eq. 13.82.

with

$$U_{\text{eff}}(\theta) = \frac{(p_\phi - p_\psi \cos \theta)^2}{2I_1 \sin^2 \theta} + \frac{p_\psi^2}{2I_3} + M g \ell \cos \theta . \quad (13.79)$$

Using energy conservation, we may write

$$dt = \pm \sqrt{\frac{I_1}{2}} \frac{d\theta}{\sqrt{E - U_{\text{eff}}(\theta)}} . \quad (13.80)$$

and thus the problem is reduced to quadratures:

$$t(\theta) = t(\theta_0) \pm \sqrt{\frac{I_1}{2}} \int_{\theta_0}^{\theta} d\vartheta \frac{1}{\sqrt{E - U_{\text{eff}}(\vartheta)}} . \quad (13.81)$$

We can gain physical insight into the motion by examining the shape of the effective potential,

$$U_{\text{eff}}(\theta) = \frac{(p_\phi - p_\psi \cos \theta)^2}{2I_1 \sin^2 \theta} + M g \ell \cos \theta + \frac{p_\psi^2}{2I_3} , \quad (13.82)$$

over the interval $\theta \in [0, \pi]$. Clearly $U_{\text{eff}}(0) = U_{\text{eff}}(\pi) = \infty$, so the motion must be bounded. What is not yet clear, but what is nonetheless revealed by some additional analysis, is that $U_{\text{eff}}(\theta)$ has a single minimum on this interval, at $\theta = \theta_0$. The turning points for the θ motion are at $\theta = \theta_a$ and $\theta = \theta_b$, where $U_{\text{eff}}(\theta_a) = U_{\text{eff}}(\theta_b) = E$. Clearly if we expand about θ_0 and write $\theta = \theta_0 + \eta$, the η motion will be harmonic, with

$$\eta(t) = \eta_0 \cos(\Omega t + \delta) , \quad \Omega = \sqrt{\frac{U''_{\text{eff}}(\theta_0)}{I_1}} . \quad (13.83)$$

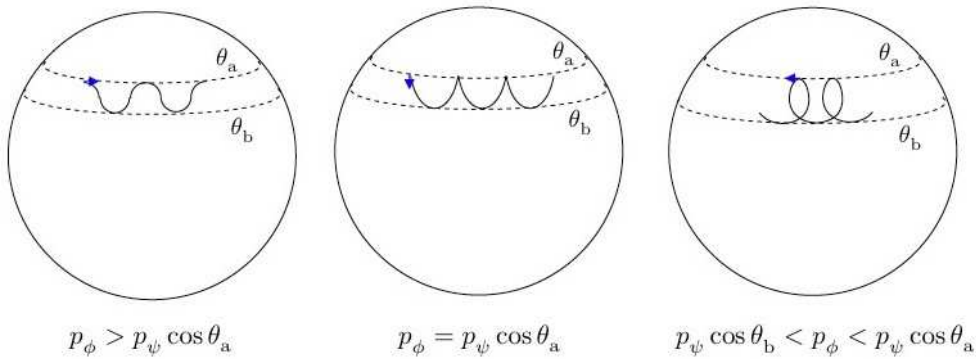


Figure 13.9: Precession and nutation of the symmetry axis of a symmetric top.

To prove that $U_{\text{eff}}(\theta)$ has these features, let us define $u \equiv \cos \theta$. Then $\dot{u} = -\dot{\theta} \sin \theta$, and from $E = \frac{1}{2}I_1 \dot{\theta}^2 + U_{\text{eff}}(\theta)$ we derive

$$\dot{u}^2 = \left(\frac{2E}{I_1} - \frac{p_\psi^2}{I_1 I_3} \right) (1 - u^2) - \frac{2Mg\ell}{I_1} (1 - u^2) u - \left(\frac{p_\phi - p_\psi u}{I_1} \right)^2 \equiv f(u) . \quad (13.84)$$

The turning points occur at $f(u) = 0$. The function $f(u)$ is cubic, and the coefficient of the cubic term is $2Mg\ell/I_1$, which is positive. Clearly $f(u = \pm 1) = -(p_\phi \mp p_\psi)^2/I_1^2$ is negative, so there must be at least one solution to $f(u) = 0$ on the interval $u \in (1, \infty)$. Clearly there can be at most three real roots for $f(u)$, since the function is cubic in u , hence there are at most two turning points on the interval $u \in [-1, 1]$. Thus, $U_{\text{eff}}(\theta)$ has the form depicted in fig. 13.8.

To apprehend the full motion of the top in an inertial frame, let us follow the symmetry axis $\hat{\mathbf{e}}_3$:

$$\hat{\mathbf{e}}_3 = \sin \theta \sin \phi \hat{\mathbf{e}}_1^0 - \sin \theta \cos \phi \hat{\mathbf{e}}_2^0 + \cos \theta \hat{\mathbf{e}}_3^0 . \quad (13.85)$$

Once we know $\theta(t)$ and $\phi(t)$ we're done. The motion $\theta(t)$ is described above: θ oscillates between turning points at θ_a and θ_b . As for $\phi(t)$, we have already derived the result

$$\dot{\phi} = \frac{p_\phi - p_\psi \cos \theta}{I_1 \sin^2 \theta} . \quad (13.86)$$

Thus, if $p_\phi > p_\psi \cos \theta_a$, then $\dot{\phi}$ will remain positive throughout the motion. If, on the other hand, we have

$$p_\psi \cos \theta_b < p_\phi < p_\psi \cos \theta_a , \quad (13.87)$$

then $\dot{\phi}$ changes sign at an angle $\theta^* = \cos^{-1}(p_\phi/p_\psi)$. The motion is depicted in Fig. 13.9. An extensive discussion of this problem is given in H. Goldstein, *Classical Mechanics*.

13.7 Rolling and Skidding Motion of Real Tops

The material in this section is based on the corresponding sections from V. Barger and M. Olsson, *Classical Mechanics: A Modern Perspective*. This is an excellent book which contains many interesting applications and examples.

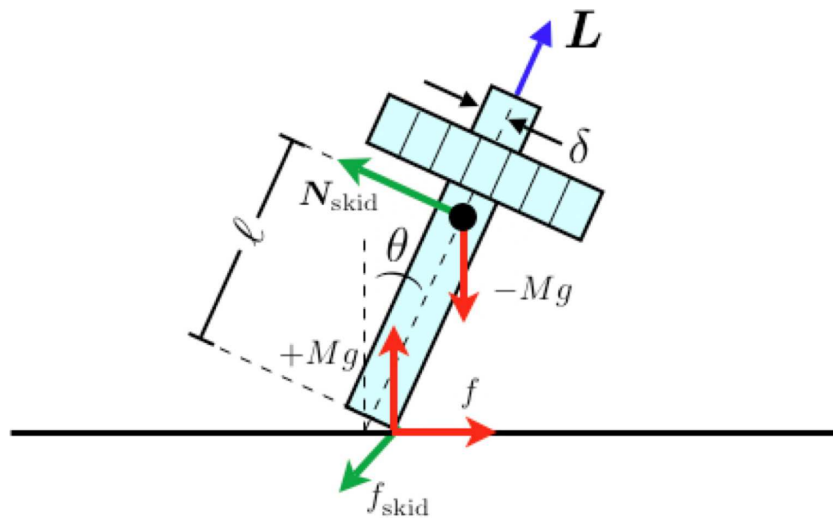


Figure 13.10: A top with a peg end. The frictional forces f and f_{skid} are shown. When the top rolls without skidding, $f_{\text{skid}} = 0$.

13.7.1 Rolling tops

In most tops, the point of contact rolls or skids along the surface. Consider the peg end top of Fig. 13.10, executing a circular rolling motion, as sketched in Fig. 13.11. There are three components to the force acting on the top: gravity, the normal force from the surface, and friction. The frictional force is perpendicular to the CM velocity, and results in centripetal acceleration of the top:

$$f = M\Omega^2\rho \leq \mu Mg , \quad (13.88)$$

where Ω is the frequency of the CM motion and μ is the coefficient of friction. If the above inequality is violated, the top starts to slip.

The frictional and normal forces combine to produce a torque $N = Mg\ell \sin \theta - f\ell \cos \theta$ about the CM². This torque is tangent to the circular path of the CM, and causes \mathbf{L} to precess. We assume that the top is spinning rapidly, so that \mathbf{L} very nearly points along the symmetry axis of the top itself. (As we'll see, this is true for slow precession but not for fast precession, where the precession frequency is proportional to ω_3 .) The precession is then governed by the equation

$$\begin{aligned} N &= Mg\ell \sin \theta - f\ell \cos \theta \\ &= |\dot{\mathbf{L}}| = |\boldsymbol{\Omega} \times \mathbf{L}| \approx \Omega I_3 \omega_3 \sin \theta , \end{aligned} \quad (13.89)$$

where $\hat{\mathbf{e}}_3$ is the instantaneous symmetry axis of the top. Substituting $f = M\Omega^2\rho$,

$$\frac{Mg\ell}{I_3 \omega_3} \left(1 - \frac{\Omega^2 \rho}{g} \operatorname{ctn} \theta \right) = \Omega , \quad (13.90)$$

which is a quadratic equation for Ω . We supplement this with the ‘no slip’ condition,

$$\omega_3 \delta = \Omega (\rho + \ell \sin \theta) , \quad (13.91)$$

²Gravity of course produces no net torque about the CM.

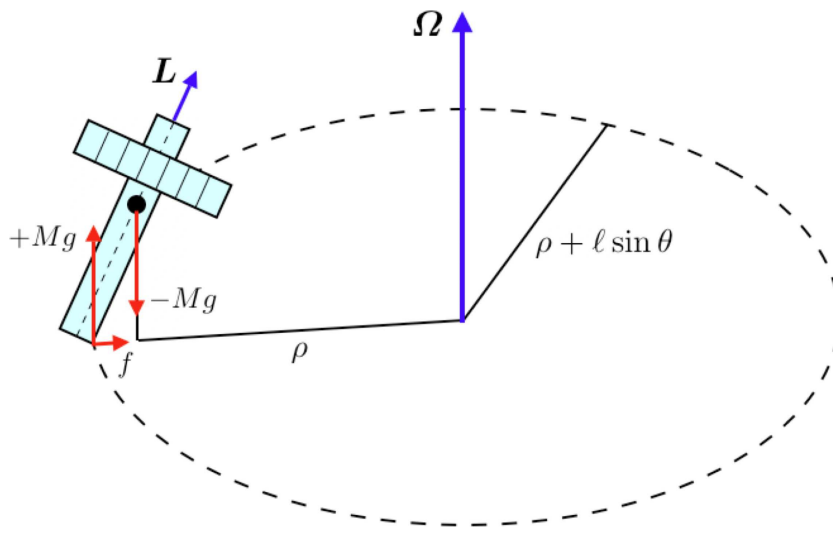


Figure 13.11: Circular rolling motion of the peg top.

resulting in two equations for the two unknowns Ω and ρ .

Substituting for $\rho(\Omega)$ and solving for Ω , we obtain

$$\Omega = \frac{I_3 \omega_3}{2M\ell^2 \cos \theta} \left\{ 1 + \frac{Mg\ell\delta}{I_3} \operatorname{ctn} \theta \pm \sqrt{\left(1 + \frac{Mg\ell\delta}{I_3} \operatorname{ctn} \theta \right)^2 - \frac{4M\ell^2}{I_3} \cdot \frac{Mg\ell}{I_3 \omega_3^2}} \right\}. \quad (13.92)$$

This in order to have a real solution we must have

$$\omega_3 \geq \frac{2M\ell^2 \sin \theta}{I_3 \sin \theta + Mg\ell\delta \cos \theta} \sqrt{\frac{g}{\ell}}. \quad (13.93)$$

If the inequality is satisfied, there are two possible solutions for Ω , corresponding to fast and slow precession. Usually one observes slow precession. Note that it is possible that $\rho < 0$, in which case the CM and the peg end lie on opposite sides of a circle from each other.

13.7.2 Skidding tops

A skidding top experiences a frictional force which opposes the skidding velocity, until $v_{\text{skid}} = 0$ and a pure rolling motion sets in. This force provides a torque which makes the top *rise*:

$$\dot{\theta} = -\frac{N_{\text{skid}}}{L} = -\frac{\mu M g \ell}{I_3 \omega_3}. \quad (13.94)$$

Suppose $\delta \approx 0$, in which case $\rho + \ell \sin \theta = 0$, from eqn. 13.91, and the point of contact remains fixed. Now recall the effective potential for a symmetric top with one point fixed:

$$U_{\text{eff}}(\theta) = \frac{(p_\phi - p_\psi \cos \theta)^2}{2I_1 \sin^2 \theta} + \frac{p_\psi^2}{2I_3} + M g \ell \cos \theta. \quad (13.95)$$

We demand $U'_{\text{eff}}(\theta_0) = 0$, which yields

$$\cos \theta_0 \cdot \beta^2 - p_\psi \sin^2 \theta_0 \cdot \beta + M g \ell I_1 \sin^4 \theta_0 = 0 , \quad (13.96)$$

where

$$\beta \equiv p_\phi - p_\psi \cos \theta_0 = I_1 \sin^2 \theta_0 \dot{\phi} . \quad (13.97)$$

Solving the quadratic equation for β , we find

$$\dot{\phi} = \frac{I_3 \omega_3}{2I_1 \cos \theta_0} \left(1 \pm \sqrt{1 - \frac{4Mg\ell I_1 \cos \theta_0}{I_3^2 \omega_3^2}} \right) . \quad (13.98)$$

This is simply a recapitulation of eqn. 13.92, with $\delta = 0$ and with $M\ell^2$ replaced by I_1 . Note $I_1 = M\ell^2$ by the parallel axis theorem if $I_1^{\text{CM}} = 0$. But to the extent that $I_1^{\text{CM}} \neq 0$, our treatment of the peg top was incorrect. It turns out to be OK, however, if the precession is slow, *i.e.* if $\Omega/\omega_3 \ll 1$.

On a level surface, $\cos \theta_0 > 0$, and therefore we must have

$$\omega_3 \geq \frac{2}{I_3} \sqrt{Mg\ell I_1 \cos \theta_0} . \quad (13.99)$$

Thus, if the top spins too slowly, it cannot maintain precession. Eqn. 13.98 says that there are two possible precession frequencies. When ω_3 is large, we have

$$\dot{\phi}_{\text{slow}} = \frac{Mg\ell}{I_3 \omega_3} + \mathcal{O}(\omega_3^{-1}) \quad , \quad \dot{\phi}_{\text{fast}} = \frac{I_3 \omega_3}{I_1 \cos \theta_0} + \mathcal{O}(\omega_3^{-3}) . \quad (13.100)$$

Again, one usually observes slow precession.

A top with $\omega_3 > \frac{2}{I_3} \sqrt{Mg\ell I_1}$ may ‘sleep’ in the vertical position with $\theta_0 = 0$. Due to the constant action of frictional forces, ω_3 will eventually drop below this value, at which time the vertical position is no longer stable. The top continues to slow down and eventually falls.

13.7.3 Tippie-top

A particularly nice example from the Barger and Olsson book is that of the tippie-top, a truncated sphere with a peg end, sketched in Fig. 13.12. The CM is close to the center of curvature, which means that there is almost no gravitational torque acting on the top. The frictional force \mathbf{f} opposes slipping, but as the top spins \mathbf{f} rotates with it, and hence the time-averaged frictional force $\langle \mathbf{f} \rangle \approx 0$ has almost no effect on the motion of the CM. A similar argument shows that the frictional torque, which is nearly horizontal, also time averages to zero:

$$\left\langle \frac{d\mathbf{L}}{dt} \right\rangle_{\text{inertial}} \approx 0 . \quad (13.101)$$

In the *body*-fixed frame, however, \mathbf{N} is roughly constant, with magnitude $N \approx \mu MgR$, where R is the radius of curvature and μ the coefficient of sliding friction. Now we invoke

$$\mathbf{N} = \frac{d\mathbf{L}}{dt} \Big|_{\text{body}} + \boldsymbol{\omega} \times \mathbf{L} . \quad (13.102)$$

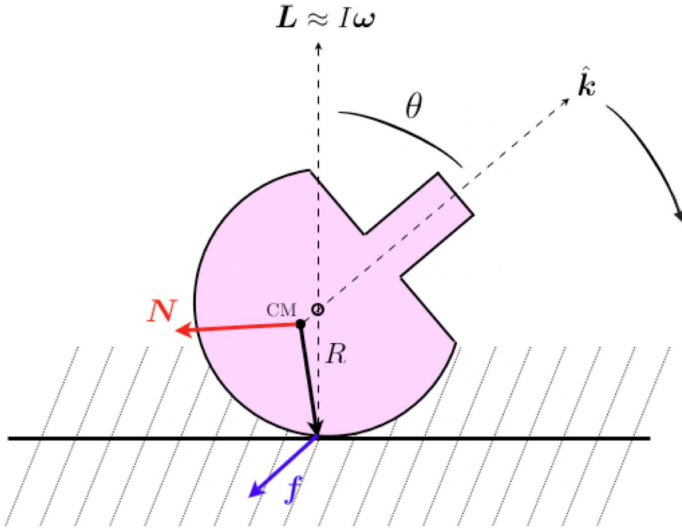


Figure 13.12: The tippie-top behaves in a counterintuitive way. Once started spinning with the peg end up, the peg axis rotates downward. Eventually the peg scrapes the surface and the top rises to the vertical in an inverted orientation.

The second term on the RHS is very small, because the tippie-top is almost spherical, hence inertia tensor is very nearly diagonal, and this means

$$\boldsymbol{\omega} \times \mathbf{L} \approx \boldsymbol{\omega} \times I\boldsymbol{\omega} = 0 . \quad (13.103)$$

Thus, $\dot{\mathbf{L}}_{\text{body}} \approx \mathbf{N}$, and taking the dot product of this equation with the unit vector $\hat{\mathbf{k}}$, we obtain

$$-N \sin \theta = \hat{\mathbf{k}} \cdot \mathbf{N} = \frac{d}{dt} (\hat{\mathbf{k}} \cdot \mathbf{L}_{\text{body}}) = -L \sin \theta \dot{\theta} . \quad (13.104)$$

Thus,

$$\dot{\theta} = \frac{N}{L} \approx \frac{\mu MgR}{I\omega} . \quad (13.105)$$

Once the stem scrapes the table, the tippie-top rises to the vertical just like any other rising top.

Chapter 14

Dynamical Systems

14.1 Introduction

14.1.1 Phase space and phase curves

Dynamics is the study of motion through phase space. The phase space of a given dynamical system is described as an N -dimensional manifold, \mathcal{M} . A (differentiable) manifold \mathcal{M} is a topological space that is locally diffeomorphic to \mathbb{R}^N .¹ Typically in this course \mathcal{M} will \mathbb{R}^N itself, but other common examples include the circle \mathbb{S}^1 , the torus \mathbb{T}^2 , the sphere \mathbb{S}^2 , etc.

Let $g_t: \mathcal{M} \rightarrow \mathcal{M}$ be a one-parameter family of transformations from \mathcal{M} to itself, with $g_{t=0} = 1$, the identity. We call g_t the t -advance mapping. It satisfies the composition rule

$$g_t g_s = g_{t+s} . \quad (14.1)$$

Let us choose a point $\varphi_0 \in \mathcal{M}$. Then we write $\varphi(t) = g_t \varphi_0$, which also is in \mathcal{M} . The set $\{g_t \varphi_0 \mid t \in \mathbb{R}, \varphi_0 \in \mathcal{M}\}$ is called a *phase curve*. A graph of the motion $\varphi(t)$ in the product space $\mathbb{R} \times \mathcal{M}$ is called an *integral curve*.

14.1.2 Vector fields

The *velocity* vector $\mathbf{V}(\varphi)$ is given by the derivative

$$\mathbf{V}(\varphi) = \frac{d}{dt} \Big|_{t=0} g_t \varphi . \quad (14.2)$$

The velocity $\mathbf{V}(\varphi)$ is an element of the *tangent space* to \mathcal{M} at φ , abbreviated $T\mathcal{M}_\varphi$. If \mathcal{M} is N -dimensional, then so is each $T\mathcal{M}_\varphi$ (for all φ). However, \mathcal{M} and $T\mathcal{M}_\varphi$ may differ topologically. For example, if $\mathcal{M} = \mathbb{S}^1$, the circle, the tangent space at any point is isomorphic to \mathbb{R} .

¹A *diffeomorphism* $F: \mathcal{M} \rightarrow \mathcal{N}$ is a differentiable map with a differentiable inverse. This is a special type of *homeomorphism*, which is a continuous map with a continuous inverse.

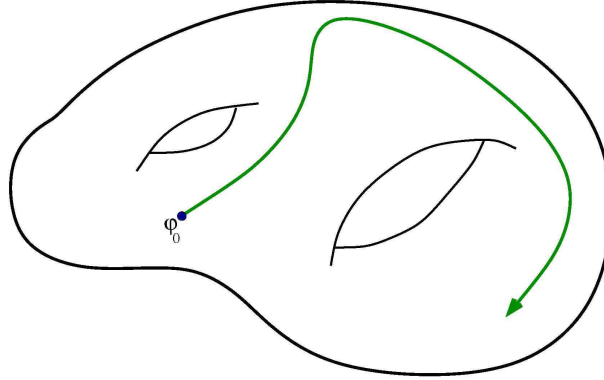


Figure 14.1: An example of a phase curve.

For our purposes, we will take $\varphi = (\varphi_1, \dots, \varphi_N)$ to be an N -tuple, *i.e.* a point in \mathbb{R}^N . The equation of motion is then

$$\frac{d}{dt} \varphi(t) = \mathbf{V}(\varphi(t)) . \quad (14.3)$$

Note that any N^{th} order ODE, of the general form

$$\frac{d^N x}{dt^N} = F\left(x, \frac{dx}{dt}, \dots, \frac{d^{N-1}x}{dt^{N-1}}\right) , \quad (14.4)$$

may be represented by the first order system $\dot{\varphi} = \mathbf{V}(\varphi)$. To see this, define $\varphi_k = d^{k-1}x/dt^{k-1}$, with $k = 1, \dots, N$. Thus, for $j < N$ we have $\dot{\varphi}_j = \varphi_{j+1}$, and $\dot{\varphi}_N = f$. In other words,

$$\overbrace{\frac{d}{dt} \begin{pmatrix} \dot{\varphi} \\ \varphi_1 \\ \vdots \\ \varphi_{N-1} \\ \varphi_N \end{pmatrix}}^{\dot{\varphi}} = \underbrace{\begin{pmatrix} \mathbf{V}(\varphi) \\ \varphi_2 \\ \vdots \\ \varphi_N \\ F(\varphi_1, \dots, \varphi_N) \end{pmatrix}}_{\mathbf{V}(\varphi)} . \quad (14.5)$$

14.1.3 Autonomous vs. non-autonomous ODEs

A dynamical system of the form $\dot{\varphi}_j = V_j(\varphi_1, \dots, \varphi_N)$ is *autonomous* provided the N functions $V_j(\varphi)$ do not depend explicitly on the independent variable t . In the non-autonomous case, we have the coupled system $\dot{\varphi}_j = V_j(\varphi_1, \dots, \varphi_N, t)$, which is equivalent to the $(N + 1)$ -dimensional dynamical system

$$\frac{d}{dt} \begin{pmatrix} \varphi_1 \\ \vdots \\ \varphi_N \\ \varphi_{N+1} \end{pmatrix} = \begin{pmatrix} V_1(\varphi_1, \dots, \varphi_{N+1}) \\ \vdots \\ V_N(\varphi_1, \dots, \varphi_{N+1}) \\ 1 \end{pmatrix} . \quad (14.6)$$

Note that one can integrate the last of these equations to get $\varphi_{N+1}(t) = t$, starting from $\varphi_{N+1}(0) = 0$. Thus, we once again have $\dot{\varphi} = \mathbf{V}(\varphi)$, now in $(N + 1)$ dimensions, and with $V_{N+1}(\varphi) = 1$.

14.1.4 Existence / uniqueness / extension theorems

Theorem : Given $\dot{\varphi} = \mathbf{V}(\varphi)$ and $\varphi(0)$, if each $\mathbf{V}(\varphi)$ is a smooth vector field over some open set $\mathcal{D} \in \mathcal{M}$, then for $\varphi(0) \in \mathcal{D}$ the initial value problem has a solution on some finite time interval $(-\tau, +\tau)$ and the solution is unique. Furthermore, the solution has a unique extension forward or backward in time, either indefinitely or until $\varphi(t)$ reaches the boundary of \mathcal{D} .

Corollary : Different trajectories never intersect!

14.1.5 Linear differential equations

A homogeneous linear N^{th} order ODE,

$$\frac{d^N x}{dt^N} + c_{N-1} \frac{d^{N-1} x}{dt^{N-1}} + \dots + c_1 \frac{dx}{dt} + c_0 x = 0 \quad (14.7)$$

may be written in matrix form, as

$$\frac{d}{dt} \begin{pmatrix} \varphi_1 \\ \varphi_2 \\ \vdots \\ \varphi_N \end{pmatrix} = \overbrace{\begin{pmatrix} 0 & 1 & 0 & \cdots & 0 \\ 0 & 0 & 1 & \cdots & 0 \\ \vdots & \vdots & \vdots & & \vdots \\ -c_0 & -c_1 & -c_2 & \cdots & -c_{N-1} \end{pmatrix}}^M \begin{pmatrix} \varphi_1 \\ \varphi_2 \\ \vdots \\ \varphi_N \end{pmatrix}. \quad (14.8)$$

Thus,

$$\dot{\varphi} = M\varphi, \quad (14.9)$$

and if the coefficients c_k are time-independent, i.e. the ODE is *autonomous*, the solution is obtained by exponentiating the constant matrix M :

$$\varphi(t) = \exp(Mt) \varphi(0); \quad (14.10)$$

the exponential of a matrix may be given meaning by its Taylor series expansion. If the ODE is not autonomous, then $M = M(t)$ is time-dependent, and the solution is given by the path-ordered exponential,

$$\varphi(t) = \mathcal{P} \exp \left\{ \int_0^t dt' M(t') \right\} \varphi(0), \quad (14.11)$$

As defined, the equation $\dot{\varphi} = \mathbf{V}(\varphi)$ is autonomous, since g_t depends only on t and on no other time variable. However, by extending the phase space from \mathcal{M} to $\mathbb{R} \times \mathcal{M}$, which is of dimension $(N+1)$, one can describe arbitrary time-dependent ODEs.

Exercise: Write the formal solution to the inhomogeneous linear system $\dot{\varphi} = M\varphi + \mathbf{b}$, where \mathbf{b} is a constant N -component vector.

14.1.6 Lyapunov functions

For a general dynamical system $\dot{\varphi} = \mathbf{V}(\varphi)$, a *Lyapunov function* $L(\varphi)$ is a function which satisfies

$$\nabla L(\varphi) \cdot \mathbf{V}(\varphi) \leq 0 . \quad (14.12)$$

There is no simple way to determine whether a Lyapunov function exists for a given dynamical system, or, if it does exist, what the Lyapunov function is. However, if a Lyapunov function can be found, then this severely limits the possible behavior of the system. This is because $L(\varphi(t))$ must be a monotonic function of time:

$$\frac{d}{dt} L(\varphi(t)) = \nabla L \cdot \frac{d\varphi}{dt} = \nabla L(\varphi) \cdot \mathbf{V}(\varphi) \leq 0 . \quad (14.13)$$

Thus, the system evolves toward a local minimum of the Lyapunov function. In general this means that oscillations are impossible in systems for which a Lyapunov function exists. For example, the relaxational dynamics of the magnetization M of a system are sometimes modeled by the equation

$$\frac{dM}{dt} = -\Gamma \frac{\partial F}{\partial M} , \quad (14.14)$$

where $F(M, T)$ is the *free energy* of the system. In this model, assuming constant temperature T , $\dot{F} = F'(M) \dot{M} = -\Gamma [F'(M)]^2 \leq 0$. So the free energy $F(M)$ itself is a Lyapunov function, and it monotonically decreases during the evolution of the system. We shall meet up with this example again in the next chapter when we discuss imperfect bifurcations.

14.2 $N = 1$ Systems

We now study phase flows in a one-dimensional phase space, governed by the equation

$$\frac{du}{dt} = f(u) . \quad (14.15)$$

Again, the equation $\dot{u} = h(u, t)$ is first order, but not autonomous, and it corresponds to the $N = 2$ system,

$$\frac{d}{dt} \begin{pmatrix} u \\ t \end{pmatrix} = \begin{pmatrix} h(u, t) \\ 1 \end{pmatrix} . \quad (14.16)$$

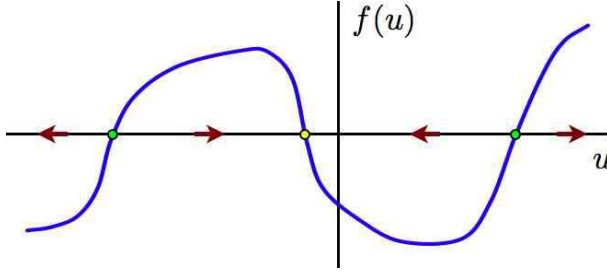
The equation 14.15 is easily integrated:

$$\frac{du}{f(u)} = dt \quad \Rightarrow \quad \boxed{t - t_0 = \int_{u_0}^u \frac{du'}{f(u')}} . \quad (14.17)$$

This gives $t(u)$; we must then invert this relationship to obtain $u(t)$.

Example : Suppose $f(u) = a - bu$, with a and b constant. Then

$$dt = \frac{du}{a - bu} = -b^{-1} d \ln(a - bu) \quad (14.18)$$

Figure 14.2: Phase flow for an $N = 1$ system.

whence

$$t = \frac{1}{b} \ln \left(\frac{a - b u(0)}{a - b u(t)} \right) \implies u(t) = \frac{a}{b} + \left(u(0) - \frac{a}{b} \right) \exp(-bt) . \quad (14.19)$$

Even if one cannot analytically obtain $u(t)$, the behavior is very simple, and easily obtained by graphical analysis. Sketch the function $f(u)$. Then note that

$$\dot{u} = f(u) \implies \begin{cases} f(u) > 0 & \dot{u} > 0 \Rightarrow \text{move to right} \\ f(u) < 0 & \dot{u} < 0 \Rightarrow \text{move to left} \\ f(u) = 0 & \dot{u} = 0 \Rightarrow \text{fixed point} \end{cases} \quad (14.20)$$

The behavior of $N = 1$ systems is particularly simple: $u(t)$ flows to the first stable fixed point encountered, where it then (after a logarithmically infinite time) stops. The motion is monotonic – the velocity \dot{u} never changes sign. Thus, *oscillations never occur for $N = 1$ phase flows.*²

14.2.1 Classification of fixed points ($N = 1$)

A *fixed point* u^* satisfies $f(u^*) = 0$. Generically, $f'(u^*) \neq 0$ at a fixed point.³ Suppose $f'(u^*) < 0$. Then to the left of the fixed point, the function $f(u < u^*)$ is positive, and the flow is to the right, *i.e.* toward u^* . To the right of the fixed point, the function $f(u > u^*)$ is negative, and the flow is to the left, *i.e.* again toward u^* . Thus, when $f'(u^*) < 0$ the fixed point is said to be *stable*, since the flow in the vicinity of u^* is to u^* . Conversely, when $f'(u^*) > 0$, the flow is always away from u^* , and the fixed point is then said to be *unstable*. Indeed, if we linearize about the fixed point, and let $\epsilon \equiv u - u^*$, then

$$\dot{\epsilon} = f'(u^*) \epsilon + \frac{1}{2} f''(u^*) \epsilon^2 + \mathcal{O}(\epsilon^3) , \quad (14.21)$$

and dropping all terms past the first on the RHS gives

$$\epsilon(t) = \exp \left[f'(u^*) t \right] \epsilon(0) . \quad (14.22)$$

²When I say ‘never’ I mean ‘sometimes’ – see the section 14.3.

³The system $f(u^*) = 0$ and $f'(u^*) = 0$ is overdetermined, with two equations for the single variable u^* .

The deviation decreases exponentially for $f'(u^*) < 0$ and increases exponentially for $f(u^*) > 0$. Note that

$$t(\epsilon) = \frac{1}{f'(u^*)} \ln \left(\frac{\epsilon}{\epsilon(0)} \right), \quad (14.23)$$

so the approach to a stable fixed point takes a logarithmically infinite time. For the unstable case, the deviation grows exponentially, until eventually the linearization itself fails.

14.2.2 Logistic equation

This model for population growth was first proposed by Verhulst in 1838. Let N denote the population in question. The dynamics are modeled by the first order ODE,

$$\frac{dN}{dt} = rN \left(1 - \frac{N}{K}\right), \quad (14.24)$$

where N , r , and K are all positive. For $N \ll K$ the growth rate is r , but as N increases a quadratic nonlinearity kicks in and the rate vanishes for $N = K$ and is negative for $N > K$. The nonlinearity models the effects of competition between the organisms for food, shelter, or other resources. Or maybe they crap all over each other and get sick. Whatever.

There are two fixed points, one at $N^* = 0$, which is unstable ($f'(0) = r > 0$). The other, at $N^* = K$, is stable ($f'(K) = -r$). The equation is adimensionalized by defining $\nu = N/K$ and $s = rt$, whence

$$\dot{\nu} = \nu(1 - \nu). \quad (14.25)$$

Integrating,

$$\frac{d\nu}{\nu(1 - \nu)} = d\ln \left(\frac{\nu}{1 - \nu} \right) = ds \implies \boxed{\nu(s) = \frac{\nu_0}{\nu_0 + (1 - \nu_0) \exp(-s)}}. \quad (14.26)$$

As $s \rightarrow \infty$, $\nu(s) = 1 - (\nu_0^{-1} - 1) e^{-s} + \mathcal{O}(e^{-2s})$, and the relaxation to equilibrium ($\nu^* = 1$) is exponential, as usual.

Another application of this model is to a simple autocatalytic reaction, such as



i.e. X catalyses the reaction $A \rightarrow X$. Assuming a fixed concentration of A , we have

$$\dot{x} = \kappa_+ a x - \kappa_- x^2, \quad (14.28)$$

where x is the concentration of X , and κ_{\pm} are the forward and backward reaction rates.

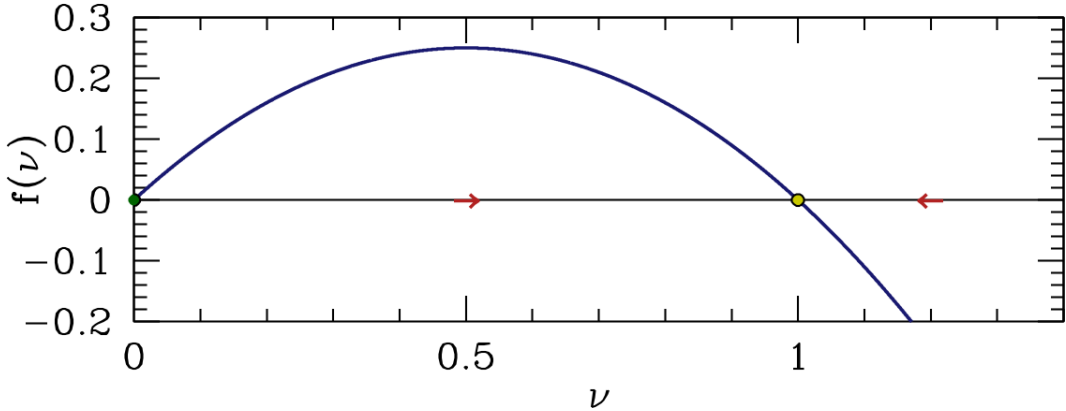


Figure 14.3: Flow diagram for the logistic equation.

14.2.3 Recommended exercises

It is instructive to sketch the phase flows for the following examples:

$$\begin{array}{ll} \dot{v} = -g & \dot{u} = A \sin(u) \\ m\dot{v} = -mg - \gamma v & \dot{u} = A(u-a)(u-b)(u-c) \\ m\dot{v} = -mg - cv^2 \operatorname{sgn}(v) & \dot{u} = au^2 - bu^3. \end{array}$$

In each case, identify all the fixed points and assess their stability. Assume all constants A, a, b, c, γ , etc. are positive.

14.2.4 Nongeneric cases with singular $f(u)$

Suppose that in the vicinity of a fixed point we have $f(u) = A|u - u^*|^\alpha$, with $A > 0$. We now analyze both sides of the fixed point.

$u < u^*$: Let $\epsilon = u^* - u$. Then

$$\dot{\epsilon} = -A\epsilon^\alpha \implies \frac{\epsilon^{1-\alpha}}{1-\alpha} = \frac{\epsilon_0^{1-\alpha}}{1-\alpha} - At, \quad (14.29)$$

hence

$$\epsilon(t) = \left[\epsilon_0^{1-\alpha} + (\alpha-1)At \right]^{\frac{1}{1-\alpha}}. \quad (14.30)$$

This, for $\alpha < 1$ the fixed point $\epsilon = 0$ is reached in a finite time: $\epsilon(t_c) = 0$, with

$$t_c = \frac{\epsilon_0^{1-\alpha}}{(1-\alpha)A}. \quad (14.31)$$

For $\alpha > 1$, we have $\lim_{t \rightarrow \infty} \epsilon(t) = 0$, but $\epsilon(t) > 0 \forall t < \infty$.

The fixed point $u = u^*$ is now *half-stable* – the flow from the left is toward u^* but from the right is away from u^* . Let's analyze the flow on either side of u^* .

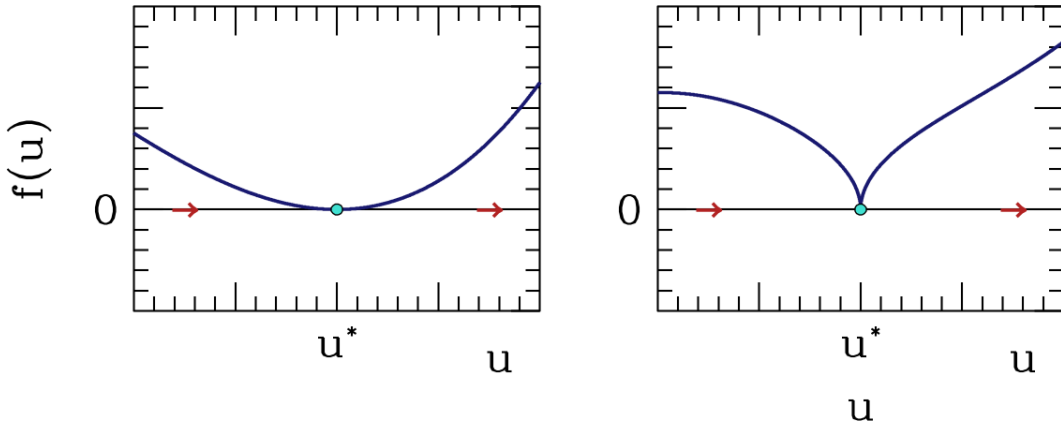


Figure 14.4: $f(u) = A |u - u^*|^\alpha$, for $\alpha > 1$ and $\alpha < 1$.

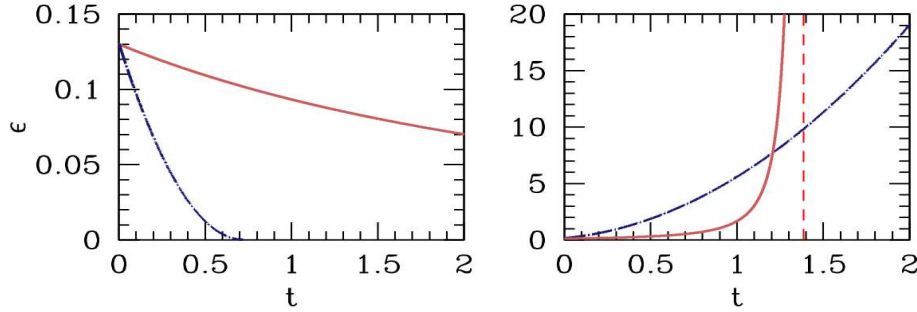


Figure 14.5: Solutions to $\dot{\epsilon} = \mp A \epsilon^\alpha$. Left panel: $\epsilon = u^* - u$, with $\alpha = 1.5$ (solid red) and $\alpha = 0.5$ (dot-dashed blue); $A = 1$ in both cases. Right panel: $\epsilon = u - u^*$, $\alpha = 1.5$ (solid red) and $\alpha = 0.5$ (dot-dashed blue); $A = 4$ in both cases

$u > u^*$: Let $\epsilon = u - u^*$. Then $\dot{\epsilon} = A \epsilon^\alpha$, and

$$\epsilon(t) = \left[\epsilon_0^{1-\alpha} + (1-\alpha)A t \right]^{\frac{1}{1-\alpha}}. \quad (14.32)$$

For $\alpha < 1$, $\epsilon(t)$ escapes to $\epsilon = \infty$ only after an infinite time. For $\alpha > 1$, the escape to infinity takes a finite time: $\epsilon(t_c) = \infty$, with

$$t_c = \frac{\epsilon_0^{1-\alpha}}{(\alpha-1)A}. \quad (14.33)$$

In both cases, higher order terms in the (nonanalytic) expansion of $f(u)$ about $u = u^*$ will eventually come into play.

14.2.5 Non-autonomous ODEs

Non-autonomous ODEs of the form $\dot{u} = h(u, t)$ are in general impossible to solve by quadratures. One can always go to the computer, but it is worth noting that in the *separable* case, $h(u, t) = f(u) g(t)$, one

can obtain the solution

$$\frac{du}{f(u)} = g(t) dt \implies \boxed{\int_{u_0}^u \frac{du'}{f(u')} = \int_0^t dt' g(t')} , \quad (14.34)$$

which implicitly gives $u(t)$. Note that \dot{u} may now change sign, and $u(t)$ may even oscillate. For an explicit example, consider the equation

$$\dot{u} = A(u + 1) \sin(\beta t) , \quad (14.35)$$

the solution of which is

$$u(t) = -1 + (u_0 + 1) \exp \left\{ \frac{A}{\beta} [1 - \cos(\beta t)] \right\} . \quad (14.36)$$

In general, the non-autonomous case defies analytic solution. Many have been studied, such as the Riccati equation,

$$\frac{du}{dt} = P(t)u^2 + Q(t)u + R(t) . \quad (14.37)$$

Riccati equations have the special and remarkable property that one can generate *all* solutions (*i.e.* with arbitrary boundary condition $u(0) = u_0$) from *any* given solution (*i.e.* with any boundary condition).

14.3 Flows on the Circle

We had remarked that oscillations are impossible for the equation $\dot{u} = f(u)$ because the flow is to the first stable fixed point encountered. If there are no stable fixed points, the flow is unbounded. However, suppose phase space itself is bounded, *e.g.* a circle \mathbb{S}^1 rather than the real line \mathbb{R} . Thus,

$$\dot{\theta} = f(\theta) , \quad (14.38)$$

with $f(\theta + 2\pi) = f(\theta)$. Now if there are no fixed points, $\theta(t)$ endlessly winds around the circle, and in this sense we can have oscillations.

14.3.1 Nonuniform oscillator

A particularly common example is that of the nonuniform oscillator,

$$\dot{\theta} = \omega - \sin \theta , \quad (14.39)$$

which has applications to electronics, biology, classical mechanics, and condensed matter physics. Note that the general equation $\dot{\theta} = \omega - A \sin \theta$ may be rescaled to the above form. A simple application is to the dynamics of a driven, overdamped pendulum. The equation of motion is

$$I\ddot{\theta} + b\dot{\theta} + I\omega_0^2 \sin \theta = N , \quad (14.40)$$

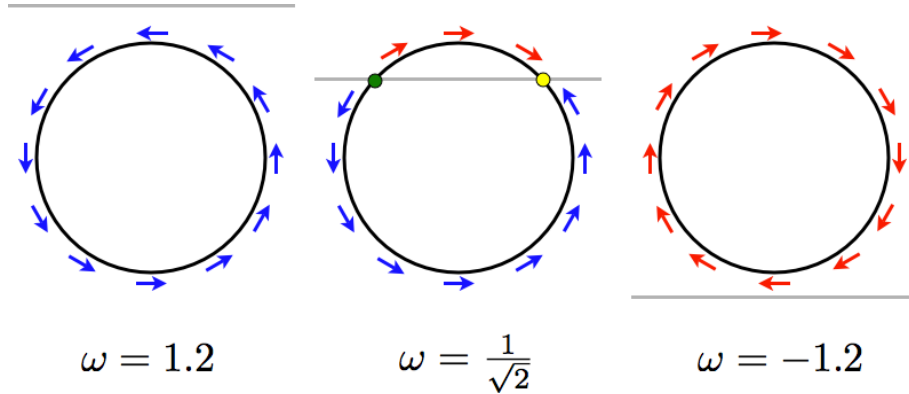


Figure 14.6: Flow for the nonuniform oscillator $\dot{\theta} = \omega - \sin \theta$ for three characteristic values of ω .

where I is the moment of inertia, b is the damping parameter, N is the external torque (presumed constant), and ω_0 is the frequency of small oscillations when $b = N = 0$. When b is large, the inertial term $I\ddot{\theta}$ may be neglected, and after rescaling we arrive at eqn. 14.39.

The book by Strogatz provides a biological example of the nonuniform oscillator: fireflies. An individual firefly will on its own flash at some frequency f . This can be modeled by the equation $\dot{\phi} = \beta$, where $\beta = 2\pi f$ is the angular frequency. A flash occurs when $\phi = 2\pi n$ for $n \in \mathbb{Z}$. When subjected to a periodic stimulus, fireflies will attempt to synchronize their flash to the flash of the stimulus. Suppose the stimulus is periodic with angular frequency Ω . The firefly synchronization is then modeled by the equation

$$\dot{\phi} = \beta - A \sin(\phi - \Omega t) . \quad (14.41)$$

Here, A is a measure of the firefly's ability to modify its natural frequency in response to the stimulus. Note that when $0 < \phi - \Omega t < \pi$, i.e. when the firefly is leading the stimulus, the dynamics tell the firefly to slow down. Conversely, when $-\pi < \phi - \Omega t < 0$, the firefly is lagging the stimulus, the dynamics tell it to speed up. Now focus on the difference $\theta \equiv \phi - \Omega t$. We have

$$\dot{\theta} = \beta - \Omega - A \sin \theta , \quad (14.42)$$

which is the nonuniform oscillator. We can adimensionalize by defining

$$s \equiv At \quad , \quad \omega \equiv \frac{\beta - \Omega}{A} , \quad (14.43)$$

yielding $\frac{d\theta}{ds} = f(\theta) = \omega - \sin \theta$.

Fixed points θ^* occur only for $|\omega| < 1$, at $\sin \theta^* = \omega$, in which case $f'(\theta^*) = -\cos \theta^*$. As we have seen above, stability requires $f'(\theta^*) < 0$, which means $\theta^* \in (-\frac{\pi}{2}, \frac{\pi}{2})$, i.e. θ^* must lie on the right half of the circle. For $|\omega| > 1$, the angular velocity never vanishes anywhere along the circle, and there are no fixed points. In this case the motion is eternally clockwise ($\omega < -1$) or counterclockwise ($\omega > +1$). The situation is depicted in Fig. 14.6.

To integrate, set $z = \exp(i\theta)$, in which case

$$\frac{dz}{ds} = -\frac{1}{2}(z^2 - 2iz\omega - 1) = -\frac{1}{2}(z - z_-)(z - z_+) , \quad (14.44)$$

where $z_{\pm} = i\omega \pm \sqrt{1 - \omega^2} \equiv \pm e^{\pm i\alpha}$, with $e^{i\alpha} = \sqrt{1 - \omega^2} + i\omega$. This yields

$$d \ln \left(\frac{z - e^{i\alpha}}{z + e^{-i\alpha}} \right) = -\cos \alpha \, ds \quad , \quad (14.45)$$

which integrates to

$$\frac{e^{i\theta(s)} - e^{i\alpha}}{e^{i\theta(s)} + e^{-i\alpha}} = \left(\frac{e^{i\theta(0)} - e^{i\alpha}}{e^{i\theta(0)} + e^{-i\alpha}} \right) \exp(-s \cos \alpha) \quad . \quad (14.46)$$

Note that $e^{i\theta(\pm\infty)} = \pm e^{\pm i\alpha}$, which lie on the appropriate halves of the circle.

For $|\omega| > 1$, the motion is periodic, with period

$$T = \int_0^{2\pi} \frac{d\theta}{|\omega| - \sin \theta} = \frac{2\pi}{\sqrt{\omega^2 - 1}} \quad . \quad (14.47)$$

14.4 Appendix I : Evolution of Phase Space Volumes

Recall the general form of a dynamical system, $\dot{\varphi} = \mathbf{V}(\varphi)$. Usually we are interested in finding integral curves $\varphi(t)$. However, consider for the moment a collection of points in phase space comprising a region \mathcal{R} . As the dynamical system evolves, this region will also evolve, so that $\mathcal{R} = \mathcal{R}(t)$. We now ask: how does the volume of $\mathcal{R}(t)$,

$$\text{vol}[\mathcal{R}(t)] = \int_{\mathcal{R}(t)} d\mu \quad , \quad (14.48)$$

where $d\mu = d\varphi_1 d\varphi_2 \cdots d\varphi_N$ is the phase space measure, change with time. We have, explicitly,

$$\begin{aligned} \text{vol}[\mathcal{R}(t+dt)] &= \int_{\mathcal{R}(t+dt)} d\mu = \int_{\mathcal{R}(t)} d\mu \left\| \frac{\partial \varphi_i(t+dt)}{\partial \varphi_j(t)} \right\| \\ &= \int_{\mathcal{R}(t)} d\mu \left\{ 1 + \nabla \cdot \mathbf{V} dt + \mathcal{O}((dt)^2) \right\} \quad , \end{aligned} \quad (14.49)$$

since

$$\frac{\partial \varphi_i(t+dt)}{\partial \varphi_j(t)} = \delta_{ij} + \frac{\partial V_i}{\partial \varphi_j} \Big|_{\varphi(t)} dt + \mathcal{O}((dt)^2) \quad , \quad (14.50)$$

and, using $\ln \det M = \text{Tr} \ln M$,

$$\det(1 + \epsilon A) = 1 + \epsilon \text{Tr} A + \mathcal{O}(\epsilon^2) \quad . \quad (14.51)$$

Thus,

$$\frac{d}{dt} \text{vol}[\mathcal{R}(t)] = \int_{\mathcal{R}(t)} d\mu \nabla \cdot \mathbf{V} = \int_{\partial\mathcal{R}(t)} d\Sigma \hat{\mathbf{n}} \cdot \mathbf{V} \quad , \quad (14.52)$$

where in the last line we have used Stokes' theorem to convert the volume integral over \mathcal{R} to a surface integral over its boundary $\partial\mathcal{R}$.

14.5 Appendix II : Lyapunov Characteristic Exponents

Suppose $\varphi(t)$ is an integral curve – *i.e.* a solution of $\dot{\varphi} = \mathbf{V}(\varphi)$. We now ask: how do nearby trajectories behave? Do they always remain close to $\varphi(t)$ for all t ? To answer this, we write $\tilde{\varphi}(t) \equiv \varphi(t) + \boldsymbol{\eta}(t)$, in which case

$$\frac{d}{dt} \eta_i(t) = M_{ij}(t) \eta_j(t) + \mathcal{O}(\eta^2), \quad (14.53)$$

where

$$M_{ij}(t) = \left. \frac{\partial V_i}{\partial \varphi_j} \right|_{\varphi(t)}. \quad (14.54)$$

The solution, valid to first order in $\delta\varphi$, is

$$\eta_i(t) = Q_{ij}(t, t_0) \eta_j(t_0), \quad (14.55)$$

where the matrix $Q(t, t_0)$ is given by the *path ordered exponential*,

$$\begin{aligned} Q(t, t_0) &= \mathcal{P} \exp \left\{ \int_{t_0}^t dt' M(t') \right\} \\ &\equiv \lim_{N \rightarrow \infty} \left(1 + \frac{\Delta t}{N} M(t_{N-1}) \right) \cdots \left(1 + \frac{\Delta t}{N} M(t_1) \right) \left(1 + \frac{\Delta t}{N} M(t_0) \right), \end{aligned} \quad (14.56)$$

with $\Delta t = t - t_0$ and $t_j = t_0 + (j/N)\Delta t$. \mathcal{P} is the *path ordering operator*, which places earlier times to the right:

$$\mathcal{P} A(t) B(t') = \begin{cases} A(t) B(t') & \text{if } t > t' \\ B(t') A(t) & \text{if } t < t'. \end{cases} \quad (14.57)$$

The distinction is important if $[A(t), B(t')] \neq 0$. Note that Q satisfies the composition property,

$$Q(t, t_0) = Q(t, t_1) Q(t_1, t_0) \quad (14.58)$$

for any $t_1 \in [t_0, t]$. When M is time-independent, as in the case of a *fixed point* where $\mathbf{V}(\varphi^*) = 0$, the path ordered exponential reduces to the ordinary exponential, and $Q(t, t_0) = \exp(M(t - t_0))$.

Generally it is impossible to analytically compute path-ordered exponentials. However, the following example may be instructive. Suppose

$$M(t) = \begin{cases} M_1 & \text{if } t/T \in [2j, 2j+1] \\ M_2 & \text{if } t/T \in [2j+1, 2j+2], \end{cases} \quad (14.59)$$

for all integer j . $M(t)$ is a ‘matrix-valued square wave’, with period $2T$. Then, integrating over one

period, from $t = 0$ to $t = 2T$, we have

$$\begin{aligned} A &\equiv \exp \left\{ \int_0^{2T} dt M(t) \right\} = e^{(M_1 + M_2) T} \\ A_{\mathcal{P}} &\equiv \mathcal{P} \exp \left\{ \int_0^{2T} dt M(t) \right\} = e^{M_2 T} e^{M_1 T}. \end{aligned} \quad (14.60)$$

In general, $A \neq A_{\mathcal{P}}$, so the path ordering has a nontrivial effect⁴.

The Lyapunov exponents are defined in the following manner. Let $\hat{\mathbf{e}}$ be an N -dimensional unit vector. Define

$$\Lambda(\varphi_0, \hat{\mathbf{e}}) \equiv \lim_{t \rightarrow \infty} \lim_{b \rightarrow 0} \frac{1}{t - t_0} \ln \left(\frac{\|\boldsymbol{\eta}(t)\|}{\|\boldsymbol{\eta}(t_0)\|} \right)_{\boldsymbol{\eta}(t_0)=b\hat{\mathbf{e}}}, \quad (14.61)$$

where $\|\cdot\|$ denotes the Euclidean norm of a vector, and where $\varphi_0 = \varphi(t_0)$. A theorem due to Oseledec guarantees that there are N such values $\Lambda_i(\varphi_0)$, depending on the choice of $\hat{\mathbf{e}}$, for a given φ_0 . Specifically, the theorem guarantees that the matrix

$$W \equiv (Q^t Q)^{1/(t-t_0)} \quad (14.62)$$

converges in the limit $t \rightarrow \infty$ for almost all φ_0 . The eigenvalues Λ_i correspond to the different eigenspaces of W . Oseledec's theorem (also called the ‘multiplicative ergodic theorem’) guarantees that the eigenspaces of W either grow ($\Lambda_i > 1$) or shrink ($\Lambda_i < 1$) exponentially fast. That is, the norm any vector lying in the i^{th} eigenspace of W will behave as $\Lambda_i^t = \exp(t \ln \Lambda_i)$ as $t \rightarrow \infty$.

Note that while $W = W^t$ is symmetric by construction, Q is simply a general real-valued $N \times N$ matrix. The left and right eigenvectors of a matrix $M \in \text{GL}(N, \mathbb{R})$ will in general be different. The set of eigenvalues λ_α is, however, common to both sets of eigenvectors. Let $\{\psi_\alpha\}$ be the right eigenvectors and $\{\chi_\alpha^*\}$ the left eigenvectors, such that

$$\begin{aligned} M_{ij} \psi_{\alpha,j} &= \lambda_\alpha \psi_{\alpha,i} \\ \chi_{\alpha,i}^* M_{ij} &= \lambda_\alpha \chi_{\alpha,j}^*. \end{aligned} \quad (14.63)$$

We can always choose the left and right eigenvectors to be orthonormal, *viz.*

$$\langle \chi_\alpha | \psi_\beta \rangle = \chi_{\alpha,i}^* \psi_{\beta,j} = \delta_{\alpha\beta}. \quad (14.64)$$

Indeed, we can define the matrix $S_{i\alpha} = \psi_{\alpha,i}$, in which case $S_{\alpha j}^{-1} = \chi_{\alpha,j}^*$, and

$$S^{-1} M S = \text{diag}(\lambda_1, \dots, \lambda_N). \quad (14.65)$$

The matrix M can always be decomposed into its eigenvectors, as

$$M_{ij} = \sum_\alpha \lambda_\alpha \psi_{\alpha,i} \chi_{\alpha,j}^*. \quad (14.66)$$

⁴If $[M_1, M_2] = 0$ then $A = A_{\mathcal{P}}$.

If we expand \mathbf{u} in terms of the right eigenvectors,

$$\boldsymbol{\eta}(t) = \sum_{\beta} C_{\beta}(t) \boldsymbol{\psi}_{\beta}(t), \quad (14.67)$$

then upon taking the inner product with $\boldsymbol{\chi}_{\alpha}$, we find that C_{α} obeys

$$\dot{C}_{\alpha} + \langle \boldsymbol{\chi}_{\alpha} | \dot{\boldsymbol{\psi}}_{\beta} \rangle C_{\beta} = \lambda_{\alpha} C_{\alpha}. \quad (14.68)$$

If $\dot{\boldsymbol{\psi}}_{\beta} = 0$, e.g. if M is time-independent, then $C_{\alpha}(t) = C_{\alpha}(0) e^{\lambda_{\alpha} t}$, and

$$\eta_i(t) = \sum_{\alpha} \overbrace{\sum_j \eta_j(0) \chi_{\alpha,j}^*}^{C_{\alpha}(0)} e^{\lambda_{\alpha} t} \psi_{\alpha,i}. \quad (14.69)$$

Thus, the component of $\boldsymbol{\eta}(t)$ along $\boldsymbol{\psi}_{\alpha}$ increases exponentially with time if $\text{Re}(\lambda_{\alpha}) > 0$, and decreases exponentially if $\text{Re}(\lambda_{\alpha}) < 0$.

Chapter 15

Bifurcations

15.1 Types of Bifurcations

15.1.1 Saddle-node bifurcation

We remarked above how $f'(u)$ is in general nonzero when $f(u)$ itself vanishes, since two equations in a single unknown is an overdetermined set. However, consider the function $F(x, \alpha)$, where α is a control parameter. If we demand $F(x, \alpha) = 0$ and $\partial_x F(x, \alpha) = 0$, we have two equations in two unknowns, and in general there will be a zero-dimensional solution set consisting of points (x_c, α_c) . The situation is depicted in Fig. 15.1.

Let's expand $F(x, \alpha)$ in the vicinity of such a point (x_c, α_c) :

$$\begin{aligned} F(x, \alpha) &= F(x_c, \alpha_c) + \frac{\partial F}{\partial x} \Big|_{(x_c, \alpha_c)} (x - x_c) + \frac{\partial F}{\partial \alpha} \Big|_{(x_c, \alpha_c)} (\alpha - \alpha_c) + \frac{1}{2} \frac{\partial^2 F}{\partial x^2} \Big|_{(x_c, \alpha_c)} (x - x_c)^2 \\ &\quad + \frac{\partial^2 F}{\partial x \partial \alpha} \Big|_{(x_c, \alpha_c)} (x - x_c)(\alpha - \alpha_c) + \frac{1}{2} \frac{\partial^2 F}{\partial \alpha^2} \Big|_{(x_c, \alpha_c)} (\alpha - \alpha_c)^2 + \dots \end{aligned} \quad (15.1)$$

$$= A(\alpha - \alpha_c) + B(x - x_c)^2 + \dots, \quad (15.2)$$

where we keep terms of lowest order in the deviations δx and $\delta \alpha$. Note that we can separately change the signs of A and B by redefining $\alpha \rightarrow -\alpha$ and/or $x \rightarrow -x$, so without loss of generality we may assume both A and B are positive. If we now rescale $u \equiv \sqrt{B/A}(x - x_c)$, $r \equiv \alpha - \alpha_c$, and $\tau = \sqrt{AB}t$, we have, neglecting the higher order terms, we obtain the ‘normal form’ of the saddle-node bifurcation,

$$\frac{du}{d\tau} = r + u^2. \quad (15.3)$$

The evolution of the flow is depicted in Fig. 15.2. For $r < 0$ there are two fixed points – one stable ($u^* = -\sqrt{-r}$) and one unstable ($u = +\sqrt{-r}$). At $r = 0$ these two nodes coalesce and annihilate each other. (The point $u^* = 0$ is half-stable precisely at $r = 0$.) For $r > 0$ there are no longer any fixed points in the vicinity of $u = 0$. In the left panel of Fig. 15.3 we show the flow in the extended (r, u) plane. The unstable and stable nodes annihilate at $r = 0$.

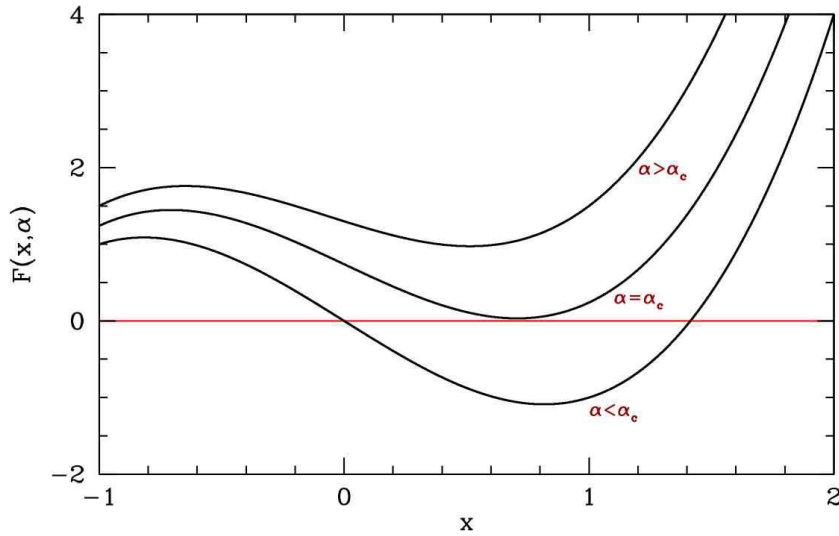


Figure 15.1: Evolution of $F(x, \alpha)$ as a function of the control parameter α .

15.1.2 Transcritical bifurcation

Another situation which arises frequently is the *transcritical bifurcation*. Consider the equation $\dot{x} = f(x)$ in the vicinity of a fixed point x^* .

$$\frac{dx}{dt} = f'(x^*) (x - x^*) + \frac{1}{2} f''(x^*)(x - x^*)^2 + \dots . \quad (15.4)$$

We rescale $u \equiv \beta (x - x^*)$ with $\beta = -\frac{1}{2} f''(x^*)$ and define $r \equiv f'(x^*)$ as the control parameter, to obtain, to order u^2 ,

$$\frac{du}{dt} = ru - u^2 . \quad (15.5)$$

Note that the sign of the u^2 term can be reversed relative to the others by sending $u \rightarrow -u$.

Consider a crude model of a laser threshold. Let n be the number of photons in the laser cavity, and N the number of excited atoms in the cavity. The dynamics of the laser are approximated by the equations

$$\begin{aligned} \dot{n} &= GNn - kn \\ N &= N_0 - \alpha n . \end{aligned} \quad (15.6)$$

Here G is the gain coefficient and k the photon decay rate. N_0 is the pump strength, and α is a numerical factor. The first equation tells us that the number of photons in the cavity grows with a rate $GN - k$; gain is proportional to the number of excited atoms, and the loss rate is a constant cavity-dependent quantity (typically through the ends, which are semi-transparent). The second equation says that the number of excited atoms is equal to the pump strength minus a term proportional to the number of photons (since the presence of a photon means an excited atom has decayed). Putting them together,

$$\dot{n} = (GN_0 - k)n - \alpha Gn^2 , \quad (15.7)$$

which exhibits a transcritical bifurcation at pump strength $N_0 = k/G$. For $N_0 < k/G$ the system acts as a lamp; for $N_0 > k/G$ the system acts as a laser.

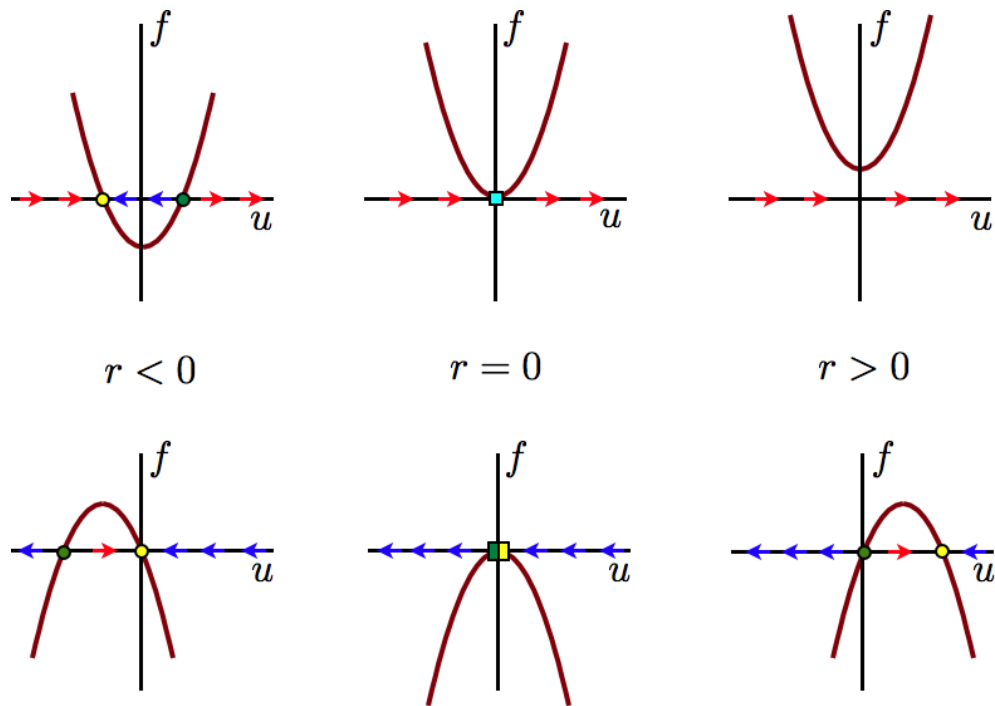


Figure 15.2: Flow diagrams for the saddle-node bifurcation $\dot{u} = r + u^2$ (top) and the transcritical bifurcation $\dot{u} = ru - u^2$ (bottom).

What happens in the transcritical bifurcation is an exchange of stability of the fixed points at $u^* = 0$ and $u^* = r$ as r passes through zero. This is depicted graphically in the bottom panel of Fig. 15.2.

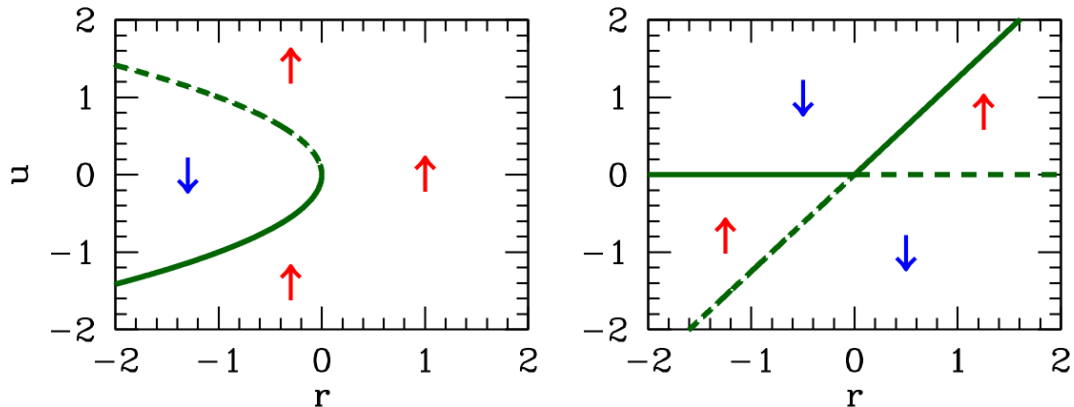


Figure 15.3: Extended phase space (r, u) flow diagrams for the saddle-node bifurcation $\dot{u} = r + u^2$ (left) and the transcritical bifurcation $\dot{u} = ru - u^2$ (right).

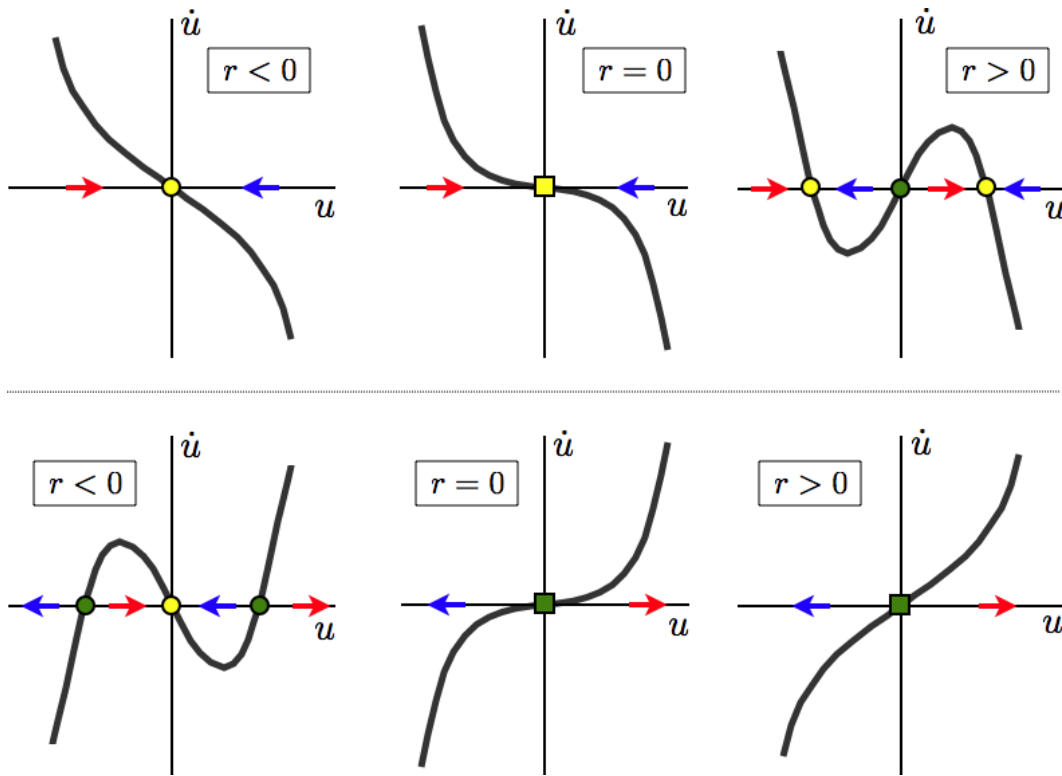


Figure 15.4: Top: supercritical pitchfork bifurcation $\dot{u} = ru - u^3$. Bottom: subcritical pitchfork bifurcation $\dot{u} = ru + u^3$.

15.1.3 Pitchfork bifurcation

The pitchfork bifurcation is commonly encountered in systems in which there is an overall parity symmetry ($u \rightarrow -u$). There are two classes of pitchfork: supercritical and subcritical. The normal form of the supercritical bifurcation is

$$\dot{u} = ru - u^3 , \quad (15.8)$$

which has fixed points at $u^* = 0$ and $u^* = \pm\sqrt{r}$. Thus, the situation is as depicted in fig. 15.4 (top panel). For $r < 0$ there is a single stable fixed point at $u^* = 0$. For $r > 0$, $u^* = 0$ is unstable, and flanked by two stable fixed points at $u^* = \pm\sqrt{r}$.

If we send $u \rightarrow -u$, $r \rightarrow -r$, and $t \rightarrow -t$, we obtain the *subcritical pitchfork*, depicted in the bottom panel of fig. 15.4. The normal form of the subcritical pitchfork bifurcation is

$$\dot{u} = ru + u^3 . \quad (15.9)$$

The fixed point structure in both supercritical and subcritical cases is shown in Fig. 15.5.

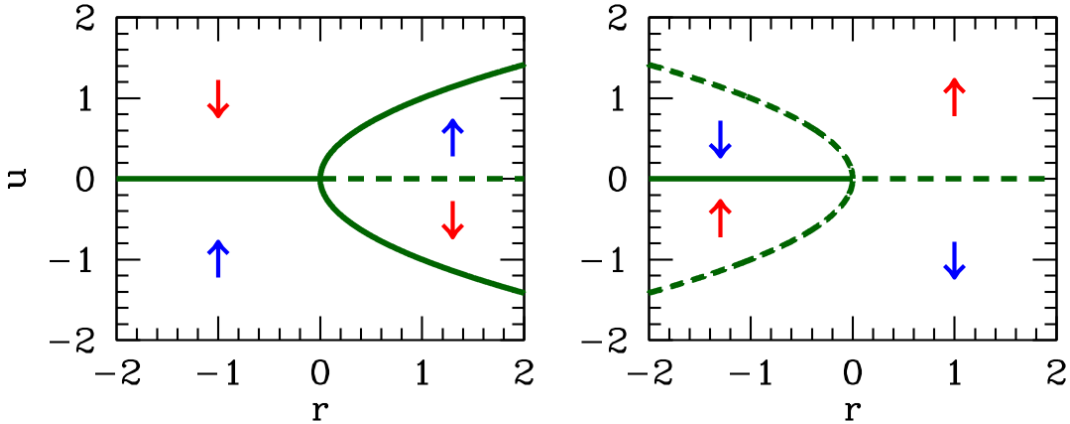


Figure 15.5: Extended phase space (r, u) flow diagrams for the supercritical pitchfork bifurcation $\dot{u} = ru - u^3$ (left), and subcritical pitchfork bifurcation $\dot{u} = ru + u^3$ (right).

15.1.4 Imperfect bifurcation

The imperfect bifurcation occurs when a symmetry-breaking term is added to the pitchfork. The normal form contains two control parameters:

$$\dot{u} = h + ru - u^3. \quad (15.10)$$

Here, the constant h breaks the parity symmetry if $u \rightarrow -u$.

This equation arises from a crude model of magnetization dynamics. Let M be the magnetization of a sample, and $F(M)$ the free energy. Assuming M is small, we can expand $F(M)$ as

$$F(M) = -HM + \frac{1}{2}aM^2 + \frac{1}{4}bM^4 + \dots, \quad (15.11)$$

where H is the external magnetic field, and a and b are temperature-dependent constants. This is called the *Landau expansion* of the free energy. We assume $b > 0$ in order that the minimum of $F(M)$ not lie at infinity. The dynamics of $M(t)$ are modeled by

$$\frac{dM}{dt} = -\Gamma \frac{\partial F}{\partial M}, \quad (15.12)$$

with $\Gamma > 0$. Thus, the magnetization evolves toward a local minimum in the free energy. Note that the free energy is a decreasing function of time:

$$\frac{dF}{dt} = \frac{\partial F}{\partial M} \frac{dM}{dt} = -\Gamma \left(\frac{\partial F}{\partial M} \right)^2. \quad (15.13)$$

By rescaling $M \equiv uM_0$ with $M_0 = (b\Gamma)^{-1/2}$ and defining $r \equiv -a\Gamma$ and $h \equiv (\Gamma^3 b)^{1/2} H$, we obtain the normal form

$$\begin{aligned} \dot{u} &= h + ru - u^3 = -\frac{\partial f}{\partial u} \\ f(u) &= -\frac{1}{2}ru^2 + \frac{1}{4}u^4 - hu. \end{aligned} \quad (15.14)$$

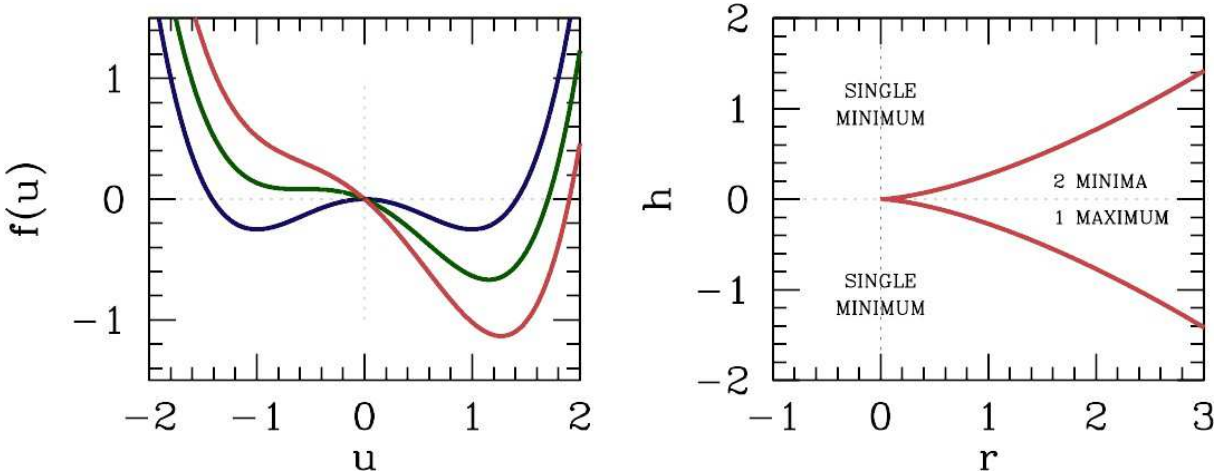


Figure 15.6: Left: scaled free energy $f(u) = -\frac{1}{2}ru^2 + \frac{1}{4}u^4 - hu$, with $h = 0$ (blue), $h = h_c$ (green), and $h = 2h_c$ (red), where $h_c = \frac{2}{3\sqrt{3}}r^{3/2}$. Right: phase diagram for the imperfect bifurcation $\dot{u} = -f'(u) = h + ru - u^3$ in the (r, h) plane.

Here, $f(u)$ is a scaled version of the free energy.

Fixed points satisfy the equation

$$u^3 - ru - h = 0 , \quad (15.15)$$

and correspond to extrema in $f(u)$. By the fundamental theorem of algebra, this cubic polynomial may be uniquely factorized over the complex plane. Since the coefficients are real, the complex conjugate \bar{u} satisfies the same equation as u , hence there are two possibilities for the roots: either (i) all three roots are real, or (ii) one root is real and the other two are a complex conjugate pair. Clearly for $r < 0$ we are in situation (ii) since $u^3 - ru$ is then monotonically increasing for $u \in \mathbb{R}$, and therefore takes the value h precisely once for u real. For $r > 0$, there is a region $h \in [-h_c(r), h_c(r)]$ over which there are three real roots. To find $h_c(r)$, we demand $f''(u) = 0$ as well as $f'(u) = 0$, which says that two roots have merged, forming an inflection point. One easily finds $h_c(r) = \frac{2}{3\sqrt{3}}r^{3/2}$.

Examples of the function $f(u)$ for $r > 0$ are shown in the left panel of Fig. 15.6 for three different values of h . For $|h| < h_c(r)$ there are three extrema satisfying $f'(u^*) = 0$: $u_1^* < u_2^* < 0 < u_3^*$, assuming (without loss of generality) that $h > 0$. Clearly u_1^* is a local minimum, u_2^* a local maximum, and u_3^* the global minimum of the function $f(u)$. The ‘phase diagram’ for this system, plotted in the (r, h) control parameter space, is shown in the right panel of Fig. 15.6.

In Fig. 15.7 we plot the fixed points $u^*(r)$ for fixed h . A saddle-node bifurcation occurs at $r = r_c(h) = \frac{3}{2^{2/3}}|h|^{2/3}$. For $h = 0$ this reduces to the supercritical pitchfork; for finite h the pitchfork is deformed and even changed topologically. Finally, in Fig. 15.7 we show the behavior of $u^*(h)$ for fixed r . When $r < 0$ the curve retraces itself as h is ramped up and down, but for $r > 0$ the system exhibits the phenomenon of *hysteresis*, i.e. there is an irreversible aspect to the behavior. Fig. 15.7 shows a *hysteresis loop* when $r > 0$.

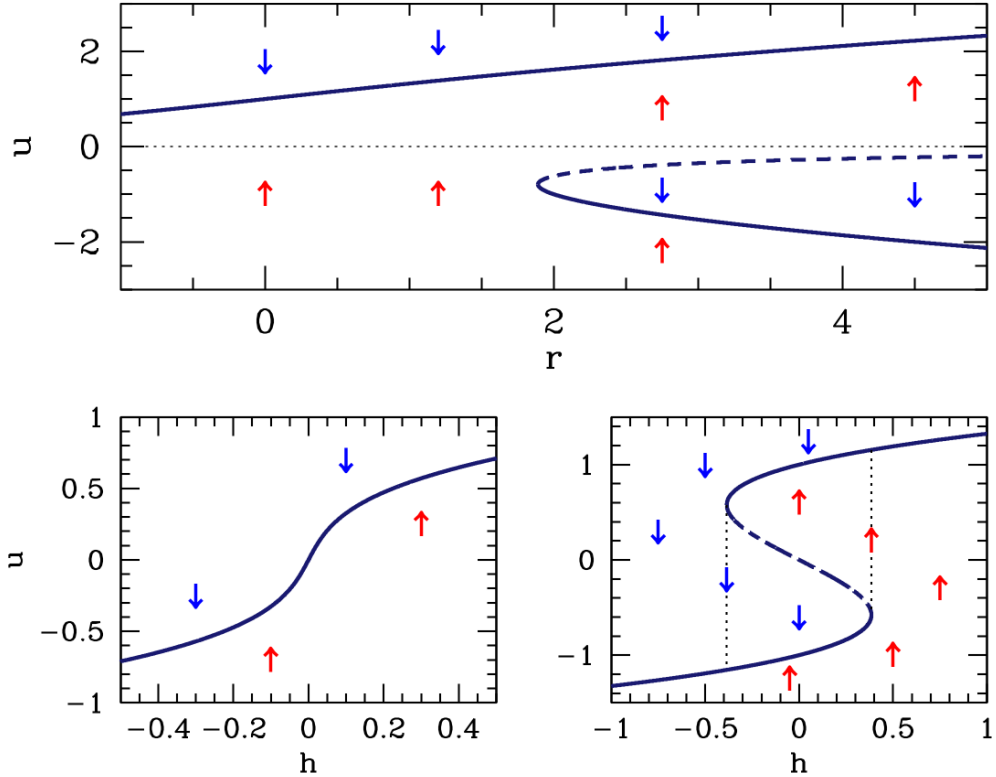


Figure 15.7: Top: extended phase space \$(r, u)\$ flow diagram for the imperfect pitchfork bifurcation \$\dot{u} = h + ru - u^3\$ for \$h = 1\$. This is in a sense a deformed supercritical pitchfork. Bottom: extended phase space \$(h, u)\$ flow diagram for the imperfect pitchfork bifurcation \$r = -0.2\$ (left panel) and \$r = 1\$ (right panel). For \$r < 0\$ the behavior is completely reversible. For \$r > 0\$, a regime of irreversibility sets in between \$-h_c\$ and \$+h_c\$, where \$h_c = 2(r/3)^{3/2}\$. The system then exhibits the phenomenon of hysteresis. The dotted vertical lines show the boundaries of the hysteresis loop.

15.2 Examples

15.2.1 Population dynamics

Consider the dynamics of a harvested population,

$$\dot{N} = rN \left(1 - \frac{N}{K}\right) - H(N) , \quad (15.16)$$

where \$r, K > 0\$, and where \$H(N)\$ is the *harvesting rate*.

(a) Suppose \$H(N) = H_0\$ is a constant. Sketch the phase flow, and identify and classify all fixed points.

Solution : We examine \$\dot{N} = f(N)\$ with

$$f(N) = rN - \frac{r}{K} N^2 - H_0 . \quad (15.17)$$

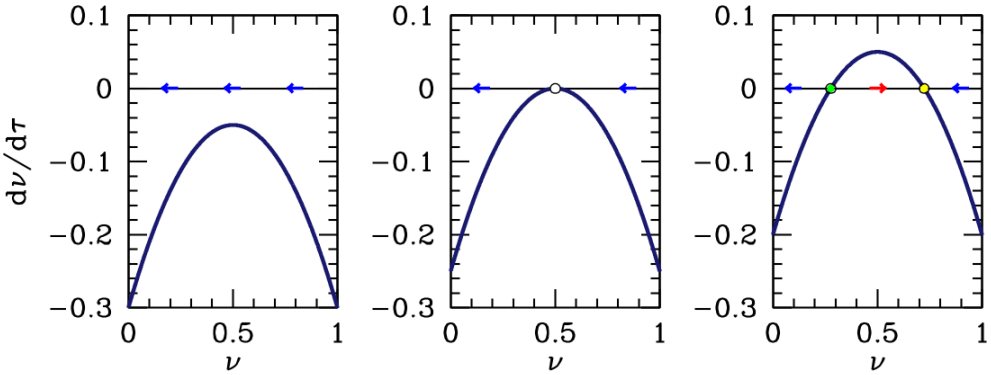


Figure 15.8: Phase flow for the constantly harvested population, $\dot{\nu} = \nu(1 - \nu) - h$, for $h = 0.30$ (left), $h = 0.25$ (center), and $h = 0.20$ (right). The critical harvesting rate is $h_c = \frac{1}{4}$.

Setting $f'(N) = 0$ yields $N = \frac{1}{2}K$. $f(N)$ is a downward-opening parabola whose maximum value is $f(\frac{1}{2}K) = \frac{1}{4}rK - H_0$. Thus, if $H_0 > \frac{1}{4}rK$, the harvesting rate is too large and the population always shrinks. A saddle-node bifurcation occurs at this value of H_0 , and for larger harvesting rates, there are fixed points at

$$N_{\pm} = \frac{1}{2}K \pm \frac{1}{2}K \sqrt{1 - \frac{4H_0}{rK}} , \quad (15.18)$$

with N_- unstable and N_+ stable. By rescaling the population $\nu = N/K$, time $\tau = rt$ and harvesting rate $h = H_0/rK$, we arrive at the equation

$$\dot{\nu} = \nu(1 - \nu) - h . \quad (15.19)$$

The critical harvesting rate is then $h_c = \frac{1}{4}$. See fig. 15.8.

(b) One defect of the constant harvesting rate model is that $N = 0$ is not a fixed point. To remedy this, consider the following model for $H(N)$ ¹:

$$H(N) = \frac{BN^2}{N^2 + A^2} , \quad (15.20)$$

where A and B are (positive) constants. Show that one can rescale (N, t) to (n, τ) , such that

$$\frac{dn}{d\tau} = \gamma n \left(1 - \frac{n}{c}\right) - \frac{n^2}{n^2 + 1} , \quad (15.21)$$

where γ and c are positive constants. Provide expressions for n , τ , γ , and c .

Solution : Examining the denominator of $H(N)$, we must take $N = An$. Dividing both sides of $\dot{N} = f(N)$ by B , we obtain

$$\frac{A}{B} \frac{dN}{dt} = \frac{rA}{B} n \left(1 - \frac{A}{K} n\right) - \frac{n^2}{n^2 + 1} ,$$

from which we glean $\tau = Bt/A$, $\gamma = rA/B$, and $c = K/A$.

¹This is a model for the dynamics of the spruce budworm population, taken from ch. 1 of J. D. Murray, *Mathematical Biology* (2nd edition, Springer, 1993).

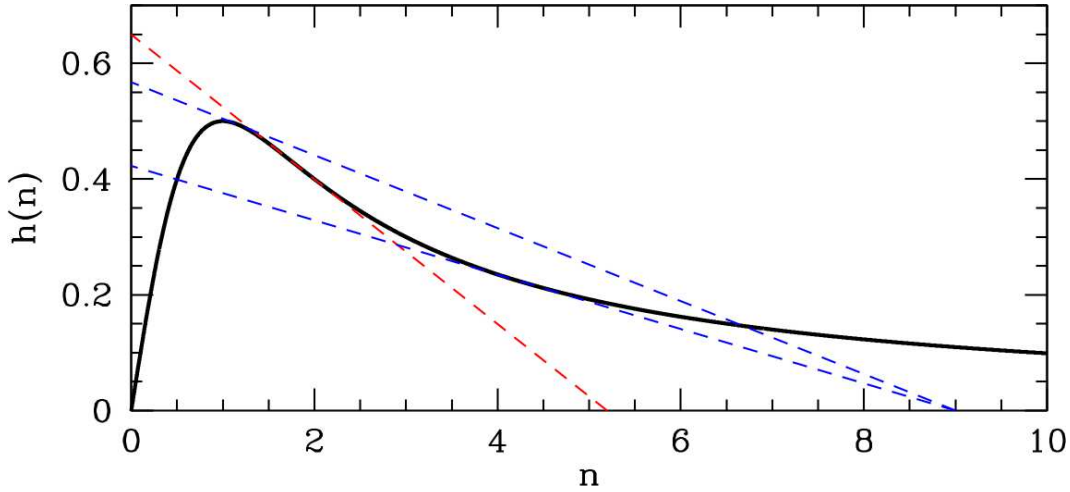


Figure 15.9: Plot of $h(n) = n/(n^2 + 1)$ (thick black curve). Straight lines show the function $y(n) = \gamma(1 - \frac{n}{c})$ for different values of c and γ . The red line is tangent to the inflection point of $h(n)$ and determines the minimum value $c^* = 3\sqrt{3}$ for a bifurcation. The blue lines show the construction for determining the location of the two bifurcations for $c > c^*$ (in this case, $c = 9$). See the analysis in the text.

(c) Show that for c sufficiently small that there is a unique asymptotic ($\tau \rightarrow \infty$) value for the (scaled) population n , for any given value of γ . Thus, there are no bifurcations as a function of the control parameter γ for c fixed and $c < c^*$.

(d) Show that for $c > c^*$, there are two bifurcations as a function of γ , and that for $\gamma_1^* < \gamma < \gamma_2^*$ the asymptotic solution is bistable, *i.e.* there are two stable values for $n(\tau \rightarrow \infty)$. Sketch the solution set ‘phase diagram’ in the (c, γ) plane. Hint: Sketch the functions $\gamma(1 - n/c)$ and $n/(n^2 + 1)$. The $n \neq 0$ fixed points are given by the intersections of these two curves. Determine the boundary of the bistable region in the (c, γ) plane parametrically in terms of n . Find c^* and $\gamma_1^*(c) = \gamma_2^*(c)$.

Solution (c) and (d) : We examine

$$\frac{dn}{d\tau} = g(n) = \left\{ \gamma \left(1 - \frac{n}{c} \right) - \frac{n}{n^2 + 1} \right\} n . \quad (15.22)$$

There is an unstable fixed point at $n = 0$, where $g'(0) = \gamma > 0$. The other fixed points occur when the term in the curly brackets vanishes. In fig. 15.9 we plot the function $h(n) \equiv n/(n^2 + 1)$ versus n . We seek the intersection of this function with a two-parameter family of straight lines, given by $y(n) = \gamma(1 - n/c)$. The n -intercept is c and the y -intercept is γ . Provided $c > c^*$ is large enough, there are two bifurcations as a function of γ , which we call $\gamma_{\pm}(c)$. These are shown as the dashed blue lines in figure 15.9 for $c = 9$.

Both bifurcations are of the saddle-node type. We determine the curves $\gamma_{\pm}(c)$ by requiring that $h(n)$ is

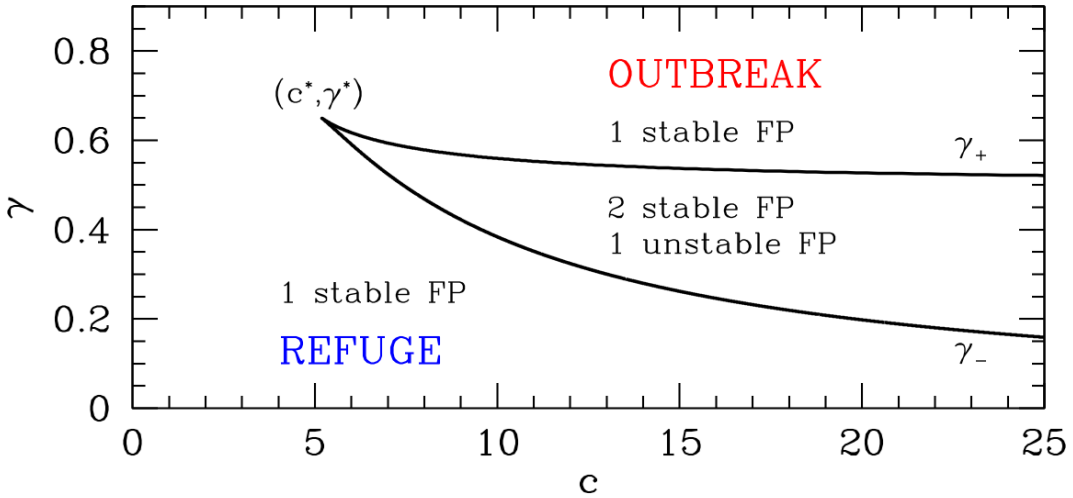


Figure 15.10: Phase diagram for the equation $\dot{n} = \gamma(1 - n/c)n - n^2/(n^2 + 1)$, labeling $n \neq 0$ fixed points. (The point $n = 0$ is always unstable.)

tangent to $y(n)$, which gives two equations:

$$\begin{aligned} h(n) &= \frac{n}{n^2 + 1} = \gamma\left(1 - \frac{n}{c}\right) = y(n) \\ h'(n) &= \frac{1 - n^2}{(n^2 + 1)^2} = -\frac{\gamma}{c} = y'(n) . \end{aligned} \quad (15.23)$$

Together, these give $\gamma(c)$ parametrically, *i.e.* as $\gamma(n)$ and $c(n)$:

$$\gamma(n) = \frac{2n^3}{(n^2 + 1)^2} , \quad c(n) = \frac{2n^3}{(n^2 - 1)} . \quad (15.24)$$

Since $h(n)$ is maximized for $n = 1$, where $h(1) = \frac{1}{2}$, there is no bifurcation occurring at values $n < 1$. If we plot $\gamma(n)$ versus $c(n)$ over the allowed range of n , we obtain the phase diagram in fig. 15.10. The cusp occurs at (c^*, γ^*) , and is determined by the requirement that the two bifurcations coincide. This supplies a third condition, namely that $h''(n) = 0$, where

$$h''(n) = \frac{2n(n^2 - 3)}{(n^2 + 1)^3} . \quad (15.25)$$

Thus $n = \sqrt{3}$, whence $c^* = 3\sqrt{3}$ and $\gamma^* = \frac{3\sqrt{3}}{8}$. For $c < c^*$, there are no bifurcations at any value of γ .

15.2.2 The Bletch

Problem: The bletch is a disgusting animal native to the Forest of Jkroo on the planet Barney. The bletch population obeys the equation

$$\frac{dN}{dt} = aN^2 - bN^3 , \quad (15.26)$$



Figure 15.11: Phase flow for the scaled bletch population, $\dot{n} = n^2 - n^3$.

where N is the number of blettes, and a and b are constants. (Blettes reproduce asexually, but only when another blette is watching. However, when there are three blettes around, they beat the @! !*\$&* out of each other.)

- (a) Sketch the phase flow for N . (Strange as the blette is, you can still rule out $N < 0$.) Identify and classify all fixed points.
- (b) The blette population is now *harvested* (they make nice shoes). To model this, we add an extra term to the dynamics:

$$\frac{dN}{dt} = -hN + aN^2 - bN^3 , \quad (15.27)$$

where h is the harvesting rate. Show that the phase flow now depends crucially on h , in that there are two qualitatively different flows, depending on whether $h < h_c(a, b)$ or $h > h_c(a, b)$. Find the critical harvesting rate $h_c(a, b)$ and sketch the phase flows for the two different regimes.

- (c) In equilibrium, the rate at which blettes are harvested is $R = hN^*$, where N^* is the equilibrium blette population. Suppose we start with $h = 0$, in which case N^* is given by the value of N at the stable fixed point you found in part (a). Now let h be increased very slowly from zero. As h is increased, the equilibrium population changes. Sketch R versus h . What value of h achieves the biggest blette harvest? What is the corresponding value of R_{\max} ?

Solution:

- (a) Setting the RHS of eqn. 15.26 to zero suggests the rescaling

$$N = \frac{a}{b} n \quad , \quad t = \frac{b}{a^2} \tau . \quad (15.28)$$

This results in

$$\frac{dn}{d\tau} = n^2 - n^3 . \quad (15.29)$$

The point $n = 0$ is a (nonlinearly) repulsive fixed point, and $n = 1$, corresponding to $N = a/b$, is attractive. The flow is shown in fig. 15.11.

By the way, the dynamics can be integrated, using the method of partial fractions, to yield

$$\frac{1}{n_0} - \frac{1}{n} + \ln \left(\frac{n}{n_0} \cdot \frac{1-n_0}{1-n} \right) = \tau . \quad (15.30)$$

(b) Upon rescaling, the harvested bletch dynamics obeys the equation

$$\frac{dn}{d\tau} = -\nu n + n^2 - n^3 , \quad (15.31)$$

where $\nu = bh/a^2$ is the dimensionless harvesting rate. Setting the RHS to zero yields $n(n^2 - n + \nu) = 0$, with solutions $n^* = 0$ and

$$n_{\pm}^* = \frac{1}{2} \pm \sqrt{\frac{1}{4} - \nu} . \quad (15.32)$$

At $\nu = \frac{1}{4}$ there is a saddle-node bifurcation, and for $\nu > \frac{1}{4}$ the only fixed point (for real n) is at $n^* = 0$ (stable) – the bletch population is then *overharvested*. For $\nu > \frac{1}{4}$, there are three solutions: a stable fixed point at $n^* = 0$, an unstable fixed point at $n^* = \frac{1}{2} - \sqrt{\frac{1}{4} - \nu}$, and a stable fixed point at $n^* = \frac{1}{2} + \sqrt{\frac{1}{4} - \nu}$. The critical harvesting rate is $\nu_c = \frac{1}{4}$, which means $h_c = a^2/4b$.

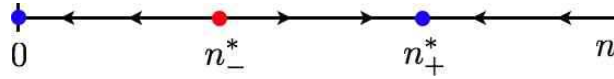


Figure 15.12: Phase flow for the harvested bletch population, $\dot{n} = -\nu n + n^2 - n^3$.

(c) The scaled bletch harvest is given by $r = \nu n_+^*(\nu)$. Note $R = h N_+^* = \frac{a^3}{b^2} r$. The optimal harvest occurs when νn^* is a maximum, which means we set

$$\frac{d}{d\nu} \left\{ \frac{1}{2}\nu + \nu \sqrt{\frac{1}{4} - \nu} \right\} = 0 \implies \nu_{\text{opt}} = \frac{2}{9} . \quad (15.33)$$

Thus, $n_+^*(\nu_{\text{opt}}) = \frac{2}{3}$ and $r_{\text{opt}} = \frac{4}{27}$, meaning $R = 4a^3/27b^2$. Note that at $\nu = \nu_c = \frac{1}{4}$ that $n_+^*(\nu_c) = \frac{1}{2}$, hence $r(\nu_c) = \frac{1}{8}$, which is smaller than $(\nu_{\text{opt}}) = \frac{2}{9}$. The harvest $r(\nu)$ discontinuously drops to zero at $\nu = \nu_c$, since for $\nu > \nu_c$ the flow is to the only stable fixed point at $n^* = 0$.

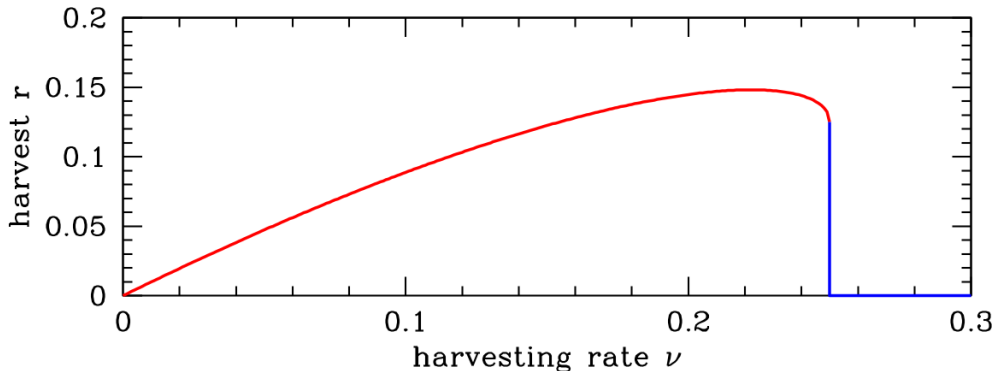


Figure 15.13: Scaled bletch harvest r versus scaled harvesting rate ν . Optimal harvesting occurs for $\nu_{\text{opt}} = \frac{2}{9}$. The critical harvesting rate is $\nu_c = \frac{1}{4}$, at which point the harvest discontinuously drops to zero.

15.3 Appendix : Landau Theory of Phase Transitions

Landau's theory of phase transitions is based on an expansion of the free energy of a thermodynamic system in terms of an *order parameter*, which is nonzero in an ordered phase and zero in a disordered phase. For example, the magnetization M of a ferromagnet in zero external field but at finite temperature typically vanishes for temperatures $T > T_c$, where T_c is the *critical temperature*, also called the *Curie temperature* in a ferromagnet. A low order expansion in powers of the order parameter is appropriate sufficiently close to T_c , *i.e.* at temperatures such that the order parameter, if nonzero, is still small.

The simplest example is the quartic free energy,

$$f(m) = f_0 + \frac{1}{2}am^2 + \frac{1}{4}bm^4 , \quad (15.34)$$

where m is a dimensionless measure of the magnetization density, and where f_0 , a , and b are all functions of the dimensionless temperature θ , which in a ferromagnet is the ratio $\theta = k_B T / \mathcal{J}$, where $\mathcal{J} = \sum_j J_{ij}$ is a sum over the couplings. Let us assume $b > 0$, which is necessary if the free energy is to be bounded from below². The equation of state ,

$$\frac{\partial f}{\partial m} = 0 = am + bm^3 , \quad (15.35)$$

has three solutions in the complex m plane: (i) $m = 0$, (ii) $m = \sqrt{-a/b}$, and (iii) $m = -\sqrt{-a/b}$. The latter two solutions lie along the (physical) real axis if $a < 0$. We assume that $a(\theta)$ is monotonically increasing, and that there exists a unique temperature θ_c where $a(\theta_c) = 0$. Minimizing f , we find

$$\begin{aligned} \theta < \theta_c &: f = f_0 - \frac{a^2}{4b} \\ \theta > \theta_c &: f = f_0 . \end{aligned} \quad (15.36)$$

The free energy is continuous at θ_c since $a(\theta_c) = 0$. The specific heat, however, is discontinuous across the transition, with

$$c(\theta_c^+) - c(\theta_c^-) = -\theta_c \frac{\partial^2}{\partial \theta^2} \Big|_{\theta=\theta_c} \left(\frac{a^2}{4b} \right) = -\frac{\theta_c [a'(\theta_c)]^2}{2b(\theta_c)} . \quad (15.37)$$

The presence of a magnetic field h breaks the \mathbb{Z}_2 symmetry of $m \rightarrow -m$. The free energy becomes

$$f(m) = f_0 + \frac{1}{2}am^2 + \frac{1}{4}bm^4 - hm , \quad (15.38)$$

and the mean field equation is

$$bm^3 + am - h = 0 . \quad (15.39)$$

This is a cubic equation for m with real coefficients, and as such it can either have three real solutions or one real solution and two complex solutions related by complex conjugation. Clearly we must have $a < 0$ in order to have three real roots, since $bm^3 + am$ is monotonically increasing otherwise. The boundary

²It is always the case that f is bounded from below, on physical grounds. Were b negative, we'd have to consider higher order terms in the Landau expansion.

between these two classes of solution sets occurs when two roots coincide, which means $f''(m) = 0$ as well as $f'(m) = 0$. Simultaneously solving these two equations, we find

$$h^*(a) = \pm \frac{2}{3^{3/2}} \frac{(-a)^{3/2}}{b^{1/2}}, \quad (15.40)$$

or, equivalently,

$$a^*(h) = -\frac{3}{2^{2/3}} b^{1/3} |h|^{2/3}. \quad (15.41)$$

If, for fixed h , we have $a < a^*(h)$, then there will be three real solutions to the mean field equation $f'(m) = 0$, one of which is a global minimum (the one for which $m \cdot h > 0$). For $a > a^*(h)$ there is only a single global minimum, at which m also has the same sign as h . If we solve the mean field equation perturbatively in h/a , we find

$$\begin{aligned} m(a, h) &= \frac{h}{a} - \frac{b h^3}{a^4} + \mathcal{O}(h^5) & (a > 0) \\ &= \frac{h}{2|a|} - \frac{3 b^{1/2} h^2}{8|a|^{5/2}} + \mathcal{O}(h^3) & (a < 0). \end{aligned} \quad (15.42)$$

15.3.1 Landau coefficients from mean field theory

A simple variational density matrix for the Ising ferromagnet yields the dimensionless free energy density

$$f(m, h, \theta) = -\frac{1}{2} m^2 - hm + \theta \left\{ \left(\frac{1+m}{2} \right) \ln \left(\frac{1+m}{2} \right) + \left(\frac{1-m}{2} \right) \ln \left(\frac{1-m}{2} \right) \right\}. \quad (15.43)$$

When m is small, it is appropriate to expand $f(m, h, \theta)$, obtaining

$$f(m, h, \theta) = -\theta \ln 2 - hm + \frac{1}{2}(\theta - 1)m^2 + \frac{\theta}{12}m^4 + \frac{\theta}{30}m^6 + \frac{\theta}{56}m^8 + \dots. \quad (15.44)$$

Thus, we identify

$$a(\theta) = \theta - 1, \quad b(\theta) = \frac{1}{3}\theta. \quad (15.45)$$

We see that $a(\theta) = 0$ at a critical temperature $\theta_c = 1$.

The free energy of eqn. 15.43 behaves qualitatively just like it does for the simple Landau expansion, where one stops at order m^4 . Consider without loss of generality the case $h > 0$. The minimum of the free energy $f(m, h, \theta)$ then lies at $m > 0$ for any θ . At low temperatures, the double well structure we found in the $h = 0$ case is tilted so that the right well lies lower in energy than the left well. This is depicted in fig. 15.15. As the temperature is raised, the local minimum at $m < 0$ vanishes, annihilating with the local maximum in a saddle-node bifurcation. To find where this happens, one sets $\frac{\partial f}{\partial m} = 0$ and $\frac{\partial^2 f}{\partial m^2} = 0$ simultaneously, resulting in

$$h^*(\theta) = \sqrt{1-\theta} - \frac{\theta}{2} \ln \left(\frac{1+\sqrt{1-\theta}}{1-\sqrt{1-\theta}} \right). \quad (15.46)$$

The solutions lie at $h = \pm h^*(\theta)$. For $\theta < \theta_c = 1$ and $h \in [-h^*(\theta), +h^*(\theta)]$, there are three solutions to the mean field equation. Equivalently we could in principle invert the above expression to obtain $\theta^*(h)$. For $\theta > \theta^*(h)$, there is only a single global minimum in the free energy $f(m)$ and there is no local minimum. Note $\theta^*(h=0) = 1$.

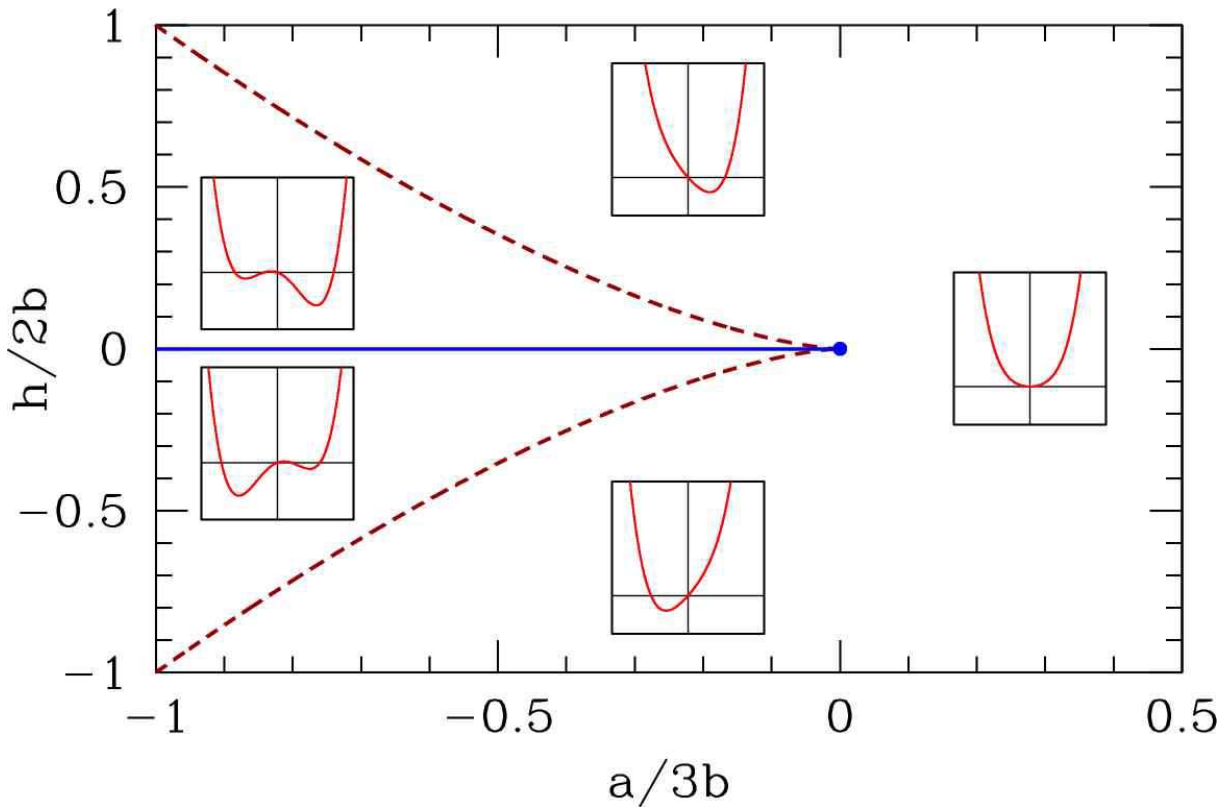


Figure 15.14: Phase diagram for the quartic mean field theory $f = f_0 + \frac{1}{2}am^2 + \frac{1}{4}bm^4 - hm$, with $b > 0$. There is a first order line at $h = 0$ extending from $a = -\infty$ and terminating in a critical point at $a = 0$. For $|h| < h^*(a)$ (dashed red line) there are three solutions to the mean field equation, corresponding to one global minimum, one local minimum, and one local maximum. Insets show behavior of the free energy $f(m)$.

15.3.2 Magnetization dynamics

Dissipative processes drive physical systems to minimum energy states. We can crudely model the dissipative dynamics of a magnet by writing the phenomenological equation

$$\frac{dm}{dt} = -\Gamma \frac{\partial f}{\partial m} . \quad (15.47)$$

This drives the free energy f to smaller and smaller values:

$$\frac{df}{dt} = \frac{\partial f}{\partial m} \frac{dm}{dt} = -\Gamma \left(\frac{\partial f}{\partial m} \right)^2 \leq 0 . \quad (15.48)$$

Clearly the *fixed point* of these dynamics, where $\dot{m} = 0$, is a solution to the mean field equation $\frac{\partial f}{\partial m} = 0$. At the solution to the mean field equation, one has

$$\frac{\partial f}{\partial m} = 0 \quad \Rightarrow \quad m = \tanh \left(\frac{m+h}{\theta} \right) . \quad (15.49)$$

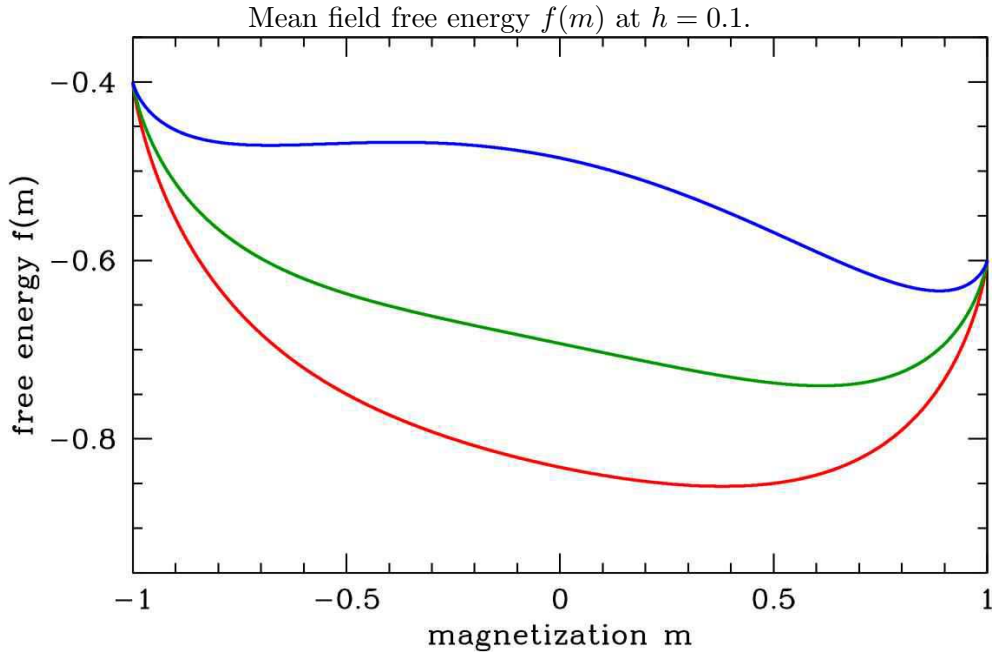


Figure 15.15: Mean field free energy $f(m)$ at $h = 0.1$. Temperatures shown: $\theta = 1.2$ (red), $\theta = 1.0$ (dark green), and $\theta = 0.7$ (blue).

The phase flow for the equation $\dot{m} = -\Gamma f'(m)$ is shown in fig. 15.16. As we have seen, for any value of h there is a temperature θ^* below which the free energy $f(m)$ has two local minima and one local maximum. When $h = 0$ the minima are degenerate, but at finite h one of the minima is a global minimum. Thus, for $\theta < \theta^*(h)$ there are three solutions to the mean field equations. In the language of dynamical systems, under the dynamics of eqn. 15.47, minima of $f(m)$ correspond to attractive fixed points and maxima to repulsive fixed points. If $h > 0$, the rightmost of these fixed points corresponds to the global minimum of the free energy. As θ is increased, this fixed point evolves smoothly. At $\theta = \theta^*$, the (metastable) local minimum and the local maximum coalesce and annihilate in a saddle-node bifurcation. However at $h = 0$ all three fixed points coalesce at $\theta = \theta_c$ and the bifurcation is a supercritical pitchfork. As a function of t at finite h , the dynamics are said to exhibit an *imperfect bifurcation*, which is a deformed supercritical pitchfork.

The solution set for the mean field equation is simply expressed by inverting the tanh function to obtain $h(\theta, m)$. One readily finds

$$h(\theta, m) = \frac{\theta}{2} \ln\left(\frac{1+m}{1-m}\right) - m . \quad (15.50)$$

As we see in the bottom panel of fig. 15.17, $m(h)$ becomes multivalued for field values $h \in [-h^*(\theta), +h^*(\theta)]$, where $h^*(\theta)$ is given in eqn. 15.46. Now imagine that $\theta < \theta_c$ and we slowly ramp the field h from a large negative value to a large positive value, and then slowly back down to its original value. On the time scale of the magnetization dynamics, we can regard $h(t)$ as a constant. Thus, $m(t)$ will flow to the nearest stable fixed point. Initially the system starts with $m = -1$ and h large and negative, and there is only one fixed point, at $m^* \approx -1$. As h slowly increases, the fixed point value m^* also slowly increases. As h exceeds $-h^*(\theta)$, a saddle-node bifurcation occurs, and two new fixed points are created

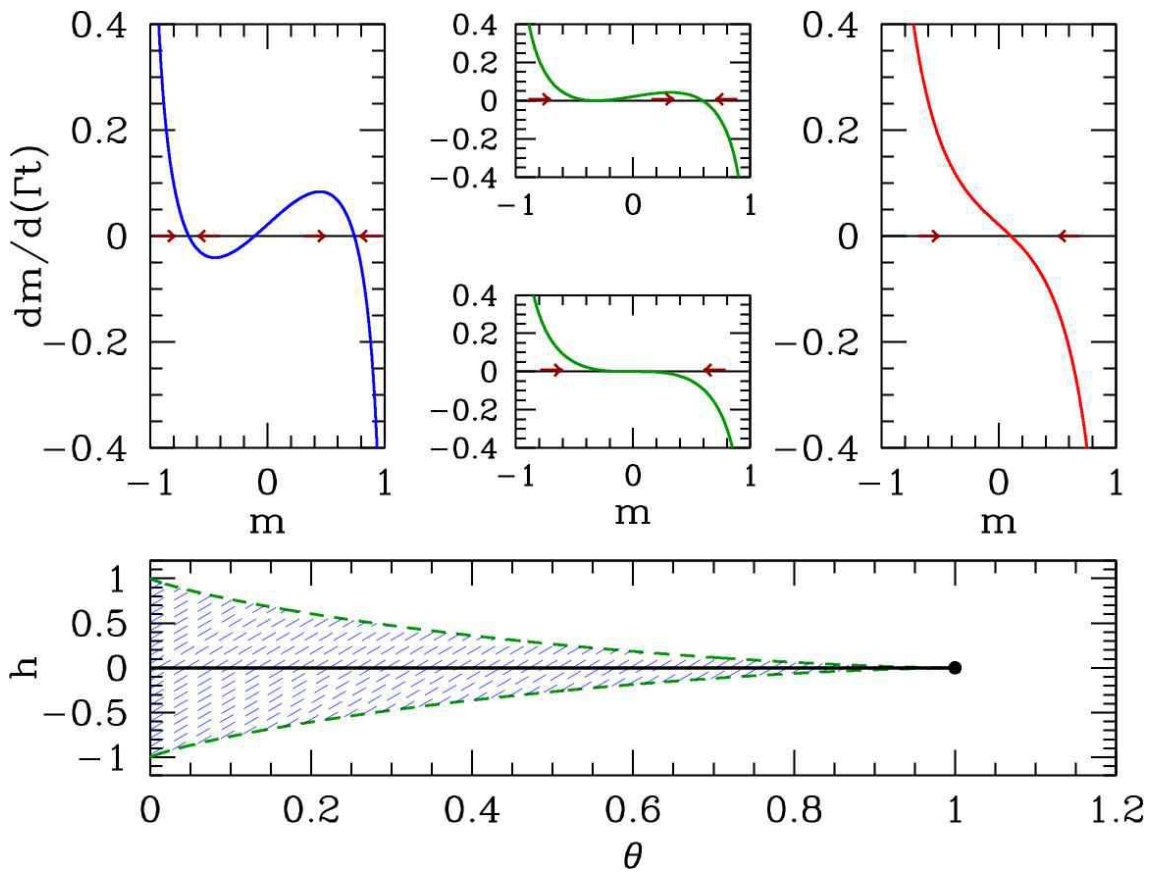


Figure 15.16: Dissipative magnetization dynamics $\dot{m} = -f'(m)$. Bottom panel shows $h^*(\theta)$ from eqn. 15.46. For (θ, h) within the blue shaded region, the free energy $f(m)$ has a global minimum plus a local minimum and a local maximum. Otherwise $f(m)$ has only a single global maximum. Top panels show an imperfect bifurcation in the magnetization dynamics at $h = 0.0215$, for which $\theta^* = 0.90$. Temperatures shown: $\theta = 0.80$ (blue), $\theta = \theta^*(h) = 0.90$ (green), and $\theta = 1.2$. The rightmost stable fixed point corresponds to the global minimum of the free energy. The bottom of the middle two upper panels shows $h = 0$, where both of the attractive fixed points and the repulsive fixed point coalesce into a single attractive fixed point (supercritical pitchfork bifurcation).

at positive m , one stable and one unstable. The global minimum of the free energy still lies at the fixed point with $m^* < 0$. However, when h crosses $h = 0$, the global minimum of the free energy lies at the most positive fixed point m^* . The dynamics, however, keep the system stuck in what is a metastable phase. This persists until $h = +h^*(\theta)$, at which point another saddle-node bifurcation occurs, and the attractive fixed point at $m^* < 0$ annihilates with the repulsive fixed point. The dynamics then act quickly to drive m to the only remaining fixed point. This process is depicted in the top panel of fig. 15.17. As one can see from the figure, the system follows a stable fixed point until the fixed point disappears, even though that fixed point may not always correspond to a global minimum of the free energy. The resulting $m(h)$ curve is then not reversible as a function of time, and it possesses a characteristic shape known as a *hysteresis loop*. Etymologically, the word *hysteresis* derives from the Greek *υστερησις*, which means ‘lagging behind’. Systems which are hysteretic exhibit a *history-dependence* to their status, which

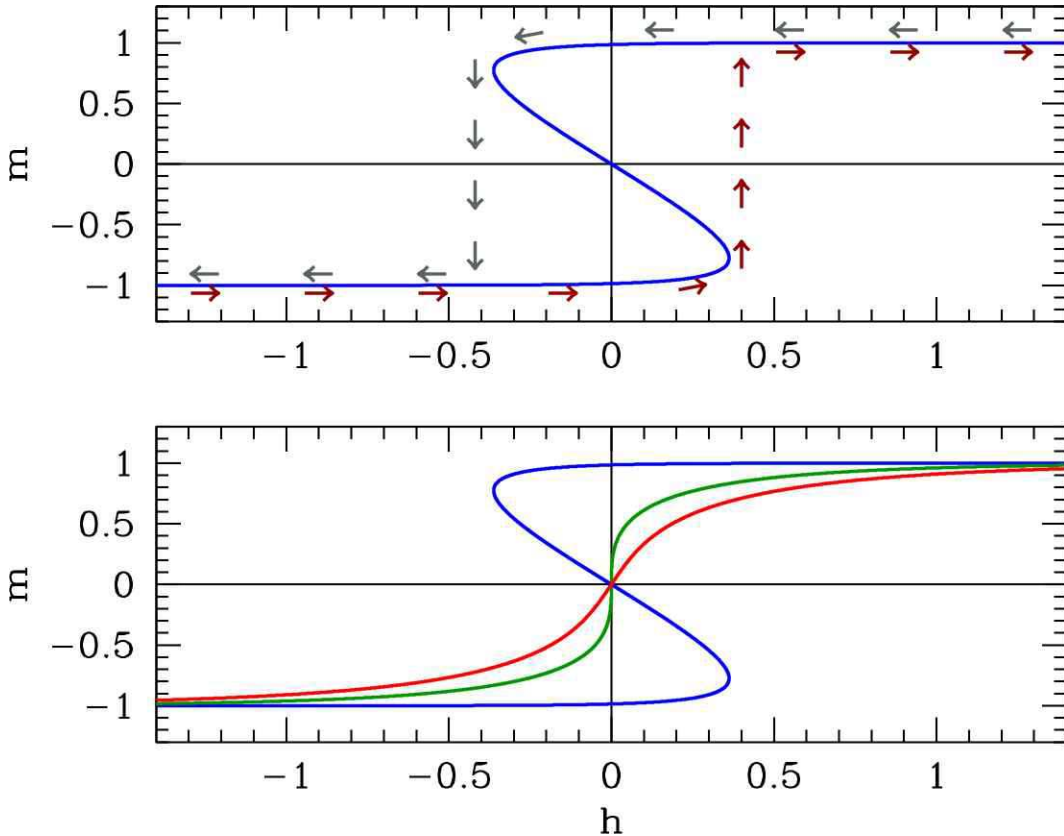


Figure 15.17: Top panel : hysteresis as a function of ramping the dimensionless magnetic field h at $\theta = 0.40$. Dark red arrows below the curve follow evolution of the magnetization on slow increase of h . Dark grey arrows above the curve follow evolution of the magnetization on slow decrease of h . Bottom panel : solution set for $m(\theta, h)$ as a function of h at temperatures $\theta = 0.40$ (blue), $\theta = \theta_c = 1.0$ (dark green), and $t = 1.25$ (red).

is not uniquely determined by external conditions. Hysteresis may be exhibited with respect to changes in applied magnetic field, changes in temperature, or changes in other externally determined parameters.

15.3.3 Cubic terms in Landau theory : first order transitions

Next, consider a free energy with a cubic term,

$$f = f_0 + \frac{1}{2}am^2 - \frac{1}{3}ym^3 + \frac{1}{4}bm^4 , \quad (15.51)$$

with $b > 0$ for stability. Without loss of generality, we may assume $y > 0$ (else send $m \rightarrow -m$). Note that we no longer have $m \rightarrow -m$ (*i.e.* \mathbb{Z}_2) symmetry. The cubic term favors positive m . What is the phase diagram in the (a, y) plane?

Extremizing the free energy with respect to m , we obtain

$$\frac{\partial f}{\partial m} = 0 = am - ym^2 + bm^3 . \quad (15.52)$$

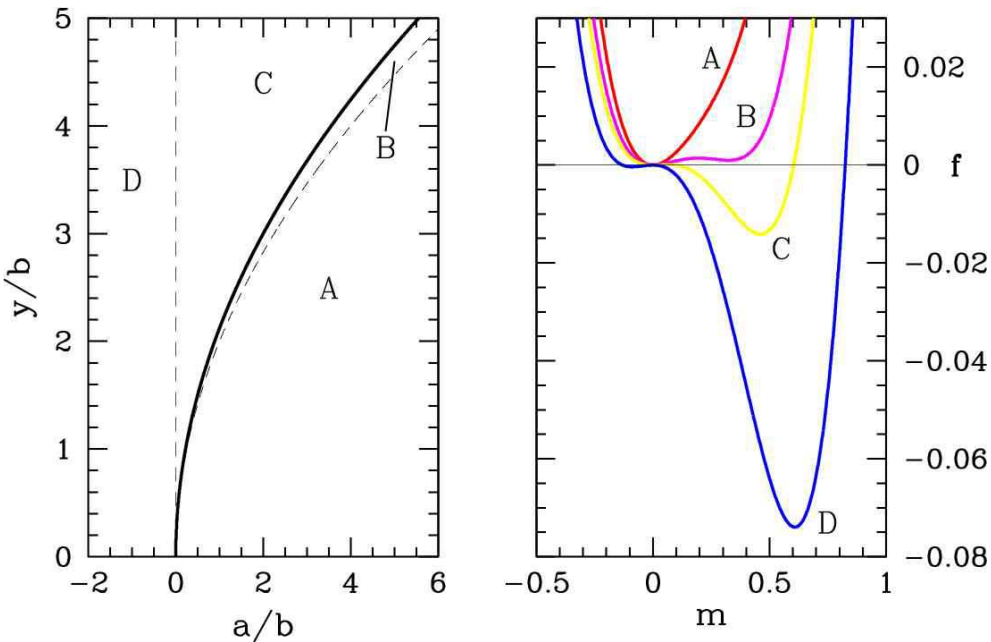


Figure 15.18: Behavior of the quartic free energy $f(m) = \frac{1}{2}am^2 - \frac{1}{3}ym^3 + \frac{1}{4}bm^4$. A: $y^2 < 4ab$; B: $4ab < y^2 < \frac{9}{2}ab$; C and D: $y^2 > \frac{9}{2}ab$. The thick black line denotes a line of first order transitions, where the order parameter is discontinuous across the transition.

This cubic equation factorizes into a linear and quadratic piece, and hence may be solved simply. The three solutions are $m = 0$ and

$$m = m_{\pm} \equiv \frac{y}{2b} \pm \sqrt{\left(\frac{y}{2b}\right)^2 - \frac{a}{b}} . \quad (15.53)$$

We now see that for $y^2 < 4ab$ there is only one real solution, at $m = 0$, while for $y^2 > 4ab$ there are three real solutions. Which solution has lowest free energy? To find out, we compare the energy $f(0)$ with $f(m_+)$ ³. Thus, we set

$$f(m) = f(0) \implies \frac{1}{2}am^2 - \frac{1}{3}ym^3 + \frac{1}{4}bm^4 = 0 , \quad (15.54)$$

and we now have two quadratic equations to solve simultaneously:

$$\begin{aligned} 0 &= a - ym + bm^2 \\ 0 &= \frac{1}{2}a - \frac{1}{3}ym + \frac{1}{4}bm^2 = 0 . \end{aligned} \quad (15.55)$$

Eliminating the quadratic term gives $m = 3a/y$. Finally, substituting $m = m_+$ gives us a relation between a , b , and y :

$$y^2 = \frac{9}{2}ab . \quad (15.56)$$

³We needn't waste our time considering the $m = m_-$ solution, since the cubic term prefers positive m .

Thus, we have the following:

$$\begin{aligned} a > \frac{y^2}{4b} & : \quad 1 \text{ real root } m = 0 \\ \frac{y^2}{4b} > a > \frac{2y^2}{9b} & : \quad 3 \text{ real roots; minimum at } m = 0 \\ \frac{2y^2}{9b} > a & : \quad 3 \text{ real roots; minimum at } m = \frac{y}{2b} + \sqrt{\left(\frac{y}{2b}\right)^2 - \frac{a}{b}} \end{aligned}$$

The solution $m = 0$ lies at a local minimum of the free energy for $a > 0$ and at a local maximum for $a < 0$. Over the range $\frac{y^2}{4b} > a > \frac{2y^2}{9b}$, then, there is a global minimum at $m = 0$, a local minimum at $m = m_+$, and a local maximum at $m = m_-$, with $m_+ > m_- > 0$. For $\frac{2y^2}{9b} > a > 0$, there is a local minimum at $a = 0$, a global minimum at $m = m_+$, and a local maximum at $m = m_-$, again with $m_+ > m_- > 0$. For $a < 0$, there is a local maximum at $m = 0$, a local minimum at $m = m_-$, and a global minimum at $m = m_+$, with $m_+ > 0 > m_-$. See fig. 15.18.

15.3.4 Magnetization dynamics

Suppose we now impose some dynamics on the system, of the simple relaxational type

$$\frac{dm}{dt} = -\Gamma \frac{\partial f}{\partial m}, \quad (15.57)$$

where Γ is a phenomenological kinetic coefficient. Assuming $y > 0$ and $b > 0$, it is convenient to adimensionalize by writing

$$m \equiv \frac{y}{b} \cdot u \quad , \quad a \equiv \frac{y^2}{b} \cdot \bar{r} \quad , \quad t \equiv \frac{b}{\Gamma y^2} \cdot s. \quad (15.58)$$

Then we obtain

$$\frac{\partial u}{\partial s} = -\frac{\partial \varphi}{\partial u}, \quad (15.59)$$

where the dimensionless free energy function is

$$\varphi(u) = \frac{1}{2}\bar{r}u^2 - \frac{1}{3}u^3 + \frac{1}{4}u^4. \quad (15.60)$$

We see that there is a single control parameter, \bar{r} . The fixed points of the dynamics are then the stationary points of $\varphi(u)$, where $\varphi'(u) = 0$, with

$$\varphi'(u) = u(\bar{r} - u + u^2). \quad (15.61)$$

The solutions to $\varphi'(u) = 0$ are then given by

$$u^* = 0 \quad , \quad u^* = \frac{1}{2} \pm \sqrt{\frac{1}{4} - \bar{r}}. \quad (15.62)$$

For $\bar{r} > \frac{1}{4}$ there is one fixed point at $u = 0$, which is attractive under the dynamics $\dot{u} = -\varphi'(u)$ since $\varphi''(0) = \bar{r}$. At $\bar{r} = \frac{1}{4}$ there occurs a saddle-node bifurcation and a pair of fixed points is generated, one

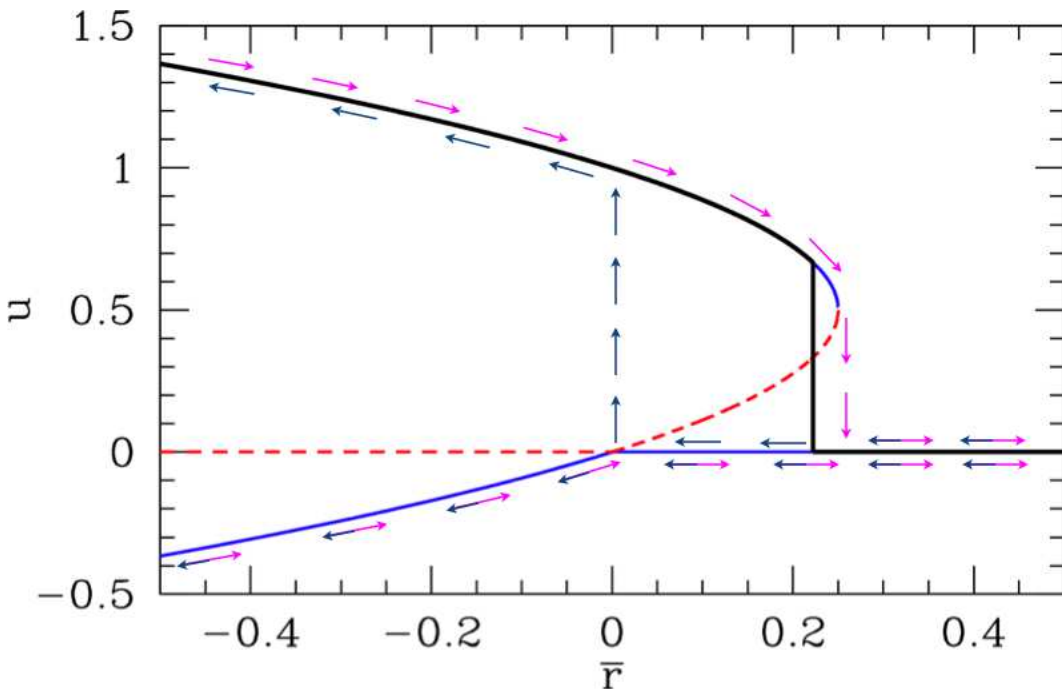


Figure 15.19: Fixed points for $\varphi(u) = \frac{1}{2}\bar{r}u^2 - \frac{1}{3}u^3 + \frac{1}{4}u^4$ and flow under the dynamics $\dot{u} = -\varphi'(u)$. Solid curves represent stable fixed points and dashed curves unstable fixed points. Magenta arrows show behavior under slowly increasing control parameter \bar{r} and dark blue arrows show behavior under slowly decreasing \bar{r} . For $u > 0$ there is a hysteresis loop. The thick black curve shows the equilibrium thermodynamic value of $u(\bar{r})$, i.e. that value which minimizes the free energy $\varphi(u)$. There is a first order phase transition at $\bar{r} = \frac{2}{9}$, where the thermodynamic value of u jumps from $u = 0$ to $u = \frac{2}{3}$.

stable and one unstable. As we see from fig. 15.14, the interior fixed point is always unstable and the two exterior fixed points are always stable. At $r = 0$ there is a transcritical bifurcation where two fixed points of opposite stability collide and bounce off one another (metaphorically speaking).

At the saddle-node bifurcation, $\bar{r} = \frac{1}{4}$ and $u = \frac{1}{2}$, and we find $\varphi(u = \frac{1}{2}; \bar{r} = \frac{1}{4}) = \frac{1}{192}$, which is positive. Thus, the thermodynamic state of the system remains at $u = 0$ until the value of $\varphi(u_+)$ crosses zero. This occurs when $\varphi(u) = 0$ and $\varphi'(u) = 0$, the simultaneous solution of which yields $\bar{r} = \frac{2}{9}$ and $u = \frac{2}{3}$.

Suppose we slowly ramp the control parameter \bar{r} up and down as a function of the dimensionless time s . Under the dynamics of eqn. 15.59, $u(s)$ flows to the first stable fixed point encountered – this is always the case for a dynamical system with a one-dimensional phase space. Then as \bar{r} is further varied, u follows the position of whatever locally stable fixed point it initially encountered. Thus, $u(\bar{r}(s))$ evolves smoothly until a bifurcation is encountered. The situation is depicted by the arrows in fig. 15.19. The equilibrium thermodynamic value for $u(\bar{r})$ is discontinuous; there is a first order phase transition at $\bar{r} = \frac{2}{9}$, as we've already seen. As r is increased, $u(\bar{r})$ follows a trajectory indicated by the magenta arrows. For an negative initial value of u , the evolution as a function of \bar{r} will be *reversible*. However, if $u(0)$ is initially positive, then the system exhibits *hysteresis*, as shown. Starting with a large positive value of \bar{r} , $u(s)$ quickly evolves to $u = 0^+$, which means a positive infinitesimal value. Then as r is decreased, the system remains at $u = 0^+$ even through the first order transition, because $u = 0$ is an attractive

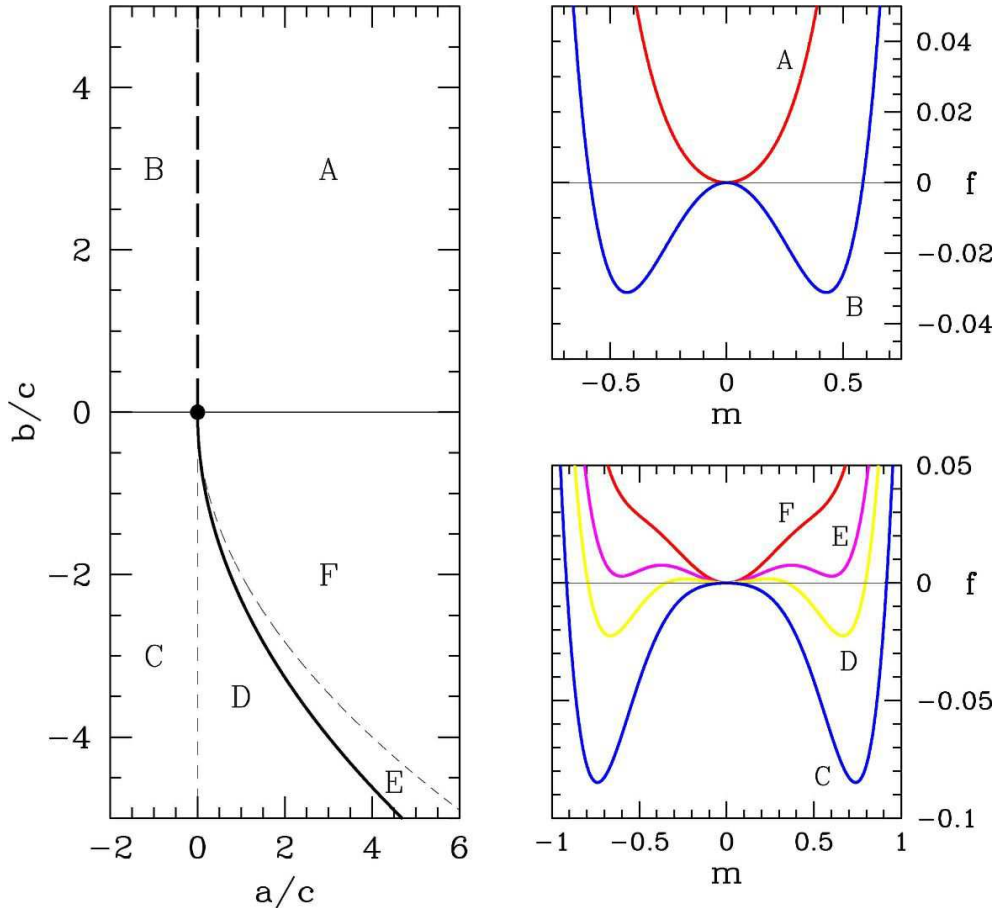


Figure 15.20: Behavior of the sextic free energy $f(m) = \frac{1}{2}am^2 + \frac{1}{4}bm^4 + \frac{1}{6}cm^6$. A: $a > 0$ and $b > 0$; B: $a < 0$ and $b > 0$; C: $a < 0$ and $b < 0$; D: $a > 0$ and $b < -\frac{4}{\sqrt{3}}\sqrt{ac}$; E: $a > 0$ and $-\frac{4}{\sqrt{3}}\sqrt{ac} < b < -2\sqrt{ac}$; F: $a > 0$ and $-2\sqrt{ac} < b < 0$. The thick dashed line is a line of second order transitions, which meets the thick solid line of first order transitions at the tricritical point, $(a, b) = (0, 0)$.

fixed point. However, once r begins to go negative, the $u = 0$ fixed point becomes repulsive, and $u(s)$ quickly flows to the stable fixed point $u_+ = \frac{1}{2} + \sqrt{\frac{1}{4} - \bar{r}}$. Further decreasing r , the system remains on this branch. If \bar{r} is later increased, then $u(s)$ remains on the upper branch past $r = 0$, until the u_+ fixed point annihilates with the unstable fixed point at $u_- = \frac{1}{2} - \sqrt{\frac{1}{4} - \bar{r}}$, at which time $u(s)$ quickly flows down to $u = 0^+$ again.

15.3.5 Sixth order Landau theory : tricritical point

Finally, consider a model with \mathbb{Z}_2 symmetry, with the Landau free energy

$$f = f_0 + \frac{1}{2}am^2 + \frac{1}{4}bm^4 + \frac{1}{6}cm^6, \quad (15.63)$$

with $c > 0$ for stability. We seek the phase diagram in the (a, b) plane. Extremizing f with respect to m , we obtain

$$\frac{\partial f}{\partial m} = 0 = m(a + bm^2 + cm^4), \quad (15.64)$$

which is a quintic with five solutions over the complex m plane. One solution is obviously $m = 0$. The other four are

$$m = \pm \sqrt{-\frac{b}{2c}} \pm \sqrt{\left(\frac{b}{2c}\right)^2 - \frac{a}{c}}. \quad (15.65)$$

For each \pm symbol in the above equation, there are two options, hence four roots in all.

If $a > 0$ and $b > 0$, then four of the roots are imaginary and there is a unique minimum at $m = 0$.

For $a < 0$, there are only three solutions to $f'(m) = 0$ for real m , since the $-$ choice for the \pm sign under the radical leads to imaginary roots. One of the solutions is $m = 0$. The other two are

$$m = \pm \sqrt{-\frac{b}{2c} + \sqrt{\left(\frac{b}{2c}\right)^2 - \frac{a}{c}}}. \quad (15.66)$$

The most interesting situation is $a > 0$ and $b < 0$. If $a > 0$ and $b < -2\sqrt{ac}$, all five roots are real. There must be three minima, separated by two local maxima. Clearly if m^* is a solution, then so is $-m^*$. Thus, the only question is whether the outer minima are of lower energy than the minimum at $m = 0$. We assess this by demanding $f(m^*) = f(0)$, where m^* is the position of the largest root (*i.e.* the rightmost minimum). This gives a second quadratic equation,

$$0 = \frac{1}{2}a + \frac{1}{4}bm^2 + \frac{1}{6}cm^4, \quad (15.67)$$

which together with equation 15.64 gives

$$b = -\frac{4}{\sqrt{3}}\sqrt{ac}. \quad (15.68)$$

Thus, we have the following, for fixed $a > 0$:

$$\begin{aligned} b > -2\sqrt{ac} &: 1 \text{ real root } m = 0 \\ -2\sqrt{ac} > b > -\frac{4}{\sqrt{3}}\sqrt{ac} &: 5 \text{ real roots; minimum at } m = 0 \\ -\frac{4}{\sqrt{3}}\sqrt{ac} > b &: 5 \text{ real roots; minima at } m = \pm \sqrt{-\frac{b}{2c} + \sqrt{\left(\frac{b}{2c}\right)^2 - \frac{a}{c}}} \end{aligned}$$

The point $(a, b) = (0, 0)$, which lies at the confluence of a first order line and a second order line, is known as a *tricritical point*.

15.3.6 Hysteresis for the sextic potential

Once again, we consider the dissipative dynamics $\dot{m} = -\Gamma f'(m)$. We adimensionalize by writing

$$m \equiv \sqrt{\frac{|b|}{c}} \cdot u, \quad a \equiv \frac{b^2}{c} \cdot \bar{r}, \quad t \equiv \frac{c}{\Gamma b^2} \cdot s. \quad (15.69)$$

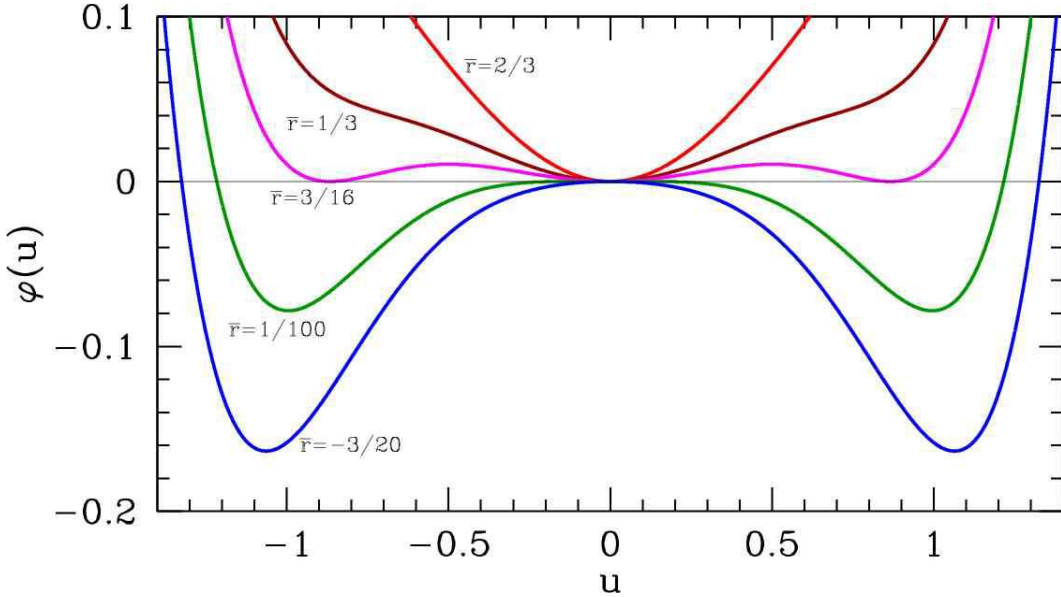


Figure 15.21: Free energy $\varphi(u) = \frac{1}{2}\bar{r}u^2 - \frac{1}{4}u^4 + \frac{1}{6}u^6$ for several different values of the control parameter \bar{r} .

Then we obtain once again the dimensionless equation

$$\frac{\partial u}{\partial s} = -\frac{\partial \varphi}{\partial u}, \quad (15.70)$$

where

$$\varphi(u) = \frac{1}{2}\bar{r}u^2 \pm \frac{1}{4}u^4 + \frac{1}{6}u^6. \quad (15.71)$$

In the above equation, the coefficient of the quartic term is positive if $b > 0$ and negative if $b < 0$. That is, the coefficient is $\text{sgn}(b)$. When $b > 0$ we can ignore the sextic term for sufficiently small u , and we recover the quartic free energy studied earlier. There is then a second order transition at $r = 0$.

New and interesting behavior occurs for $b > 0$. The fixed points of the dynamics are obtained by setting $\varphi'(u) = 0$. We have

$$\begin{aligned} \varphi(u) &= \frac{1}{2}\bar{r}u^2 - \frac{1}{4}u^4 + \frac{1}{6}u^6 \\ \varphi'(u) &= u(\bar{r} - u^2 + u^4). \end{aligned} \quad (15.72)$$

Thus, the equation $\varphi'(u) = 0$ factorizes into a linear factor u and a quartic factor $u^4 - u^2 + \bar{r}$ which is quadratic in u^2 . Thus, we can easily obtain the roots:

$$\begin{aligned} \bar{r} < 0 & : u^* = 0, u^* = \pm \sqrt{\frac{1}{2} + \sqrt{\frac{1}{4} - \bar{r}}} \\ 0 < \bar{r} < \frac{1}{4} & : u^* = 0, u^* = \pm \sqrt{\frac{1}{2} + \sqrt{\frac{1}{4} - \bar{r}}}, u^* = \pm \sqrt{\frac{1}{2} - \sqrt{\frac{1}{4} - \bar{r}}} \\ \bar{r} > \frac{1}{4} & : u^* = 0. \end{aligned} \quad (15.73)$$

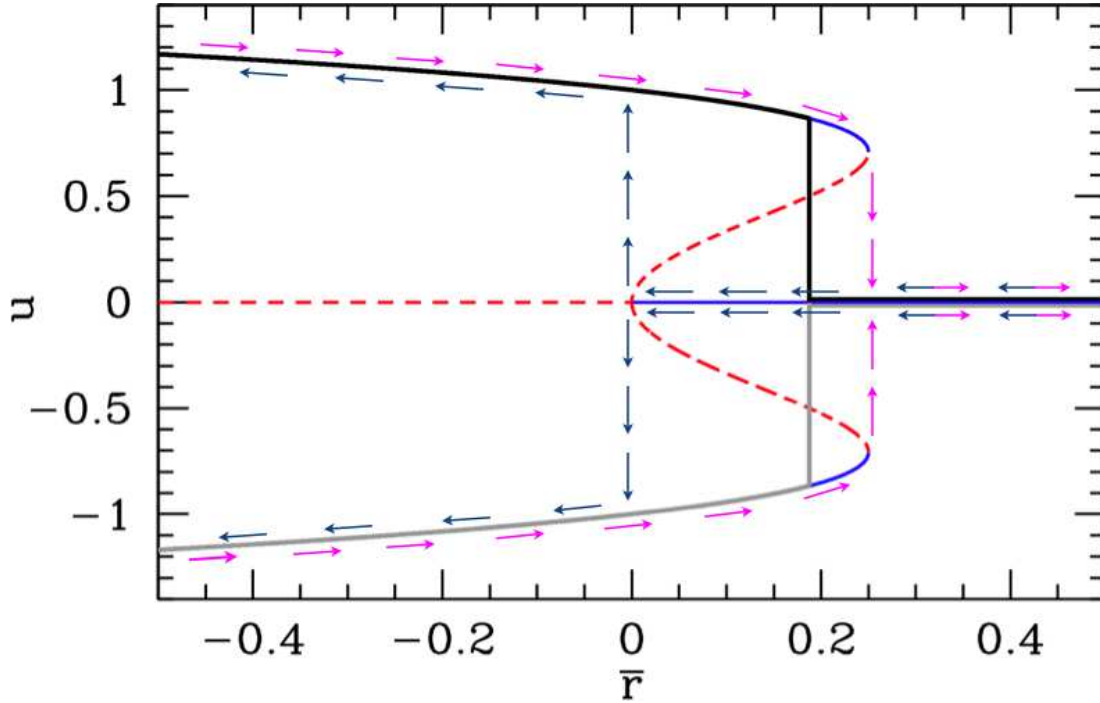


Figure 15.22: Fixed points $\varphi'(u^*) = 0$ for the sextic potential $\varphi(u) = \frac{1}{2}\bar{r}u^2 - \frac{1}{4}u^4 + \frac{1}{6}u^6$, and corresponding dynamical flow (arrows) under $\dot{u} = -\varphi'(u)$. Solid curves show stable fixed points and dashed curves show unstable fixed points. The thick solid black and solid grey curves indicate the equilibrium thermodynamic values for u ; note the overall $u \rightarrow -u$ symmetry. Within the region $\bar{r} \in [0, \frac{1}{4}]$ the dynamics are irreversible and the system exhibits the phenomenon of hysteresis. There is a first order phase transition at $\bar{r} = \frac{3}{16}$.

In fig. 15.22, we plot the fixed points and the hysteresis loops for this system. At $\bar{r} = \frac{1}{4}$, there are two symmetrically located saddle-node bifurcations at $u = \pm \frac{1}{\sqrt{2}}$. We find $\varphi(u = \pm \frac{1}{\sqrt{2}}, \bar{r} = \frac{1}{4}) = \frac{1}{48}$, which is positive, indicating that the stable fixed point $u^* = 0$ remains the thermodynamic minimum for the free energy $\varphi(u)$ as \bar{r} is decreased through $\frac{1}{4}$. Setting $\varphi(u) = 0$ and $\varphi'(u) = 0$ simultaneously, we obtain $\bar{r} = \frac{3}{16}$ and $u = \pm \frac{\sqrt{3}}{2}$. The thermodynamic value for u therefore jumps discontinuously from $u = 0$ to $u = \pm \frac{\sqrt{3}}{2}$ (either branch) at $\bar{r} = \frac{3}{16}$; this is a first order transition.

Under the dissipative dynamics considered here, the system exhibits hysteresis, as indicated in the figure, where the arrows show the evolution of $u(s)$ for very slowly varying $\bar{r}(s)$. When the control parameter \bar{r} is large and positive, the flow is toward the sole fixed point at $u^* = 0$. At $\bar{r} = \frac{1}{4}$, two simultaneous saddle-node bifurcations take place at $u^* = \pm \frac{1}{\sqrt{2}}$; the outer branch is stable and the inner branch unstable in both cases. At $r = 0$ there is a subcritical pitchfork bifurcation, and the fixed point at $u^* = 0$ becomes unstable.

Suppose one starts off with $\bar{r} \gg \frac{1}{4}$ with some value $u > 0$. The flow $\dot{u} = -\varphi'(u)$ then rapidly results in $u \rightarrow 0^+$. This is the ‘high temperature phase’ in which there is no magnetization. Now let r increase slowly, using s as the dimensionless time variable. The scaled magnetization $u(s) = u^*(\bar{r}(s))$ will remain pinned at the fixed point $u^* = 0^+$. As \bar{r} passes through $\bar{r} = \frac{1}{4}$, two new stable values of u^* appear, but our system remains at $u = 0^+$, since $u^* = 0$ is a stable fixed point. But after the subcritical pitchfork,

$u^* = 0$ becomes unstable. The magnetization $u(s)$ then flows rapidly to the stable fixed point at $u^* = \frac{1}{\sqrt{2}}$, and follows the curve $u^*(\bar{r}) = \left(\frac{1}{2} + (\frac{1}{4} - \bar{r})^{1/2}\right)^{1/2}$ for all $r < 0$.

Now suppose we start increasing r (*i.e.* increasing temperature). The magnetization follows the stable fixed point $u^*(\bar{r}) = \left(\frac{1}{2} + (\frac{1}{4} - \bar{r})^{1/2}\right)^{1/2}$ past $\bar{r} = 0$, beyond the first order phase transition point at $\bar{r} = \frac{3}{16}$, and all the way up to $\bar{r} = \frac{1}{4}$, at which point this fixed point is annihilated at a saddle-node bifurcation. The flow then rapidly takes $u \rightarrow u^* = 0^+$, where it remains as r continues to be increased further.

Within the region $\bar{r} \in [0, \frac{1}{4}]$ of control parameter space, the dynamics are said to be *irreversible* and the behavior of $u(s)$ is said to be *hysteretic*.

Chapter 16

Two-Dimensional Phase Flows

We've seen how, for one-dimensional dynamical systems $\dot{u} = f(u)$, the possibilities in terms of the behavior of the system are in fact quite limited. Starting from an arbitrary initial condition $u(0)$, the phase flow is monotonically toward the first stable fixed point encountered. (That point may lie at infinity.) No oscillations are possible¹. For $N = 2$ phase flows, a richer set of possibilities arises, as we shall now see.

16.1 Harmonic Oscillator and Pendulum

16.1.1 Simple harmonic oscillator

A one-dimensional harmonic oscillator obeys the equation of motion,

$$m \frac{d^2x}{dt^2} = -kx , \quad (16.1)$$

where m is the mass and k the force constant (of a spring). If we define $v = \dot{x}$, this may be written as the $N = 2$ system,

$$\frac{d}{dt} \begin{pmatrix} x \\ v \end{pmatrix} = \begin{pmatrix} 0 & 1 \\ -\Omega^2 & 0 \end{pmatrix} \begin{pmatrix} x \\ v \end{pmatrix} = \begin{pmatrix} v \\ -\Omega^2 x \end{pmatrix} , \quad (16.2)$$

where $\Omega = \sqrt{k/m}$ has the dimensions of frequency (inverse time). The solution is well known:

$$\begin{aligned} x(t) &= x_0 \cos(\Omega t) + \frac{v_0}{\Omega} \sin(\Omega t) \\ v(t) &= v_0 \cos(\Omega t) - \Omega x_0 \sin(\Omega t) . \end{aligned} \quad (16.3)$$

The phase curves are ellipses:

$$\Omega x^2(t) + \Omega^{-1} v^2(t) = C , \quad (16.4)$$

where the constant $C = \Omega x_0^2 + \Omega^{-1} v_0^2$. A sketch of the phase curves and of the phase flow is shown in Fig. 16.1. Note that the x and v axes have different dimensions. Note also that the origin is a fixed

¹If phase space itself is multiply connected, e.g. a circle, then the system can oscillate by moving around the circle.

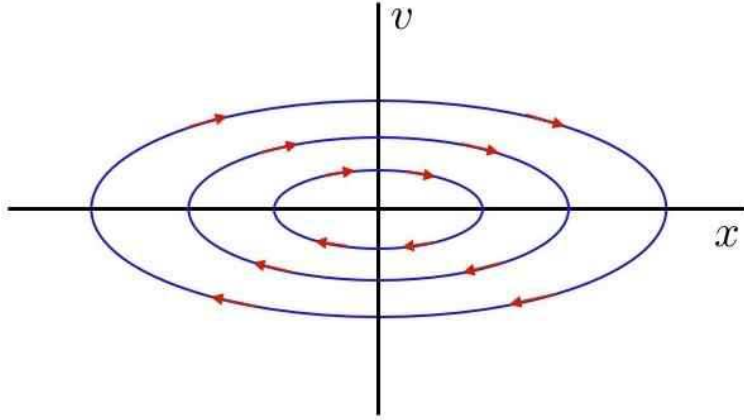


Figure 16.1: Phase curves for the harmonic oscillator.

point, however, unlike the $N = 1$ systems studied in the first lecture, here the phase flow can avoid the fixed points, and oscillations can occur.

Incidentally, eqn. 16.2 is linear, and may be solved by the following method. Write the equation as $\dot{\varphi} = M\varphi$, with

$$\varphi = \begin{pmatrix} x \\ \dot{x} \end{pmatrix} \quad \text{and} \quad M = \begin{pmatrix} 0 & 1 \\ -\Omega^2 & 0 \end{pmatrix} \quad (16.5)$$

The formal solution to $\dot{\varphi} = M\varphi$ is

$$\varphi(t) = e^{Mt} \varphi(0) . \quad (16.6)$$

What do we mean by the exponential of a matrix? We mean its Taylor series expansion:

$$e^{Mt} = \mathbb{I} + Mt + \frac{1}{2!} M^2 t^2 + \frac{1}{3!} M^3 t^3 + \dots . \quad (16.7)$$

Note that

$$M^2 = \begin{pmatrix} 0 & 1 \\ -\Omega^2 & 0 \end{pmatrix} \begin{pmatrix} 0 & 1 \\ -\Omega^2 & 0 \end{pmatrix} = \begin{pmatrix} -\Omega^2 & 0 \\ 0 & -\Omega^2 \end{pmatrix} = -\Omega^2 \mathbb{I} , \quad (16.8)$$

hence

$$M^{2k} = (-\Omega^2)^k \mathbb{I} \quad , \quad M^{2k+1} = (-\Omega^2)^k M . \quad (16.9)$$

Thus,

$$\begin{aligned} e^{Mt} &= \sum_{k=0}^{\infty} \frac{1}{(2k)!} (-\Omega^2 t^2)^k \cdot \mathbb{I} + \sum_{k=0}^{\infty} \frac{1}{(2k+1)!} (-\Omega^2 t^2)^k \cdot Mt \\ &= \cos(\Omega t) \cdot \mathbb{I} + \Omega^{-1} \sin(\Omega t) \cdot M = \begin{pmatrix} \cos(\Omega t) & \Omega^{-1} \sin(\Omega t) \\ -\Omega \sin(\Omega t) & \cos(\Omega t) \end{pmatrix} . \end{aligned} \quad (16.10)$$

Plugging this into eqn. 16.6, we obtain the desired solution.

For the damped harmonic oscillator, we have

$$\ddot{x} + 2\beta \dot{x} + \Omega^2 x = 0 \quad \Rightarrow \quad M = \begin{pmatrix} 0 & 1 \\ -\Omega^2 & -2\beta \end{pmatrix} . \quad (16.11)$$

The phase curves then spiral inward to the fixed point at $(0, 0)$.

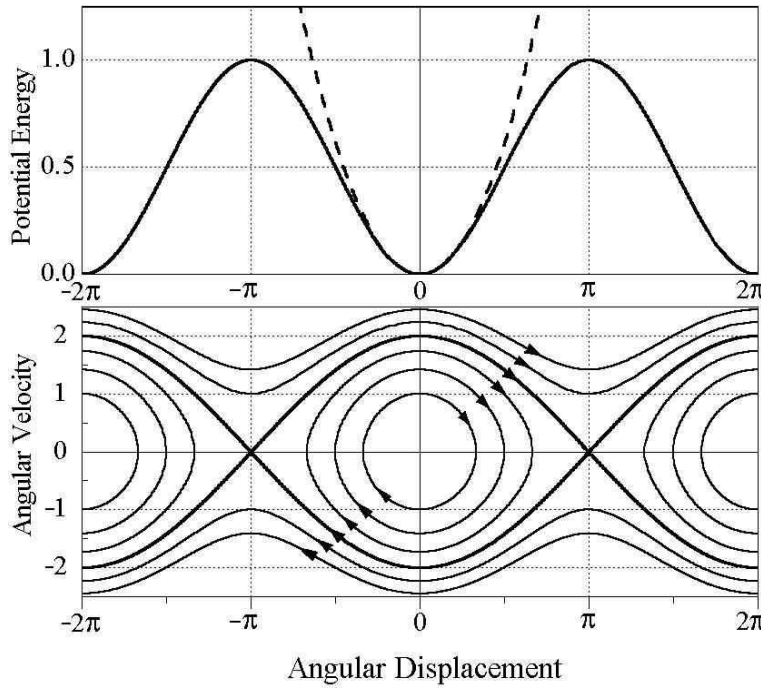


Figure 16.2: Phase curves for the simple pendulum. The *separatrix* divides phase space into regions of vibration and libration.

16.1.2 Pendulum

Next, consider the simple pendulum, composed of a mass point m affixed to a massless rigid rod of length ℓ .

$$m\ell^2 \ddot{\theta} = -mg\ell \sin \theta . \quad (16.12)$$

This is equivalent to

$$\frac{d}{dt} \begin{pmatrix} \theta \\ \omega \end{pmatrix} = \begin{pmatrix} \omega \\ -\Omega^2 \sin \theta \end{pmatrix} , \quad (16.13)$$

where $\omega = \dot{\theta}$ is the angular velocity, and where $\Omega = \sqrt{g/\ell}$ is the natural frequency of small oscillations.

The phase curves for the pendulum are shown in Fig. 16.2. The small oscillations of the pendulum are essentially the same as those of a harmonic oscillator. Indeed, within the small angle approximation, $\sin \theta \approx \theta$, and the pendulum equations of motion are exactly those of the harmonic oscillator. These oscillations are called *librations*. They involve a back-and-forth motion in real space, and the phase space motion is contractable to a point, in the topological sense. However, if the initial angular velocity is large enough, a qualitatively different kind of motion is observed, whose phase curves are *rotations*. In this case, the pendulum bob keeps swinging around in the same direction, because, as we'll see in a later lecture, the total energy is sufficiently large. The phase curve which separates these two topologically distinct motions is called a *separatrix*.

16.2 General $N = 2$ Systems

The general form to be studied is

$$\frac{d}{dt} \begin{pmatrix} x \\ y \end{pmatrix} = \begin{pmatrix} V_x(x, y) \\ V_y(x, y) \end{pmatrix}. \quad (16.14)$$

Special cases include autonomous second order ODEs, *viz.*

$$\ddot{x} = f(x, \dot{x}) \quad \Rightarrow \quad \frac{d}{dt} \begin{pmatrix} x \\ v \end{pmatrix} = \begin{pmatrix} v \\ f(x, v) \end{pmatrix}, \quad (16.15)$$

of the type which occur in one-dimensional mechanics.

16.2.1 The damped driven pendulum

Another example is that of the damped and driven harmonic oscillator,

$$\frac{d^2\phi}{ds^2} + \gamma \frac{d\phi}{ds} + \sin \phi = j. \quad (16.16)$$

This is equivalent to a model of a resistively and capacitively shunted Josephson junction, depicted in fig. 16.3. If ϕ is the superconducting phase difference across the junction, the current through the junction is given by $I_J = I_c \sin \phi$, where I_c is the *critical current*. The current carried by the resistor is $I_R = V/R$ from Ohm's law, and the current from the capacitor is $I_C = \dot{Q}$. Finally, the *Josephson relation* relates the voltage V across the junction to the superconducting phase difference ϕ : $V = (\hbar/2e)\dot{\phi}$. Summing up the parallel currents, we have that the total current I is given by

$$I = \frac{\hbar C}{2e} \ddot{\phi} + \frac{\hbar}{2eR} \dot{\phi} + I_c \sin \phi, \quad (16.17)$$

which, again, is equivalent to a damped, driven pendulum.

This system also has a mechanical analog. Define the 'potential'

$$U(\phi) = -I_c \cos \phi - I\phi. \quad (16.18)$$

The equation of motion is then

$$\frac{\hbar C}{2e} \ddot{\phi} + \frac{\hbar}{2eR} \dot{\phi} = -\frac{\partial U}{\partial \phi}. \quad (16.19)$$

Thus, the combination $\hbar C/2e$ plays the role of the inertial term (mass, or moment of inertia), while the combination $\hbar/2eR$ plays the role of a damping coefficient. The potential $U(\phi)$ is known as the *tilted washboard potential*, for obvious reasons. (Though many of you have perhaps never seen a washboard.)

The model is adimensionalized by defining the Josephson plasma frequency ω_p and the RC time constant τ :

$$\omega_p \equiv \sqrt{\frac{2eI_c}{\hbar C}}, \quad , \quad \tau \equiv RC. \quad (16.20)$$

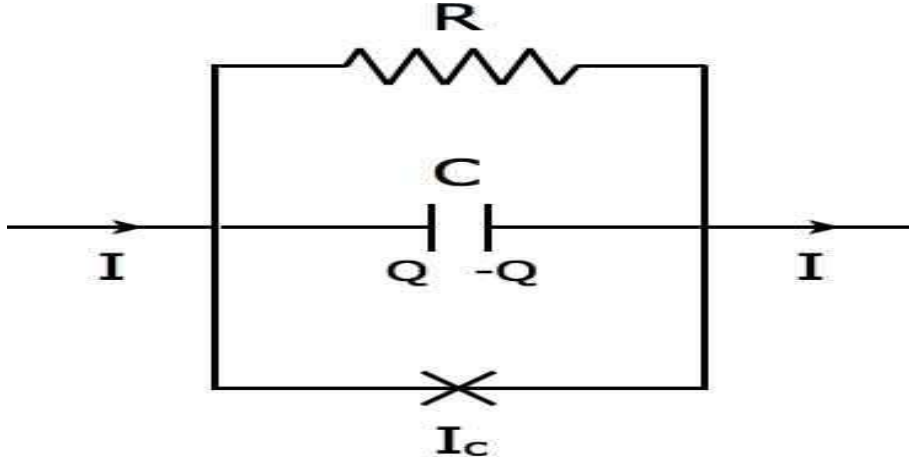


Figure 16.3: . The resistively and capacitively shunted Josephson junction. The Josephson junction is the X element at the bottom of the figure.

The dimensionless combination $\omega_p\tau$ then enters the adimensionalized equation as the sole control parameter:

$$\frac{I}{I_c} = \frac{d^2\phi}{ds^2} + \frac{1}{\omega_p\tau} \frac{d\phi}{ds} + \sin \phi , \quad (16.21)$$

where $s = \omega_p t$. In the Josephson junction literature, the quantity $\beta \equiv 2eI_cR^2C/\hbar = (\omega_p\tau)^2$, known as the *McCumber-Stewart* parameter, is a dimensionless measure of the damping (large β means small damping). In terms of eqn. 16.16, we have $\gamma = (\omega_p\tau)^{-1}$ and $j = I/I_c$.

We can write the second order ODE of eqn. 16.16 as two coupled first order ODEs:

$$\frac{d}{dt} \begin{pmatrix} \phi \\ \omega \end{pmatrix} = \begin{pmatrix} \omega \\ j - \sin \phi - \gamma \omega \end{pmatrix} , \quad (16.22)$$

where $\omega = \dot{\phi}$. Phase space is a cylinder, $\mathbb{S}^1 \times \mathbb{R}^1$.

The quantity $\omega_p\tau$ typically ranges from 10^{-3} to 10^3 in Josephson junction applications. If $\omega_p\tau$ is small, then the system is heavily damped, and the inertial term $d^2\phi/ds^2$ can be neglected. One then obtains the $N = 1$ system

$$\gamma \frac{d\phi}{ds} = j - \sin \phi . \quad (16.23)$$

If $|j| < 1$, then $\phi(s)$ evolves to the first stable fixed point encountered, where $\phi^* = \sin^{-1}(j)$ and $\cos \phi^* = \sqrt{1 - j^2}$. Since $\phi(s) \rightarrow \phi^*$ is asymptotically a constant, the voltage drop V must then vanish, as a consequence of the Josephson relation $V = (\hbar/2e)\phi$. This, there is current flowing with no voltage drop!

If $|j| > 1$, the RHS never vanishes, in which case $\phi(s)$ is monotonic. We then can integrate the differential equation

$$dt = \frac{\hbar}{2eR} \cdot \frac{d\phi}{I - I_c \sin \phi} . \quad (16.24)$$

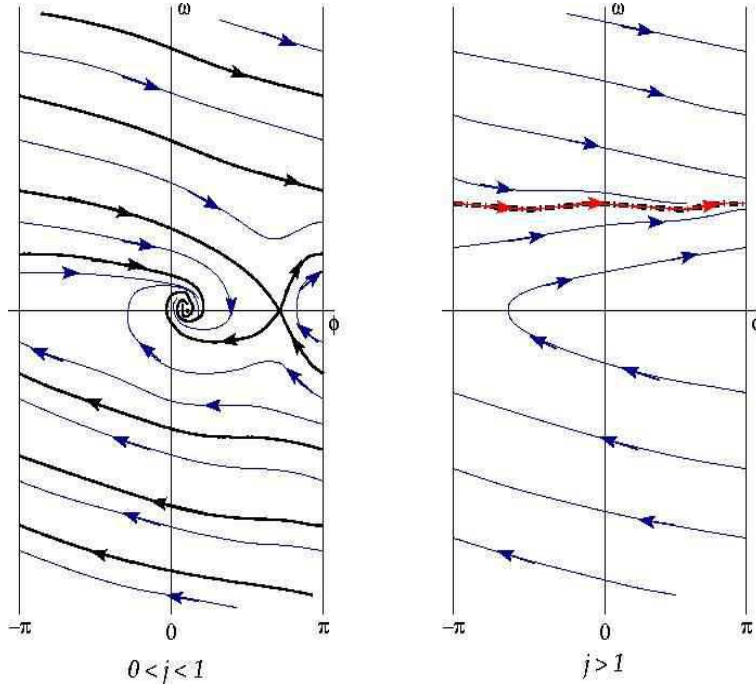


Figure 16.4: Phase flows for the equation $\ddot{\phi} + \gamma^{-1}\dot{\phi} + \sin \phi = j$. Left panel: $0 < j < 1$; note the separatrix (in black), which flows into the stable and unstable fixed points. Right panel: $j > 1$. The red curve overlying the thick black dot-dash curve is a *limit cycle*.

Asymptotically the motion is periodic, with the period T obtained by integrating over the interval $\phi \in [0, 2\pi]$. One finds

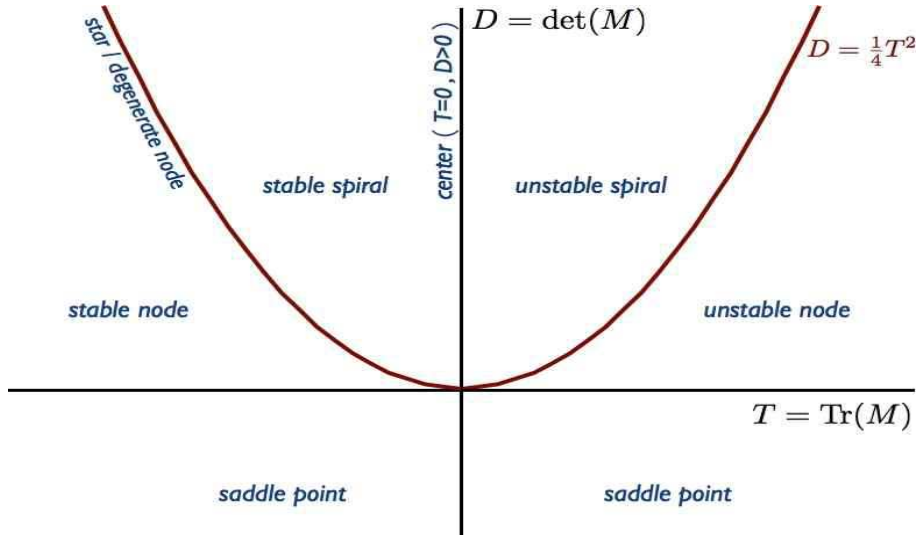
$$T = \frac{\hbar}{2eR} \cdot \frac{2\pi}{\sqrt{I^2 - I_c^2}} . \quad (16.25)$$

The time-averaged voltage drop is then

$$\langle V \rangle = \frac{\hbar}{2e} \langle \dot{\phi} \rangle = \frac{\hbar}{2e} \cdot \frac{2\pi}{T} = R\sqrt{I^2 - I_c^2} . \quad (16.26)$$

This is the physics of the *current-biased resistively and capacitively shunted Josephson junction* in the strong damping limit. It is ‘current-biased’ because we are specifying the current I . Note that Ohm’s law is recovered at large values of I .

For general $\omega_p\tau$, we can still say quite a bit. At a fixed point, both components of the vector field $\mathbf{V}(\phi, \omega)$ must vanish. This requires $\omega = 0$ and $j = \sin \phi$. Therefore, there are two fixed points for $|j| < 1$, one a saddle point and the other a stable spiral. For $|j| > 1$ there are no fixed points, and asymptotically the function $\phi(t)$ tends to a periodic *limit cycle* $\phi_{LC}(t)$. The flow is sketched for two representative values of j in Fig. 16.4.

Figure 16.5: Complete classification of fixed points for the $N = 2$ system.

16.2.2 Classification of $N = 2$ fixed points

Suppose we have solved the fixed point equations $V_x(x^*, y^*) = 0$ and $V_y(x^*, y^*) = 0$. Let us now expand about the fixed point, writing

$$\begin{aligned}\dot{x} &= \frac{\partial V_x}{\partial x} \Bigg|_{(x^*, y^*)} (x - x^*) + \frac{\partial V_x}{\partial y} \Bigg|_{(x^*, y^*)} (y - y^*) + \dots \\ \dot{y} &= \frac{\partial V_y}{\partial x} \Bigg|_{(x^*, y^*)} (x - x^*) + \frac{\partial V_y}{\partial y} \Bigg|_{(x^*, y^*)} (y - y^*) + \dots .\end{aligned}\tag{16.27}$$

We define

$$u_1 = x - x^* \quad , \quad u_2 = y - y^* ,\tag{16.28}$$

which, to linear order, satisfy

$$\frac{d}{dt} \begin{pmatrix} u_1 \\ u_2 \end{pmatrix} = \underbrace{\begin{pmatrix} a & b \\ c & d \end{pmatrix}}_M \begin{pmatrix} u_1 \\ u_2 \end{pmatrix} + \mathcal{O}(u^2) .\tag{16.29}$$

The formal solution to $\dot{\mathbf{u}} = M\mathbf{u}$ is

$$\mathbf{u}(t) = \exp(Mt) \mathbf{u}(0) ,\tag{16.30}$$

where $\exp(Mt) = \sum_{n=0}^{\infty} \frac{1}{n!} (Mt)^n$ is the exponential of the matrix Mt .

The behavior of the system is determined by the eigenvalues of M , which are roots of the characteristic equation $P(\lambda) = 0$, where

$$\begin{aligned}P(\lambda) &= \det(\lambda\mathbb{I} - M) \\ &= \lambda^2 - T\lambda + D ,\end{aligned}\tag{16.31}$$

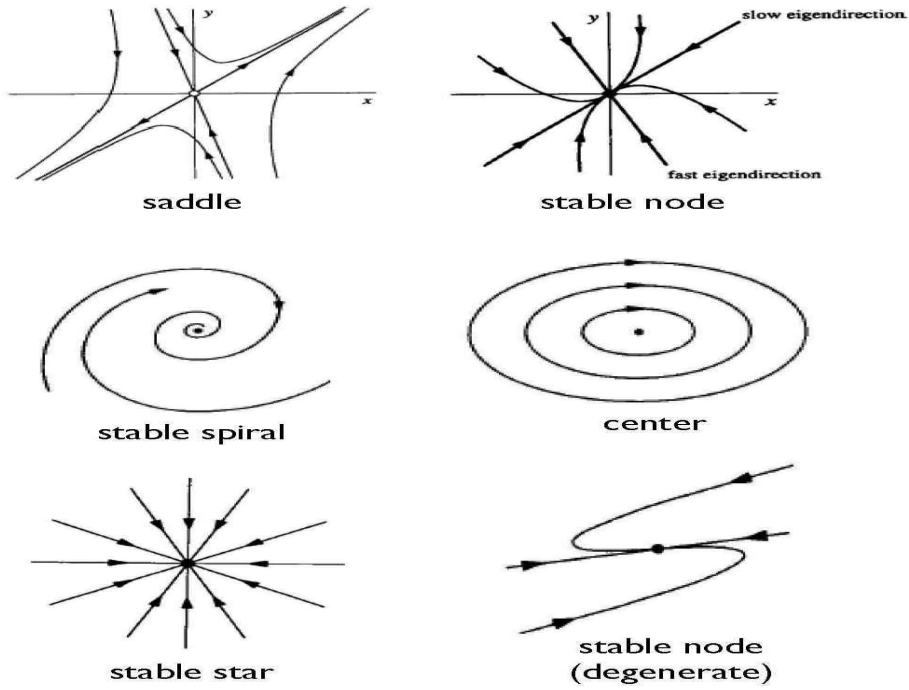


Figure 16.6: Fixed point zoo for $N = 2$ systems. Not shown: unstable versions of node, spiral, and star (reverse direction of arrows to turn stable into unstable).

with $T = a + d = \text{Tr}(M)$ and $D = ad - bc = \det(M)$. The two eigenvalues are therefore

$$\lambda_{\pm} = \frac{1}{2} \left(T \pm \sqrt{T^2 - 4D} \right) . \quad (16.32)$$

To see why the eigenvalues control the behavior, let us expand $\mathbf{u}(0)$ in terms of the eigenvectors of M . Since M is not necessarily symmetric, we should emphasize that we expand $\mathbf{u}(0)$ in terms of the *right* eigenvectors of M , which satisfy

$$M\psi_a = \lambda_a \psi_a , \quad (16.33)$$

where the label a runs over the symbols $+$ and $-$, as in (16.32). We write

$$\mathbf{u}(t) = \sum_a C_a(t) \psi_a . \quad (16.34)$$

Since (we assume) the eigenvectors are *linearly independent*, the equation $\dot{\mathbf{u}} = M\mathbf{u}$ becomes

$$\dot{C}_a = \lambda_a C_a , \quad (16.35)$$

with solution

$$C_a(t) = e^{\lambda_a t} C_a(0) . \quad (16.36)$$

Thus, the coefficients of the eigenvectors ψ_a will *grow* in magnitude if $|\lambda_a| > 1$, and will *shrink* if $|\lambda_a| < 1$.

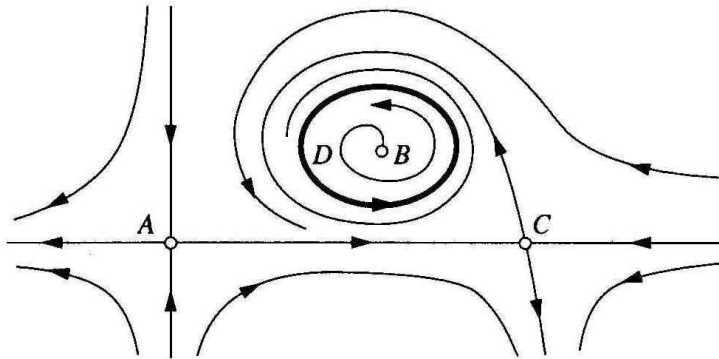


Figure 16.7: Phase portrait for an $N = 2$ flow including saddles (A,C), unstable spiral (B), and limit cycle (D).

16.2.3 The fixed point zoo

- **Saddles** : When $D < 0$, both eigenvalues are real; one is positive and one is negative, i.e. $\lambda_+ > 0$ and $\lambda_- < 0$. The right eigenvector ψ_- is thus the *stable direction* while ψ_+ is the *unstable direction*.
- **Nodes** : When $0 < D < \frac{1}{4}T^2$, both eigenvalues are real and of the same sign. Thus, both right eigenvectors correspond to stable or to unstable directions, depending on whether $T < 0$ (stable; $\lambda_- < \lambda_+ < 0$) or $T > 0$ (unstable; $\lambda_+ > \lambda_- > 0$). If λ_\pm are distinct, one can distinguish *fast* and *slow* eigendirections, based on the magnitude of the eigenvalues.
- **Spirals** : When $D > \frac{1}{4}T^2$, the discriminant $T^2 - 4D$ is negative, and the eigenvalues come in a complex conjugate pair: $\lambda_- = \lambda_+^*$. The real parts are given by $\text{Re}(\lambda_\pm) = \frac{1}{2}T$, so the motion is stable (i.e. collapsing to the fixed point) if $T < 0$ and unstable (i.e. diverging from the fixed point) if $T > 0$. The motion is easily shown to correspond to a spiral. One can check that the spiral rotates counterclockwise for $a > d$ and clockwise for $a < d$.
- **Degenerate Cases** : When $T = 0$ we have $\lambda_\pm = \pm\sqrt{-D}$. For $D < 0$ we have a saddle, but for $D > 0$ both eigenvalues are imaginary: $\lambda_\pm = \pm i\sqrt{D}$. The orbits do not collapse to a point, nor do they diverge to infinity, in the $t \rightarrow \infty$ limit, as they do in the case of the stable and unstable spiral. The fixed point is called a *center*, and it is surrounded by closed trajectories.

When $D = \frac{1}{4}T^2$, the discriminant vanishes and the eigenvalues are degenerate. If the rank of M is two, the fixed point is a stable ($T < 0$) or unstable ($T > 0$) *star*. If M is degenerate and of rank one, the fixed point is a *degenerate node*.

When $D = 0$, one of the eigenvalues vanishes. This indicates a *fixed line* in phase space, since any point on that line will not move. The fixed line can be stable or unstable, depending on whether the remaining eigenvalue is negative (stable, $T < 0$), or positive (unstable, $T > 0$).

16.2.4 Limit cycles

Putting it all together, an example of a phase portrait is shown in Fig. 16.7. Note the presence of an *isolated, closed trajectory*, which is called a *limit cycle*. Many self-sustained physical oscillations, *i.e.* oscillations with no external forcing, exhibit limit cycle behavior. Limit cycles, like fixed points, can be stable or unstable, or partially stable. Limit cycles are inherently nonlinear. While the linear equation $\dot{\varphi} = M\varphi$ can have periodic solutions if M has purely imaginary eigenvalues, these periodic trajectories are not *isolated*, because $\lambda\varphi(t)$ is also a solution. The amplitude of these linear oscillations is fixed by the initial conditions, whereas for limit cycles, the amplitude is inherent from the dynamics itself, and the initial conditions are irrelevant (for a stable limit cycle).

In fig. 16.8 we show simple examples of stable, unstable, and half-stable limit cycles. As we shall see when we study nonlinear oscillations, the Van der Pol oscillator,

$$\ddot{x} + \mu(x^2 - 1)\dot{x} + x = 0 , \quad (16.37)$$

with $\mu > 0$ has a stable limit cycle. The physics is easy to apprehend. The coefficient of the \dot{x} term in the equation of motion is positive for $|x| > 1$ and negative for $|x| < 1$. Interpreting this as a coefficient of friction, we see that the friction is positive, *i.e.* dissipating energy, when $|x| > 1$ but *negative*, *i.e.* accumulating energy, for $|x| < 1$. Thus, any small motion with $|x| < 1$ is *amplified* due to the negative friction, and would increase without bound were it not for the fact that the friction term reverses its sign and becomes dissipative for $|x| > 1$. The limit cycle for $\mu \gg 1$ is shown in fig. 16.9.

16.2.5 Andronov-Hopf bifurcation

A bifurcation between a spiral and a limit cycle is known as an *Andronov-Hopf bifurcation*. As a simple example, consider the $N = 2$ system,

$$\begin{aligned} \dot{x} &= ax - by - C(x^2 + y^2)x \\ \dot{y} &= bx + ay - C(x^2 + y^2)y , \end{aligned} \quad (16.38)$$

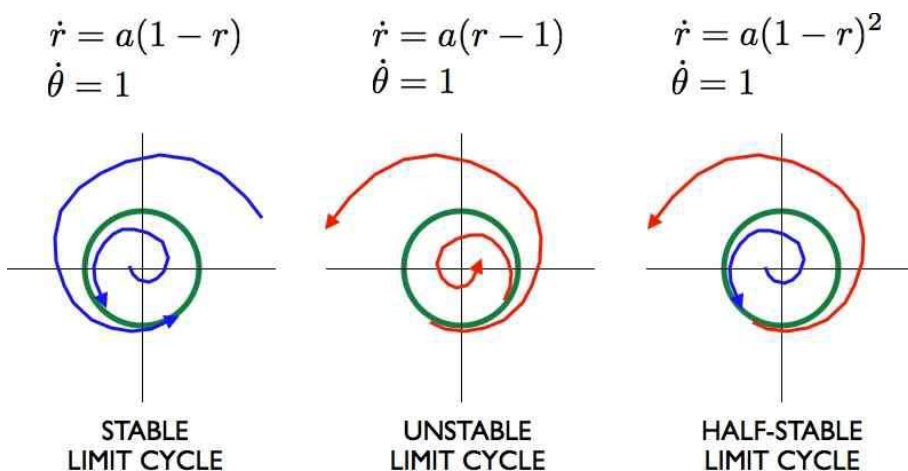


Figure 16.8: Stable, unstable, and half-stable limit cycles.

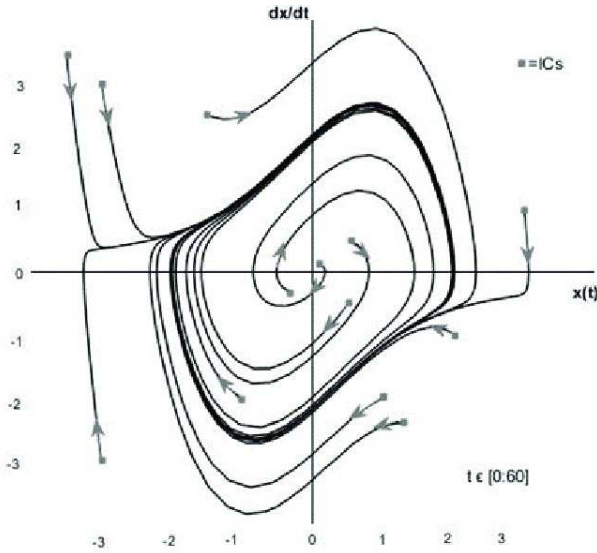


Figure 16.9: Limit cycle of the Van der Pol oscillator for $\mu = 1$.

where a , b , and C are real. Clearly the origin is a fixed point, at which one finds the eigenvalues $\lambda = a \pm ib$. Thus, the fixed point is a stable spiral if $a < 0$ and an unstable spiral if $a > 0$.

Written in terms of the complex variable $z = x + iy$, these two equations collapse to the single equation

$$\dot{z} = (a + ib) z - C |z|^2 z . \quad (16.39)$$

The dynamics are also simple in polar coordinates $r = |z|$, $\theta = \arg(z)$:

$$\begin{aligned} \dot{r} &= ar - Cr^3 \\ \dot{\theta} &= b . \end{aligned} \quad (16.40)$$

The phase diagram, for fixed $b > 0$, is depicted in Fig. 16.10. For positive a/C , there is a limit cycle at $r = \sqrt{a/C}$. In both cases, the limit cycle disappears as a crosses the value $a^* = 0$ and is replaced by a stable ($a < 0, C > 0$) or unstable ($a > 0, C < 0$) spiral.

This example also underscores the following interesting point. Adding a small nonlinear term C has no fundamental effect on the fixed point behavior so long as $a \neq 0$, when the fixed point is a stable or unstable spiral. In general, fixed points which are attractors (stable spirals or nodes), repellers (unstable spirals or nodes), or saddles are *robust* with respect to the addition of a small nonlinearity. But the fixed point behavior in the marginal cases – centers, stars, degenerate nodes, and fixed lines – is strongly affected by the presence of even a small nonlinearity. In this example, the FP is a center when $a = 0$. But as the (r, θ) dynamics shows, a small nonlinearity will destroy the center and turn the FP into an attractor ($C > 0$) or a repeller ($C < 0$).

16.2.6 Fixed points for $N = 3$ systems

For an $N = 2$ system, there are five generic types of fixed points. They are classified according to the eigenvalues of the linearized dynamics at the fixed point. For a real 2×2 matrix, the eigenvalues must

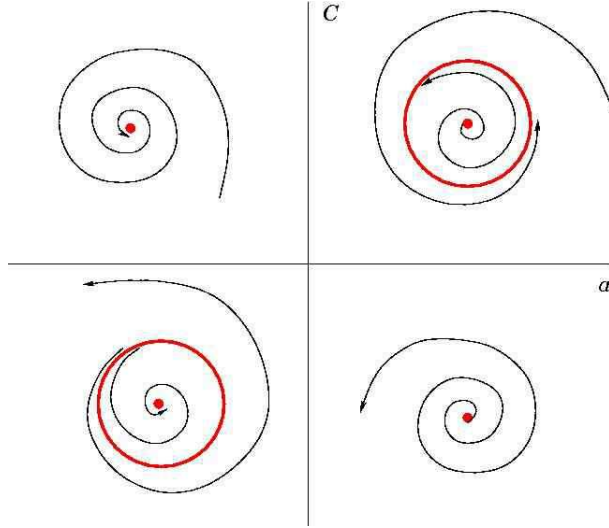


Figure 16.10: Hopf bifurcation: for $C > 0$ the bifurcation is supercritical, between stable spiral and stable limit cycle. For $C < 0$ the bifurcation is subcritical, between unstable spiral and unstable limit cycle. The bifurcation occurs at $a = 0$ in both cases.

be real or else must be a complex conjugate pair. The five types of fixed points are then

- | | | |
|--|---|---------------------|
| $\lambda_1 > 0, \lambda_2 > 0$ | : | (1) unstable node |
| $\lambda_1 > 0, \lambda_2 < 0$ | : | (2) saddle point |
| $\lambda_1 < 0, \lambda_2 < 0$ | : | (3) stable node |
| $\operatorname{Re} \lambda_1 > 0, \lambda_2 = \lambda_1^*$ | : | (4) unstable spiral |
| $\operatorname{Re} \lambda_1 < 0, \lambda_2 = \lambda_1^*$ | : | (5) stable spiral |

How many possible generic fixed points are there for an $N = 3$ system?

For a general real 3×3 matrix M , the characteristic polynomial $P(\lambda) = \det(\lambda - M)$ satisfies $P(\lambda^*) = P(\lambda)$. Thus, if λ is a root then so is λ^* . This means that the eigenvalues are either real or else come in complex conjugate pairs. There are then ten generic possibilities for the three eigenvalues:

- | | | | |
|------|-------------------------|---|--|
| (1) | unstable node | : | $\lambda_1 > \lambda_2 > \lambda_3 > 0$ |
| (2) | ($++-$) saddle | : | $\lambda_1 > \lambda_2 > 0 > \lambda_3$ |
| (3) | ($+--$) saddle | : | $\lambda_1 > 0 > \lambda_2 > \lambda_3$ |
| (4) | stable node | : | $0 > \lambda_1 > \lambda_2 > \lambda_3$ |
| (5) | unstable spiral-node | : | $\lambda_1 > \operatorname{Re} \lambda_{2,3} > 0 ; \operatorname{Im} \lambda_2 = -\operatorname{Im} \lambda_3$ |
| (6) | unstable spiral-node | : | $\operatorname{Re} \lambda_{1,2} > \lambda_3 > 0 ; \operatorname{Im} \lambda_1 = -\operatorname{Im} \lambda_2$ |
| (7) | stable spiral-node | : | $0 > \lambda_1 > \operatorname{Re} \lambda_{2,3} ; \operatorname{Im} \lambda_2 = -\operatorname{Im} \lambda_3$ |
| (8) | stable spiral-node | : | $0 > \operatorname{Re} \lambda_{1,2} > \lambda_3 ; \operatorname{Im} \lambda_1 = -\operatorname{Im} \lambda_2$ |
| (9) | ($+--$) spiral-saddle | : | $\lambda_1 > 0 > \operatorname{Re} \lambda_{2,3} ; \operatorname{Im} \lambda_2 = -\operatorname{Im} \lambda_3$ |
| (10) | ($++-$) spiral-saddle | : | $\operatorname{Re} \lambda_{1,2} > 0 > \lambda_3 ; \operatorname{Im} \lambda_1 = -\operatorname{Im} \lambda_2 .$ |

16.3 Population Biology : Lotka-Volterra Models

Consider two species with populations N_1 and N_2 , respectively. We model the evolution of these populations by the coupled ODEs

$$\begin{aligned}\frac{dN_1}{dt} &= aN_1 + bN_1N_2 + cN_1^2 \\ \frac{dN_2}{dt} &= dN_2 + eN_1N_2 + fN_2^2,\end{aligned}\tag{16.41}$$

where $\{a, b, c, d, e, f\}$ are constants. We can eliminate some constants by rescaling $N_{1,2}$. This results in the following:

$$\begin{aligned}\dot{x} &= x(r - \mu x - ky) \\ \dot{y} &= y(r' - \mu'y - k'x)\end{aligned},\tag{16.42}$$

where μ , and μ' can each take on one of three possible values $\{0, \pm 1\}$. By rescaling time, we can eliminate the scale of either of r or r' as well. Typically, intra-species competition guarantees $\mu = \mu' = +1$. The remaining coefficients (r, k, k') are real may also be of either sign. The values and especially the signs of the various coefficients have a physical (or biological) significance. For example, if $k < 0$ it means that x grows due to the presence of y . The effect of y on x may be of the same sign ($kk' > 0$) or of opposite sign ($kk' < 0$).

16.3.1 Rabbits and foxes

As an example, consider the model

$$\begin{aligned}\dot{x} &= x - xy \\ \dot{y} &= -\beta y + xy.\end{aligned}\tag{16.43}$$

The quantity x might represent the (scaled) population of rabbits and y the population of foxes in an ecosystem. There are two fixed points: at $(0, 0)$ and at $(\beta, 1)$. Linearizing the dynamics about these fixed points, one finds that $(0, 0)$ is a saddle while $(\beta, 1)$ is a center. Let's do this explicitly.

The first step is to find the fixed points (x^*, y^*) . To do this, we set $\dot{x} = 0$ and $\dot{y} = 0$. From $\dot{x} = x(1-y) = 0$ we have that $x = 0$ or $y = 1$. Suppose $x = 0$. The second equation, $\dot{y} = (x - \beta)y$ then requires $y = 0$. So $\mathbf{P}_1 = (0, 0)$ is a fixed point. The other possibility is that $y = 1$, which then requires $x = \beta$. So $\mathbf{P}_2 = (\beta, 1)$ is the second fixed point. Those are the only possibilities.

We now compute the linearized dynamics at these fixed points. The linearized dynamics are given by $\dot{\varphi} = M\varphi$, with

$$M = \begin{pmatrix} \partial\dot{x}/\partial x & \partial\dot{x}/\partial y \\ \partial\dot{y}/\partial x & \partial\dot{y}/\partial y \end{pmatrix} = \begin{pmatrix} 1-y & -x \\ y & x-\beta \end{pmatrix}.\tag{16.44}$$

Evaluating M at \mathbf{P}_1 and \mathbf{P}_2 , we find

$$M_1 = \begin{pmatrix} 1 & 0 \\ 0 & -\beta \end{pmatrix}, \quad M_2 = \begin{pmatrix} 0 & -\beta \\ 1 & 0 \end{pmatrix}. \quad (16.45)$$

The eigenvalues are easily found:

$$\begin{aligned} \mathbf{P}_1 : \lambda_+ &= 1, \lambda_- = -\beta \\ \mathbf{P}_2 : \lambda_+ &= i\sqrt{\beta}, \lambda_- = -i\sqrt{\beta}. \end{aligned} \quad (16.46)$$

Thus \mathbf{P}_1 is a saddle point and \mathbf{P}_2 is a center.

As we saw earlier, generally speaking we expect nonlinear terms to transform centers to stable or unstable spirals, possibly with a limit cycle. However for the Lotka-Volterra system there is a conserved quantity. Consider the general predator-prey system

$$\begin{aligned} \dot{x} &= (a - b y) x \\ \dot{y} &= -(c - d x) y, \end{aligned} \quad (16.47)$$

where a , b , c , and d are all positive constants. Now consider the function

$$H \equiv dx + b y - c \ln x - a \ln y. \quad (16.48)$$

Then

$$\frac{\partial H}{\partial x} = d - \frac{c}{x}, \quad \frac{\partial H}{\partial y} = b. \quad (16.49)$$

Thus, we have $\dot{x} = -xy \frac{\partial H}{\partial y}$ and $\dot{y} = xy \frac{\partial H}{\partial x}$. If we define $p \equiv \ln x$ and $q \equiv \ln y$, then we have

$$\dot{q} = \frac{\partial H}{\partial p}, \quad \dot{p} = -\frac{\partial H}{\partial q} \quad (16.50)$$

with

$$H(q, p) = d e^p + b e^q - c p - a q. \quad (16.51)$$

So the system is a Hamiltonian system in disguise, and we know that for Hamiltonian systems the only possible fixed points are saddles and centers. The phase curves are level sets of the function H .

16.3.2 Rabbits and sheep

In the rabbits and foxes model of eqs. 16.43, the rabbits are the food for the foxes. This means $k = 1$ but $k' = -1$, *i.e.* the fox population is enhanced by the presence of rabbits, but the rabbit population is diminished by the presence of foxes. Consider now a model in which the two species (rabbits and sheep, say) compete for food:

$$\begin{aligned} \dot{x} &= x(r - x - ky) \\ \dot{y} &= y(1 - y - k'x), \end{aligned} \quad (16.52)$$

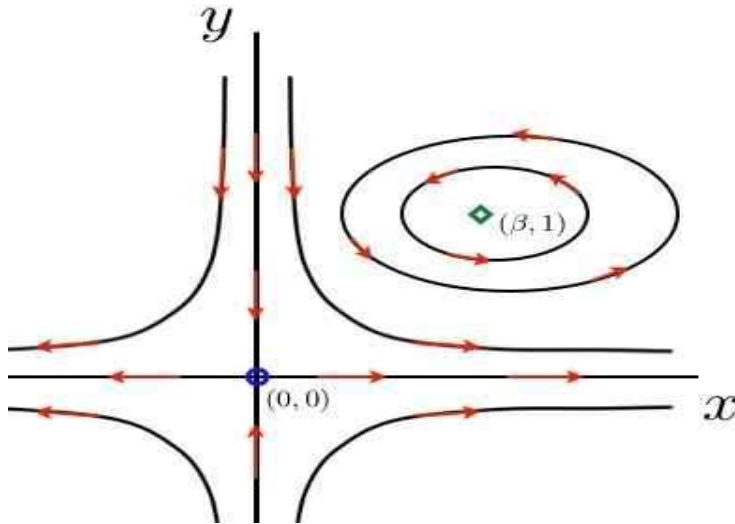


Figure 16.11: Phase flow for the rabbits *vs.* foxes Lotka-Volterra model of eqs. 16.43.

with r , k , and k' all positive. Note that when either population x or y vanishes, the remaining population is governed by the logistic equation, *i.e.* it will flow to a nonzero fixed point.

The matrix of derivatives, which is to be evaluated at each fixed point in order to assess its stability, is

$$M = \begin{pmatrix} \partial \dot{x} / \partial x & \partial \dot{x} / \partial y \\ \partial \dot{y} / \partial x & \partial \dot{y} / \partial y \end{pmatrix} = \begin{pmatrix} r - 2x - ky & -kx \\ -k'y & 1 - 2y - k'x \end{pmatrix}. \quad (16.53)$$

At each fixed point, we must evaluate $D = \det(M)$ and $T = \text{Tr}(M)$ and apply the classification scheme of Fig. 16.5.

- $\mathbf{P}_1 = (0, 0)$: This is the trivial state with no rabbits ($x = 0$) and no sheep ($y = 0$). The linearized dynamics gives $M_1 = \begin{pmatrix} r & 0 \\ 0 & 1 \end{pmatrix}$, which corresponds to an unstable node.
- $\mathbf{P}_2 = (r, 0)$: Here we have rabbits but no sheep. The linearized dynamics gives $M_2 = \begin{pmatrix} -r & -rk \\ 0 & 1 - rk' \end{pmatrix}$. For $rk' > 1$ this is a stable node; for $rk' < 1$ it is a saddle point.
- $\mathbf{P}_3 = (0, 1)$: Here we have sheep but no rabbits. The linearized dynamics gives $M_3 = \begin{pmatrix} r - k & 0 \\ -k' & -1 \end{pmatrix}$. For $k > r$ this is a stable node; for $k < r$ it is a saddle.
- There is one remaining fixed point – a nontrivial one where both x and y are nonzero. To find it, we set $\dot{x} = \dot{y} = 0$, and divide out by x and y respectively, to get

$$\begin{aligned} x + ky &= r \\ kx' + y &= 1. \end{aligned} \quad (16.54)$$

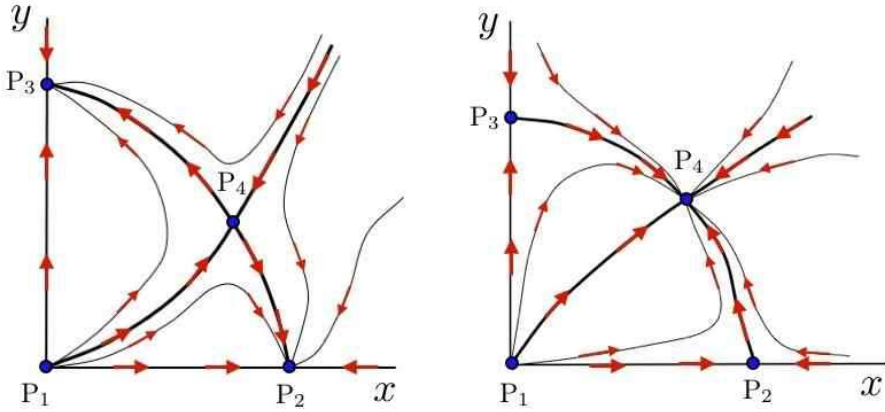


Figure 16.12: Two possible phase flows for the rabbits *vs.* sheep model of eqs. 16.52. Left panel: $k > r > k'^{-1}$. Right panel: $k < r < k'^{-1}$.

This is a simple rank 2 inhomogeneous linear system. If the fixed point \mathbf{P}_4 is to lie in the physical quadrant ($x > 0, y > 0$), then either (i) $k > r$ and $k' > r^{-1}$ or (ii) $k < r$ and $k' < r^{-1}$. The solution is

$$\mathbf{P}_4 = \begin{pmatrix} 1 & k \\ k' & 1 \end{pmatrix}^{-1} \begin{pmatrix} r \\ 1 \end{pmatrix} = \frac{1}{1 - kk'} \begin{pmatrix} r - k \\ 1 - rk' \end{pmatrix}. \quad (16.55)$$

The linearized dynamics then gives

$$M_4 = \frac{1}{1 - kk'} \begin{pmatrix} k - r & k(k - r) \\ k'(rk' - 1) & rk' - 1 \end{pmatrix}, \quad (16.56)$$

yielding

$$\begin{aligned} T &= \frac{rk' - 1 + k - r}{1 - kk'} \\ D &= \frac{(k - r)(rk' - 1)}{1 - kk'} . \end{aligned} \quad (16.57)$$

The classification of this fixed point can vary with parameters. Consider the case $r = 1$. If $k = k' = 2$ then both \mathbf{P}_2 and \mathbf{P}_3 are stable nodes. At \mathbf{P}_4 , one finds $T = -\frac{2}{3}$ and $D = -\frac{1}{3}$, corresponding to a saddle point. In this case it is the fate of one population to die out at the expense of the other, and which one survives depends on initial conditions. If instead we took $k = k' = \frac{1}{2}$, then $T = -\frac{4}{3}$ and $D = \frac{1}{3}$, corresponding to a stable node (node $D < \frac{1}{4}T^2$ in this case). The situation is depicted in Fig. 16.12.

16.4 Poincaré-Bendixson Theorem

Although $N = 2$ systems are much richer than $N = 1$ systems, they are still ultimately rather impoverished in terms of their long-time behavior. If an orbit does not flow off to infinity or asymptotically

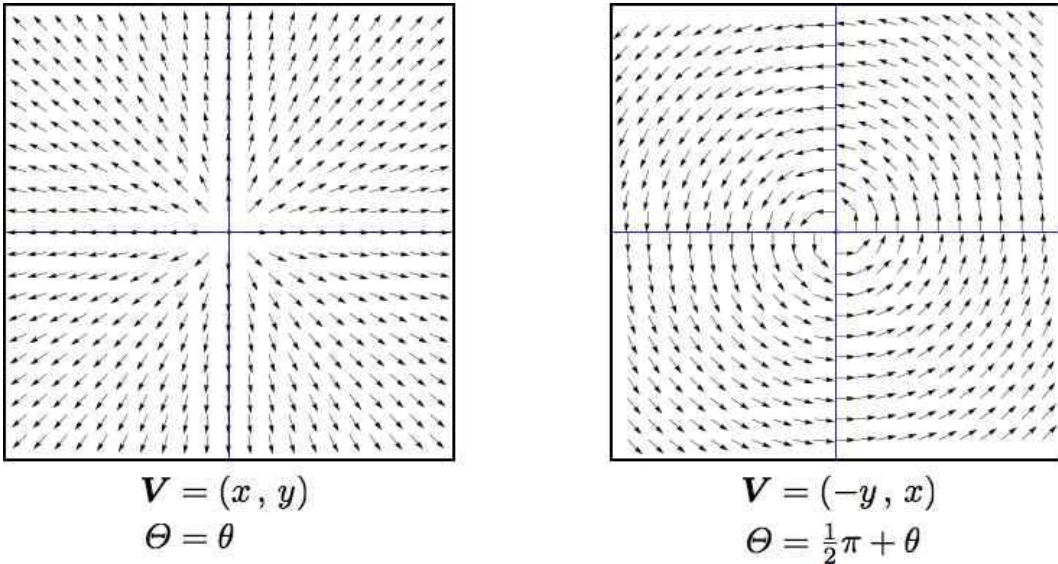


Figure 16.13: Two singularities with index +1. The direction field $\hat{\mathbf{V}} = \mathbf{V}/|\mathbf{V}|$ is shown in both cases.

approach a stable fixed point (node or spiral or nongeneric example), the only remaining possibility is limit cycle behavior. This is the content of the *Poincaré-Bendixson theorem*, which states:

- IF Ω is a compact (*i.e.* closed and bounded) subset of phase space,
- AND $\dot{\varphi} = \mathbf{V}(\varphi)$ is continuously differentiable on Ω ,
- AND Ω contains no fixed points (*i.e.* $\mathbf{V}(\varphi)$ never vanishes in Ω),
- AND a phase curve $\varphi(t)$ is always confined to Ω ,
- ◊ THEN $\varphi(t)$ is either closed or approaches a closed trajectory in the limit $t \rightarrow \infty$.

Thus, under the conditions of the theorem, Ω must contain a closed orbit.

One way to prove that $\varphi(t)$ is confined to Ω is to establish that $\mathbf{V} \cdot \hat{\mathbf{n}} \leq 0$ everywhere on the boundary $\partial\Omega$, which means that the phase flow is always directed inward (or tangent) along the boundary. Let's analyze an example from the book by Strogatz. Consider the system

$$\begin{aligned}\dot{r} &= r(1 - r^2) + \lambda r \cos \theta \\ \dot{\theta} &= 1,\end{aligned}\tag{16.58}$$

with $0 < \lambda < 1$. Then define

$$a \equiv \sqrt{1 - \lambda} \quad , \quad b \equiv \sqrt{1 + \lambda} \tag{16.59}$$

and

$$\Omega \equiv \left\{ (r, \theta) \mid a < r < b \right\}. \tag{16.60}$$

On the boundaries of Ω , we have

$$\begin{aligned} r = a : \dot{r} &= \lambda a (1 + \cos \theta) \\ r = b : \dot{r} &= -\lambda b (1 - \cos \theta) . \end{aligned} \quad (16.61)$$

We see that the radial component of the flow is inward along both $r = a$ and $r = b$. Thus, any trajectory which starts inside Ω can never escape. The Poincaré-Bendixson theorem tells us that the trajectory will approach a stable limit cycle in the limit $t \rightarrow \infty$.

It is only with $N \geq 3$ systems that the interesting possibility of chaotic behavior emerges.

16.5 Index Theory

Consider a smooth two-dimensional vector field $\mathbf{V}(\varphi)$. The angle that the vector \mathbf{V} makes with respect to the $\hat{\varphi}_1$ and $\hat{\varphi}_2$ axes is a scalar field,

$$\Theta(\varphi) = \tan^{-1} \left(\frac{V_2(\varphi)}{V_1(\varphi)} \right) . \quad (16.62)$$

So long as \mathbf{V} has finite length, the angle Θ is well-defined. In particular, we expect that we can integrate $\nabla \Theta$ over a closed curve \mathcal{C} in phase space to get

$$\oint_{\mathcal{C}} d\varphi \cdot \nabla \Theta = 0 . \quad (16.63)$$

However, this can fail if $\mathbf{V}(\varphi)$ vanishes (or diverges) at one or more points in the interior of \mathcal{C} . In general, if we define

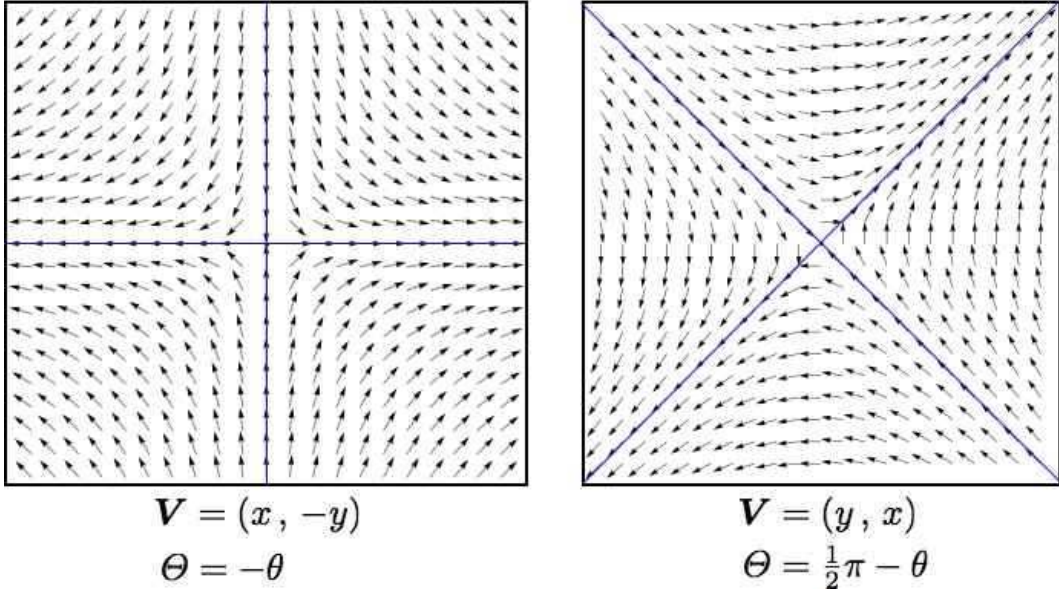
$$W_{\mathcal{C}}(\mathbf{V}) = \frac{1}{2\pi} \oint_{\mathcal{C}} d\varphi \cdot \nabla \Theta , \quad (16.64)$$

then $W_{\mathcal{C}}(\mathbf{V}) \in \mathbb{Z}$ is an integer valued function of \mathcal{C} , which is the change in Θ around the curve \mathcal{C} . This must be an integer, because Θ is well-defined only up to multiples of 2π . Note that *differential changes* of Θ are in general well-defined.

Thus, if $\mathbf{V}(\varphi)$ is finite, meaning neither infinite nor infinitesimal, *i.e.* \mathbf{V} neither diverges nor vanishes anywhere in $\text{int}(\mathcal{C})$, then $W_{\mathcal{C}}(\mathbf{V}) = 0$. Assuming that \mathbf{V} never diverges, any singularities in Θ must arise from points where $\mathbf{V} = 0$, which in general occurs at isolated points, since it entails two equations in the two variables (φ_1, φ_2) .

The index of a two-dimensional vector field $\mathbf{V}(\varphi)$ at a *point* φ is the integer-valued winding of \mathbf{V} about that point:

$$\begin{aligned} \text{ind}(\mathbf{V}) &= \lim_{\varphi_0 \rightarrow 0} \frac{1}{2\pi} \oint_{\mathcal{C}_{\varphi_0}(\varphi_0)} d\varphi \cdot \nabla \Theta \\ &= \lim_{\varphi_0 \rightarrow 0} \frac{1}{2\pi} \oint_{\mathcal{C}_{\varphi_0}(\varphi_0)} d\varphi \cdot \frac{V_1 \nabla V_2 - V_2 \nabla V_1}{V_1^2 + V_2^2} , \end{aligned} \quad (16.65)$$

Figure 16.14: Two singularities with index -1 .

where $\mathcal{C}_a(\varphi_0)$ is a circle of radius a surrounding the point φ_0 . The index of a closed curve \mathcal{C} is given by the sum of the indices at all the singularities enclosed by the curve:²

$$W_{\mathcal{C}}(\mathbf{V}) = \sum_{\varphi_i \in \text{int}(\mathcal{C})} \text{ind}(\mathbf{V}) . \quad (16.66)$$

As an example, consider the vector fields plotted in fig. 16.13. We have:

$$\begin{aligned} \mathbf{V} = (x, -y) &\implies \Theta = -\theta \\ \mathbf{V} = (-y, x) &\implies \Theta = \theta + \frac{1}{2}\pi . \end{aligned} \quad (16.67)$$

The index is the same, $+1$, in both cases, even though the first corresponds to an unstable node and the second to a center. Any $N = 2$ fixed point with $\det M > 0$ has index $+1$.

Fig. 16.14 shows two vector fields, each with index -1 :

$$\begin{aligned} \mathbf{V} = (x, y) &\implies \Theta = \theta \\ \mathbf{V} = (y, x) &\implies \Theta = -\theta + \frac{1}{2}\pi \end{aligned} \quad (16.68)$$

In both cases, the fixed point is a saddle.

As an example of the content of eqn. 16.66, consider the vector fields in eqn. 16.15. The left panel shows the vector field $\mathbf{V} = (x^2 - y^2, 2xy)$, which has a single fixed point, at the origin $(0, 0)$, of index $+2$. The

²Technically, we should weight the index at each enclosed singularity by the signed number of times the curve \mathcal{C} encloses that singularity. For simplicity and clarity, we assume that the curve \mathcal{C} is homeomorphic to the circle \mathbb{S}^1 .

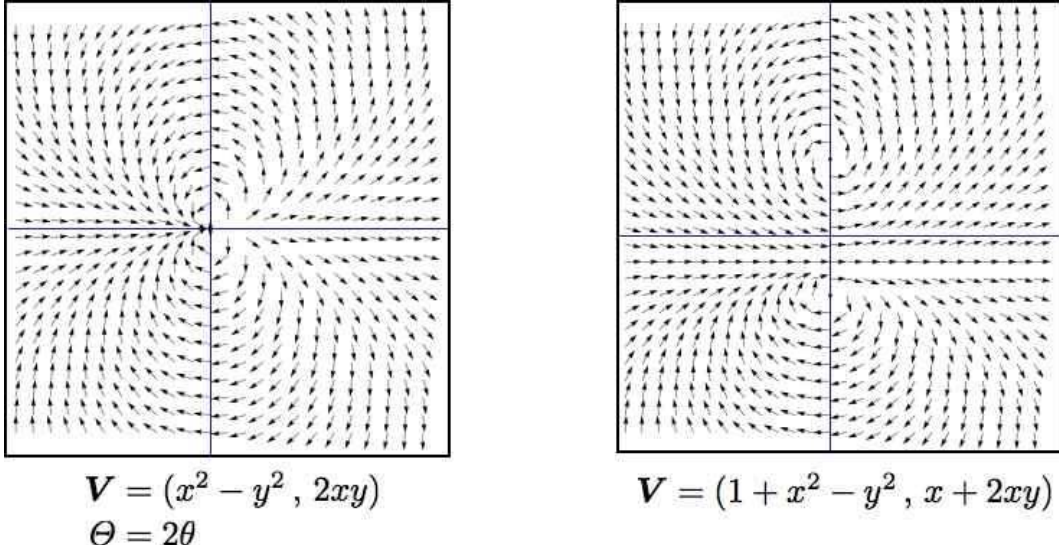


Figure 16.15: Left panel: a singularity with index +2. Right panel: two singularities each with index +1. Note that the long distance behavior of \mathbf{V} is the same in both cases.

right panel shows the vector field $\mathbf{V} = (1 + x^2 - y^2, x + 2xy)$, which has fixed points (x^*, y^*) at $(0, 1)$ and $(0, -1)$. The linearized dynamics is given by the matrix

$$M = \begin{pmatrix} \frac{\partial \dot{x}}{\partial x} & \frac{\partial \dot{x}}{\partial y} \\ \frac{\partial \dot{y}}{\partial x} & \frac{\partial \dot{y}}{\partial y} \end{pmatrix} = \begin{pmatrix} 2x & -2y \\ 1 + 2y & 2x \end{pmatrix}. \quad (16.69)$$

Thus,

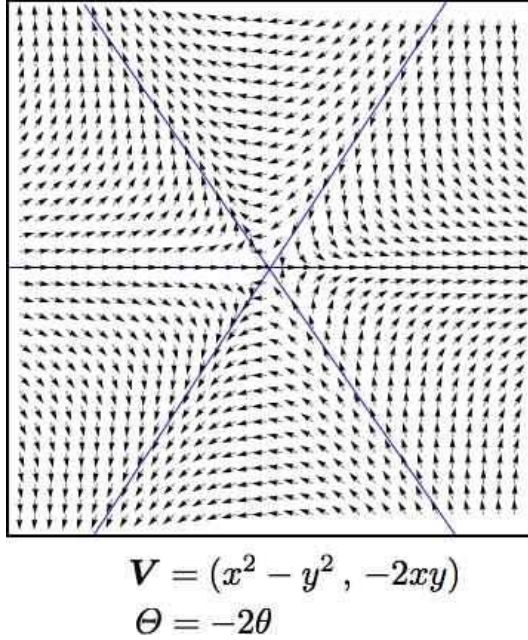
$$M_{(0,1)} = \begin{pmatrix} 0 & -2 \\ 2 & 0 \end{pmatrix}, \quad M_{(0,-1)} = \begin{pmatrix} 0 & 2 \\ -2 & 0 \end{pmatrix}. \quad (16.70)$$

At each of these fixed points, we have $T = 0$ and $D = 4$, corresponding to a center, with index +1. If we consider a square-ish curve \mathcal{C} around the periphery of each figure, the vector field is almost the same along such a curve for both the left and right panels, and the winding number is $W_{\mathcal{C}}(\mathbf{V}) = +2$.

Finally, consider the vector field shown in fig. 16.16, with $\mathbf{V} = (x^2 - y^2, -2xy)$. Clearly $\Theta = -2\theta$, and the index of the singularity at $(0, 0)$ is -2 .

To recapitulate some properties of the index / winding number:

- The index $\text{ind}_{\varphi_0}(\mathbf{V})$ of an $N = 2$ vector field \mathbf{V} at a point φ_0 is the winding number of \mathbf{V} about that point.
- The winding number $W_{\mathcal{C}}(\mathbf{V})$ of a curve \mathcal{C} is the sum of the indices of the singularities enclosed by that curve.
- Smooth deformations of \mathcal{C} do not change its winding number. One must instead “stretch” \mathcal{C} over a fixed point singularity in order to change $W_{\mathcal{C}}(\mathbf{V})$.

Figure 16.16: A vector field with index -2 .

- Uniformly rotating each vector in the vector field by an angle β has the effect of sending $\Theta \rightarrow \Theta + \beta$; this leaves all indices and winding numbers invariant.
- Nodes and spirals, whether stable or unstable, have index $+1$ (ss do the special cases of centers, stars, and degenerate nodes). Saddle points have index -1 .
- Clearly any closed orbit must lie on a curve \mathcal{C} of index $+1$.

16.5.1 Gauss-Bonnet Theorem

There is a deep result in mathematics, the Gauss-Bonnet theorem, which connects the local *geometry* of a two-dimensional manifold to its global *topological structure*. The content of the theorem is as follows:

$$\int_{\mathcal{M}} dA K = 2\pi \chi(\mathcal{M}) = 2\pi \sum_i \text{ind}(\mathbf{V}) , \quad (16.71)$$

where \mathcal{M} is a 2-manifold (a topological space locally homeomorphic to \mathbb{R}^2), K is the local *Gaussian curvature* of \mathcal{M} , which is given by $K = (R_1 R_2)^{-1}$, where $R_{1,2}$ are the principal radii of curvature at a given point, and dA is the differential area element. The quantity $\chi(\mathcal{M})$ is called the *Euler characteristic* of \mathcal{M} and is given by $\chi(\mathcal{M}) = 2 - 2g$, where g is the *genus* of \mathcal{M} , which is the number of holes (or handles) of \mathcal{M} . Furthermore, $\mathbf{V}(\varphi)$ is *any* smooth vector field on \mathcal{M} , and φ_i are the singularity points of that vector field, which are fixed points of the dynamics $\dot{\varphi} = \mathbf{V}(\varphi)$.

To apprehend the content of the Gauss-Bonnet theorem, it is helpful to consider an example. Let $\mathcal{M} = \mathbb{S}^2$ be the unit 2-sphere, as depicted in fig. 16.17. At any point on the unit 2-sphere, the radii of curvature

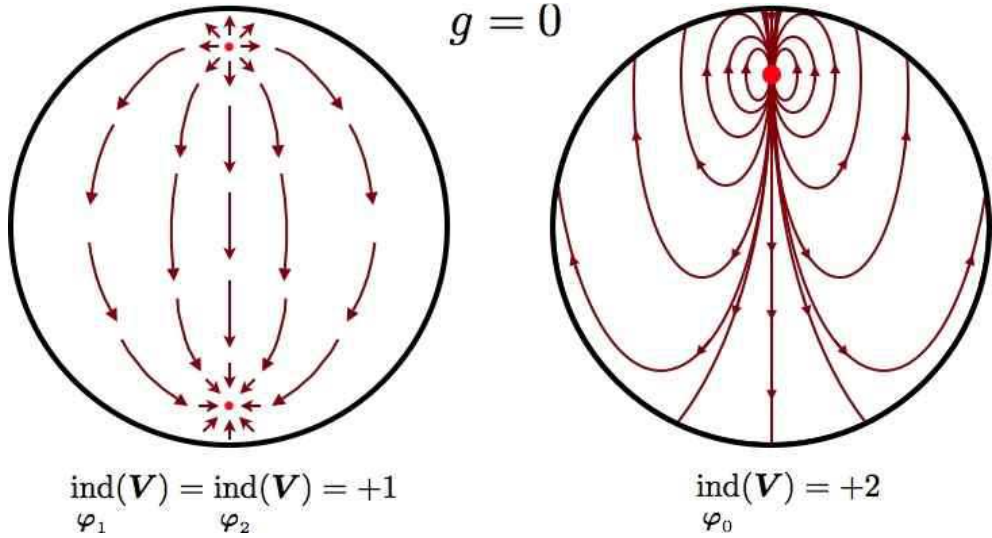


Figure 16.17: Two smooth vector fields on the sphere S^2 , which has genus $g = 0$. Left panel: two index +1 singularities. Right panel: one index +2 singularity.

are degenerate and both equal to $R = 1$, hence $K = 1$. If we integrate the Gaussian curvature over the sphere, we thus get $4\pi = 2\pi \chi(S^2)$, which says $\chi(S^2) = 2 - 2g = 2$, which agrees with $g = 0$ for the sphere. Furthermore, the Gauss-Bonnet theorem says that *any* smooth vector field on S^2 *must* have a singularity or singularities, with the total index summed over the singularities equal to +2. The vector field sketched in the left panel of fig. 16.17 has two index +1 singularities, which could be taken at the north and south poles, but which could be anywhere. Another possibility, depicted in the right panel of fig. 16.17, is that there is a one singularity with index +2.

In fig. 16.18 we show examples of manifolds with genii $g = 1$ and $g = 2$. The case $g = 1$ is the familiar 2-torus, which is topologically equivalent to a product of circles: $T^2 \simeq S^1 \times S^1$, and is thus coordinatized by two angles θ_1 and θ_2 . A smooth vector field pointing in the direction of increasing θ_1 never vanishes, and thus has no singularities, consistent with $g = 1$ and $\chi(T^2) = 0$. Topologically, one can define a torus as the quotient space $\mathbb{R}^2/\mathbb{Z}^2$, or as a square with opposite sides identified. This is what mathematicians call a ‘flat torus’ – one with curvature $K = 0$ everywhere. Of course, such a torus cannot be embedded in three-dimensional Euclidean space; a two-dimensional figure embedded in a three-dimensional Euclidean space inherits a metric due to the embedding, and for a physical torus, like the surface of a bagel, the Gaussian curvature is only zero *on average*.

The $g = 2$ surface \mathcal{M} shown in the right panel of fig. 16.18 has Euler characteristic $\chi(\mathcal{M}) = -2$, which means that any smooth vector field on \mathcal{M} must have singularities with indices totalling -2 . One possibility, depicted in the figure, is to have two saddle points with index -1 ; one of these singularities is shown in the figure (the other would be on the opposite side).

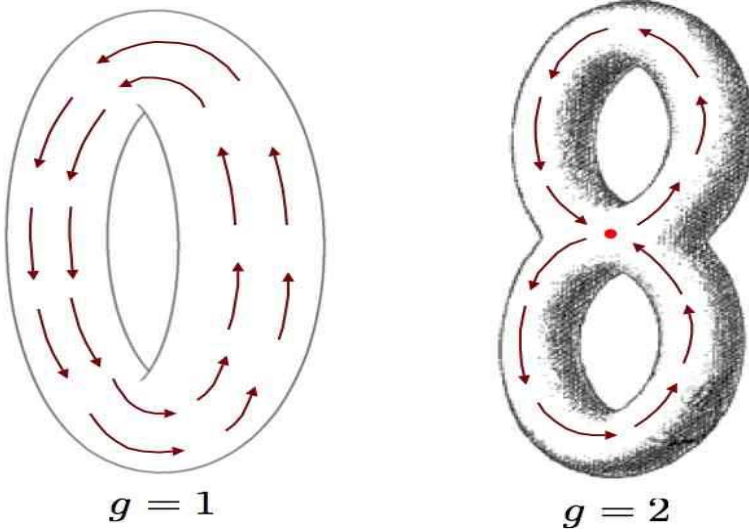


Figure 16.18: Smooth vector fields on the torus \mathbb{T}^2 ($g = 1$), and on a 2-manifold \mathcal{M} of genus $g = 2$.

16.5.2 Singularities and topology

For any $N = 1$ system $\dot{x} = f(x)$, we can identify a ‘charge’ Q with any generic fixed point x^* by setting

$$Q = \text{sgn}\left[f'(x^*)\right], \quad (16.72)$$

where $f(x^*) = 0$. The total charge contained in a region $[x_1, x_2]$ is then

$$Q_{12} = \frac{1}{2} \text{sgn}\left[f(x_2)\right] - \frac{1}{2} \text{sgn}\left[f(x_1)\right]. \quad (16.73)$$

It is easy to see that Q_{12} is the sum of the charges of all the fixed points lying within the interval $[x_1, x_2]$.

In higher dimensions, we have the following general construction. Consider an N -dimensional dynamical system $\dot{\mathbf{x}} = \mathbf{V}(\mathbf{x})$, and let $\hat{\mathbf{n}}(\mathbf{x})$ be the unit vector field defined by

$$\hat{\mathbf{n}}(\mathbf{x}) = \frac{\mathbf{V}(\mathbf{x})}{|\mathbf{V}(\mathbf{x})|}. \quad (16.74)$$

Consider now a unit sphere in $\hat{\mathbf{n}}$ space, which is of dimension $(N - 1)$. If we integrate over this surface, we obtain

$$\Omega_N = \oint d\sigma_a n^a = \frac{2\pi^{(N-1)/2}}{\Gamma(\frac{N-1}{2})}, \quad (16.75)$$

which is the surface area of the unit sphere \mathbb{S}^{N-1} . Thus, $\Omega_2 = 2\pi$, $\Omega_3 = 4\pi$, $\Omega_4 = 2\pi^2$, etc.

Now consider a change of variables over the surface of the sphere, to the set $(\xi_1, \dots, \xi_{N-1})$. We then have

$$\Omega_N = \oint_{\mathbb{S}^{N-1}} d\sigma_a n^a = \oint d^{N-1}\xi \epsilon_{a_1 \dots a_N} n^{a_1} \frac{\partial n^{a_2}}{\partial \xi_1} \dots \frac{\partial n^{a_N}}{\partial \xi_{N-1}} \quad (16.76)$$

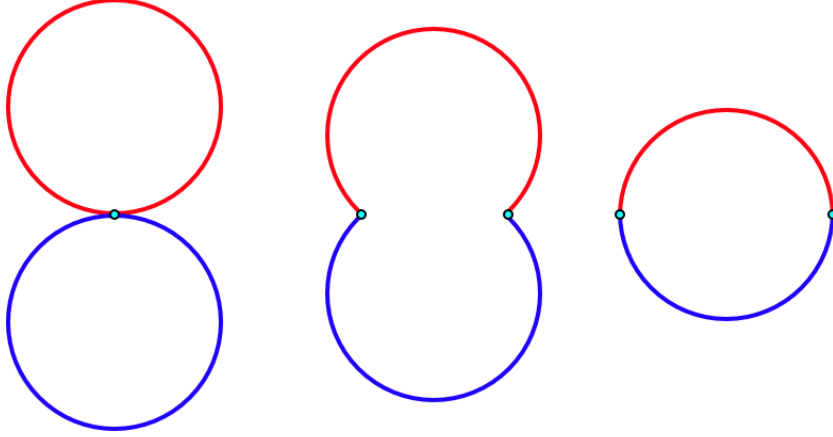


Figure 16.19: Composition of two circles. The same general construction applies to the merging of n -spheres \mathbb{S}^n , called the *wedge sum*.

The topological charge is then

$$Q = \frac{1}{\Omega_N} \oint d^{N-1}\xi \epsilon_{a_1 \dots a_N} n^{a_1} \frac{\partial n^{a_2}}{\partial \xi_1} \dots \frac{\partial n^{a_N}}{\partial \xi_{N-1}} \quad (16.77)$$

The quantity Q is an *integer topological invariant* which characterizes the map from the surface $(\xi_1, \dots, \xi_{N-1})$ to the unit sphere $|\hat{n}| = 1$. In mathematical parlance, Q is known as the *Pontrjagin index* of this map.

This analytical development recapitulates some basic topology. Let \mathcal{M} be a topological space and consider a map from the circle \mathbb{S}^1 to \mathcal{M} . We can compose two such maps by merging the two circles, as shown in fig. 16.19. Two maps are said to be *homotopic* if they can be smoothly deformed into each other. Any two homotopic maps are said to belong to the same *equivalence class* or *homotopy class*. For general \mathcal{M} , the homotopy classes may be multiplied using the composition law, resulting in a group structure. The group is called the *fundamental group* of the manifold \mathcal{M} , and is abbreviated $\pi_1(\mathcal{M})$. If $\mathcal{M} = \mathbb{S}^2$, then any such map can be smoothly contracted to a point on the 2-sphere, which is to say a trivial map. We then have $\pi_1(\mathcal{M}) = 0$. If $\mathcal{M} = \mathbb{S}^1$, the maps can wind nontrivially, and the homotopy classes are labeled by a single integer winding number: $\pi_1(\mathbb{S}^1) = \mathbb{Z}$. The winding number of the composition of two such maps is the sum of their individual winding numbers. If $\mathcal{M} = \mathbb{T}^2$, the maps can wind nontrivially around either of the two cycles of the 2-torus. We then have $\pi_1(\mathbb{T}^2) = \mathbb{Z}^2$, and in general $\pi_1(\mathbb{T}^n) = \mathbb{Z}^n$. This makes good sense, since an n -torus is topologically equivalent to a product of n circles. In some cases, $\pi_1(\mathcal{M})$ can be nonabelian, as is the case when \mathcal{M} is the genus $g = 2$ structure shown in the right hand panel of fig. 16.18.

In general we define the n^{th} *homotopy group* $\pi_n(\mathcal{M})$ as the group under composition of maps from \mathbb{S}^n to \mathcal{M} . For $n \geq 2$, $\pi_n(\mathcal{M})$ is abelian. If $\dim(\mathcal{M}) < n$, then $\pi_n(\mathcal{M}) = 0$. In general, $\pi_n(\mathbb{S}^n) = \mathbb{Z}$. These n^{th} homotopy classes of the n -sphere are labeled by their Pontrjagin index Q .

Finally, we ask what is Q in terms of the eigenvalues and eigenvectors of the linearized map

$$M_{ij} = \left. \frac{\partial V_i}{\partial x_j} \right|_{x^*} . \quad (16.78)$$

For simple cases where all the λ_i are nonzero, we have

$$Q = \operatorname{sgn} \left(\prod_{i=1}^N \lambda_i \right) . \quad (16.79)$$

16.6 Appendix : Example Problem

Consider the two-dimensional phase flow,

$$\begin{aligned} \dot{x} &= \frac{1}{2}x + xy - 2x^3 \\ \dot{y} &= \frac{5}{2}y + xy - y^2 . \end{aligned} \quad (16.80)$$

(a) Find and classify all fixed points.

Solution : We have

$$\begin{aligned} \dot{x} &= x \left(\frac{1}{2} + y - 2x^2 \right) \\ \dot{y} &= y \left(\frac{5}{2} + x - y \right) . \end{aligned} \quad (16.81)$$

The matrix of first derivatives is

$$M = \begin{pmatrix} \frac{\partial \dot{x}}{\partial x} & \frac{\partial \dot{x}}{\partial y} \\ \frac{\partial \dot{y}}{\partial x} & \frac{\partial \dot{y}}{\partial y} \end{pmatrix} = \begin{pmatrix} \frac{1}{2} + y - 6x^2 & x \\ y & \frac{5}{2} + x - 2y \end{pmatrix} . \quad (16.82)$$

There are six fixed points.

$(x, y) = (0, 0)$: The derivative matrix is

$$M = \begin{pmatrix} \frac{1}{2} & 0 \\ 0 & \frac{5}{2} \end{pmatrix} . \quad (16.83)$$

The determinant is $D = \frac{5}{4}$ and the trace is $T = 3$. Since $D < \frac{1}{4}T^2$ and $T > 0$, this is an unstable node. (Duh! One can read off both eigenvalues are real and positive.) Eigenvalues: $\lambda_1 = \frac{1}{2}$, $\lambda_2 = \frac{5}{2}$.

$(x, y) = (0, \frac{5}{2})$: The derivative matrix is

$$M = \begin{pmatrix} 3 & 0 \\ \frac{5}{2} & -\frac{5}{2} \end{pmatrix} , \quad (16.84)$$

for which $D = -\frac{15}{4}$ and $T = \frac{1}{2}$. The determinant is negative, so this is a saddle. Eigenvalues: $\lambda_1 = -\frac{5}{2}$, $\lambda_2 = 3$.

$(x, y) = (-\frac{1}{2}, 0)$: The derivative matrix is

$$M = \begin{pmatrix} -1 & -\frac{1}{2} \\ 0 & 2 \end{pmatrix} , \quad (16.85)$$

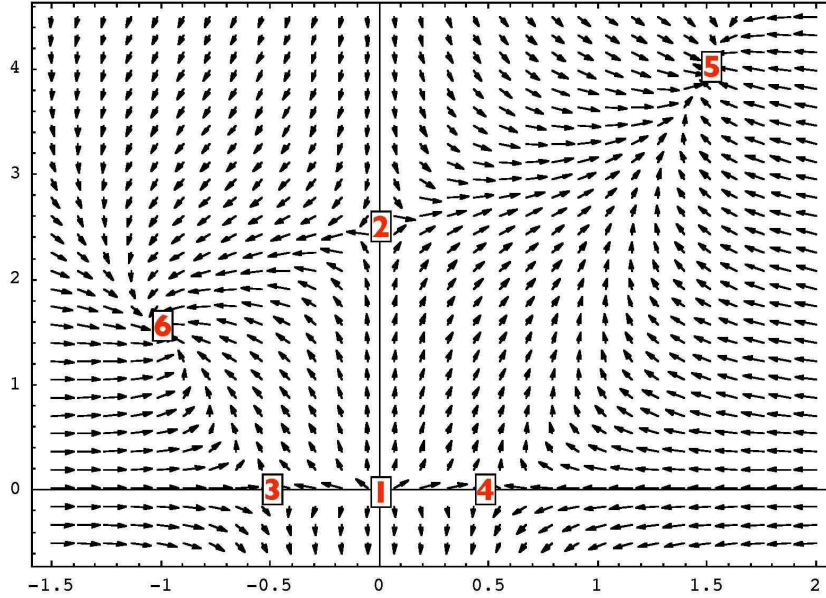


Figure 16.20: Sketch of phase flow for $\dot{x} = \frac{1}{2}x + xy - 2x^3$, $\dot{y} = \frac{5}{2}y + xy - y^2$. Fixed point classifications are in the text.

for which $D = -2$ and $T = +1$. The determinant is negative, so this is a saddle. Eigenvalues: $\lambda_1 = -1$, $\lambda_2 = 2$.

$(x, y) = (\frac{1}{2}, 0)$: The derivative matrix is

$$M = \begin{pmatrix} -1 & \frac{1}{2} \\ 0 & 3 \end{pmatrix}, \quad (16.86)$$

for which $D = -3$ and $T = +2$. The determinant is negative, so this is a saddle. Eigenvalues: $\lambda_1 = -1$, $\lambda_2 = 3$.

$(x, y) = (\frac{3}{2}, 4)$: This is one root obtained by setting $y = x + \frac{5}{2}$ and solving $\frac{1}{2} + y - 2x^2 = 3 + x - 2x^2 = 0$, giving $x = -1$ and $x = +\frac{3}{2}$. The derivative matrix is

$$M = \begin{pmatrix} -9 & \frac{3}{2} \\ 4 & -4 \end{pmatrix}, \quad (16.87)$$

for which $D = 30$ and $T = -13$. Since $D < \frac{1}{4}T^2$ and $T < 0$, this corresponds to a stable node. Eigenvalues: $\lambda_1 = -10$, $\lambda_2 = -3$.

$(x, y) = (-1, \frac{3}{2})$: This is the second root obtained by setting $y = x + \frac{5}{2}$ and solving $\frac{1}{2} + y - 2x^2 = 3 + x - 2x^2 = 0$, giving $x = -1$ and $x = +\frac{3}{2}$. The derivative matrix is

$$M = \begin{pmatrix} -4 & -1 \\ \frac{3}{2} & -\frac{3}{2} \end{pmatrix}, \quad (16.88)$$

for which $D = \frac{15}{2}$ and $T = -\frac{11}{2}$. Since $D < \frac{1}{4}T^2$ and $T < 0$, this corresponds to a stable node. Eigenvalues: $\lambda_1 = -3$, $\lambda_2 = -\frac{5}{2}$.

(b) Sketch the phase flow.

Solution : The flow is sketched in fig. 16.20. Thanks to Evan Bierman for providing the **Mathematica** code.

Chapter 17

Maps, Strange Attractors, and Chaos

17.1 One-dimensional Maps

Consider the simple case of a one-dimensional map,

$$x_{n+1} = f(x_n) . \quad (17.1)$$

A fixed point of the map satisfies $x = f(x)$. Writing the solution as x^* and expanding about the fixed point, we write $x = x^* + u$ and obtain

$$u_{n+1} = f'(x^*) u_n + \mathcal{O}(u^2) . \quad (17.2)$$

Thus, the fixed point is stable if $|f'(x^*)| < 1$, since successive iterates of u then get smaller and smaller. The fixed point is unstable if $|f'(x^*)| > 1$.

Perhaps the most important and most studied of the one-dimensional maps is the logistic map, where $f(x) = rx(1 - x)$, defined on the interval $x \in [0, 1]$. This has a fixed point at $x^* = 1 - r^{-1}$ if $r > 1$. We then have $f'(x^*) = 2 - r$, so the fixed point is stable if $r \in (1, 3)$. What happens for $r > 3$? We can explore the behavior of the iterated map by drawing a *cobweb diagram*, shown in fig. 17.1. We sketch, on the same graph, the curves $y = x$ (in blue) and $y = f(x)$ (in black). Starting with a point x on the line $y = x$, we move vertically until we reach the curve $y = f(x)$. To iterate, we then move horizontally to the line $y = x$ and repeat the process. We see that for $r = 3.4$ the fixed point x^* is unstable, but there is a stable two-cycle, defined by the equations

$$\begin{aligned} x_2 &= rx_1(1 - x_1) \\ x_1 &= rx_2(1 - x_2) . \end{aligned} \quad (17.3)$$

The second iterate of $f(x)$ is then

$$f^{(2)}(x) = f(f(x)) = r^2 x(1 - x)(1 - rx + rx^2) . \quad (17.4)$$

Setting $x = f^{(2)}(x)$, we obtain a cubic equation. Since $x - x^*$ must be a factor, we can divide out by this monomial and obtain a quadratic equation for x_1 and x_2 . We find

$$x_{1,2} = \frac{1 + r \pm \sqrt{(r + 1)(r - 3)}}{2r} . \quad (17.5)$$

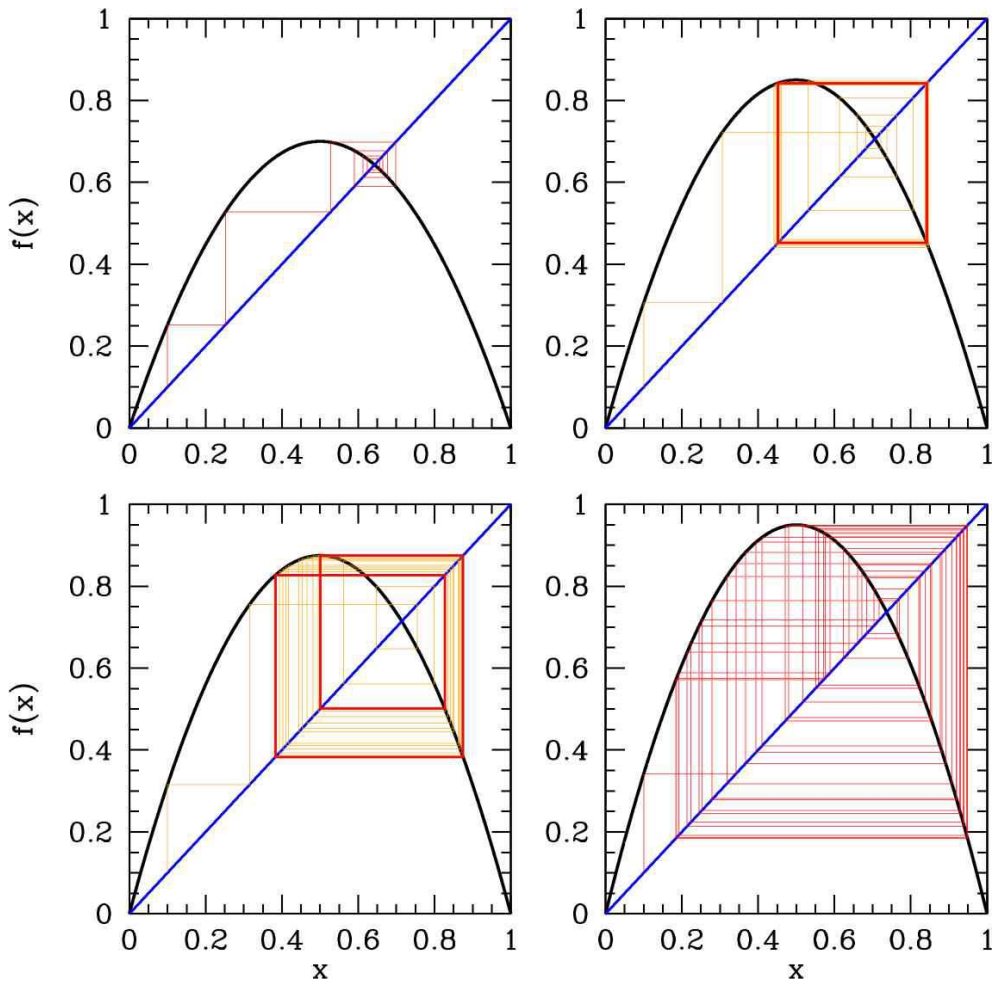


Figure 17.1: Cobweb diagram showing iterations of the logistic map $f(x) = rx(1-x)$ for $r = 2.8$ (upper left), $r = 3.4$ (upper right), $r = 3.5$ (lower left), and $r = 3.8$ (lower right). Note the single stable fixed point for $r = 2.8$, the stable two-cycle for $r = 3.4$, the stable four-cycle for $r = 3.5$, and the chaotic behavior for $r = 3.8$.

How stable is this 2-cycle? We find

$$\frac{d}{dx}f^{(2)}(x) = r^2(1 - 2x_1)(1 - 2x_2) = -r^2 + 2r + 4 . \quad (17.6)$$

The condition that the 2-cycle be stable is then

$$-1 < r^2 - 2r - 4 < 1 \quad \Rightarrow \quad r \in [3, 1 + \sqrt{6}] . \quad (17.7)$$

At $r = 1 + \sqrt{6} = 3.4494897\dots$ there is a bifurcation to a 4-cycle, as can be seen in fig. 17.2.

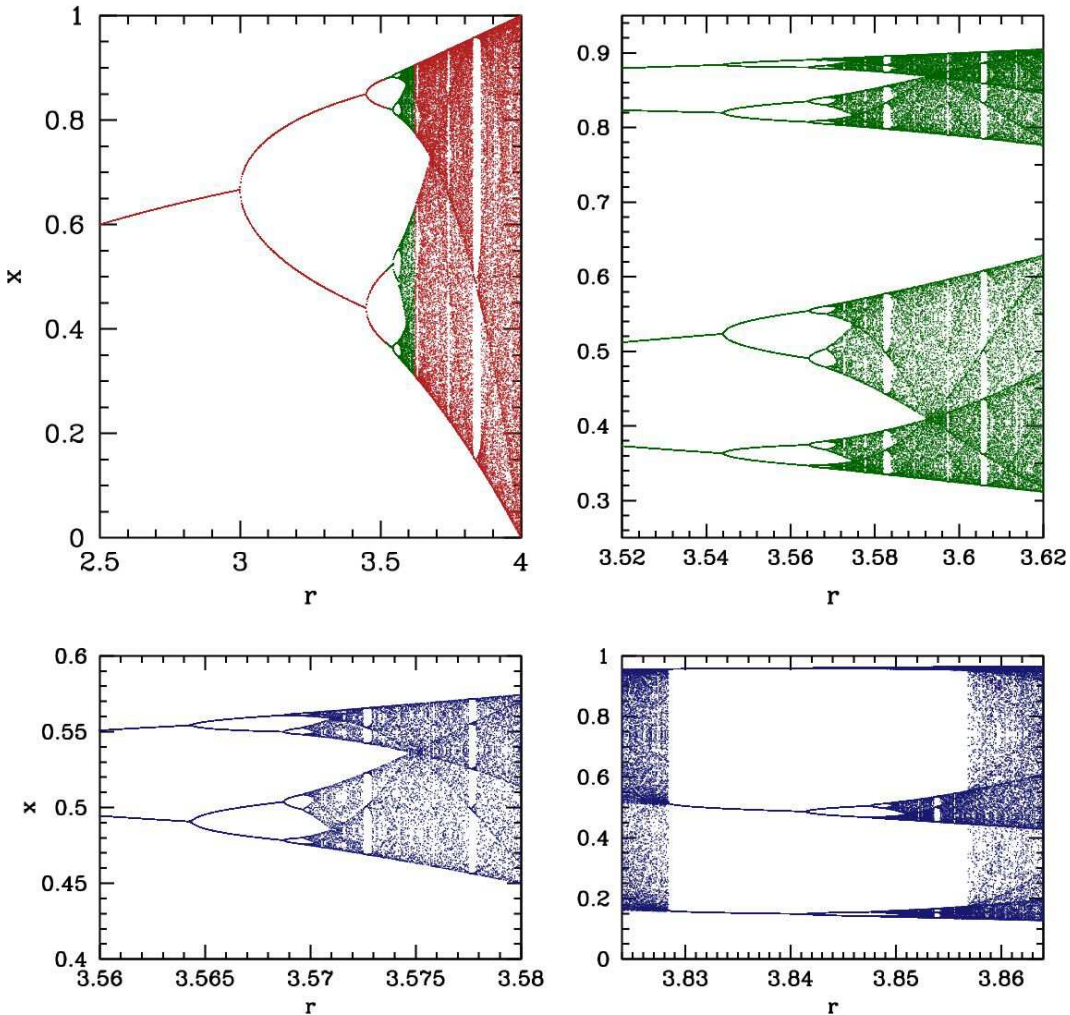


Figure 17.2: Iterates of the logistic map $f(x) = rx(1 - x)$.

17.1.1 Lyapunov Exponents

The *Lyapunov exponent* $\lambda(x)$ of the iterated map $f(x)$ at point x is defined to be

$$\lambda(x) = \lim_{n \rightarrow \infty} \frac{1}{n} \ln \left| \frac{df^{(n)}(x)}{dx} \right| = \lim_{n \rightarrow \infty} \frac{1}{n} \sum_{j=1}^n \ln |f'(x_j)| , \quad (17.8)$$

where $x_{j+1} \equiv f(x_j)$. The significance of the Lyapunov exponent is the following. If $\text{Re}(\lambda(x)) > 0$ then two initial conditions near x will exponentially separate under the iterated map. For the *tent map*,

$$f(x) = \begin{cases} 2rx & \text{if } x < \frac{1}{2} \\ 2r(1-x) & \text{if } x \geq \frac{1}{2} , \end{cases} \quad (17.9)$$

one easily finds $\lambda(x) = \ln(2r)$ independent of x . Thus, if $r > \frac{1}{2}$ the Lyapunov exponent is positive, meaning that every neighboring pair of initial conditions will eventually separate exponentially under

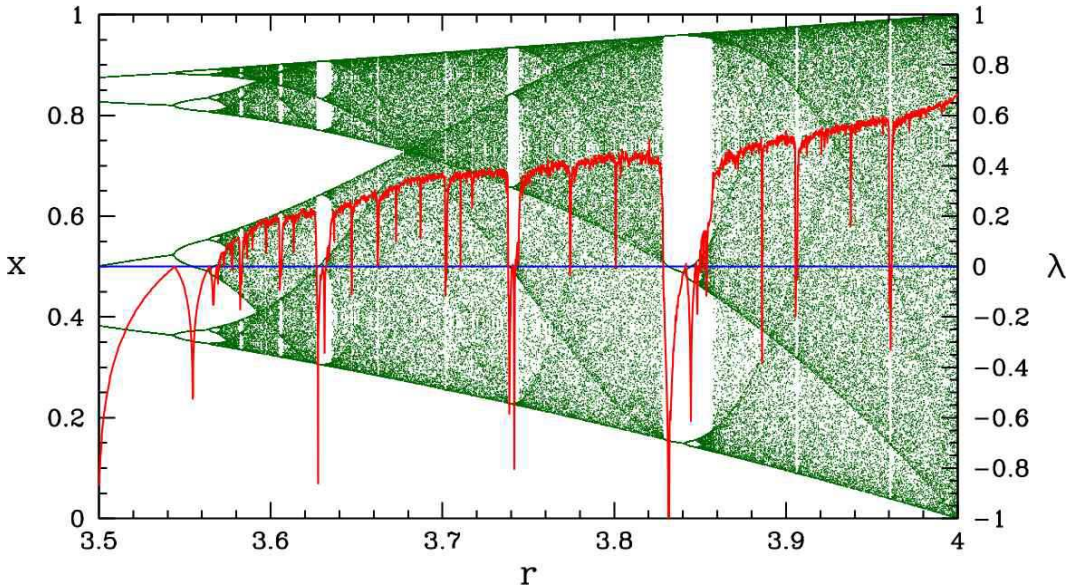


Figure 17.3: Lyapunov exponent (in red) for the logistic map.

repeated application of the map. The Lyapunov exponent for the logistic map is depicted in fig. 17.3.

17.1.2 Chaos in the logistic map

What happens in the logistic map for $r > 1 + \sqrt{6}$? At this point, the 2-cycle becomes unstable and a stable 4-cycle develops. However, this soon goes unstable and is replaced by a stable 8-cycle, as the right hand panel of fig. 17.2 shows. The first eight values of r where bifurcations occur are given by

$$\begin{aligned} r_1 &= 3, \quad r_2 = 1 + \sqrt{6} = 3.4494897, \quad r_3 = 3.544096, \quad r_4 = 3.564407, \\ r_5 &= 3.568759, \quad r_6 = 3.569692, \quad r_7 = 3.569891, \quad r_8 = 3.569934, \dots \end{aligned} \quad (17.10)$$

Feigenbaum noticed that these numbers seemed to be converging exponentially. With the *Ansatz*

$$r_\infty - r_k = \frac{c}{\delta^k}, \quad (17.11)$$

one finds

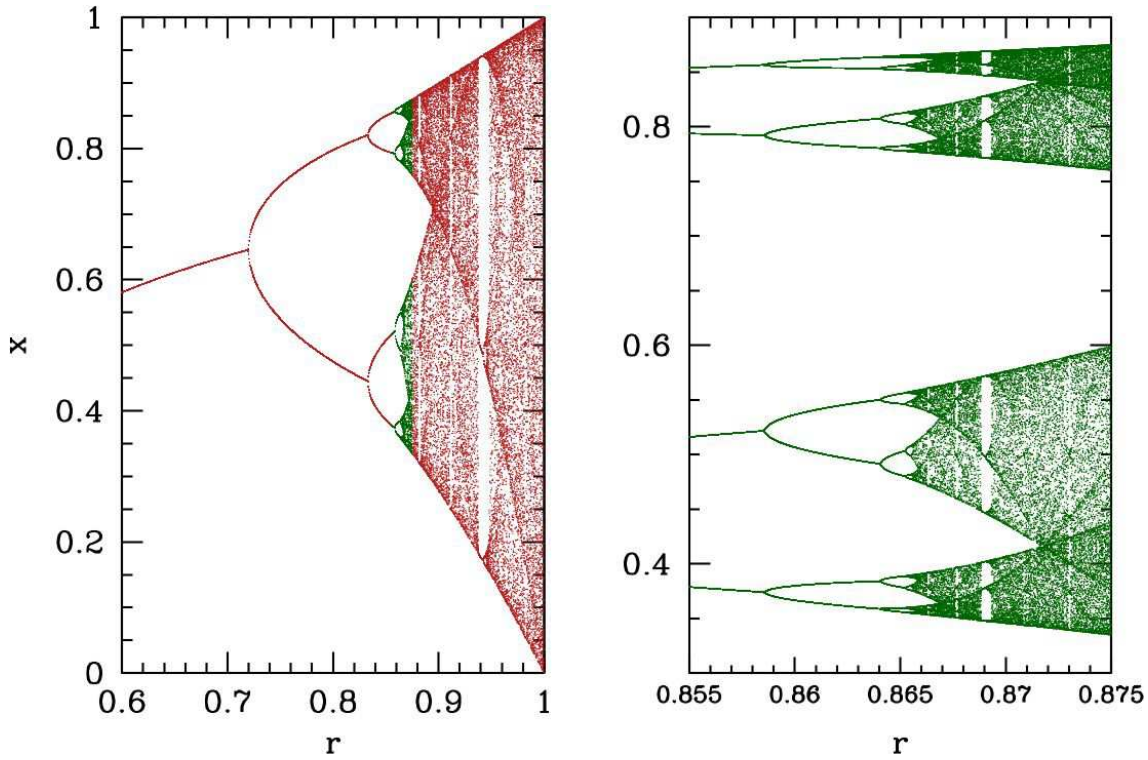
$$\delta = \frac{r_k - r_{k-1}}{r_{k+1} - r_k}, \quad (17.12)$$

and taking the limit $k \rightarrow \infty$ from the above data one finds

$$\delta = 4.669202, \quad c = 2.637, \quad r_\infty = 3.5699456. \quad (17.13)$$

There's a very nifty way of thinking about the chaos in the logistic map at the special value $r = 4$. If we define $x_n \equiv \sin^2 \theta_n$, then we find

$$\theta_{n+1} = 2\theta_n. \quad (17.14)$$

Figure 17.4: Iterates of the sine map $f(x) = r \sin(\pi x)$.

Now let us write

$$\theta_0 = \pi \sum_{k=1}^{\infty} \frac{b_k}{2^k}, \quad (17.15)$$

where each b_k is either 0 or 1. In other words, the $\{b_k\}$ are the digits in the binary decimal expansion of θ_0/π . Now $\theta_n = 2^n \theta_0$, hence

$$\theta_n = \pi \sum_{k=1}^{\infty} \frac{b_{n+k}}{2^k}. \quad (17.16)$$

We now see that the logistic map has the effect of *shifting* to the left the binary digits of θ_n/π to yield θ_{n+1}/π . With each such shift, leftmost digit falls off the edge of the world, as it were, since it results in an overall contribution to θ_{n+1} which is zero modulo π . This very emphatically demonstrates the sensitive dependence on initial conditions which is the hallmark of chaotic behavior, for eventually two very close initial conditions, differing by $\Delta\theta \sim 2^{-m}$, will, after m iterations of the logistic map, come to differ by $\mathcal{O}(1)$.

17.1.3 Intermittency

Successive period doubling is one route to chaos, as we've just seen. Another route is *intermittency*. Intermittency works like this. At a particular value of our control parameter r , the map exhibits a stable periodic cycle, such as the stable 3-cycle at $r = 3.829$, as shown in the bottom panel of fig. 17.5. If we

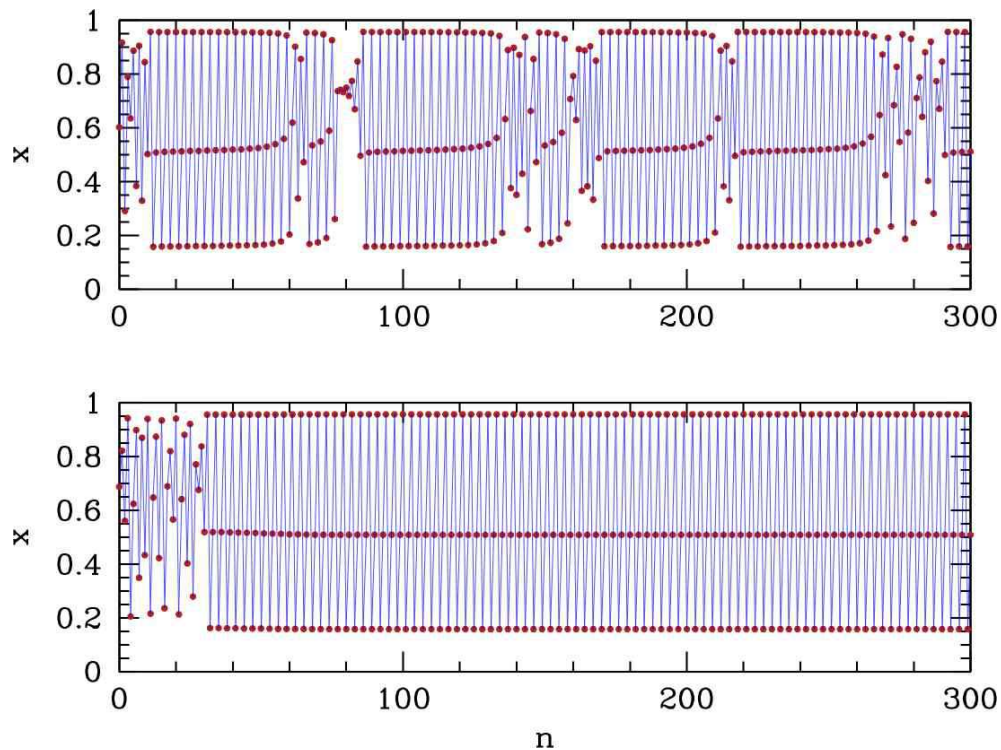


Figure 17.5: Intermittency in the logistic map in the vicinity of the 3-cycle. Top panel: $r = 3.828$, showing intermittent behavior. Bottom panel: $r = 3.829$, showing a stable 3-cycle.

then vary the control parameter slightly in a certain direction, the periodic behavior persists for a finite number of iterations, followed by a *burst*, which is an interruption of the regular periodicity, followed again by periodic behavior, *ad infinitum*. There are three types of intermittent behavior, depending on whether the Lyapunov exponent λ goes through $\text{Re}(\lambda) = 0$ while $\text{Im}(\lambda) = 0$ (type-I intermittency), or with $\text{Im}(\lambda) = \pi$ (type-III intermittency), or, as is possible for two-dimensional maps, with $\text{Im}(\lambda) = \eta$, a general real number.

17.2 Maps from Time-Dependent Hamiltonian Systems

17.2.1 Parametric Oscillator

Consider the equation

$$\ddot{x} + \omega_0^2(t)x = 0 , \quad (17.17)$$

where the oscillation frequency is a function of time. Equivalently,

$$\frac{d}{dt} \begin{pmatrix} x \\ \dot{x} \end{pmatrix} = \underbrace{\begin{pmatrix} M(t) & \varphi(t) \\ 0 & 1 \end{pmatrix}}_{\text{matrix}} \begin{pmatrix} x \\ \dot{x} \end{pmatrix} . \quad (17.18)$$

The formal solution is the path-ordered exponential,

$$\varphi(t) = \mathcal{P} \exp \left\{ \int_0^t dt' M(t') \right\} \varphi(0) . \quad (17.19)$$

Let's consider an example in which

$$\omega(t) = \begin{cases} (1 + \epsilon) \omega_0 & \text{if } 2n\tau \leq t \leq (2n + 1)\tau \\ (1 - \epsilon) \omega_0 & \text{if } (2n + 1)\tau \leq t \leq (2n + 2)\tau . \end{cases} \quad (17.20)$$

Define $\varphi_n \equiv \varphi(2n\tau)$. Then

$$\varphi_{n+1} = \exp(M_- \tau) \exp(M_+ \tau) \varphi_n \equiv \mathcal{U} \varphi_n , \quad (17.21)$$

where

$$M_\pm = \begin{pmatrix} 0 & 1 \\ -\omega_\pm^2 & 0 \end{pmatrix} , \quad (17.22)$$

with $\omega_\pm \equiv (1 \pm \epsilon) \omega_0$. Note that $M_\pm^2 = -\omega_\pm^2 \mathbb{I}$ is a multiple of the identity. Evaluating the Taylor series for the exponential, one finds

$$\mathcal{U}_\pm \equiv \exp(M_\pm t) = \begin{pmatrix} \cos \omega_\pm \tau & \omega_\pm^{-1} \sin \omega_\pm \tau \\ -\omega_\pm \sin \omega_\pm \tau & \cos \omega_\pm \tau \end{pmatrix} , \quad (17.23)$$

from which we derive the evolution matrix

$$\mathcal{U} \equiv \mathcal{U}_- \mathcal{U}_+ = \begin{pmatrix} \cos \omega_- \tau & \omega_-^{-1} \sin \omega_- \tau \\ -\omega_- \sin \omega_- \tau & \cos \omega_- \tau \end{pmatrix} \begin{pmatrix} \cos \omega_+ \tau & \omega_+^{-1} \sin \omega_+ \tau \\ -\omega_+ \sin \omega_+ \tau & \cos \omega_+ \tau \end{pmatrix} \equiv \begin{pmatrix} a & b \\ c & d \end{pmatrix}$$

with

$$\begin{aligned} a &= \cos \omega_- \tau \cos \omega_+ \tau - \frac{\omega_+}{\omega_-} \sin \omega_- \tau \sin \omega_+ \tau \\ b &= \frac{1}{\omega_+} \cos \omega_- \tau \sin \omega_+ \tau + \frac{1}{\omega_-} \sin \omega_- \tau \cos \omega_+ \tau \\ c &= -\omega_+ \cos \omega_- \tau \sin \omega_+ \tau - \omega_- \sin \omega_- \tau \cos \omega_+ \tau \\ d &= \cos \omega_- \tau \cos \omega_+ \tau - \frac{\omega_-}{\omega_+} \sin \omega_- \tau \sin \omega_+ \tau . \end{aligned} \quad (17.24)$$

Note that \mathcal{U}_\pm are each symplectic, hence $\det \exp(M_\pm \tau) = 1$, and therefore \mathcal{U} is also symplectic with $\det \mathcal{U} = 1$. Also note that

$$P(\lambda) = \det(\mathcal{U} - \lambda \cdot \mathbb{I}) = \lambda^2 - T\lambda + \Delta , \quad (17.25)$$

where $T = a + d = \text{Tr } \mathcal{U}$ and $\Delta = ad - bc = \det \mathcal{U}$. The eigenvalues of \mathcal{U} are

$$\lambda_\pm = \frac{1}{2}T \pm \frac{1}{2}\sqrt{T^2 - 4\Delta} . \quad (17.26)$$

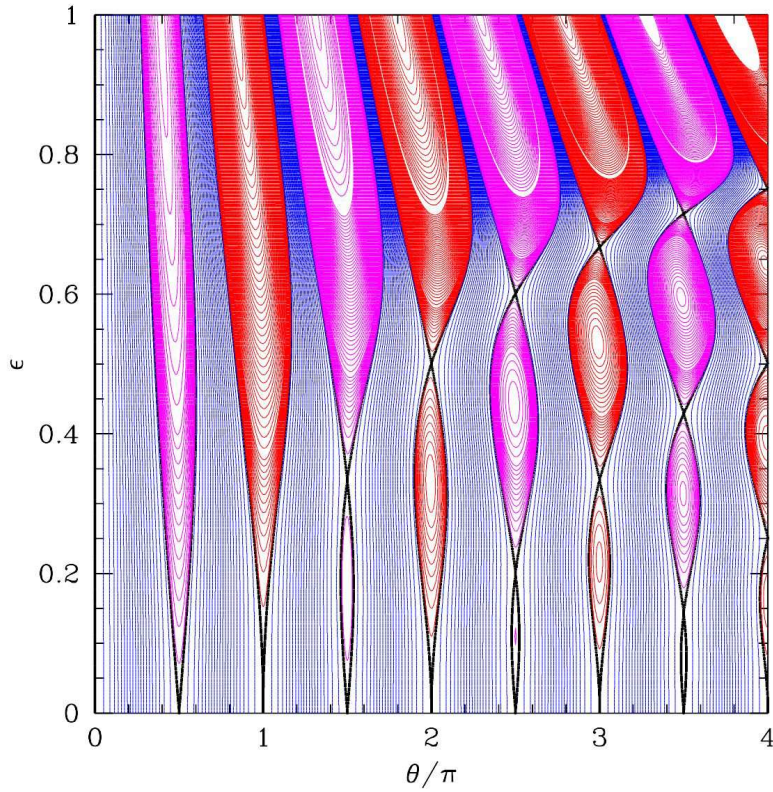


Figure 17.6: Phase diagram for the parametric oscillator in the (θ, ϵ) plane. Thick black lines correspond to $T = \pm 2$. Blue regions: $|T| < 2$. Red regions: $T > 2$. Magenta regions: $T < -2$.

In our case, $\Delta = 1$. There are two cases to consider:

$$\begin{aligned} |T| < 2 : \lambda_+ = \lambda_-^* = e^{i\delta} &, \quad \delta = \cos^{-1} \frac{1}{2}T \\ |T| > 2 : \lambda_+ = \lambda_-^{-1} = \pm e^\mu &, \quad \mu = \cosh^{-1} \frac{1}{2}|T| . \end{aligned} \quad (17.27)$$

When $|T| < 2$, φ remains bounded; when $|T| > 2$, $|\varphi|$ increases exponentially with time. Note that phase space volumes are preserved by the dynamics.

To investigate more fully, let $\theta \equiv \omega_0\tau$. The period of the frequency oscillations is $\Delta t = 2\tau$, *i.e.* $\omega_{\text{pump}} = \pi/\tau$ is the frequency at which the system is ‘pumped’, so

$$\frac{\theta}{\pi} = \frac{\omega_0}{\omega_{\text{pump}}} = \frac{T_{\text{pump}}}{T_0} , \quad (17.28)$$

where $T_0 = 2\pi/\omega_0$ is the unperturbed natural frequency and $T_{\text{pump}} = \Delta t = 2\tau$. One finds $T = \text{Tr } \mathcal{U}$ is given by

$$T = \frac{2 \cos(2\theta) - 2\epsilon^2 \cos(2\epsilon\theta)}{1 - \epsilon^2} . \quad (17.29)$$

We are interested in the boundaries in the (θ, ϵ) plane where $|T| = 2$. Setting $T = +2$, we write $\theta = n\pi + \delta$, which means $T_{\text{pump}} \approx nT_0$. Expanding for small δ and ϵ , we obtain the relation

$$\delta^2 = \epsilon^4 \theta^2 \quad \Rightarrow \quad \epsilon = \pm \left| \frac{\delta}{n\pi} \right|^{1/2}. \quad (17.30)$$

Setting $T = -2$, we write $\theta = (n + \frac{1}{2})\pi + \delta$, i.e. $T_{\text{pump}} \approx (n + \frac{1}{2})T_0$. This gives

$$\delta^2 = \epsilon^2 \quad \Rightarrow \quad \epsilon = \pm \delta. \quad (17.31)$$

The full phase diagram in the (θ, ϵ) plane is shown in Fig. 17.6. A physical example is pumping a swing. By extending your legs periodically, you effectively change the length $\ell(t)$ of the pendulum, resulting in a time-dependent $\omega_0(t) = \sqrt{g/\ell(t)}$.

17.2.2 Kicked dynamics

A related model is described by the *kicked dynamics* of the Hamiltonian

$$H(t) = T(p) + V(q) K(t), \quad (17.32)$$

where

$$K(t) = \tau \sum_{n=-\infty}^{\infty} \delta(t - n\tau) \quad (17.33)$$

is the kicking function. The potential thus winks on and off with period τ . Note that

$$\lim_{\tau \rightarrow 0} K(t) = 1. \quad (17.34)$$

In the $\tau \rightarrow 0$ limit, the system is continuously kicked, and is equivalent to motion in a time-independent external potential $V(q)$.

The equations of motion are

$$\dot{q} = T'(p) \quad , \quad \dot{p} = -V'(q) K(t). \quad (17.35)$$

Integrating these equations, we obtain the map

$$\begin{aligned} q_{n+1} &= q_n + \tau T'(p_n) \\ p_{n+1} &= p_n - \tau V'(q_{n+1}). \end{aligned} \quad (17.36)$$

Note that the determinant of Jacobean of the map is unity:

$$\det \frac{\partial(q_{n+1}, p_{n+1})}{\partial(q_n, p_n)} = \det \begin{pmatrix} 1 & \tau T''(p_n) \\ -\tau V''(q_{n+1}) & 1 - \tau^2 T''(p_n) V''(q_{n+1}) \end{pmatrix} = 1. \quad (17.37)$$

This means that the map preserves phase space volumes.

Consider, for example, the Hamiltonian $H(t) = \frac{L^2}{2T} - V\cos(\phi) K(t)$, where L is the angular momentum conjugate to ϕ . This results in the map

$$\begin{aligned} \phi_{n+1} &= \phi_n + 2\pi\epsilon J_n \\ J_{n+1} &= J_n - \epsilon \sin \phi_{n+1}, \end{aligned} \quad (17.38)$$

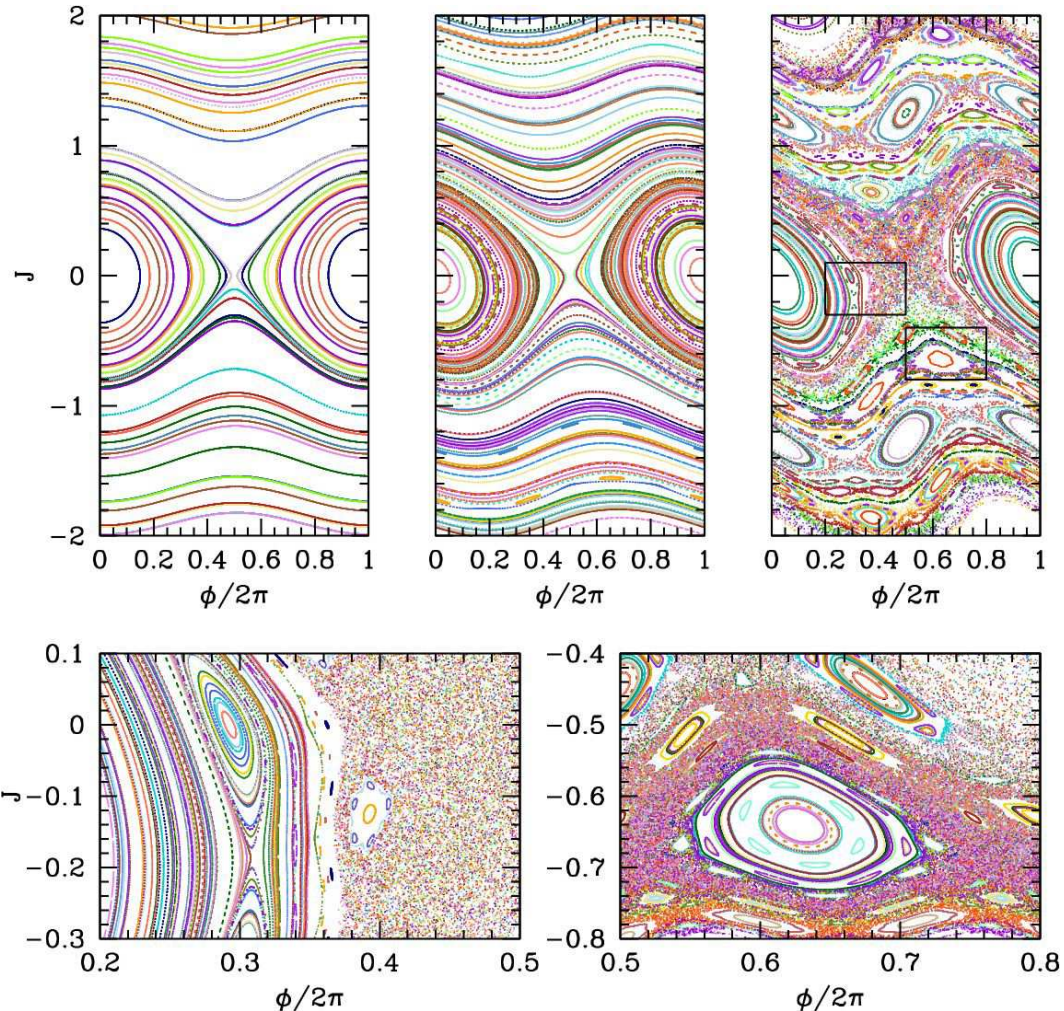


Figure 17.7: Top: the standard map, as defined in the text. Four values of the ϵ parameter are shown: $\epsilon = 0.01$ (left), $\epsilon = 0.2$ (center), and $\epsilon = 0.4$ (right). Bottom: details of the $\epsilon = 0.4$ map.

where $J_n = L_n/\sqrt{2\pi IV}$ and $\epsilon = \tau\sqrt{V/2\pi I}$. This is the standard map¹, which we encountered earlier, albeit in a slightly different form. In the limit $\epsilon \rightarrow 0$, we may define $\dot{\phi} = (\phi_{n+1} - \phi_n)/\epsilon$ and $\dot{J} = (J_{n+1} - J_n)/\epsilon$, and we recover the continuous time dynamics $\dot{\phi} = 2\pi J$ and $\dot{J} = -\sin \phi$. These dynamics preserve the energy function $E = \pi J^2 - \cos \phi$. There is a separatrix at $E = 1$, given by $J(\phi) = \pm \frac{2}{\pi} |\cos(\phi/2)|$. We see from fig. 17.7 that this separatrix is the first structure to be replaced by a chaotic fuzz as ϵ increases from zero to a small finite value.

Another well-studied system is the *kicked Harper model*, for which

$$H(t) = -V_1 \cos\left(\frac{2\pi p}{P}\right) - V_2 \cos\left(\frac{2\pi q}{Q}\right) K(t) . \quad (17.39)$$

¹The standard map us usually written in the form $x_{n+1} = x_n + \mathcal{J}_n$ and $\mathcal{J}_{n+1} = \mathcal{J}_n - k \sin(2\pi x_{n+1})$. We can recover our version by rescaling $\phi_n = 2\pi x_n$, $\mathcal{J}_n \equiv \sqrt{k} J_n$ and defining $\epsilon \equiv \sqrt{k}$.

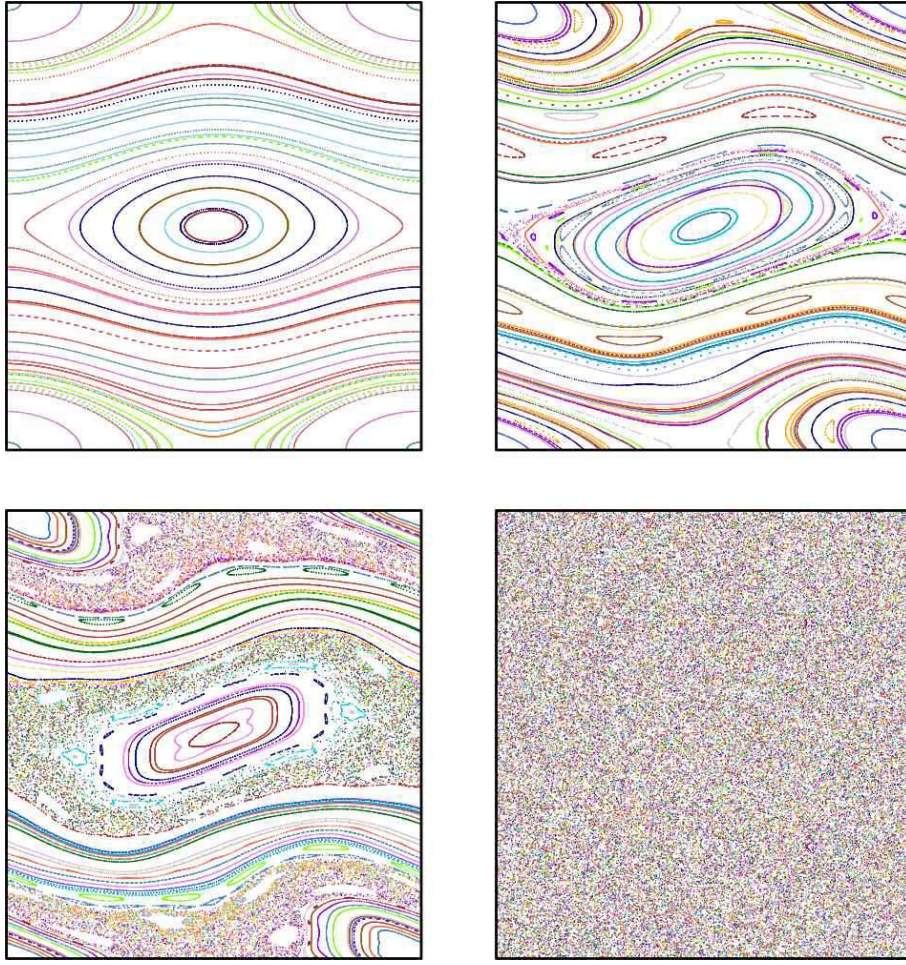


Figure 17.8: The kicked Harper map, with $\alpha = 2$, and with $\epsilon = 0.01, 0.125, 0.2$, and 5.0 (clockwise from upper left). The phase space here is the unit torus, $\mathbb{T}^2 = [0, 1] \times [0, 1]$.

With $x = q/Q$ and $y = p/P$, Hamilton's equations generate the map

$$\begin{aligned} x_{n+1} &= x_n + \epsilon \alpha \sin(2\pi y_n) \\ y_{n+1} &= y_n - \frac{\epsilon}{\alpha} \sin(2\pi x_{n+1}) , \end{aligned} \tag{17.40}$$

where $\epsilon = 2\pi\tau\sqrt{V_1 V_2}/PQ$ and $\alpha = \sqrt{V_1/V_2}$ are dimensionless parameters. In this case, the conserved energy is

$$E = -\alpha^{-1} \cos(2\pi x) - \alpha \cos(2\pi y) . \tag{17.41}$$

There are then two separatrices, at $E = \pm(\alpha - \alpha^{-1})$, with equations $\alpha \cos(\pi y) = \pm \sin(\pi x)$ and $\alpha \sin(\pi y) = \pm \cos(\pi x)$. Again, as is apparent from fig. 17.8, the separatrix is the first structure to be destroyed at finite ϵ . This also occurs for the standard map – there is a transition to *global stochasticity* at a critical value of ϵ .

Note that the kicking function may be written as

$$K(t) = \tau \sum_{n=-\infty}^{\infty} \delta(t - n\tau) = \sum_{m=-\infty}^{\infty} \cos\left(\frac{2\pi mt}{\tau}\right) , \quad (17.42)$$

a particularly handy result known as the *Poisson summation formula*. This, a kicked Hamiltonian may be written as

$$H(J, \phi, t) = H_0(J) + V(\phi) \sum_{m=-\infty}^{\infty} \cos\left(\frac{2\pi mt}{\tau}\right) . \quad (17.43)$$

The $m = 0$ term generates the continuous time dynamics $\dot{\phi} = \omega_0(J)$, $\dot{J} = -V'(\phi)$. For the standard map, these are the dynamics of a simple pendulum. The $m \neq 0$ terms are responsible for resonances and the formation of so-called ‘stochastic layers’.

17.3 Local Stability and Lyapunov Exponents

17.3.1 The fate of nearly separated initial conditions under iteration

Consider a map \hat{T} acting on a phase space of dimension $2N$ (*i.e.* N position degrees of freedom). We ask what is the fate of two nearby initial conditions, ξ_0 and $\xi_0 + d\xi$, under the iterated map. Under the first iteration, we have $\xi_0 \rightarrow \xi_1 = \hat{T}\xi_0$ and

$$\xi_0 + d\xi \longrightarrow \xi_1 + M(\xi_0) d\xi , \quad (17.44)$$

where $M(\xi)$ is a matrix given by the *linearization of \hat{T} at ξ* , *viz.*

$$M_{ij}(\xi) = \frac{\partial(\hat{T}\xi)_i}{\partial\xi_j} . \quad (17.45)$$

Let’s iterate again. Clearly $\xi_1 \rightarrow \xi_2 = \hat{T}^2\xi_0$ and

$$\xi_1 + M(\xi_0) d\xi \longrightarrow \xi_2 + M(\xi_1)M(\xi_0) d\xi . \quad (17.46)$$

After n iterations, we clearly have $\hat{T}^n\xi_0 = \xi_n$ and

$$\hat{T}^n(\xi_0 + d\xi) = \xi_n + M(\xi_{n-1}) \cdots M(\xi_0) d\xi , \quad (17.47)$$

and we define $R^{(n)}(\xi) = M(\hat{T}^n\xi) \cdots M(\hat{T}\xi)M(\xi)$, whose matrix elements may be written as $R_{ij}^{(n)}(\xi) = \partial(\hat{T}^n\xi)_i / \partial\xi_j$.

Since the map \hat{T} is presumed to be canonical, at each stage $M(\xi_j) \in \text{Sp}(2N)$, and since the product of symplectic matrices is a symplectic matrix, $R^{(n)}(\xi) \in \text{Sp}(2N)$. It is easy to see that for any real symplectic matrix R , the eigenvalues come in unimodular conjugate pairs $\{e^{i\delta}, e^{-i\delta}\}$, in real pairs $\{\lambda, \lambda^{-1}\}$ with $\lambda \in \mathbb{R}$, or in quartets $\{\lambda, \lambda^{-1}, \lambda^*, \lambda^{*-1}\}$ with $\lambda \in \mathbb{C}$, where λ^* is the complex conjugate of λ . This

follows from analysis of the characteristic polynomial $P(\lambda) = \det(\lambda - R)$ given the symplectic condition² $R^t \mathbb{J} R = \mathbb{J}$. Let $\{\lambda_j^{(n)}(\xi)\}$ be the eigenvalues of $R^{(n)}(\xi)$, with $j \in \{1, \dots, 2N\}$. One defines the *Lyapunov exponents*,

$$\nu_j(\xi) = \lim_{n \rightarrow \infty} \frac{1}{n} \ln |\lambda_j^{(n)}(\xi)| . \quad (17.48)$$

These may be ordered such that $\nu_1 \leq \nu_2 \leq \dots \leq \nu_{2N}$. Positive Lyapunov exponents correspond to an exponential stretching (as a function of the iteration number n), while negative ones correspond to an exponential squeezing.

As an example, consider the Arnol'd cat map, which is an automorphism of the torus $\mathbb{T}^2 = \mathbb{S}^1 \times \mathbb{S}^1$, given by³

$$\begin{aligned} q_{n+1} &= (K + 1) q_n + p_n \\ p_{n+1} &= K q_n + p_n , \end{aligned} \quad (17.49)$$

where $K \in \mathbb{Z}$, and where both q_n and p_n are defined modulo unity, so $(q_n, p_n) \in [0, 1] \times [0, 1]$. Note that K must be an integer in order for the map to be smooth on the torus, *i.e.* it is left unchanged by displacing either coordinate by an integer distance. The map is already linear, hence we can read off

$$M = \frac{\partial(q_{n+1}, p_{n+1})}{\partial(q_n, p_n)} = \begin{pmatrix} K+1 & 1 \\ K & 1 \end{pmatrix} , \quad (17.50)$$

which is independent of (q_n, p_n) . The inverse map also has integer coefficients:

$$M^{-1} = \begin{pmatrix} 1 & -1 \\ -K & K+1 \end{pmatrix} . \quad (17.51)$$

Since $\det M = 1$, the cat map is canonical, *i.e.* it preserves phase space volumes. The eigenvalues of M are the roots of the characteristic polynomial $P(\lambda) = \lambda^2 - (K+2)\lambda - K$, and are given by

$$\lambda_{\pm} = 1 + \frac{1}{2}K \pm \sqrt{K + \frac{1}{4}K^2} . \quad (17.52)$$

Thus, for $K \in \{-4, -3, -2, -1, 0\}$, the eigenvalues come in pairs $e^{\pm i\delta_K}$, with $\delta_{-4} = \pi$, $\delta_{-3} = \frac{2}{3}\pi$, $\delta_{-2} = \frac{1}{2}\pi$, $\delta_{-1} = \frac{1}{3}\pi$, and $\delta_0 = 0$. For $K < -4$ or $K > 0$, the eigenvalues are (λ, λ^{-1}) with $\lambda > 1$ and $0 < \lambda^{-1} < 1$, corresponding, respectively, to stretching and squeezing. The Lyapunov exponents are $\nu_{\pm} = \ln |\lambda_{\pm}|$.

17.3.2 Kolmogorov-Sinai entropy

Let $\Gamma < \infty$ be our phase space (at constant energy, for a Hamiltonian system), and $\{\Delta_j\}$ a partition of disjoint sets whose union is Γ . The simplest arrangement to think of is for each Δ_j to correspond to a little hypercube; stacking up all the hypercube builds the entire phase space. Now apply the inverse

²One has $P(\lambda) = \det(\lambda - R) = \det(\lambda - R^t) = \det(\lambda + \mathbb{J}R^{-1}\mathbb{J}) = \det(\lambda^{-1} - R) \cdot \lambda^{2N} / \det R$ and therefore if λ is a root of the characteristic polynomial, then so is λ^{-1} . Since $R = R^*$, one also has $P(\lambda^*) = [P(\lambda)]^*$, hence if λ is a root, then so is λ^* . From $\text{Pf}(R^t \mathbb{J} R) = \det(R) \text{Pf}(\mathbb{J})$, where Pf is the Pfaffian, one has $\det R = 1$.

³The map in Eqn. 17.49 is a generalized version of Arnol'd's original cat map, which had $K = 1$.

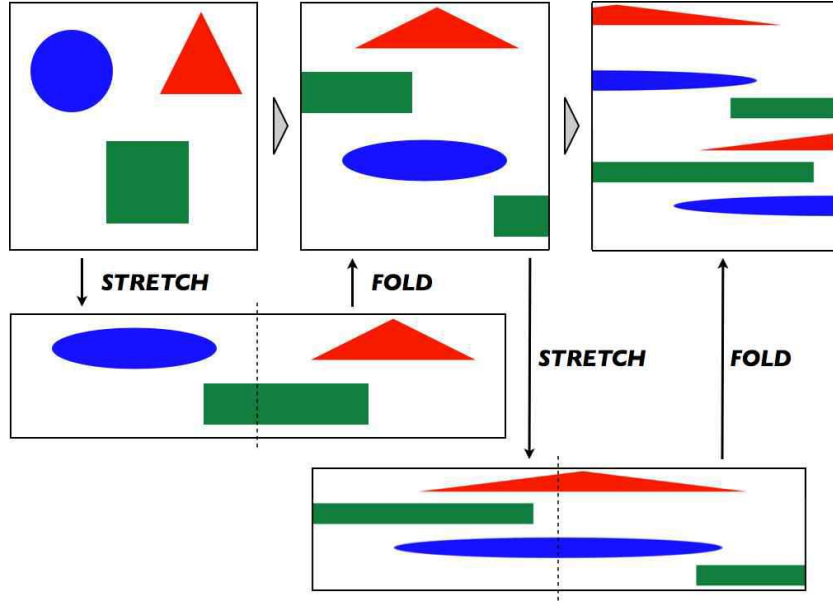


Figure 17.9: The baker's transformation involves stretching/squeezing and ‘folding’ (cutting and restacking).

map \hat{T}^{-1} to each Δ_j , and form the intersections $\Delta_{jk} \equiv \Delta_j \cap \hat{T}^{-1}\Delta_k$. If $\sum_j \mu(\Delta_j) = \mu(\Gamma) \equiv 1$, then $\sum_{j,k} \mu(\Delta_{jk}) = 1$. Iterating further, we obtain $\Delta_{jkl} = \Delta_{jk} \equiv \Delta_j \cap \hat{T}^{-1}\Delta_k \cap \hat{T}^{-2}\Delta_l$, etc.

The entropy of a distribution $\{p_a\}$ is defined to be $S = -\sum_a p_a \ln p_a$. Accordingly we define

$$S_L(\boldsymbol{\Delta}) = - \sum_{j_1} \cdots \sum_{j_L} \mu(\Delta_{j_1 \cdots j_L}) \ln \mu(\Delta_{j_1 \cdots j_L}) . \quad (17.53)$$

This is a function of both the iteration number L as well as the initial set $\boldsymbol{\Delta} = \{\Delta_1, \dots, \Delta_r\}$, where r is the number of subregions in our original partition. We then define the Kolmogorov-Sinai entropy to be

$$h_{\text{KS}} \equiv \sup_{\boldsymbol{\Delta}} \lim_{L \rightarrow \infty} \frac{1}{L} S_L(\boldsymbol{\Delta}) . \quad (17.54)$$

Here \sup stands for *supremum*, meaning we maximize over all partitions $\boldsymbol{\Delta}$.

Consider, for example, the *baker's transformation* (see Fig. 17.9), which stretches, cuts, stacks, and compresses the torus according to

$$(q', p') = \hat{T}(q, p) = \begin{cases} (2q, \frac{1}{2}p) & \text{if } 0 \leq p < \frac{1}{2} \\ (2q - 1, \frac{1}{2}p + \frac{1}{2}) & \text{if } \frac{1}{2} \leq p < 1 \end{cases} \quad (17.55)$$

It is not difficult to convince oneself that the KS entropy for the baker's transformation is $h_{\text{KS}} = \ln 2$. On the other hand, for a simple translation map which takes $(q, p) \rightarrow (q', p') = (q + \alpha, p + \beta)$, it is easy to see that $h_{\text{KS}} = 0$. The KS entropy is related to the Lyapunov exponents through the formula

$$h_{\text{KS}} = \sum_j \nu_j \Theta(\nu_j) . \quad (17.56)$$

The RHS is the sum over all the positive Lyapunov exponents $\gamma_j > 0$. Actually, this formula presumes that the γ_j do not vary in phase space, but in general this is not the case. The more general result is known as *Pesin's entropy formula*,

$$h_{\text{KS}} = \int_{\Gamma} d\mu(\xi) \sum_j \nu_j(\xi) \Theta(\nu_j(\xi)) . \quad (17.57)$$

17.4 The Lorenz Model and Chaos

17.4.1 Attractors

An *attractor* of a dynamical system $\dot{\varphi} = \mathbf{V}(\varphi)$ is the set of φ values that the system evolves to after a sufficiently long time. For $N = 1$ the only possible attractors are stable fixed points. For $N = 2$, we have stable nodes and spirals, but also stable limit cycles. For $N > 2$ the situation is qualitatively different, and a fundamentally new type of set, the *strange attractor*, emerges.

A strange attractor is basically a bounded set on which nearby orbits diverge exponentially (*i.e.* there exists at least one positive Lyapunov exponent). To envision such a set, consider a flat rectangle, like a piece of chewing gum. Now fold the rectangle over, stretch it, and squash it so that it maintains its original volume. Keep doing this. Two points which started out nearby to each other will eventually, after a sufficiently large number of folds and stretches, grow far apart. Formally, a strange attractor is a *fractal*, and may have *noninteger Hausdorff dimension*. (We won't discuss fractals and Hausdorff dimension here.)

The canonical example of an $N = 3$ strange attractor is found in the Lorenz model. E. N. Lorenz, in a seminal paper from the early 1960's, reduced the essential physics of the coupled *partial* differential equations describing Rayleigh-Benard convection (a fluid slab of finite thickness, heated from below – in Lorenz's case a model of the atmosphere warmed by the ocean) to a set of twelve coupled nonlinear *ordinary* differential equations. Lorenz's intuition was that his weather model should exhibit recognizable patterns over time. What he found instead was that in some cases, changing his initial conditions by a part in a thousand rapidly led to totally different behavior. This *sensitive dependence on initial conditions* is a hallmark of chaotic systems.

17.4.2 The Lorenz equations

The essential physics (or mathematics?) of Lorenz's $N = 12$ system is elicited by the reduced $N = 3$ system,

$$\begin{aligned} \dot{X} &= -\sigma X + \sigma Y \\ \dot{Y} &= rX - Y - XZ \\ \dot{Z} &= XY - bZ , \end{aligned} \quad (17.58)$$

where σ , r , and b are all real and positive. Here t is the familiar time variable (appropriately scaled), and (X, Y, Z) represent linear combinations of physical fields, such as global wind current and poleward

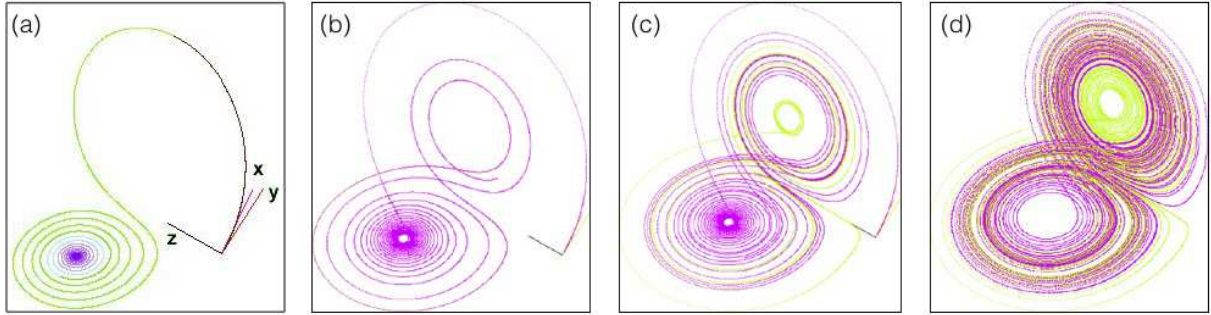


Figure 17.10: (a) Evolution of the Lorenz equations for $\sigma = 10$, $b = \frac{8}{3}$, and $r = 15$, with initial conditions $(X, Y, Z) = (0, 1, 0)$, projected onto the (X, Z) plane. The attractor is a stable spiral. (b) - (d) Chaotic regime ($r = 28$) evolution showing sensitive dependence on initial conditions. The magenta and green curves differ in their initial X coordinate by 10^{-5} . (Source: Wikipedia)

temperature gradient. These equations possess a symmetry under $(X, Y, Z) \rightarrow (-X, -Y, Z)$, but what is most important is the presence of nonlinearities in the second and third equations.

The Lorenz system is *dissipative* because phase space volumes contract:

$$\nabla \cdot \mathbf{V} = \frac{\partial \dot{X}}{\partial X} + \frac{\partial \dot{Y}}{\partial Y} + \frac{\partial \dot{Z}}{\partial Z} = -(\sigma + b + 1) . \quad (17.59)$$

Thus, volumes contract under the flow. Another property is the following. Let

$$F(X, Y, Z) = \frac{1}{2}X^2 + \frac{1}{2}Y^2 + \frac{1}{2}(Z - r - \sigma)^2 . \quad (17.60)$$

Then

$$\begin{aligned} \dot{F} &= X\dot{X} + Y\dot{Y} + (Z - r - \sigma)\dot{Z} \\ &= -\sigma X^2 - Y^2 - b(Z - \frac{1}{2}r - \frac{1}{2}\sigma)^2 + \frac{1}{4}b(r + \sigma)^2 . \end{aligned} \quad (17.61)$$

Thus, $\dot{F} < 0$ outside an ellipsoid, which means that all solutions must remain bounded in phase space for all times.

17.4.3 Fixed point analysis

Setting $\dot{X} = \dot{Y} = \dot{Z} = 0$, we find three solutions. One solution which is always present is $X^* = Y^* = Z^* = 0$. If we linearize about this solution, we obtain

$$\frac{d}{dt} \begin{pmatrix} \delta X \\ \delta Y \\ \delta Z \end{pmatrix} = \begin{pmatrix} -\sigma & \sigma & 0 \\ r & -1 & 0 \\ 0 & 0 & -b \end{pmatrix} \begin{pmatrix} \delta X \\ \delta Y \\ \delta Z \end{pmatrix} . \quad (17.62)$$

The eigenvalues of the linearized dynamics are found to be

$$\begin{aligned} \lambda_{1,2} &= -\frac{1}{2}(1 + \sigma) \pm \frac{1}{2}\sqrt{(1 + \sigma)^2 + 4\sigma(r - 1)} \\ \lambda_3 &= -b , \end{aligned} \quad (17.63)$$

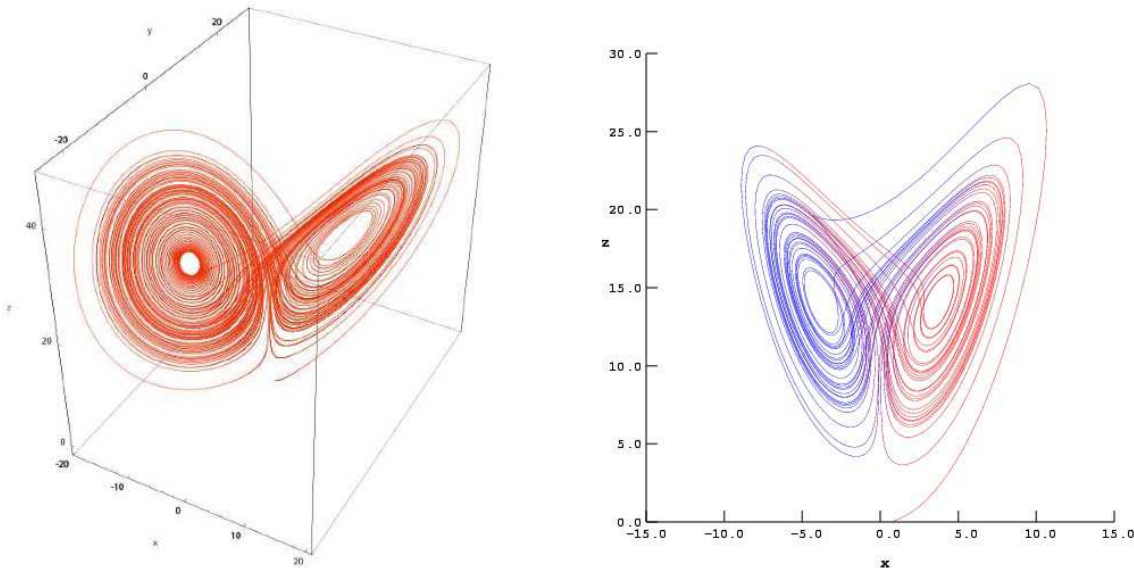


Figure 17.11: Left: Evolution of the Lorenz equations for $\sigma = 10$, $b = \frac{8}{3}$, and $r = 28$, with initial conditions $(X_0, Y_0, Z_0) = (0, 1, 0)$, showing the ‘strange attractor’. Right: The Lorenz attractor, projected onto the (X, Z) plane. (Source: Wikipedia)

and thus if $0 < r < 1$ all three eigenvalues are negative, and the fixed point is a stable node. If, however, $r > 1$, then $\lambda_2 > 0$ and the fixed point is attractive in two directions but repulsive in a third, corresponding to a three-dimensional version of a saddle point.

For $r > 1$, a new pair of solutions emerges, with

$$X^* = Y^* = \pm\sqrt{b(r-1)} , \quad Z^* = r-1 . \quad (17.64)$$

Linearizing about either one of these fixed points, we find

$$\frac{d}{dt} \begin{pmatrix} \delta X \\ \delta Y \\ \delta Z \end{pmatrix} = \begin{pmatrix} -\sigma & \sigma & 0 \\ 1 & -1 & -X^* \\ X^* & X^* & -b \end{pmatrix} \begin{pmatrix} \delta X \\ \delta Y \\ \delta Z \end{pmatrix} . \quad (17.65)$$

The characteristic polynomial of the linearized map is

$$P(\lambda) = \lambda^3 + (b + \sigma + 1)\lambda^2 + b(\sigma + r)\lambda + 2b(r - 1) . \quad (17.66)$$

Since b , σ , and r are all positive, $P'(\lambda) > 0$ for all $\lambda \geq 0$. Since $P(0) = 2b(r - 1) > 0$, we may conclude that there is always at least one eigenvalue λ_1 which is real and negative. The remaining two eigenvalues are either both real and negative, or else they occur as a complex conjugate pair: $\lambda_{2,3} = \alpha \pm i\beta$. The fixed point is stable provided $\alpha < 0$. The stability boundary lies at $\alpha = 0$. Thus, we set

$$P(i\beta) = [2b(r - 1) - (b + \sigma + 1)\beta^2] + i[b(\sigma + r) - \beta^2]\beta = 0 , \quad (17.67)$$

which results in two equations. Solving these two equations for $r(\sigma, b)$, we find

$$r_c = \frac{\sigma(\sigma + b + 3)}{\sigma - b - 1} . \quad (17.68)$$

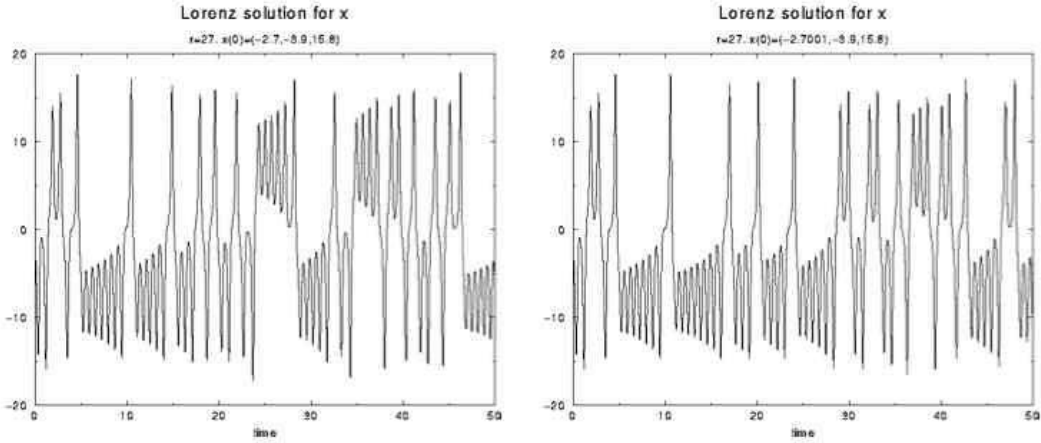


Figure 17.12: $X(t)$ for the Lorenz equations with $\sigma = 10$, $b = \frac{8}{3}$, $r = 28$, and initial conditions $(X_0, Y_0, Z_0) = (-2.7, -3.9, 15.8)$, and initial conditions $(X_0, Y_0, Z_0) = (-2.7001, -3.9, 15.8)$.

The fixed point is stable for $r \in [1, r_c]$. These fixed points correspond to steady convection. The approach to this fixed point is shown in Fig. 17.10.

The Lorenz system has commonly been studied with $\sigma = 10$ and $b = \frac{8}{3}$. This means that the volume collapse is very rapid, since $\nabla \cdot \mathbf{V} = -\frac{41}{3} \approx -13.67$, leading to a volume contraction of $e^{-41/3} \simeq 1.16 \times 10^{-6}$ per unit time. For these parameters, one also has $r_c = \frac{470}{19} \approx 24.74$. The capture by the strange attractor is shown in Fig. 17.11.

In addition to the new pair of fixed points, a strange attractor appears for $r > r_s \simeq 24.06$. In the narrow interval $r \in [24.06, 24.74]$ there are then *three* stable attractors, two of which correspond to steady convection and the third to chaos. Over this interval, there is also hysteresis. *I.e.* starting with a convective state for $r < 24.06$, the system remains in the convective state until $r = 24.74$, when the convective fixed point becomes unstable. The system is then driven to the strange attractor, corresponding to chaotic dynamics. Reversing the direction of r , the system remains chaotic until $r = 24.06$, when the strange attractor loses its own stability.

17.4.4 Poincaré section

One method used by Lorenz in analyzing his system was to plot its *Poincaré section*. This entails placing one constraint on the coordinates (X, Y, Z) to define a two-dimensional surface Σ , and then considering the intersection of this surface Σ with a given phase curve for the Lorenz system. Lorenz chose to set $\dot{Z} = 0$, which yields the surface $Z = b^{-1}XY$. Note that since $\dot{Z} = 0$, $Z(t)$ takes its maximum and minimum values on this surface; see the left panel of Fig. 17.13. By plotting the values of the maxima Z_N as the integral curve successively passed through this surface, Lorenz obtained results such as those shown in the right panel of Fig. 17.13, which has the form of a one-dimensional map and may be analyzed as such. Thus, chaos in the Lorenz attractor can be related to chaos in a particular one-dimensional map, known as the *return map* for the Lorenz system.

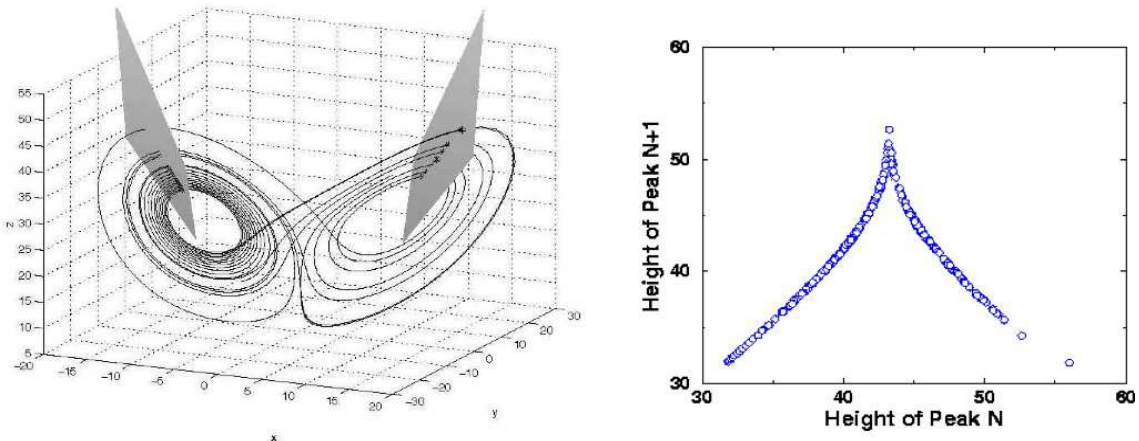


Figure 17.13: Left: Lorenz attractor for $b = \frac{8}{3}$, $\sigma = 10$, and $r = 28$. Maxima of Z are depicted by stars. Right: Relation between successive maxima Z_N along the strange attractor.

17.4.5 Rössler System

The strange attractor is one of the hallmarks of the Lorenz system. Another simple dynamical system which possesses a strange attractor is the Rössler system. This is also described by $N = 3$ coupled ordinary differential equations, *viz.*

$$\begin{aligned}\dot{X} &= -Y - Z \\ \dot{Y} &= Z + aY \\ \dot{Z} &= b + Z(X - c),\end{aligned}\tag{17.69}$$

typically studied as a function of c for $a = b = \frac{1}{5}$. In Fig. 17.15, we present results from work by Crutchfield *et al.* (1980). The transition from simple limit cycle to strange attractor proceeds via a sequence of period-doubling bifurcations, as shown in the figure. A convenient diagnostic for examining this period-doubling route to chaos is the *power spectral density*, or PSD, defined for a function $F(t)$ as

$$\Phi_F(\omega) = \left| \int_{-\infty}^{\infty} \frac{d\omega}{2\pi} F(t) e^{-i\omega t} \right|^2 = |\hat{F}(\omega)|^2.\tag{17.70}$$

As one sees in Fig. 17.15, as c is increased past each critical value, the PSD exhibits a series of frequency halvings (*i.e.* period doublings). All harmonics of the lowest frequency peak are present. In the chaotic region, where $c > c_\infty \approx 4.20$, the PSD also includes a noisy broadband background.

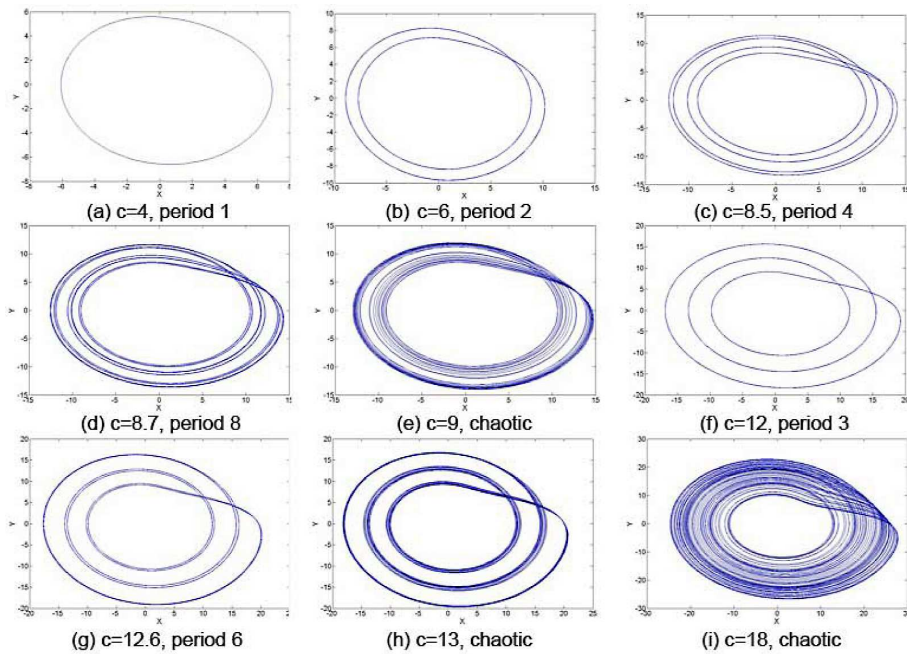


Figure 17.14: Period doubling bifurcations of the Rössler attractor, projected onto the (x, y) plane, for nine values of c , with $a = b = \frac{1}{10}$.

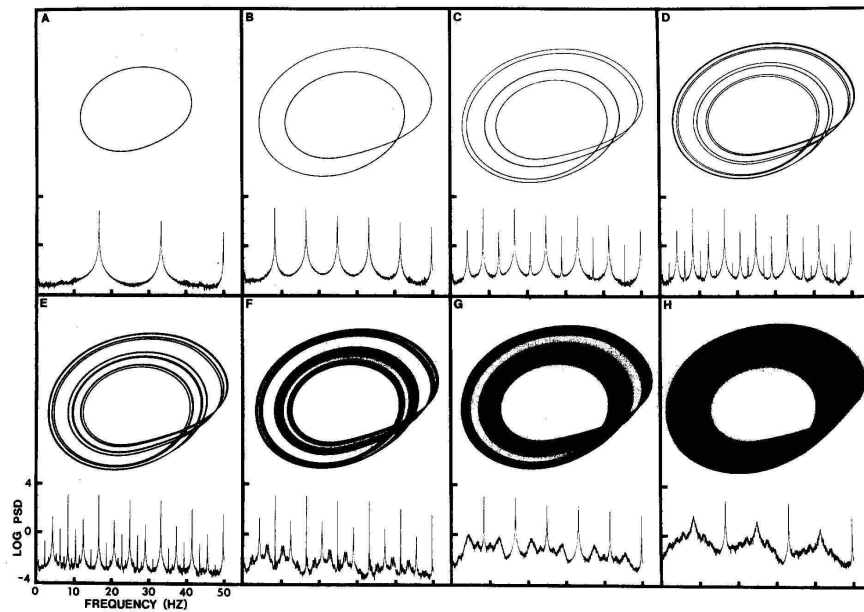


Figure 17.15: Period doubling bifurcations of the Rössler attractor with $a = b = \frac{1}{5}$, projected onto the (X, Y) plane, for eight values of c , and corresponding power spectral density for $Z(t)$. (a) $c = 2.6$; (b) $c = 3.5$; (c) $c = 4.1$; (d) $c = 4.18$; (e) $c = 4.21$; (f) $c = 4.23$; (g) $c = 4.30$; (h) $c = 4.60$.

Chapter 18

Continuum Mechanics

18.1 Continuum Mechanics of the String

18.1.1 Lagrangian formulation

Consider a string of linear mass density $\mu(x)$ under tension $\tau(x)$.¹ Let the string move in a plane, such that its shape is described by a smooth function $y(x)$, the vertical displacement of the string at horizontal position x , as depicted in fig. 18.1. The action is a functional of the height $y(x, t)$, where the coordinate along the string, x , and time, t , are the two independent variables. Consider a differential element of the string extending from x to $x + dx$. The change in length relative to the unstretched ($y = 0$) configuration is

$$d\ell = \sqrt{dx^2 + dy^2} - dx = \frac{1}{2} \left(\frac{\partial y}{\partial x} \right)^2 dx + \mathcal{O}(dx^2) . \quad (18.1)$$

The differential potential energy is then

$$dU = \tau(x) d\ell = \frac{1}{2} \tau(x) \left(\frac{\partial y}{\partial x} \right)^2 dx . \quad (18.2)$$

The differential kinetic energy is simply

$$dT = \frac{1}{2} \mu(x) \left(\frac{\partial y}{\partial t} \right)^2 dx . \quad (18.3)$$

We can then write

$$L = \int dx \mathcal{L} , \quad (18.4)$$

where the *Lagrangian density* \mathcal{L} is

$$\mathcal{L}(y, \dot{y}, y'; x, t) = \frac{1}{2} \mu(x) \left(\frac{\partial y}{\partial t} \right)^2 - \frac{1}{2} \tau(x) \left(\frac{\partial y}{\partial x} \right)^2 . \quad (18.5)$$

¹As an example of a string with a position-dependent tension, consider a string of length ℓ freely suspended from one end at $z = 0$ in a gravitational field. The tension is then $\tau(z) = \mu g(\ell - z)$.

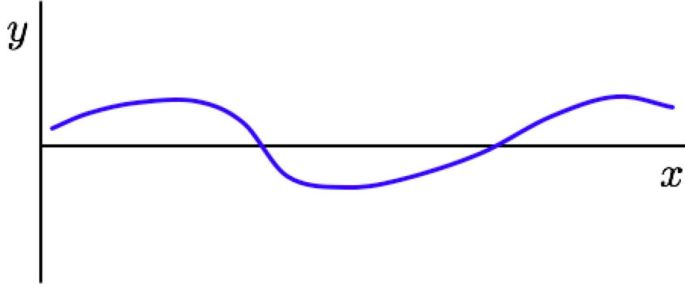


Figure 18.1: A string is described by the vertical displacement field $y(x, t)$.

The action for the string is now a double integral,

$$S = \int_{t_a}^{t_b} dt \int_{x_a}^{x_b} dx \mathcal{L}(y, \dot{y}, y'; x, t) , \quad (18.6)$$

where $y(x, t)$ is the vertical displacement field. Typically, we have $\mathcal{L} = \frac{1}{2}\mu\dot{y}^2 - \frac{1}{2}\tau y'^2$. The first variation of S is

$$\begin{aligned} \delta S = & \int_{x_a}^{x_b} dx \int_{t_a}^{t_b} dt \left[\frac{\partial \mathcal{L}}{\partial y} - \frac{\partial}{\partial x} \left(\frac{\partial \mathcal{L}}{\partial y'} \right) - \frac{\partial}{\partial t} \left(\frac{\partial \mathcal{L}}{\partial \dot{y}} \right) \right] \delta y \\ & + \int_{x_a}^{x_b} dx \left[\frac{\partial \mathcal{L}}{\partial \dot{y}} \delta y \right]_{t=t_a}^{t=t_b} + \int_{t_a}^{t_b} dt \left[\frac{\partial \mathcal{L}}{\partial y'} \delta y \right]_{x=x_b}^{x=x_a} , \end{aligned} \quad (18.7)$$

which simply recapitulates the general result from eqn. 18.181. There are two boundary terms, one of which is an integral over time and the other an integral over space. The first boundary term vanishes provided $\delta y(x, t_a) = \delta y(x, t_b) = 0$. The second boundary term vanishes provided $\tau(x) y'(x) \delta y(x) = 0$ at $x = x_a$ and $x = x_b$, for all t . Assuming $\tau(x)$ does not vanish, this can happen in one of two ways: at each endpoint either $y(x)$ is fixed or $y'(x)$ vanishes.

Assuming that either $y(x)$ is fixed or $y'(x) = 0$ at the endpoints $x = x_a$ and $x = x_b$, the Euler-Lagrange equations for the string are obtained by setting $\delta S = 0$:

$$\begin{aligned} 0 = \frac{\delta S}{\delta y(x, t)} &= \frac{\partial \mathcal{L}}{\partial y} - \frac{\partial}{\partial t} \left(\frac{\partial \mathcal{L}}{\partial \dot{y}} \right) - \frac{\partial}{\partial x} \left(\frac{\partial \mathcal{L}}{\partial y'} \right) \\ &= \frac{\partial}{\partial x} \left[\tau(x) \frac{\partial y}{\partial x} \right] - \mu(x) \frac{\partial^2 y}{\partial t^2} , \end{aligned} \quad (18.8)$$

where $y' = \frac{\partial y}{\partial x}$ and $\dot{y} = \frac{\partial y}{\partial t}$. When $\tau(x) = \tau$ and $\mu(x) = \mu$ are both constants, we obtain the Helmholtz equation,

$$\frac{1}{c^2} \frac{\partial^2 y}{\partial t^2} - \frac{\partial^2 y}{\partial x^2} = 0 , \quad (18.9)$$

which is the wave equation for the string, where $c = \sqrt{\tau/\mu}$ has dimensions of velocity. We will now see that c is the speed of wave propagation on the string.

18.1.2 d'Alembert's Solution to the Wave Equation

Let us define two new variables,

$$u \equiv x - ct \quad , \quad v \equiv x + ct . \quad (18.10)$$

We then have

$$\begin{aligned} \frac{\partial}{\partial x} &= \frac{\partial u}{\partial x} \frac{\partial}{\partial u} + \frac{\partial v}{\partial x} \frac{\partial}{\partial v} = \frac{\partial}{\partial u} + \frac{\partial}{\partial v} \\ \frac{1}{c} \frac{\partial}{\partial t} &= \frac{1}{c} \frac{\partial u}{\partial t} \frac{\partial}{\partial u} + \frac{1}{c} \frac{\partial v}{\partial t} \frac{\partial}{\partial v} = -\frac{\partial}{\partial u} + \frac{\partial}{\partial v} . \end{aligned} \quad (18.11)$$

Thus,

$$\frac{1}{c^2} \frac{\partial^2}{\partial t^2} - \frac{\partial^2}{\partial x^2} = -4 \frac{\partial^2}{\partial u \partial v} . \quad (18.12)$$

Thus, the wave equation may be solved:

$$\frac{\partial^2 y}{\partial u \partial v} = 0 \quad \Rightarrow \quad y(u, v) = f(u) + g(v) , \quad (18.13)$$

where $f(u)$ and $g(v)$ are arbitrary functions. For the moment, we work with an infinite string, so we have no spatial boundary conditions to satisfy. Note that $f(u)$ describes a right-moving disturbance, and $g(v)$ describes a left-moving disturbance:

$$y(x, t) = f(x - ct) + g(x + ct) . \quad (18.14)$$

We do, however, have boundary conditions in time. At $t = 0$, the configuration of the string is given by $y(x, 0)$, and its instantaneous vertical velocity is $\dot{y}(x, 0)$. We then have

$$\begin{aligned} y(x, 0) &= f(x) + g(x) \\ \dot{y}(x, 0) &= -c f'(x) + c g'(x) , \end{aligned} \quad (18.15)$$

hence

$$\begin{aligned} f'(x) &= \frac{1}{2} y'(x, 0) - \frac{1}{2c} \dot{y}(x, 0) \\ g'(x) &= \frac{1}{2} y'(x, 0) + \frac{1}{2c} \dot{y}(x, 0) , \end{aligned} \quad (18.16)$$

and integrating we obtain the right and left moving components

$$\begin{aligned} f(\xi) &= \frac{1}{2} y(\xi, 0) - \frac{1}{2c} \int_0^\xi d\xi' \dot{y}(\xi', 0) - \mathcal{C} \\ g(\xi) &= \frac{1}{2} y(\xi, 0) + \frac{1}{2c} \int_0^\xi d\xi' \dot{y}(\xi', 0) + \mathcal{C} , \end{aligned} \quad (18.17)$$

where \mathcal{C} is an arbitrary constant. Adding these together, we obtain the full solution

$$y(x, t) = \frac{1}{2} [y(x - ct, 0) + y(x + ct, 0)] + \frac{1}{2c} \int_{x-ct}^{x+ct} d\xi \dot{y}(\xi, 0) , \quad (18.18)$$

valid for all times.

18.1.3 Energy density and energy current

The Hamiltonian density for a string is

$$\mathcal{H} = \wp \dot{y} - \mathcal{L} , \quad (18.19)$$

where $\wp = \partial \mathcal{L} / \partial \dot{y} = \mu \dot{y}$ is the momentum density *transverse* to the string. Thus,

$$\mathcal{H} = \frac{\wp^2}{2\mu} + \frac{1}{2}\tau y'^2 . \quad (18.20)$$

Expressed in terms of \dot{y} rather than \wp , this is the energy density \mathcal{E} ,

$$\mathcal{E} = \frac{1}{2}\mu \dot{y}^2 + \frac{1}{2}\tau y'^2 . \quad (18.21)$$

We now evaluate $\dot{\mathcal{E}}$ for a solution to the equations of motion:

$$\begin{aligned} \frac{\partial \mathcal{E}}{\partial t} &= \mu \frac{\partial y}{\partial t} \frac{\partial^2 y}{\partial t^2} + \tau \frac{\partial y}{\partial x} \frac{\partial^2 y}{\partial t \partial x} = \frac{\partial y}{\partial t} \frac{\partial}{\partial x} \left(\tau \frac{\partial y}{\partial x} \right) + \tau \frac{\partial y}{\partial x} \frac{\partial^2 y}{\partial t \partial x} \\ &= \frac{\partial}{\partial x} \left[\tau \frac{\partial y}{\partial x} \frac{\partial y}{\partial t} \right] \equiv -\frac{\partial j_{\mathcal{E}}}{\partial x} , \end{aligned} \quad (18.22)$$

where the *energy current density* (or energy flux) *along the string* is

$$j_{\mathcal{E}} = -\tau \frac{\partial y}{\partial x} \frac{\partial y}{\partial t} . \quad (18.23)$$

We therefore have that solutions of the equation of motion also obey the energy *continuity equation*

$$\frac{\partial \mathcal{E}}{\partial t} + \frac{\partial j_{\mathcal{E}}}{\partial x} = 0 . \quad (18.24)$$

Let us integrate the above equation between points x_1 and x_2 . We obtain

$$\frac{\partial}{\partial t} \int_{x_1}^{x_2} dx \mathcal{E}(x, t) = - \int_{x_1}^{x_2} dx \frac{\partial j_{\mathcal{E}}(x, t)}{\partial x} = j_{\mathcal{E}}(x_1, t) - j_{\mathcal{E}}(x_2, t) , \quad (18.25)$$

which says that the time rate of change of the energy contained in the interval $[x_1, x_2]$ is equal to the difference between the entering and exiting energy flux.

When $\tau(x) = \tau$ and $\mu(x) = \mu$, we have

$$y(x, t) = f(x - ct) + g(x + ct) \quad (18.26)$$

and we find

$$\begin{aligned} \mathcal{E}(x, t) &= \tau[f'(x - ct)]^2 + \tau[g'(x + ct)]^2 \\ j_{\mathcal{E}}(x, t) &= c\tau[f'(x - ct)]^2 - c\tau[g'(x + ct)]^2 , \end{aligned} \quad (18.27)$$

which are each sums over right-moving and left-moving contributions.

Another example is the Klein-Gordon system, for which the Lagrangian density is

$$\mathcal{L} = \frac{1}{2}\mu\dot{y}^2 - \frac{1}{2}\tau y'^2 - \frac{1}{2}\beta y^2 . \quad (18.28)$$

One obtains the equation of motion $\mu\ddot{y} = \tau y'' - \beta y$ and the energy density

$$\mathcal{E} = \frac{1}{2}\mu\dot{y}^2 + \frac{1}{2}\tau y'^2 + \frac{1}{2}\beta y^2 . \quad (18.29)$$

It is left as an exercise to the student to check that the energy current, $j_{\mathcal{E}}$, is the same as in the Helmholtz case: $j_{\mathcal{E}} = -\tau\dot{y}y'$. Energy continuity is again given by $\partial_t \mathcal{E} + \partial_x j_{\mathcal{E}} = 0$. Note that solutions to the Klein-Gordon equation of motion are not of the D'Alembert form.

Momentum flux density and stress energy tensor

Let's now examine the spatial derivative \mathcal{E}' . For the Helmholtz equation, $\mathcal{E} = \frac{1}{2}\mu\dot{y}^2 + \frac{1}{2}\tau y'^2$. We assume $\mu(x) = \mu$ and $\tau(x) = \tau$ are constant. Then

$$\frac{\partial \mathcal{E}}{\partial x} = \mu\dot{y}\dot{y}' + \tau y'y'' = \frac{\partial}{\partial t}(\mu\dot{y}y') , \quad (18.30)$$

where we have invoked the equation of motion $\tau y'' = \mu\ddot{y}$. Thus, we may write

$$\frac{\partial \Pi}{\partial t} + \frac{\partial j_{\Pi}}{\partial x} = 0 , \quad (18.31)$$

where

$$\Pi = -\mu \frac{\partial y}{\partial t} \frac{\partial y}{\partial x} = \frac{j_{\mathcal{E}}}{c^2} , \quad j_{\Pi} = \mathcal{E} . \quad (18.32)$$

is the *momentum flux density along the string*. Eqn. 18.31 is thus a continuity equation for momentum, with the *energy density* playing the role of the *momentum current*. Note that Π and $\varphi = \mu\dot{y}$ have the same dimensions, but the former is the momentum density *along the string* while the latter is the momentum density *transverse to the string*. We may now write

$$\left(\frac{\partial}{\partial t} \quad \frac{\partial}{\partial x} \right) \underbrace{\begin{pmatrix} \mathcal{E} & -\Pi \\ j_{\mathcal{E}} & -j_{\Pi} \end{pmatrix}}_{T^{\mu}_{\nu}} = 0 , \quad (18.33)$$

where $\Pi = j_{\mathcal{E}}/c^2$ and $j_{\Pi} = \mathcal{E}$ for the Helmholtz model. In component notation this is neatly expressed as $\partial_{\mu} T_{\nu}^{\mu} = 0$, where T_{ν}^{μ} is the *stress-energy tensor* and $\partial_{\mu} = (\partial_t, \partial_x)$.

Below in Eqn. 18.184, we will see how the general result for the stress-energy tensor is

$$T_{\nu}^{\mu} = \frac{\partial \mathcal{L}}{\partial(\partial_{\mu} y)} \partial_{\nu} y - \delta_{\nu}^{\mu} \mathcal{L} , \quad (18.34)$$

where $\mu, \nu \in \{0, 1\}$. For $\mathcal{L} = \frac{1}{2}\mu\dot{y}^2 - \frac{1}{2}\tau y'^2$, we recover the stress-energy tensor for the Helmholtz model in Eqn. 18.33. For the Klein-Gordon model, $\mathcal{L} = \frac{1}{2}\mu\dot{y}^2 - \frac{1}{2}\tau y'^2 - \frac{1}{2}\beta y^2$, we find once again $T_0^0 = -\Pi$ but $T_1^1 = -\frac{1}{2}\mu\dot{y}^2 - \frac{1}{2}\tau y'^2 + \frac{1}{2}\beta y^2$ so $T_1^1 \neq -\mathcal{E}$.

Energy and momentum continuity in electrodynamics

A similar energy continuity equation pertains in electrodynamics. Recall $\mathcal{E} = \frac{1}{8\pi}(\mathbf{E}^2 + \mathbf{B}^2)$ is the energy density. We then have

$$\begin{aligned} \frac{\partial \mathcal{E}}{\partial t} &= \frac{1}{4\pi} \left(\mathbf{E} \cdot \frac{\partial \mathbf{E}}{\partial t} + \mathbf{B} \cdot \frac{\partial \mathbf{B}}{\partial t} \right) \\ &= \frac{1}{4\pi} \mathbf{E} \cdot (c \boldsymbol{\nabla} \times \mathbf{B} - 4\pi \mathbf{J}) + \frac{1}{4\pi} \mathbf{B} \cdot (-c \boldsymbol{\nabla} \times \mathbf{E}) \\ &= -\mathbf{E} \cdot \mathbf{J} - \boldsymbol{\nabla} \cdot \underbrace{\left(\frac{c}{4\pi} \mathbf{E} \times \mathbf{B} \right)}_{\text{Poynting vector } \mathbf{S}} . \end{aligned} \quad (18.35)$$

Thus,

$$\frac{\partial \mathcal{E}}{\partial t} + \boldsymbol{\nabla} \cdot \mathbf{S} = -\mathbf{J} \cdot \mathbf{E} , \quad (18.36)$$

which resembles a continuity equation, but with a ‘sink’ term on the RHS to account for the local power dissipated. If $\mathbf{J} = \sigma \mathbf{E}$, where σ is the conductivity, then $\mathbf{J} \cdot \mathbf{E} = \sigma \mathbf{E}^2$, which accounts for *Ohmic dissipation*.

The stress-energy tensor for Maxwell theory is given by

$$T_{\nu}^{\mu} = \begin{pmatrix} \mathcal{E} & -S_x/c & -S_y/c & -S_z/c \\ S_x/c & \sigma_{xx} & \sigma_{xy} & \sigma_{xz} \\ S_y/c & \sigma_{yx} & \sigma_{yy} & \sigma_{yz} \\ S_z/c & \sigma_{zx} & \sigma_{zy} & \sigma_{zz} \end{pmatrix} \quad (18.37)$$

where $\mathcal{E} = \frac{1}{8\pi}(\mathbf{E}^2 + \mathbf{B}^2)$ is the energy density, $\mathbf{S} = \frac{c}{4\pi} \mathbf{E} \times \mathbf{B}$ is the Poynting vector, and

$$\sigma_{ij} = \frac{1}{4\pi} \left\{ -E_i E_j - B_i B_j + \frac{1}{2} \delta_{ij} (\mathbf{E}^2 + \mathbf{B}^2) \right\} \quad (18.38)$$

is the *Maxwell stress tensor*. One again has $\partial_{\mu} T_{\nu}^{\mu} = 0$, this time with $\partial_{\mu} = (\frac{1}{c}\partial_t, \partial_x, \partial_y, \partial_z)$.

18.1.4 Reflection at an interface

Consider a semi-infinite string on the interval $[0, \infty]$, with $y(0, t) = 0$. We can still invoke d'Alembert's solution, $y(x, t) = f(x - ct) + g(x + ct)$, but we must demand

$$y(0, t) = f(-ct) + g(ct) = 0 \quad \Rightarrow \quad f(\xi) = -g(-\xi) . \quad (18.39)$$

Thus,

$$y(x, t) = g(ct + x) - g(ct - x) . \quad (18.40)$$

Now suppose $g(\xi)$ describes a pulse, and is nonzero only within a neighborhood of $\xi = 0$. For large negative values of t , the right-moving part, $-g(ct - x)$, is negligible everywhere, since $x > 0$ means that the argument $ct - x$ is always large and negative. On the other hand, the left moving part $g(ct + x)$ is nonzero for $x \approx -ct > 0$. Thus, for $t < 0$ we have a left-moving pulse incident from the right. For $t > 0$, the situation is reversed, and the left-moving component is negligible, and we have a right moving reflected wave. However, the minus sign in eqn. 18.39 means that the reflected wave is *inverted*.

If instead of fixing the endpoint at $x = 0$ we attach this end of the string to a massless ring which frictionlessly slides up and down a vertical post, then we must have $y'(0, t) = 0$, else there is a finite vertical force on the massless ring, resulting in infinite acceleration. We again write $y(x, t) = f(x - ct) + g(x + ct)$, and we invoke

$$y'(0, t) = f'(-ct) + g'(ct) \quad \Rightarrow \quad f'(\xi) = -g'(-\xi) , \quad (18.41)$$

which, upon integration, yields $f(\xi) = g(-\xi)$, and therefore

$$y(x, t) = g(ct + x) + g(ct - x) . \quad (18.42)$$

The reflected pulse is now 'right-side up', in contrast to the situation with a fixed endpoint.

18.1.5 Mass point on a string

Next, consider the case depicted in Fig. 18.4, where a point mass m is affixed to an infinite string at $x = 0$. Let us suppose that at large negative values of t , a right moving wave $f(ct - x)$ is incident from the left. The full solution may then be written as a sum of incident, reflected, and transmitted waves:

$$\begin{aligned} x < 0 & : y(x, t) = f(ct - x) + g(ct + x) \\ x > 0 & : y(x, t) = h(ct - x) . \end{aligned} \quad (18.43)$$

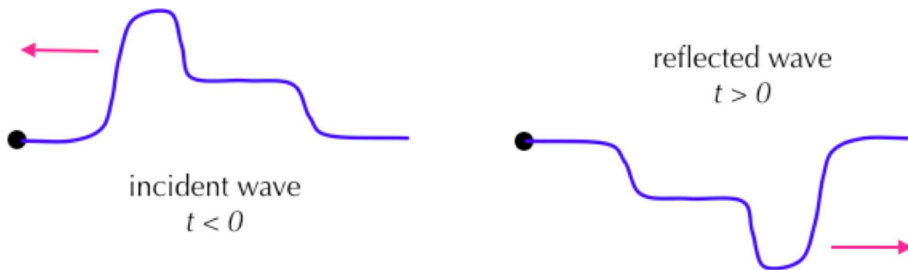


Figure 18.2: Reflection of a pulse at an interface at $x = 0$, with $y(0, t) = 0$.

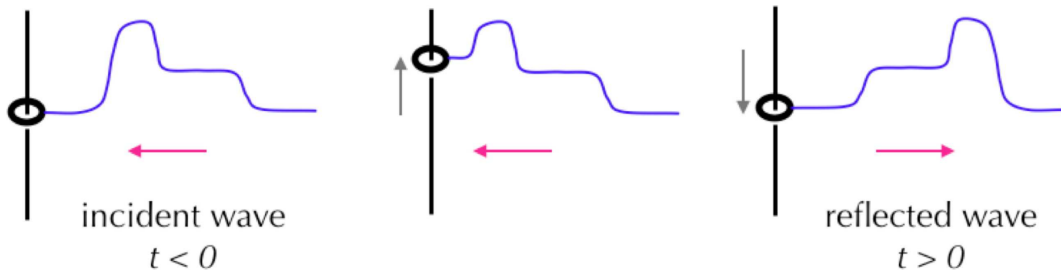


Figure 18.3: Reflection of a pulse at an interface at $x = 0$, with $y'(0, t) = 0$.

At $x = 0$, we invoke Newton's second Law, $F = ma$:

$$m \ddot{y}(0, t) = \tau y'(0^+, t) - \tau y'(0^-, t) . \quad (18.44)$$

Any discontinuity in the derivative $y'(x, t)$ at $x = 0$ results in an acceleration of the point mass. Note that

$$y'(0^-, t) = -f'(ct) + g'(ct) , \quad y'(0^+, t) = -h'(ct) . \quad (18.45)$$

Further invoking continuity at $x = 0$, i.e. $y(0^-, t) = y(0^+, t)$, we have

$$h(\xi) = f(\xi) + g(\xi) , \quad (18.46)$$

and eqn. 18.44 becomes

$$g''(\xi) + \frac{2\tau}{mc^2} g'(\xi) = -f''(\xi) . \quad (18.47)$$

We solve this equation by Fourier analysis:

$$f(\xi) = \int_{-\infty}^{\infty} \frac{dk}{2\pi} \hat{f}(k) e^{ik\xi} , \quad \hat{f}(k) = \int_{-\infty}^{\infty} d\xi f(\xi) e^{-ik\xi} . \quad (18.48)$$

Defining $\kappa \equiv 2\tau/mc^2 = 2\mu/m$, we have

$$[-k^2 + i\kappa k] \hat{g}(k) = k^2 \hat{f}(k) . \quad (18.49)$$

We may now write $\hat{g}(k) = r(k) \hat{f}(k)$ and $\hat{h}(k) = t(k) \hat{f}(k)$, where

$$r(k) = -\frac{k}{k - i\kappa} , \quad t(k) = -\frac{i\kappa}{k - i\kappa} \quad (18.50)$$

are the *reflection and transmission amplitudes*, respectively.

Energy conservation

Note that $t(k) = 1 + r(k)$. This relation follows from continuity at $x = 0$, which entails $h(\xi) = f(\xi) + g(\xi)$, hence $\hat{h}(k) = \hat{f}(k) + \hat{g}(k)$. What is also true – if there is no dissipation – is

$$|r(k)|^2 + |t(k)|^2 = 1 , \quad (18.51)$$

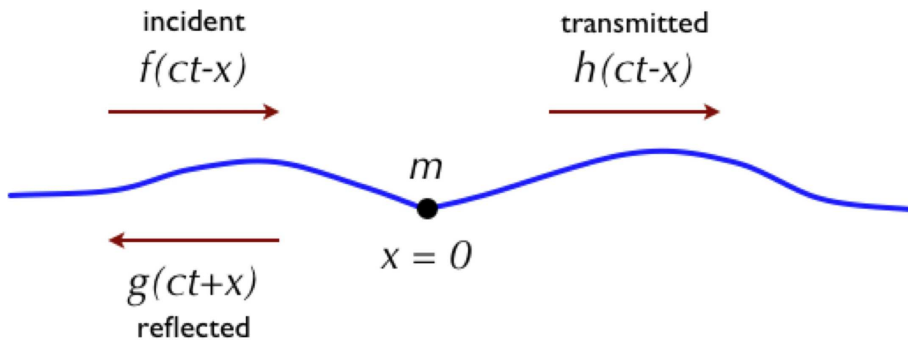


Figure 18.4: Reflection and transmission at an impurity. A point mass m is affixed to an infinite string at $x = 0$.

which is a statement of energy conservation. Integrating the energy density of the string itself, one finds

$$\begin{aligned} E_{\text{string}}(t) &= \int_{-\infty}^{\infty} dx \left(\frac{1}{2}\mu \dot{y}^2 + \frac{1}{2}\tau y'^2 \right) \\ &= \tau \int_{ct}^{\infty} d\xi [f'(\xi)]^2 + \tau \int_{-\infty}^{ct} d\xi ([g'(\xi)]^2 + [h'(\xi)]^2). \end{aligned} \quad (18.52)$$

What is missing from this expression is the kinetic energy of the mass point. However, as $t \rightarrow \pm\infty$, the kinetic energy of the mass point vanishes; it starts from rest, and as $t \rightarrow \infty$ it shakes off all its energy into waves on the string. Therefore

$$\begin{aligned} E_{\text{string}}(-\infty) &= \tau \int_{-\infty}^{\infty} d\xi [f'(\xi)]^2 = \tau \int_{-\infty}^{\infty} \frac{dk}{2\pi} k^2 |\hat{f}(k)|^2 \\ E_{\text{string}}(+\infty) &= \tau \int_{-\infty}^{\infty} d\xi ([g'(\xi)]^2 + [h'(\xi)]^2) = \tau \int_{-\infty}^{\infty} \frac{dk}{2\pi} k^2 (|r(k)|^2 + |t(k)|^2) |\hat{f}(k)|^2, \end{aligned} \quad (18.53)$$

and since the profile $\hat{f}(k)$ is arbitrary we conclude that Eqn. 18.51 must hold *for every value of the wavevector k* . It must be stressed energy conservation holds *only if there is no dissipation*. Dissipation could be modeled by adding a friction term $-\gamma \dot{y}(0, t)$ to the RHS of Eqn. 18.44. In this case, $dE_{\text{string}}(t)/dt$ would be negative, corresponding to the energy loss due to friction.

Real space form of the solution

Getting back to our solution, in real space we have

$$\begin{aligned} h(\xi) &= \int_{-\infty}^{\infty} \frac{dk}{2\pi} t(k) \hat{f}(k) e^{ik\xi} \\ &= \int_{-\infty}^{\infty} d\xi' \left[\int_{-\infty}^{\infty} \frac{dk}{2\pi} t(k) e^{ik(\xi - \xi')} \right] f(\xi') \equiv \int_{-\infty}^{\infty} d\xi' \mathcal{T}(\xi - \xi') f(\xi') , \end{aligned} \quad (18.54)$$

where

$$\mathcal{T}(\xi - \xi') = \int_{-\infty}^{\infty} \frac{dk}{2\pi} t(k) e^{ik(\xi - \xi')} , \quad (18.55)$$

is the transmission kernel in real space. For our example with $r(k) = -i\kappa/(k - i\kappa)$, the integral is done easily using the method of contour integration:

$$\mathcal{T}(\xi - \xi') = \int_{-\infty}^{\infty} \frac{dk}{2\pi} \frac{-i\kappa}{k - i\kappa} e^{ik(\xi - \xi')} = \kappa e^{-\kappa(\xi - \xi')} \Theta(\xi - \xi') . \quad (18.56)$$

Therefore,

$$h(\xi) = \kappa \int_{-\infty}^{\xi} d\xi' e^{-\kappa(\xi - \xi')} f(\xi') , \quad (18.57)$$

and of course $g(\xi) = h(\xi) - f(\xi)$. Note that $m = \infty$ means $\kappa = 0$, in which case $r(k) = -1$ and $t(k) = 0$. Thus we recover the inversion of the pulse shape under reflection found earlier.

For example, let the incident pulse shape be $f(\xi) = b \Theta(a - |\xi|)$. Then

$$\begin{aligned} h(\xi) &= \kappa \int_{-\infty}^{\xi} d\xi' e^{-\kappa(\xi - \xi')} b \Theta(a - \xi') \Theta(a + \xi') \\ &= b e^{-\kappa\xi} [e^{\kappa \min(a, \xi)} - e^{-\kappa a}] \Theta(\xi + a) . \end{aligned} \quad (18.58)$$

Taking cases,

$$h(\xi) = \begin{cases} 0 & \text{if } \xi < -a \\ b(1 - e^{-\kappa(a+\xi)}) & \text{if } -a < \xi < a \\ 2b e^{-\kappa\xi} \sinh(\kappa a) & \text{if } \xi > a . \end{cases} \quad (18.59)$$

In Fig. 18.5 we show the reflection and transmission of this square pulse for two different values of κa .

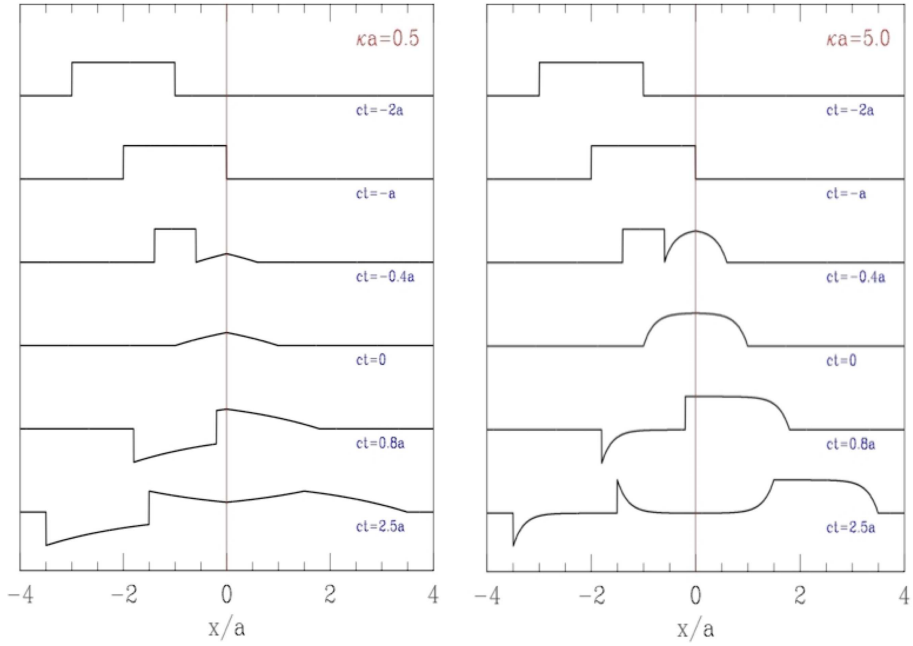


Figure 18.5: Reflection and transmission of a square wave pulse by a point mass at $x = 0$. The configuration of the string is shown for six different times, for $\kappa a = 0.5$ (left panel) and $\kappa a = 5.0$ (right panel). Note that the $\kappa a = 0.5$ case, which corresponds to a large mass $m = 2\mu/\kappa$, results in strong reflection with inversion, and weak transmission. For large κ , corresponding to small mass m , the reflection is weak and the transmission is strong.

18.1.6 Interface between strings of different mass density

Consider the situation in fig. 18.6, where the string for $x < 0$ is of density μ_L and for $x > 0$ is of density μ_R . The d'Alembert solution in the two regions, with an incoming wave from the left, is

$$\begin{aligned} x < 0: \quad y(x, t) &= f(c_L t - x) + g(c_L t + x) \\ x > 0: \quad y(x, t) &= h(c_R t - x) . \end{aligned} \tag{18.60}$$

At $x = 0$ we have

$$\begin{aligned} f(c_L t) + g(c_L t) &= h(c_R t) \\ -f'(c_L t) + g'(c_L t) &= -h'(c_R t) , \end{aligned} \tag{18.61}$$

where the second equation follows from $\tau y'(0^+, t) = \tau y'(0^-, t)$, so there is no finite vertical force on the infinitesimal interval bounding $x = 0$, which contains infinitesimal mass. Defining $\alpha \equiv c_R/c_L$, we integrate the second of these equations and have

$$f(\xi) + g(\xi) = h(\alpha \xi) \quad , \quad f(\xi) - g(\xi) = \alpha^{-1} h(\alpha \xi) . \tag{18.62}$$

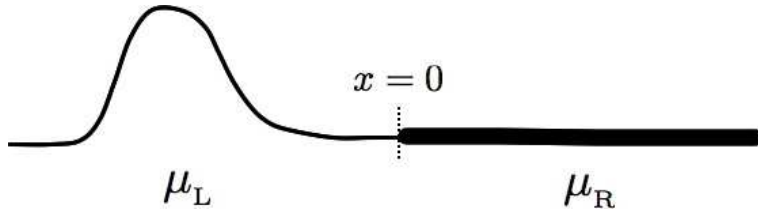


Figure 18.6: A string formed from two semi-infinite regions of different densities.

Note that $y(\pm\infty, 0) = 0$ fixes the constant of integration. The solution is then

$$g(\xi) = \frac{\alpha - 1}{\alpha + 1} f(\xi) \quad , \quad h(\xi) = \frac{2\alpha}{\alpha + 1} f(\xi/\alpha) . \quad (18.63)$$

Thus,

$$\begin{aligned} x < 0: \quad y(x, t) &= f(c_L t - x) + \left(\frac{\alpha - 1}{\alpha + 1} \right) f(c_L t + x) \\ x > 0: \quad y(x, t) &= \frac{2\alpha}{\alpha + 1} f((c_R t - x)/\alpha) . \end{aligned} \quad (18.64)$$

It is instructive to compute the total energy in the string. For large negative values of the time t , the entire disturbance is confined to the region $x < 0$. The energy is

$$E(-\infty) = \tau \int_{-\infty}^{\infty} d\xi [f'(\xi)]^2 . \quad (18.65)$$

For large positive times, the wave consists of the left-moving reflected $g(\xi)$ component in the region $x < 0$ and the right-moving transmitted component $h(\xi)$ in the region $x > 0$. The energy in the reflected wave is

$$E_L(+\infty) = \tau \left(\frac{\alpha - 1}{\alpha + 1} \right)^2 \int_{-\infty}^{\infty} d\xi [f'(\xi)]^2 . \quad (18.66)$$

For the transmitted portion, we use

$$y'(x > 0, t) = \frac{2}{\alpha + 1} f'((c_R t - x)/\alpha) \quad (18.67)$$

to obtain

$$E_R(\infty) = \frac{4\tau}{(\alpha + 1)^2} \int_{-\infty}^{\infty} d\xi [f'(\xi/\alpha)]^2 = \frac{4\alpha\tau}{(\alpha + 1)^2} \int_{-\infty}^{\infty} d\xi [f'(\xi)]^2 . \quad (18.68)$$

Thus, $E_L(\infty) + E_R(\infty) = E(-\infty)$, and energy is conserved.

18.1.7 Finite Strings : Bernoulli's Solution

Suppose $x_a = 0$ and $x_b = L$ are the boundaries of the string, where $y(0, t) = y(L, t) = 0$. Again we write

$$y(x, t) = f(x - ct) + g(x + ct) . \quad (18.69)$$

Applying the boundary condition at $x_a = 0$ gives, as earlier,

$$y(x, t) = g(ct + x) - g(ct - x) . \quad (18.70)$$

Next, we apply the boundary condition at $x_b = L$, which results in

$$g(ct + L) - g(ct - L) = 0 \implies g(\xi) = g(\xi + 2L) . \quad (18.71)$$

Thus, $g(\xi)$ is periodic, with period $2L$. Any such function may be written as a Fourier sum,

$$g(\xi) = \sum_{n=1}^{\infty} \left\{ \mathcal{A}_n \cos\left(\frac{n\pi\xi}{L}\right) + \mathcal{B}_n \sin\left(\frac{n\pi\xi}{L}\right) \right\} . \quad (18.72)$$

The full solution for $y(x, t)$ is then

$$\begin{aligned} y(x, t) &= g(ct + x) - g(ct - x) \\ &= \left(\frac{2}{\mu L}\right)^{1/2} \sum_{n=1}^{\infty} \sin\left(\frac{n\pi x}{L}\right) \left\{ A_n \cos\left(\frac{n\pi ct}{L}\right) + B_n \sin\left(\frac{n\pi ct}{L}\right) \right\} , \end{aligned} \quad (18.73)$$

where $A_n = \sqrt{2\mu L} \mathcal{B}_n$ and $B_n = -\sqrt{2\mu L} \mathcal{A}_n$. This is known as Bernoulli's solution.

We define the functions

$$\psi_n(x) \equiv \left(\frac{2}{\mu L}\right)^{1/2} \sin\left(\frac{n\pi x}{L}\right) . \quad (18.74)$$

We also write

$$k_n \equiv \frac{n\pi x}{L} , \quad \omega_n \equiv \frac{n\pi c}{L} , \quad n = 1, 2, 3, \dots, \infty . \quad (18.75)$$

Thus, $\psi_n(x) = \sqrt{2/\mu L} \sin(k_n x)$ has $(n+1)$ nodes at $x = jL/n$, for $j \in \{0, \dots, n\}$. Note that

$$\langle \psi_m | \psi_n \rangle \equiv \int_0^L dx \mu \psi_m(x) \psi_n(x) = \delta_{mn} . \quad (18.76)$$

Furthermore, this basis is complete:

$$\mu \sum_{n=1}^{\infty} \psi_n(x) \psi_n(x') = \delta(x - x') . \quad (18.77)$$

Our general solution is thus equivalent to

$$y(x, 0) = \sum_{n=1}^{\infty} A_n \psi_n(x) , \quad \dot{y}(x, 0) = \sum_{n=1}^{\infty} \frac{n\pi c}{L} B_n \psi_n(x) . \quad (18.78)$$

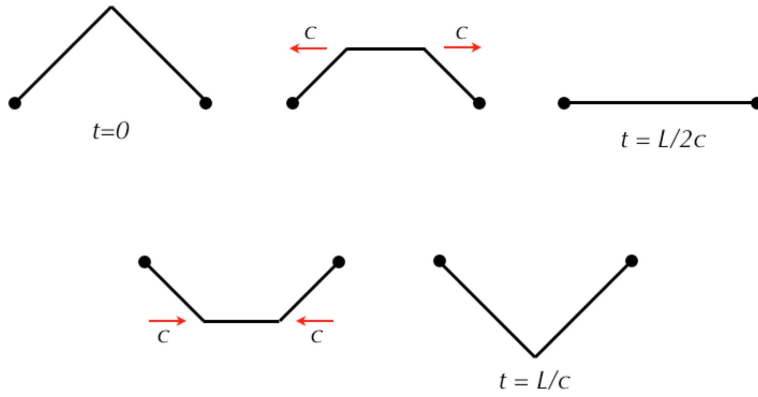


Figure 18.7: Evolution of a string with fixed ends starting from an isosceles triangle shape.

The Fourier coefficients $\{A_n, B_n\}$ may be extracted from the initial data using the orthonormality of the basis functions and their associated resolution of unity:

$$A_n = \int_0^L dx \mu \psi_n(x) y(x, 0) \quad , \quad B_n = \frac{L}{n\pi c} \int_0^L dx \mu \psi_n(x) \dot{y}(x, 0) . \quad (18.79)$$

As an example, suppose our initial configuration is a triangle, with

$$y(x, 0) = \begin{cases} 2bx/L & \text{if } 0 \leq x \leq \frac{1}{2}L \\ 2b(L-x)/L & \text{if } \frac{1}{2}L \leq x \leq L , \end{cases} \quad (18.80)$$

and $\dot{y}(x, 0) = 0$. Then $B_n = 0$ for all n , while

$$\begin{aligned} A_n &= \left(\frac{2\mu}{L}\right)^{1/2} \cdot \frac{2b}{L} \left\{ \int_0^{L/2} dx x \sin\left(\frac{n\pi x}{L}\right) + \int_{L/2}^L dx (L-x) \sin\left(\frac{n\pi x}{L}\right) \right\} \\ &= (2\mu L)^{1/2} \cdot \frac{4b}{n^2 \pi^2} \sin\left(\frac{1}{2}n\pi\right) \delta_{n,\text{odd}} , \end{aligned} \quad (18.81)$$

after changing variables to $x = L\theta/n\pi$ and using $\theta \sin \theta d\theta = d(\sin \theta - \theta \cos \theta)$. Another way to write this is to separately give the results for even and odd coefficients:

$$A_{2k} = 0 \quad , \quad A_{2k+1} = \frac{4b}{\pi^2} (2\mu L)^{1/2} \cdot \frac{(-1)^k}{(2k+1)^2} . \quad (18.82)$$

Note that each $\psi_{2k}(x) = -\psi_{2k}(L-x)$ is antisymmetric about the midpoint $x = \frac{1}{2}L$, for all k . Since our initial conditions are that $y(x, 0)$ is symmetric about $x = \frac{1}{2}L$, none of the even order eigenfunctions can enter into the expansion, precisely as we have found. The d'Alembert solution to this problem is particularly simple and is shown in Fig. 18.7. Note that $g(x) = \frac{1}{2}y(x, 0)$ must be extended to the entire real line. We know that $g(x) = g(x+2L)$ is periodic with spatial period $2L$, but how to we extend $g(x)$ from the interval $[0, L]$ to the interval $[-L, 0]$? To do this, we use $y(x, 0) = g(x) - g(-x)$, which says that $g(x)$ must be *antisymmetric*, i.e. $g(x) = -g(-x)$. Equivalently, $\dot{y}(x, 0) = cg'(x) - cg'(-x) = 0$, which integrates to $g(x) = -g(-x)$.

18.2 Sturm-Liouville Theory

18.2.1 Mathematical formalism

Consider the Lagrangian density

$$\mathcal{L} = \frac{1}{2} \mu(x) \dot{y}^2 - \frac{1}{2} \tau(x) y'^2 - \frac{1}{2} v(x) y^2 . \quad (18.83)$$

The last term is new and has the physical interpretation of a harmonic potential which attracts the string to the line $y = 0$. The Euler-Lagrange equations are then

$$-\frac{\partial}{\partial x} \left[\tau(x) \frac{\partial y}{\partial x} \right] + v(x) y = -\mu(x) \frac{\partial^2 y}{\partial t^2} . \quad (18.84)$$

This equation is invariant under time translation. Thus, if $y(x, t)$ is a solution, then so is $y(x, t + t_0)$, for any t_0 . This means that the solutions can be chosen to be eigenstates of the operator ∂_t , which is to say $y(x, t) = \psi(x) e^{-i\omega t}$. Because the coefficients are real, both y and y^* are solutions, and taking linear combinations we have

$$y(x, t) = \psi(x) \cos(\omega t + \phi) . \quad (18.85)$$

Plugging this into eqn. 18.84, we obtain

$$-\frac{d}{dx} \left[\tau(x) \psi'(x) \right] + v(x) \psi(x) = \omega^2 \mu(x) \psi(x) . \quad (18.86)$$

This is the Sturm-Liouville equation. There are four types of boundary conditions that we shall consider:

1. Fixed endpoint: $\psi(x) = 0$, where $x = x_{a,b}$.
2. Natural: $\tau(x) \psi'(x) = 0$, where $x = x_{a,b}$.
3. Periodic: $\psi(x) = \psi(x + L)$, where $L = x_b - x_a$.
4. Mixed homogeneous: $\alpha \psi(x) + \beta \psi'(x) = 0$, where $x = x_{a,b}$.

The Sturm-Liouville equation is an eigenvalue equation. The eigenfunctions $\{\psi_n(x)\}$ satisfy

$$-\frac{d}{dx} \left[\tau(x) \psi'_n(x) \right] + v(x) \psi_n(x) = \omega_n^2 \mu(x) \psi_n(x) . \quad (18.87)$$

Now suppose we have a second solution $\psi_m(x)$, satisfying

$$-\frac{d}{dx} \left[\tau(x) \psi'_m(x) \right] + v(x) \psi_m(x) = \omega_m^2 \mu(x) \psi_m(x) . \quad (18.88)$$

Now multiply (18.87)* by $\psi_m(x)$ and (18.88) by $\psi_n^*(x)$ and subtract, yielding

$$\begin{aligned} \psi_n^* \frac{d}{dx} \left[\tau \psi'_m \right] - \psi_m \frac{d}{dx} \left[\tau \psi'^*_n \right] &= (\omega_n^{*2} - \omega_m^2) \mu \psi_m \psi_n^* \\ &= \frac{d}{dx} \left[\tau \psi_n^* \psi'_m - \tau \psi_m \psi'^*_n \right] . \end{aligned} \quad (18.89)$$

We integrate this equation over the length of the string, to get

$$(\omega_n^{*2} - \omega_m^2) \int_{x_a}^{x_b} dx \mu(x) \psi_n^*(x) \psi_m(x) = \left[\tau(x) \psi_n^*(x) \psi'_m(x) - \tau(x) \psi_m(x) \psi'^*_n(x) \right]_{x_a}^{x_b} = 0 . \quad (18.90)$$

The term in square brackets vanishes for any of the four types of boundary conditions articulated above. Thus, we have

$$(\omega_n^{*2} - \omega_m^2) \langle \psi_n | \psi_m \rangle = 0 , \quad (18.91)$$

where the inner product is defined as

$$\langle \psi | \phi \rangle \equiv \int_{x_a}^{x_b} dx \mu(x) \psi^*(x) \phi(x) . \quad (18.92)$$

The distribution $\mu(x)$ is non-negative definite. Setting $m = n$, we have $\langle \psi_n | \psi_n \rangle \geq 0$, and hence $\omega_n^{*2} = \omega_n^2$, which says that $\omega_n^2 \in \mathbb{R}$. When $\omega_m^2 \neq \omega_n^2$, the eigenfunctions are orthogonal with respect to the above inner product. In the case of degeneracies, we may invoke the Gram-Schmidt procedure, which orthogonalizes the eigenfunctions within a given degenerate subspace. Since the Sturm-Liouville equation is linear, we may normalize the eigenfunctions, taking

$$\langle \psi_m | \psi_n \rangle = \delta_{mn} . \quad (18.93)$$

Finally, since the coefficients in the Sturm-Liouville equation are all real, we can and henceforth do choose the eigenfunctions themselves to be real.

Another important result, which we will not prove here, is the *completeness* of the eigenfunction basis. Completeness means

$$\mu(x) \sum_n \psi_n^*(x) \psi_n(x') = \delta(x - x') . \quad (18.94)$$

Thus, any function can be expanded in the eigenbasis, *viz.*

$$\phi(x) = \sum_n C_n \psi_n(x) , \quad C_n = \langle \psi_n | \phi \rangle . \quad (18.95)$$

18.2.2 Variational method

Consider the functional

$$\omega^2[\psi(x)] = \frac{\frac{1}{2} \int_{x_a}^{x_b} dx \left\{ \tau(x) \psi'^2(x) + v(x) \psi^2(x) \right\}}{\frac{1}{2} \int_{x_a}^{x_b} dx \mu(x) \psi^2(x)} \equiv \frac{\mathcal{N}}{\mathcal{D}} . \quad (18.96)$$

The variation is

$$\delta\omega^2 = \frac{\delta\mathcal{N}}{\mathcal{D}} - \frac{\mathcal{N}\delta\mathcal{D}}{\mathcal{D}^2} = \frac{\delta\mathcal{N} - \omega^2 \delta\mathcal{D}}{\mathcal{D}} . \quad (18.97)$$

Thus, $\delta\omega^2 = 0$ requires $\delta\mathcal{N} = \omega^2 \delta\mathcal{D}$, which says

$$-\frac{d}{dx} \left[\tau(x) \frac{d\psi(x)}{dx} \right] + v(x) \psi(x) = \omega^2 \mu(x) \psi(x) , \quad (18.98)$$

which is the Sturm-Liouville equation. In obtaining this equation, we have dropped a boundary term, which is correct provided

$$\left[\tau(x) \psi'(x) \psi(x) \right]_{x=x_a}^{x=x_b} = 0 . \quad (18.99)$$

This condition is satisfied for any of the first three classes of boundary conditions: $\psi = 0$ (fixed endpoint), $\tau\psi' = 0$ (natural), or $\psi(x_a) = \psi(x_b)$, $\psi'(x_a) = \psi'(x_b)$ (periodic). For the fourth class of boundary conditions, $\alpha\psi + \beta\psi' = 0$ (mixed homogeneous), the Sturm-Liouville equation may still be derived, provided one uses a slightly different functional,

$$\omega^2 [\psi(x)] = \frac{\tilde{\mathcal{N}}}{\mathcal{D}} \quad \text{with} \quad \tilde{\mathcal{N}} = \mathcal{N} + \frac{\alpha}{2\beta} \left[\tau(x_b) \psi^2(x_b) - \tau(x_a) \psi^2(x_a) \right] , \quad (18.100)$$

since then

$$\begin{aligned} \delta\tilde{\mathcal{N}} - \tilde{\mathcal{N}} \delta\mathcal{D} &= \int_{x_a}^{x_b} dx \left\{ -\frac{d}{dx} \left[\tau(x) \frac{d\psi(x)}{dx} \right] + v(x) \psi(x) - \omega^2 \mu(x) \psi(x) \right\} \delta\psi(x) \\ &\quad + \left[\tau(x) \left(\psi'(x) + \frac{\alpha}{\beta} \psi(x) \right) \delta\psi(x) \right]_{x=x_a}^{x=x_b} , \end{aligned} \quad (18.101)$$

and the last term vanishes as a result of the boundary conditions.

For all four classes of boundary conditions we may write

$$\omega^2 [\psi(x)] = \frac{\int_{x_a}^{x_b} dx \psi(x) \overbrace{\left[-\frac{d}{dx} \tau(x) \frac{d}{dx} + v(x) \right]}^K \psi(x)}{\int_{x_a}^{x_b} dx \mu(x) \psi^2(x)} \quad (18.102)$$

If we expand $\psi(x)$ in the basis of eigenfunctions of the Sturm-Liouville operator K ,

$$\psi(x) = \sum_{n=1}^{\infty} \mathcal{C}_n \psi_n(x) , \quad (18.103)$$

we obtain

$$\omega^2 [\psi(x)] = \omega^2 (\mathcal{C}_1, \dots, \mathcal{C}_{\infty}) = \frac{\sum_{j=1}^{\infty} |\mathcal{C}_j|^2 \omega_j^2}{\sum_{k=1}^{\infty} |\mathcal{C}_k|^2} . \quad (18.104)$$

If $\omega_1^2 \leq \omega_2^2 \leq \dots$, then we see that $\omega^2 \geq \omega_1^2$, so an arbitrary function $\psi(x)$ will always yield an upper bound to the lowest eigenvalue.

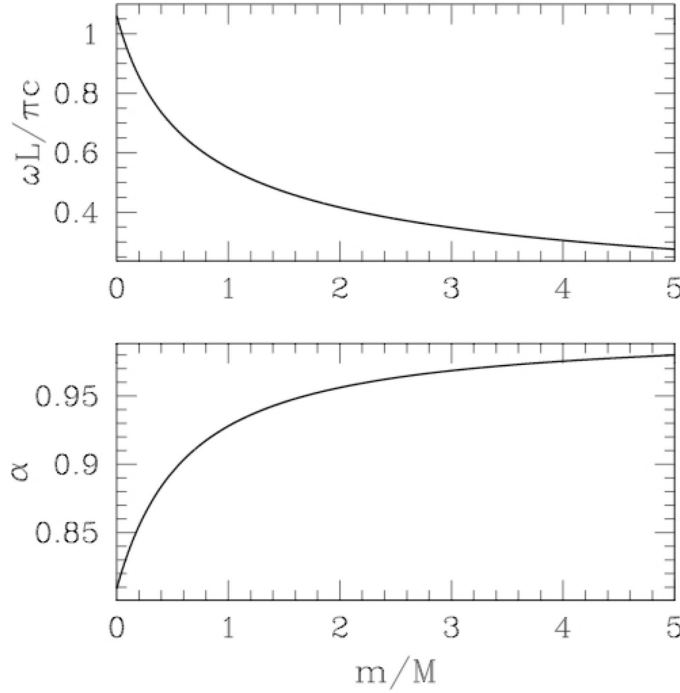


Figure 18.8: One-parameter variational solution for a string with a point mass m at $x = \frac{1}{2}L$.

As an example, consider a violin string ($v = 0$) with a mass m affixed in the center. We write $\mu(x) = \mu + m\delta(x - \frac{1}{2}L)$, hence

$$\omega^2[\psi(x)] = \frac{\tau \int_0^L dx \psi'^2(x)}{m \psi^2(\frac{1}{2}L) + \mu \int_0^L dx \psi^2(x)} \quad (18.105)$$

Now consider a trial function

$$\psi(x) = \begin{cases} A x^\alpha & \text{if } 0 \leq x \leq \frac{1}{2}L \\ A (L-x)^\alpha & \text{if } \frac{1}{2}L \leq x \leq L . \end{cases} \quad (18.106)$$

The functional $\omega^2[\psi(x)]$ now becomes an ordinary function of the trial parameter α , with

$$\omega^2(\alpha) = \frac{2\tau \int_0^{L/2} dx \alpha^2 x^{2\alpha-2}}{m (\frac{1}{2}L)^{2\alpha} + 2\mu \int_0^{L/2} dx x^{2\alpha}} = \left(\frac{2c}{L}\right)^2 \cdot \frac{\alpha^2(2\alpha+1)}{(2\alpha-1)[1+(2\alpha+1)\frac{m}{M}]} , \quad (18.107)$$

where $M = \mu L$ is the mass of the string alone. We minimize $\omega^2(\alpha)$ to obtain the optimal solution of this form:

$$\frac{d}{d\alpha} \omega^2(\alpha) = 0 \implies 4\alpha^2 - 2\alpha - 1 + (2\alpha+1)^2 (\alpha-1) \frac{m}{M} = 0 . \quad (18.108)$$

For $m/M \rightarrow 0$, we obtain $\alpha = \frac{1}{4}(1 + \sqrt{5}) \approx 0.809$. The variational estimate for the eigenvalue is then 6.00% larger than the exact answer $\omega_1^0 = \pi c/L$. In the opposite limit, $m/M \rightarrow \infty$, the inertia of the string may be neglected. The normal mode is then piecewise linear, in the shape of an isosceles triangle with base L and height y . The equation of motion is then $m\ddot{y} = -2\tau \cdot (y/\frac{1}{2}L)$, assuming $|y/L| \ll 1$. Thus, $\omega_1 = (2c/L)\sqrt{M/m}$. This is reproduced exactly by the variational solution, for which $\alpha \rightarrow 1$ as $m/M \rightarrow \infty$.

18.3 Continua in Higher Dimensions

18.3.1 General formalism

In higher dimensions, we generalize the operator K as follows:

$$K = -\frac{\partial}{\partial x^\alpha} \tau_{\alpha\beta}(\mathbf{x}) \frac{\partial}{\partial x^\beta} + v(\mathbf{x}) . \quad (18.109)$$

The eigenvalue equation is again

$$K\psi(\mathbf{x}) = \omega^2 \mu(\mathbf{x}) \psi(\mathbf{x}) , \quad (18.110)$$

and the *Green's function* (see §18.7) satisfies

$$[K - \omega^2 \mu(\mathbf{x})] G_\omega(\mathbf{x}, \mathbf{x}') = \delta(\mathbf{x} - \mathbf{x}') , \quad (18.111)$$

and has the eigenfunction expansion,

$$G_\omega(\mathbf{x}, \mathbf{x}') = \sum_{n=1}^{\infty} \frac{\psi_n(\mathbf{x}) \psi_n(\mathbf{x}')}{\omega_n^2 - \omega^2} . \quad (18.112)$$

The eigenfunctions form a complete and orthonormal basis:

$$\begin{aligned} \mu(\mathbf{x}) \sum_{n=1}^{\infty} \psi_n(\mathbf{x}) \psi_n(\mathbf{x}') &= \delta(\mathbf{x} - \mathbf{x}') \\ \int_{\Omega} d\mathbf{x} \mu(\mathbf{x}) \psi_m(\mathbf{x}) \psi_n(\mathbf{x}) &= \delta_{mn} , \end{aligned} \quad (18.113)$$

where Ω is the region of space in which the continuous medium exists. For purposes of simplicity, we consider here fixed boundary conditions $u(\mathbf{x}, t)|_{\partial\Omega} = 0$, where $\partial\Omega$ is the boundary of Ω . The general solution to the wave equation

$$\left[\mu(\mathbf{x}) \frac{\partial^2}{\partial t^2} - \frac{\partial}{\partial x^\alpha} \tau_{\alpha\beta}(\mathbf{x}) \frac{\partial}{\partial x^\beta} + v(\mathbf{x}) \right] u(\mathbf{x}, t) = 0 \quad (18.114)$$

is

$$u(\mathbf{x}, t) = \sum_{n=1}^{\infty} C_n \psi_n(\mathbf{x}) \cos(\omega_n t + \delta_n) . \quad (18.115)$$

The variational approach generalizes as well. We define

$$\mathcal{N}[\psi(\mathbf{x})] = \int_{\Omega} d\mathbf{x} \left[\tau_{\alpha\beta} \frac{\partial\psi}{\partial x^\alpha} \frac{\partial\psi}{\partial x^\beta} + v \psi^2 \right] \quad (18.116)$$

$$\mathcal{D}[\psi(\mathbf{x})] = \int_{\Omega} d\mathbf{x} \mu \psi^2 , \quad (18.117)$$

and

$$\omega^2[\psi(\mathbf{x})] = \frac{\mathcal{N}[\psi(\mathbf{x})]}{\mathcal{D}[\psi(\mathbf{x})]} . \quad (18.118)$$

Setting the variation $\delta\omega^2 = 0$ recovers the eigenvalue equation $K\psi = \omega^2\mu\psi$.

18.3.2 Membranes

Consider a surface where the height z is a function of the lateral coordinates x and y :

$$z = u(x, y) . \quad (18.119)$$

The equation of the surface is then

$$F(x, y, z) = z - u(x, y) = 0 . \quad (18.120)$$

Let the differential element of surface area be dS . The projection of this element onto the (x, y) plane is

$$dA = dx dy = \hat{\mathbf{n}} \cdot \hat{\mathbf{z}} dS . \quad (18.121)$$

The unit normal $\hat{\mathbf{n}}$ is given by

$$\hat{\mathbf{n}} = \frac{\nabla F}{|\nabla F|} = \frac{\hat{\mathbf{z}} - \nabla u}{\sqrt{1 + (\nabla u)^2}} . \quad (18.122)$$

Thus,

$$dS = \frac{dx dy}{\hat{\mathbf{n}} \cdot \hat{\mathbf{z}}} = \sqrt{1 + (\nabla u)^2} dx dy . \quad (18.123)$$

The potential energy for a deformed surface can take many forms. In the case we shall consider here, we consider only the effect of surface tension σ , and we write the potential energy functional as

$$U[u(x, y, t)] = \sigma \int dS = U_0 + \frac{1}{2} \sigma \int dA (\nabla u)^2 + \dots . \quad (18.124)$$

The kinetic energy functional is

$$T[u(x, y, t)] = \frac{1}{2} \int dA \mu(\mathbf{x}) (\partial_t u)^2 . \quad (18.125)$$

Thus, the action is

$$S[u(\mathbf{x}, t)] = \int d^2x \mathcal{L}(u, \nabla u, \partial_t u, \mathbf{x}) , \quad (18.126)$$

where the Lagrangian density is

$$\mathcal{L} = \frac{1}{2}\mu(\mathbf{x}) (\partial_t u)^2 - \frac{1}{2}\sigma(\mathbf{x}) (\nabla u)^2 , \quad (18.127)$$

where here we have allowed both $\mu(\mathbf{x})$ and $\sigma(\mathbf{x})$ to depend on the spatial coordinates. The equations of motion are

$$\begin{aligned} 0 &= \frac{\partial}{\partial t} \frac{\partial \mathcal{L}}{\partial (\partial_t u)} + \nabla \cdot \frac{\partial \mathcal{L}}{\partial \nabla u} - \frac{\partial \mathcal{L}}{\partial u} \\ &= \mu(\mathbf{x}) \frac{\partial^2 u}{\partial t^2} - \nabla \cdot \left\{ \sigma(\mathbf{x}) \nabla u \right\} . \end{aligned} \quad (18.128)$$

18.3.3 Helmholtz equation

When μ and σ are each constant, we obtain the Helmholtz equation:

$$\left(\nabla^2 - \frac{1}{c^2} \frac{\partial^2}{\partial t^2} \right) u(\mathbf{x}, t) = 0 , \quad (18.129)$$

with $c = \sqrt{\sigma/\mu}$. The d'Alembert solution still works – waves of arbitrary shape can propagate *in a fixed direction* $\hat{\mathbf{k}}$:

$$u(\mathbf{x}, t) = f(\hat{\mathbf{k}} \cdot \mathbf{x} - ct) . \quad (18.130)$$

This is called a *plane wave* because the three dimensional generalization of this wave has wavefronts which are planes. In our case, it might better be called a *line wave*, but people will look at you funny if you say that, so we'll stick with *plane wave*. Note that the locus of points of constant f satisfies

$$\phi(\mathbf{x}, t) = \hat{\mathbf{k}} \cdot \mathbf{x} - ct = \text{constant} , \quad (18.131)$$

and setting $d\phi = 0$ gives

$$\hat{\mathbf{k}} \cdot \frac{d\mathbf{x}}{dt} = c , \quad (18.132)$$

which means that the velocity along $\hat{\mathbf{k}}$ is c . The component of \mathbf{x} perpendicular to $\hat{\mathbf{k}}$ is arbitrary, hence the regions of constant ϕ correspond to lines which are orthogonal to $\hat{\mathbf{k}}$.

Owing to the linearity of the wave equation, we can construct arbitrary superpositions of plane waves. The most general solution is written

$$u(\mathbf{x}, t) = \int \frac{d^2 k}{(2\pi)^2} \left[A(\mathbf{k}) e^{i(\mathbf{k} \cdot \mathbf{x} - ckt)} + B(\mathbf{k}) e^{i(\mathbf{k} \cdot \mathbf{x} + ckt)} \right] . \quad (18.133)$$

The first term in the bracket on the RHS corresponds to a plane wave moving in the $+\hat{\mathbf{k}}$ direction, and the second term to a plane wave moving in the $-\hat{\mathbf{k}}$ direction.

18.3.4 Rectangles

Consider a rectangular membrane where $x \in [0, a]$ and $y \in [0, b]$, and subject to the boundary conditions $u(0, y) = u(a, y) = u(x, 0) = u(x, b) = 0$. We try a solution of the form

$$u(x, y, t) = X(x) Y(y) T(t) . \quad (18.134)$$

This technique is known as *separation of variables*. Dividing the Helmholtz equation by u then gives

$$\frac{1}{X} \frac{\partial^2 X}{\partial x^2} + \frac{1}{Y} \frac{\partial^2 Y}{\partial y^2} = \frac{1}{c^2} \frac{1}{T} \frac{\partial^2 T}{\partial t^2} . \quad (18.135)$$

The first term on the LHS depends only on x . The second term on the LHS depends only on y . The RHS depends only on t . Therefore, each of these terms must individually be constant. We write

$$\frac{1}{X} \frac{\partial^2 X}{\partial x^2} = -k_x^2 , \quad \frac{1}{Y} \frac{\partial^2 Y}{\partial y^2} = -k_y^2 , \quad \frac{1}{T} \frac{\partial^2 T}{\partial t^2} = -\omega^2 , \quad (18.136)$$

with

$$k_x^2 + k_y^2 = \frac{\omega^2}{c^2} . \quad (18.137)$$

Thus, $\omega = \pm c|\mathbf{k}|$. The most general solution is then

$$\begin{aligned} X(x) &= A \cos(k_x x) + B \sin(k_x x) \\ Y(y) &= C \cos(k_y y) + D \sin(k_y y) \\ T(t) &= E \cos(\omega t) + F \sin(\omega t) . \end{aligned} \quad (18.138)$$

The boundary conditions now demand

$$A = 0 , \quad C = 0 , \quad \sin(k_x a) = 0 , \quad \sin(k_y b) = 0 . \quad (18.139)$$

Thus, the most general solution subject to the boundary conditions is

$$u(x, y, t) = \sum_{m=1}^{\infty} \sum_{n=1}^{\infty} \mathcal{A}_{mn} \sin\left(\frac{m\pi x}{a}\right) \sin\left(\frac{n\pi y}{b}\right) \cos(\omega_{mn} t + \delta_{mn}) , \quad (18.140)$$

where

$$\omega_{mn} = \sqrt{\left(\frac{m\pi c}{a}\right)^2 + \left(\frac{n\pi c}{b}\right)^2} . \quad (18.141)$$

18.3.5 Circles

For a circular membrane, such as a drumhead, it is convenient to work in two-dimensional polar coordinates (r, φ) . The Laplacian is then

$$\nabla^2 = \frac{1}{r} \frac{\partial}{\partial r} r \frac{\partial}{\partial r} + \frac{1}{r^2} \frac{\partial^2}{\partial \varphi^2} . \quad (18.142)$$

We seek a solution to the Helmholtz equation which satisfies the boundary conditions $u(r = a, \varphi, t) = 0$. Once again, we invoke the separation of variables method, writing

$$u(r, \varphi, t) = R(r) \Phi(\varphi) T(t) , \quad (18.143)$$

resulting in

$$\frac{1}{R} \frac{1}{r} \frac{\partial}{\partial r} \left(r \frac{\partial R}{\partial r} \right) + \frac{1}{r^2} \frac{1}{\Phi} \frac{\partial^2 \Phi}{\partial \varphi^2} = \frac{1}{c^2} \frac{1}{T} \frac{\partial^2 T}{\partial t^2} . \quad (18.144)$$

The azimuthal and temporal functions are

$$\Phi(\varphi) = e^{im\varphi} , \quad T(t) = \cos(\omega t + \delta) , \quad (18.145)$$

where m is an integer in order that the function $u(r, \varphi, t)$ be single-valued. The radial equation is then

$$\frac{\partial^2 R}{\partial r^2} + \frac{1}{r} \frac{\partial R}{\partial r} + \left(\frac{\omega^2}{c^2} - \frac{m^2}{r^2} \right) R = 0 . \quad (18.146)$$

This is Bessel's equation, with solution

$$R(r) = A J_m \left(\frac{\omega r}{c} \right) + B N_m \left(\frac{\omega r}{c} \right) , \quad (18.147)$$

where $J_m(z)$ and $N_m(z)$ are the Bessel and Neumann functions of order m , respectively. Since the Neumann functions diverge at $r = 0$, we must exclude them, setting $B = 0$ for each m .

We now invoke the boundary condition $u(r = a, \varphi, t) = 0$. This requires

$$J_m \left(\frac{\omega a}{c} \right) = 0 \quad \Rightarrow \quad \omega = \omega_{m\ell} = x_{m\ell} \frac{c}{a} , \quad (18.148)$$

where $J_m(x_{m\ell}) = 0$, i.e. $x_{m\ell}$ is the ℓ^{th} zero of $J_m(x)$. The most general solution is therefore

$$u(r, \varphi, t) = \sum_{m=0}^{\infty} \sum_{\ell=1}^{\infty} \mathcal{A}_{m\ell} J_m(x_{m\ell} r/a) \cos(m\varphi + \beta_{m\ell}) \cos(\omega_{m\ell} t + \delta_{m\ell}) . \quad (18.149)$$

18.3.6 Sound in fluids

Let $\varrho(\mathbf{x}, t)$ and $\mathbf{v}(\mathbf{x}, t)$ be the density and velocity fields in a fluid. Mass conservation requires

$$\frac{\partial \varrho}{\partial t} + \nabla \cdot (\varrho \mathbf{v}) = 0 . \quad (18.150)$$

This is the continuity equation for mass.

Focus now on a small packet of fluid of infinitesimal volume dV . The total force on this fluid element is $d\mathbf{F} = (-\nabla p + \varrho \mathbf{g}) dV$. By Newton's Second Law,

$$d\mathbf{F} = (\varrho dV) \frac{d\mathbf{v}}{dt} \quad (18.151)$$

Note that the chain rule gives

$$\frac{d\mathbf{v}}{dt} = \frac{\partial \mathbf{v}}{\partial t} + (\mathbf{v} \cdot \nabla) \mathbf{v} . \quad (18.152)$$

Thus, dividing eqn. 18.151 by dV , we obtain

$$\varrho \left(\frac{\partial \mathbf{v}}{\partial t} + (\mathbf{v} \cdot \nabla) \mathbf{v} \right) = -\nabla p + \varrho \mathbf{g} . \quad (18.153)$$

This is the inviscid (*i.e.* zero viscosity) form of the Navier-Stokes equation.

Locally the fluid can also be described in terms of thermodynamic variables $p(\mathbf{x}, t)$ (pressure) and $T(\mathbf{x}, t)$ (temperature). For a one-component fluid there is necessarily an equation of state of the form $p = p(\varrho, T)$. Thus, we may write

$$dp = \left. \frac{\partial p}{\partial \varrho} \right|_T d\varrho + \left. \frac{\partial p}{\partial T} \right|_\varrho dT . \quad (18.154)$$

We now make the following approximations. First, we assume that the fluid is close to equilibrium at $\mathbf{v} = 0$, meaning we write $p = \bar{p} + \delta p$ and $\varrho = \bar{\varrho} + \delta\varrho$, and assume that δp , $\delta\varrho$, and \mathbf{v} are small. The smallness of \mathbf{v} means we can neglect the nonlinear term $(\mathbf{v} \cdot \nabla) \mathbf{v}$ in eqn. 18.153. Second, we neglect gravity (more on this later). The continuity equation then takes the form

$$\frac{\partial \delta\varrho}{\partial t} + \bar{\varrho} \nabla \cdot \mathbf{v} = 0 , \quad (18.155)$$

and the Navier-Stokes equation becomes

$$\bar{\varrho} \frac{\partial \mathbf{v}}{\partial t} = -\nabla \delta p . \quad (18.156)$$

Taking the time derivative of the former, and then invoking the latter of these equations yields

$$\frac{\partial^2 \delta\varrho}{\partial t^2} = \nabla^2 p = \left(\frac{\partial p}{\partial \varrho} \right) \nabla^2 \delta\varrho \equiv c^2 \nabla^2 \delta\varrho . \quad (18.157)$$

The speed of wave propagation, *i.e.* the speed of sound, is given by

$$c = \sqrt{\frac{\partial p}{\partial \varrho}} . \quad (18.158)$$

Finally, we must make an assumption regarding the conditions under which the derivative $\partial p / \partial \varrho$ is computed. If the fluid is an excellent conductor of heat, then the temperature will equilibrate quickly and it is a good approximation to take the derivative at fixed temperature. The resulting value of c is called the *isothermal* sound speed c_T . If, on the other hand, the fluid is a poor conductor of heat, as is the case for air, then it is more appropriate to take the derivative at constant entropy, yielding the *adiabatic* sound speed. Thus,

$$c_T = \sqrt{\left(\frac{\partial p}{\partial \varrho} \right)_T} , \quad c_S = \sqrt{\left(\frac{\partial p}{\partial \varrho} \right)_S} . \quad (18.159)$$

In an ideal gas, $c_S/c_T = \sqrt{\gamma}$, where $\gamma = c_p/c_V$ is the ratio of the specific heat at constant pressure to that at constant volume. For a (mostly) diatomic gas like air (comprised of N₂ and O₂ and just a little Ar), $\gamma = \frac{7}{5}$. Note that one can write $c^2 = 1/\varrho\kappa$, where

$$\kappa = \frac{1}{\varrho} \left(\frac{\partial \varrho}{\partial p} \right) \quad (18.160)$$

is the *compressibility*, which is the inverse of the *bulk modulus*. Again, one must specify whether one is talking about κ_T or κ_S . For reference in air at $T = 293\text{K}$, using $M = 28.8\text{ g/mol}$, one obtains $c_T = 290.8\text{ m/s}$ and $c_S = 344.0\text{ m/s}$. In H₂O at 293K, $c = 1482\text{ m/s}$. In Al at 273K, $c = 6420\text{ m/s}$.

If we retain gravity, the wave equation becomes

$$\frac{\partial^2 \delta\varrho}{\partial t^2} = c^2 \nabla^2 \delta\varrho - \mathbf{g} \cdot \nabla \delta\varrho . \quad (18.161)$$

The dispersion relation is then

$$\omega(\mathbf{k}) = \sqrt{c^2 k^2 + i\mathbf{g} \cdot \mathbf{k}} . \quad (18.162)$$

We are permitted to ignore the effects of gravity so long as $c^2 k^2 \gg gk$. In terms of the wavelength $\lambda = 2\pi/k$, this requires

$$\lambda \ll \frac{2\pi c^2}{g} = 75.9\text{ km} \text{ (at } T = 293\text{K)} . \quad (18.163)$$

18.4 Dispersion

18.4.1 Helmholtz *versus* Klein-Gordon equations

The one-dimensional Helmholtz equation $\ddot{y} = c^2 y''$ is solved by a plane wave

$$y(x, t) = A e^{ikx} e^{-i\omega t} , \quad (18.164)$$

provided $\omega = \pm ck$. We say that there are *two branches* to the *dispersion relation* $\omega(k)$ for this equation. In general, we may add solutions, due to the linearity of the Helmholtz equation. The most general solution is then

$$\begin{aligned} y(x, t) &= \int_{-\infty}^{\infty} \frac{dk}{2\pi} \left[\hat{f}(k) e^{ik(x-ct)} + \hat{g}(k) e^{ik(x+ct)} \right] \\ &= f(x - ct) + g(x + ct) , \end{aligned} \quad (18.165)$$

which is consistent with d'Alembert's solution.

The Klein-Gordon equation, $\ddot{\phi} = c^2 \phi'' - \gamma^2 \phi$, also has a plane wave solution as in Eqn. 18.164, but with dispersion branches $\omega = \pm W(k)$ with $W(k) = \pm(\gamma^2 + c^2 k^2)^{1/2}$. The general solution is then

$$\phi(x, t) = \int_{-\infty}^{\infty} \frac{dk}{2\pi} \left[\hat{A}(k) e^{ikx} e^{-iW(k)t} + \hat{B}(k) e^{ikx} e^{iW(k)t} \right] , \quad (18.166)$$

which is not of the D'Alembert form.

18.4.2 Schrödinger's equation

Consider now the free particle Schrödinger equation in one space dimension,

$$i\hbar \frac{\partial \psi}{\partial t} = -\frac{\hbar^2}{2m} \frac{\partial^2 \psi}{\partial x^2}. \quad (18.167)$$

The function $\psi(x, t)$ is the quantum mechanical wavefunction for a particle of mass m moving freely along a one-dimensional line. The *probability density* for finding the particle at position x at time t is

$$\rho(x, t) = |\psi(x, t)|^2. \quad (18.168)$$

Conservation of probability therefore requires

$$\int_{-\infty}^{\infty} dx |\psi(x, t)|^2 = 1. \quad (18.169)$$

This condition must hold at all times t .

As is the case with the Helmholtz and Klein-Gordon equations, the Schrödinger equation is solved by a plane wave of the form

$$\psi(x, t) = A e^{ikx} e^{-i\omega t}, \quad (18.170)$$

where the dispersion relation now only has one branch, and is given by

$$\omega(k) = \frac{\hbar k^2}{2m}. \quad (18.171)$$

The most general solution is then

$$\psi(x, t) = \int_{-\infty}^{\infty} \frac{dk}{2\pi} \hat{\psi}(k) e^{ikx} e^{-i\hbar k^2 t / 2m}. \quad (18.172)$$

Let's suppose we start at time $t = 0$ with a Gaussian wavepacket,

$$\psi(x, 0) = (\pi \ell_0^2)^{-1/4} e^{-x^2/2\ell_0^2} e^{ik_0 x}. \quad (18.173)$$

To find the amplitude $\hat{\psi}(k)$, we perform the Fourier transform:

$$\hat{\psi}(k) = \int_{-\infty}^{\infty} dx \psi(x, 0) e^{-ikx} = \sqrt{2} (\pi \ell_0^2)^{-1/4} e^{-(k-k_0)^2 \ell_0^2 / 2}. \quad (18.174)$$

We now compute $\psi(x, t)$ valid for all times t :

$$\begin{aligned} \psi(x, t) &= \sqrt{2} (\pi \ell_0^2)^{-1/4} \int_{-\infty}^{\infty} \frac{dk}{2\pi} e^{ikx} e^{-(k-k_0)^2 \ell_0^2 / 2} e^{ikx} e^{-i\hbar k^2 t / 2m} \\ &= (\pi \ell_0^2)^{-1/4} (1 + it/\tau)^{-1/2} \exp \left[-\frac{(x - \hbar k_0 t / m)^2}{2 \ell_0^2 (1 + t^2/\tau^2)} \right] \\ &\quad \times \exp \left[\frac{i(2k_0 \ell_0^2 x + x^2 t / \tau - k_0^2 \ell_0^4 t / \tau)}{2 \ell_0^2 (1 + t^2/\tau^2)} \right], \end{aligned} \quad (18.175)$$

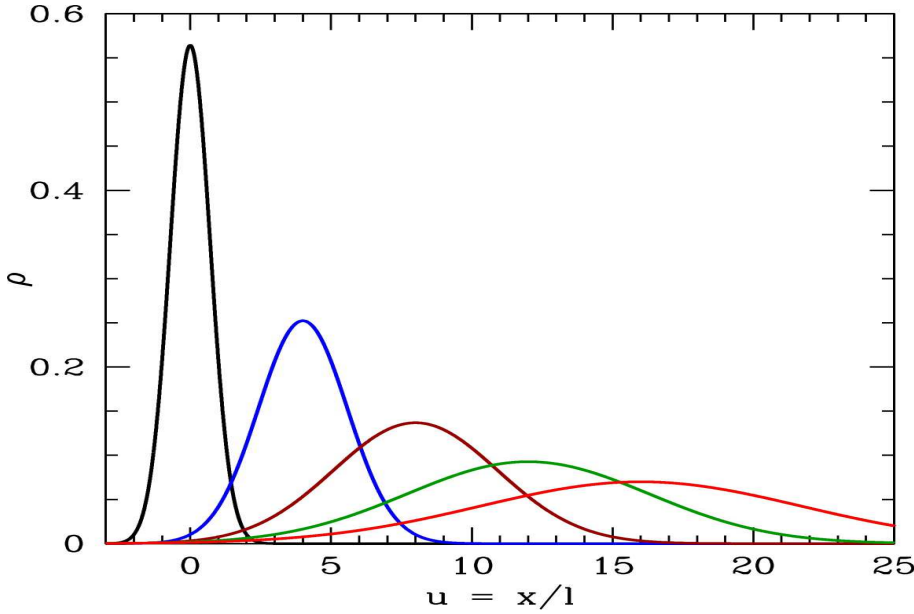


Figure 18.9: Wavepacket spreading for $k_0 \ell_0 = 2$ with $t/\tau = 0, 2, 4, 6$, and 8 .

where $\tau \equiv m\ell_0^2/\hbar$. The probability density is then the normalized Gaussian

$$\rho(x, t) = \frac{1}{\sqrt{\pi \ell^2(t)}} e^{-(x-v_0 t)^2/\ell^2(t)} , \quad (18.176)$$

where $v_0 = \hbar k_0/m$ and

$$\ell(t) = \ell_0 \sqrt{1 + t^2/\tau^2} . \quad (18.177)$$

Note that $\ell(t)$ gives the width of the wavepacket, and that this width increases as a function of time, with $\ell(t \gg \tau) \simeq \ell_0 t/\tau$.

Unlike the case of the Helmholtz equation, the solution to the Schrödinger equation does not retain its shape as it moves. This phenomenon is known as the *spreading of the wavepacket*. In fig. 18.9, we show the motion and spreading of the wavepacket.

For a given plane wave $e^{ikx} e^{-i\omega(k)t}$, the wavefronts move at the *phase velocity*

$$v_p(k) = \frac{\omega(k)}{k} . \quad (18.178)$$

The center of the wavepacket, however, travels at the *group velocity*

$$v_g(k) = \left. \frac{d\omega}{dk} \right|_{k_0} , \quad (18.179)$$

where $k = k_0$ is the maximum of $|\hat{\psi}(k)|^2$.

18.5 General Field Theoretic Formulation

Continuous systems possess an infinite number of degrees of freedom. They are described by a set of fields $\phi_a(\mathbf{x}, t)$ which depend on space and time. These fields may represent local displacement, pressure, velocity, etc. The equations of motion of the fields are again determined by extremizing the action, which, in turn, is an integral of the *Lagrangian density* over all space and time. Extremization yields a set of (generally coupled) *partial* differential equations.

18.5.1 Euler-Lagrange equations for classical field theories

Suppose $\phi_a(\mathbf{x})$ depends on n independent variables, $\{x^1, x^2, \dots, x^n\}$. Consider the functional

$$S[\{\phi_a(\mathbf{x})\}] = \int_{\Omega} d\mathbf{x} \mathcal{L}(\phi_a, \partial_\mu \phi_a, \mathbf{x}), \quad (18.180)$$

i.e. the *Lagrangian density* \mathcal{L} is a function of the fields ϕ_a and their partial derivatives $\partial\phi_a/\partial x^\mu$. Here Ω is a region in \mathbb{R}^n . Then the first variation of S is

$$\begin{aligned} \delta S &= \int_{\Omega} d\mathbf{x} \left\{ \frac{\partial \mathcal{L}}{\partial \phi_a} \delta \phi_a + \frac{\partial \mathcal{L}}{\partial (\partial_\mu \phi_a)} \frac{\partial \delta \phi_a}{\partial x^\mu} \right\} \\ &= \oint_{\partial\Omega} d\Sigma n^\mu \frac{\partial \mathcal{L}}{\partial (\partial_\mu \phi_a)} \delta \phi_a + \int_{\Omega} d\mathbf{x} \left\{ \frac{\partial \mathcal{L}}{\partial \phi_a} - \frac{\partial}{\partial x^\mu} \left(\frac{\partial \mathcal{L}}{\partial (\partial_\mu \phi_a)} \right) \right\} \delta \phi_a, \end{aligned} \quad (18.181)$$

where $\partial\Omega$ is the $(n-1)$ -dimensional boundary of Ω , $d\Sigma$ is the differential surface area, and n^μ is the unit normal. If we demand either $\partial\mathcal{L}/\partial(\partial_\mu \phi_a)|_{\partial\Omega} = 0$ or $\delta \phi_a|_{\partial\Omega} = 0$, the surface term vanishes, and we conclude

$$\frac{\delta S}{\delta \phi_a(\mathbf{x})} = \left[\frac{\partial \mathcal{L}}{\partial \phi_a} - \frac{\partial}{\partial x^\mu} \left(\frac{\partial \mathcal{L}}{\partial (\partial_\mu \phi_a)} \right) \right]_x, \quad (18.182)$$

where the subscript means we are to evaluate the term in brackets at \mathbf{x} . In a mechanical system, one of the n independent variables (usually x^0), is the time t . However, we may be interested in a time-independent context in which we wish to extremize the energy functional, for example. In any case, setting the first variation of S to zero yields the Euler-Lagrange equations,

$$\delta S = 0 \quad \Rightarrow \quad \frac{\partial \mathcal{L}}{\partial \phi_a} - \frac{\partial}{\partial x^\mu} \left(\frac{\partial \mathcal{L}}{\partial (\partial_\mu \phi_a)} \right) = 0 \quad (18.183)$$

The stress-energy tensor is defined as

$$T^\mu_\nu = \sum_a \frac{\partial \mathcal{L}}{\partial (\partial_\mu \phi_a)} \partial_\nu \phi_a - \delta^\mu_\nu \mathcal{L}. \quad (18.184)$$

When $\mathcal{L} = \mathcal{L}(\phi_a, \partial_\mu \phi_a)$ is independent of the independent variables \mathbf{x} , one has that the stress-energy tensor is conserved: $\partial_\mu T^\mu_\nu = 0$. (Students should check this result.)

Maxwell theory

The Lagrangian density for an electromagnetic field with sources is

$$\mathcal{L} = -\frac{1}{16\pi} F_{\mu\nu} F^{\mu\nu} - J_\mu A^\mu . \quad (18.185)$$

The equations of motion are then

$$\frac{\partial \mathcal{L}}{\partial A^\nu} - \frac{\partial}{\partial x^\nu} \left(\frac{\partial \mathcal{L}}{\partial (\partial^\mu A^\nu)} \right) = 0 \quad \Rightarrow \quad \partial_\mu F^{\mu\nu} = 4\pi J^\nu , \quad (18.186)$$

which are Maxwell's equations.

18.5.2 Conserved currents in field theory

Recall the result of Noether's theorem for mechanical systems:

$$\frac{d}{dt} \left(\frac{\partial L}{\partial \dot{q}_\sigma} \frac{\partial \tilde{q}_\sigma}{\partial \zeta} \right)_{\zeta=0} = 0 , \quad (18.187)$$

where $\tilde{q}_\sigma = \tilde{q}_\sigma(q, \zeta)$ is a one-parameter (ζ) family of transformations of the generalized coordinates which leaves L invariant. We generalize to field theory by replacing

$$q_\sigma(t) \longrightarrow \phi_a(\mathbf{x}, t) , \quad (18.188)$$

where $\{\phi_a(\mathbf{x}, t)\}$ are a set of fields, which are functions of the independent variables $\{x, y, z, t\}$. We will adopt covariant relativistic notation and write for four-vector $x^\mu = (ct, x, y, z)$. The generalization of $dQ/dt = 0$ is

$$\frac{\partial}{\partial x^\mu} \left(\frac{\partial \mathcal{L}}{\partial (\partial_\mu \phi_a)} \frac{\partial \tilde{\phi}_a}{\partial \zeta} \right)_{\zeta=0} = 0 , \quad (18.189)$$

where there is an implied sum on both μ and a . We can write this as $\partial_\mu J^\mu = 0$, where

$$J^\mu \equiv \frac{\partial \mathcal{L}}{\partial (\partial_\mu \phi_a)} \frac{\partial \tilde{\phi}_a}{\partial \zeta} \Big|_{\zeta=0} . \quad (18.190)$$

We call $Q = J^0/c$ the *total charge*. If we assume $\mathbf{J} = 0$ at the spatial boundaries of our system, then integrating the conservation law $\partial_\mu J^\mu$ over the spatial region Ω gives

$$\frac{dQ}{dt} = \int_{\Omega} d^3x \partial_0 J^0 = - \int_{\Omega} d^3x \nabla \cdot \mathbf{J} = - \oint_{\partial\Omega} d\Sigma \hat{\mathbf{n}} \cdot \mathbf{J} = 0 , \quad (18.191)$$

assuming $\mathbf{J} = 0$ at the boundary $\partial\Omega$.

As an example, consider the case of a complex scalar field, with Lagrangian density²

$$\mathcal{L}(\psi, \psi^*, \partial_\mu \psi, \partial_\mu \psi^*) = \frac{1}{2} K(\partial_\mu \psi^*)(\partial^\mu \psi) - U(\psi^* \psi) . \quad (18.192)$$

²We raise and lower indices using the Minkowski metric $g_{\mu\nu} = \text{diag}(+, -, -, -)$.

This is invariant under the transformation $\psi \rightarrow e^{i\zeta} \psi$, $\psi^* \rightarrow e^{-i\zeta} \psi^*$. Thus,

$$\frac{\partial \tilde{\psi}}{\partial \zeta} = i e^{i\zeta} \psi \quad , \quad \frac{\partial \tilde{\psi}^*}{\partial \zeta} = -i e^{-i\zeta} \psi^* , \quad (18.193)$$

and, summing over both ψ and ψ^* fields, we have

$$\begin{aligned} J^\mu &= \frac{\partial \mathcal{L}}{\partial (\partial_\mu \psi)} \cdot (i\psi) + \frac{\partial \mathcal{L}}{\partial (\partial_\mu \psi^*)} \cdot (-i\psi^*) \\ &= \frac{K}{2i} (\psi^* \partial^\mu \psi - \psi \partial^\mu \psi^*) . \end{aligned} \quad (18.194)$$

The potential, which depends on $|\psi|^2$, is independent of ζ . Hence, this form of conserved 4-current is valid for an entire class of potentials.

18.5.3 Gross-Pitaevskii model

As one final example of a field theory, consider the Gross-Pitaevskii model, with

$$\mathcal{L} = i\hbar \psi^* \frac{\partial \psi}{\partial t} - \frac{\hbar^2}{2m} \nabla \psi^* \cdot \nabla \psi - g (|\psi|^2 - n_0)^2 . \quad (18.195)$$

This describes a Bose fluid with repulsive short-ranged interactions. Here $\psi(\mathbf{x}, t)$ is again a complex scalar field, and ψ^* is its complex conjugate. Using the Leibniz rule, we have

$$\begin{aligned} \delta S[\psi^*, \psi] &= S[\psi^* + \delta\psi^*, \psi + \delta\psi] \\ &= \int dt \int d^d x \left\{ i\hbar \psi^* \frac{\partial \delta\psi}{\partial t} + i\hbar \delta\psi^* \frac{\partial \psi}{\partial t} - \frac{\hbar^2}{2m} \nabla \psi^* \cdot \nabla \delta\psi \right. \\ &\quad \left. - \frac{\hbar^2}{2m} \nabla \delta\psi^* \cdot \nabla \psi - 2g (|\psi|^2 - n_0) (\psi^* \delta\psi + \psi \delta\psi^*) \right\} \\ &= \int dt \int d^d x \left\{ \left[-i\hbar \frac{\partial \psi^*}{\partial t} + \frac{\hbar^2}{2m} \nabla^2 \psi^* - 2g (|\psi|^2 - n_0) \psi^* \right] \delta\psi \right. \\ &\quad \left. + \left[i\hbar \frac{\partial \psi}{\partial t} + \frac{\hbar^2}{2m} \nabla^2 \psi - 2g (|\psi|^2 - n_0) \psi \right] \delta\psi^* \right\} , \end{aligned} \quad (18.196)$$

where we have integrated by parts where necessary and discarded the boundary terms. Extremizing $S[\psi^*, \psi]$ therefore results in the *nonlinear Schrödinger equation* (NLSE),

$$i\hbar \frac{\partial \psi}{\partial t} = -\frac{\hbar^2}{2m} \nabla^2 \psi + 2g (|\psi|^2 - n_0) \psi \quad (18.197)$$

as well as its complex conjugate,

$$-i\hbar \frac{\partial \psi^*}{\partial t} = -\frac{\hbar^2}{2m} \nabla^2 \psi^* + 2g (|\psi|^2 - n_0) \psi^* . \quad (18.198)$$

Note that these equations are indeed the Euler-Lagrange equations:

$$\begin{aligned}\frac{\delta S}{\delta \psi} &= \frac{\partial \mathcal{L}}{\partial \psi} - \frac{\partial}{\partial x^\mu} \left(\frac{\partial \mathcal{L}}{\partial \partial_\mu \psi} \right) \\ \frac{\delta S}{\delta \psi^*} &= \frac{\partial \mathcal{L}}{\partial \psi^*} - \frac{\partial}{\partial x^\mu} \left(\frac{\partial \mathcal{L}}{\partial \partial_\mu \psi^*} \right),\end{aligned}\tag{18.199}$$

with $x^\mu = (t, \mathbf{x})$ the space-time four-vector³. Plugging in

$$\frac{\partial \mathcal{L}}{\partial \psi} = -2g(|\psi|^2 - n_0)\psi^* \quad , \quad \frac{\partial \mathcal{L}}{\partial \partial_t \psi} = i\hbar\psi^* \quad , \quad \frac{\partial \mathcal{L}}{\partial \nabla \psi} = -\frac{\hbar^2}{2m}\nabla\psi^*\tag{18.200}$$

and

$$\frac{\partial \mathcal{L}}{\partial \psi^*} = i\hbar\psi - 2g(|\psi|^2 - n_0)\psi \quad , \quad \frac{\partial \mathcal{L}}{\partial \partial_t \psi^*} = 0 \quad , \quad \frac{\partial \mathcal{L}}{\partial \nabla \psi^*} = -\frac{\hbar^2}{2m}\nabla\psi,\tag{18.201}$$

we recover the NLSE and its conjugate.

The Gross-Pitaevskii model also possesses a U(1) invariance, under

$$\psi(\mathbf{x}, t) \rightarrow \tilde{\psi}(\mathbf{x}, t) = e^{i\zeta}\psi(\mathbf{x}, t) \quad , \quad \psi^*(\mathbf{x}, t) \rightarrow \tilde{\psi}^*(\mathbf{x}, t) = e^{-i\zeta}\psi^*(\mathbf{x}, t).\tag{18.202}$$

Thus, the conserved Noether current is then

$$J^\mu = \frac{\partial \mathcal{L}}{\partial \partial_\mu \psi} \frac{\partial \tilde{\psi}}{\partial \zeta} \Big|_{\zeta=0} + \frac{\partial \mathcal{L}}{\partial \partial_\mu \psi^*} \frac{\partial \tilde{\psi}^*}{\partial \zeta} \Big|_{\zeta=0}\tag{18.203}$$

so that

$$J^0 = -\hbar|\psi|^2 \quad , \quad \mathbf{J} = -\frac{\hbar^2}{2im}(\psi^*\nabla\psi - \psi\nabla\psi^*).\tag{18.204}$$

Dividing out by \hbar , taking $J^0 \equiv -\hbar\rho$ and $\mathbf{J} \equiv -\hbar\mathbf{j}$, we obtain the continuity equation,

$$\frac{\partial \rho}{\partial t} + \nabla \cdot \mathbf{j} = 0,\tag{18.205}$$

where

$$\rho = |\psi|^2 \quad , \quad \mathbf{j} = \frac{\hbar}{2im}(\psi^*\nabla\psi - \psi\nabla\psi^*).\tag{18.206}$$

are the particle density and the particle current, respectively.

18.6 Appendix : Three Strings

Problem: Three identical strings are connected to a ring of mass m as shown in fig. 18.10. The linear mass density of each string is σ and each string is under identical tension τ . In equilibrium, all strings

³In the nonrelativistic case, there is no utility in defining $x^0 = ct$, so we simply define $x^0 = t$.

are coplanar. All motion on the string is in the \hat{z} -direction, which is perpendicular to the equilibrium plane. The ring slides frictionlessly along a vertical pole.

It is convenient to describe each string as a half line $[-\infty, 0]$. We can choose coordinates x_1 , x_2 , and x_3 for the three strings, respectively. For each string, the ring lies at $x_i = 0$.

A pulse is sent down the first string. After a time, the pulse arrives at the ring. Transmitted waves are sent down the other two strings, and a reflected wave down the first string. The solution to the wave equation in the strings can be written as follows. In string #1, we have

$$z = f(ct - x_1) + g(ct + x_1). \quad (18.207)$$

In the other two strings, we may write $z = h_A(ct + x_2)$ and $z = h_B(ct + x_3)$, as indicated in the figure.

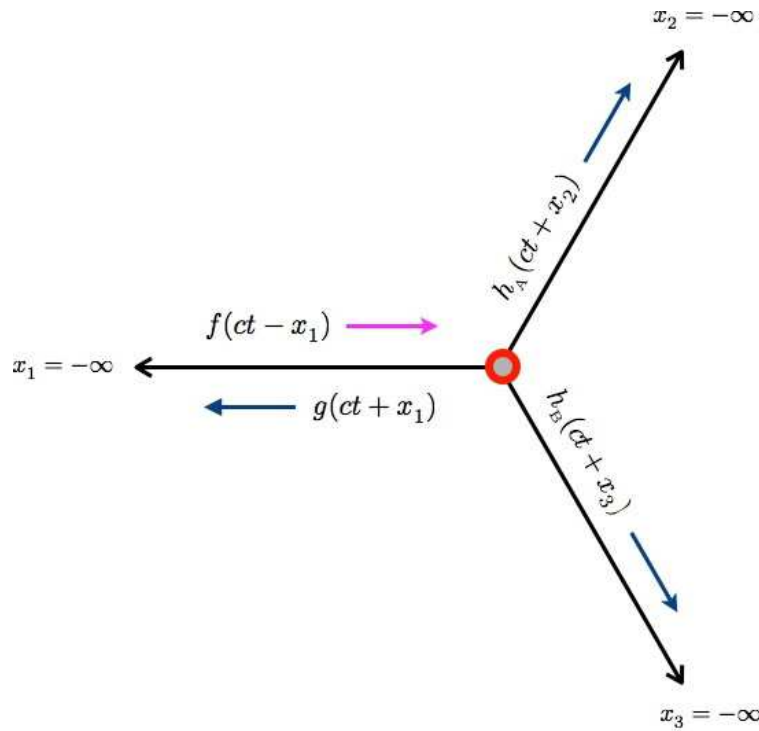


Figure 18.10: Three identical strings arranged symmetrically in a plane, attached to a common end. All motion is in the direction perpendicular to this plane. The red ring, whose mass is m , slides frictionlessly in this direction along a pole.

- (a) Write the wave equation in string #1. Define all constants.
- (b) Write the equation of motion for the ring.
- (c) Solve for the reflected wave $g(\xi)$ in terms of the incident wave $f(\xi)$. You may write this relation in terms of the Fourier transforms $\hat{f}(k)$ and $\hat{g}(k)$.
- (d) Suppose a very long wavelength pulse of maximum amplitude A is incident on the ring. What is the maximum amplitude of the reflected pulse? What do we mean by “very long wavelength”?

Solution:

(a) The wave equation is

$$\frac{\partial^2 z}{\partial x^2} = \frac{1}{c^2} \frac{\partial^2 z}{\partial t^2}, \quad (18.208)$$

where x is the coordinate along the string, and $c = \sqrt{\tau/\sigma}$ is the speed of wave propagation.

(b) Let Z be the vertical coordinate of the ring. Newton's second law says $m\ddot{Z} = F$, where the force on the ring is the sum of the vertical components of the tension in the three strings at $x = 0$:

$$F = -\tau \left[-f'(ct) + g'(ct) + h'_A(ct) + h'_B(ct) \right], \quad (18.209)$$

where prime denotes differentiation with respect to argument.

(c) To solve for the reflected wave, we must eliminate the unknown functions $h_{A,B}$ and then obtain g in terms of f . This is much easier than it might at first seem. We start by demanding continuity at the ring. This means

$$Z(t) = f(ct) + g(ct) = h_A(ct) = h_B(ct) \quad (18.210)$$

for all t . We can immediately eliminate $h_{A,B}$:

$$h_A(\xi) = h_B(\xi) = f(\xi) + g(\xi), \quad (18.211)$$

for all ξ . Newton's second law from part (b) may now be written as

$$mc^2 [f''(\xi) + g''(\xi)] = -\tau [f'(\xi) + 3g'(\xi)]. \quad (18.212)$$

This linear ODE becomes a simple linear algebraic equation for the Fourier transforms,

$$f(\xi) = \int_{-\infty}^{\infty} \frac{dk}{2\pi} \hat{f}(k) e^{ik\xi}, \quad (18.213)$$

etc. We readily obtain

$$\hat{g}(k) = -\left(\frac{k - iQ}{k - 3iQ} \right) \hat{f}(k), \quad (18.214)$$

where $Q \equiv \tau/mc^2$ has dimensions of inverse length. Since $h_{A,B} = f + g$, we have

$$\hat{h}_A(k) = \hat{h}_B(k) = -\left(\frac{2iQ}{k - 3iQ} \right) \hat{f}(k). \quad (18.215)$$

(d) For a very long wavelength pulse, composed of plane waves for which $|k| \ll Q$, we have $\hat{g}(k) \approx -\frac{1}{3} \hat{f}(k)$. Thus, the reflected pulse is inverted, and is reduced by a factor $\frac{1}{3}$ in amplitude. Note that for a very short wavelength pulse, for which $k \gg Q$, we have perfect reflection with inversion, and no transmission. This is due to the inertia of the ring.

It is straightforward to generalize this problem to one with n strings. The transmission into each of the $(n - 1)$ channels is of course identical (by symmetry). One then finds the reflection and transmission amplitudes

$$r(k) = -\left(\frac{k - i(n - 2)Q}{k - inQ}\right), \quad t(k) = -\left(\frac{2iQ}{k - inQ}\right). \quad (18.216)$$

Conservation of energy means that the sum of the squares of the reflection amplitude and all the $(n - 1)$ transmission amplitudes must be unity:

$$|r(k)|^2 + (n - 1) |t(k)|^2 = 1. \quad (18.217)$$

18.7 Appendix : Green's Functions for Strings

18.7.1 Inhomogeneous Sturm-Liouville problem

Suppose we add a forcing term,

$$\mu(x) \frac{\partial^2 y}{\partial t^2} - \frac{\partial}{\partial x} \left[\tau(x) \frac{\partial y}{\partial x} \right] + v(x) y = \operatorname{Re} \left[\mu(x) f(x) e^{-i\omega t} \right]. \quad (18.218)$$

We write the solution as

$$y(x, t) = \operatorname{Re} \left[y(x) e^{-i\omega t} \right], \quad (18.219)$$

where

$$-\frac{d}{dx} \left[\tau(x) \frac{dy(x)}{dx} \right] + v(x) y(x) - \omega^2 \mu(x) y(x) = \mu(x) f(x), \quad (18.220)$$

or

$$\left[K - \omega^2 \mu(x) \right] y(x) = \mu(x) f(x), \quad (18.221)$$

where K is a differential operator,

$$K \equiv -\frac{d}{dx} \tau(x) \frac{d}{dx} + v(x). \quad (18.222)$$

Note that the eigenfunctions of K are the $\{\psi_n(x)\}$:

$$K \psi_n(x) = \omega_n^2 \mu(x) \psi_n(x). \quad (18.223)$$

The formal solution to equation 18.221 is then

$$y(x) = \left[K - \omega^2 \mu \right]_{x,x'}^{-1} \mu(x') f(x') = \int_{x_a}^{x_b} dx' \mu(x') G_\omega(x, x') f(x'). \quad (18.224)$$

What do we mean by the term in brackets? If we define the *Green's function*

$$G_\omega(x, x') \equiv \left[K - \omega^2 \mu \right]_{x,x'}^{-1}, \quad (18.225)$$

what this means is

$$\left[K - \omega^2 \mu(x) \right] G_\omega(x, x') = \delta(x - x') . \quad (18.226)$$

Note that the Green's function may be expanded in terms of the (real) eigenfunctions, as

$$G_\omega(x, x') = \sum_n \frac{\psi_n(x) \psi_n(x')}{\omega_n^2 - \omega^2} , \quad (18.227)$$

which follows from completeness of the eigenfunctions:

$$\mu(x) \sum_{n=1}^{\infty} \psi_n(x) \psi_n(x') = \delta(x - x') . \quad (18.228)$$

The expansion in eqn. 18.227 is formally exact, but difficult to implement, since it requires summing over an infinite set of eigenfunctions. It is more practical to construct the Green's function from solutions to the homogeneous Sturm Liouville equation, as follows. When $x \neq x'$, we have that $(K - \omega^2 \mu) G_\omega(x, x') = 0$, which is a homogeneous ODE of degree two. Consider first the interval $x \in [x_a, x']$. A second order homogeneous ODE has two solutions, and further invoking the boundary condition at $x = x_a$, there is a unique solution, up to a multiplicative constant. Call this solution $y_1(x)$. Next, consider the interval $x \in [x', x_b]$. Once again, there is a unique solution to the homogeneous Sturm-Liouville equation, up to a multiplicative constant, which satisfies the boundary condition at $x = x_b$. Call this solution $y_2(x)$. We then can write

$$G_\omega(x, x') = \begin{cases} A(x') y_1(x) & \text{if } x_a \leq x < x' \\ B(x') y_2(x) & \text{if } x' < x \leq x_b \end{cases} . \quad (18.229)$$

Here, $A(x')$ and $B(x')$ are undetermined functions. We now invoke the inhomogeneous Sturm-Liouville equation,

$$-\frac{d}{dx} \left[\tau(x) \frac{dG_\omega(x, x')}{dx} \right] + v(x) G_\omega(x, x') - \omega^2 \mu(x) G_\omega(x, x') = \delta(x - x') . \quad (18.230)$$

We integrate this from $x = x' - \epsilon$ to $x = x' + \epsilon$, where ϵ is a positive infinitesimal. This yields

$$\tau(x') \left[A(x') y'_1(x') - B(x') y'_2(x') \right] = 1 . \quad (18.231)$$

Continuity of $G_\omega(x, x')$ itself demands

$$A(x') y_1(x') = B(x') y_2(x') . \quad (18.232)$$

Solving these two equations for $A(x')$ and $B(x')$, we obtain

$$A(x') = -\frac{y_2(x')}{\tau(x') \mathcal{W}_{y_1, y_2}(x')} , \quad B(x') = -\frac{y_1(x')}{\tau(x') \mathcal{W}_{y_1, y_2}(x')} , \quad (18.233)$$

where $\mathcal{W}_{y_1, y_2}(x)$ is the *Wronskian*

$$\begin{aligned}\mathcal{W}_{y_1, y_2}(x) &= \det \begin{pmatrix} y_1(x) & y_2(x) \\ y'_1(x) & y'_2(x) \end{pmatrix} \\ &= y_1(x) y'_2(x) - y_2(x) y'_1(x).\end{aligned}\tag{18.234}$$

Now it is easy to show that $\mathcal{W}_{y_1, y_2}(x) \tau(x) = \mathcal{W} \tau$ is a constant. This follows from

$$\begin{aligned}0 &= y_2 K y_1 - y_2 K y_1 \\ &= \frac{d}{dx} \left\{ \tau(x) [y_1 y'_2 - y_2 y'_1] \right\}.\end{aligned}\tag{18.235}$$

Thus, we have

$$G_\omega(x, x') = \begin{cases} -y_1(x) y_2(x')/\mathcal{W} & \text{if } x_a \leq x < x' \\ -y_1(x') y_2(x)/\mathcal{W} & \text{if } x' < x \leq x_b, \end{cases}\tag{18.236}$$

or, in compact form,

$$G_\omega(x, x') = -\frac{y_1(x_<) y_2(x_>)}{\mathcal{W} \tau},\tag{18.237}$$

where $x_< = \min(x, x')$ and $x_> = \max(x, x')$.

As an example, consider a uniform string (*i.e.* μ and τ constant, $v = 0$) with fixed endpoints at $x_a = 0$ and $x_b = L$. The normalized eigenfunctions are

$$\psi_n(x) = \sqrt{\frac{2}{\mu L}} \sin\left(\frac{n\pi x}{L}\right),\tag{18.238}$$

and the eigenvalues are $\omega_n = n\pi c/L$. The Green's function is

$$G_\omega(x, x') = \frac{2}{\mu L} \sum_{n=1}^{\infty} \frac{\sin(n\pi x/L) \sin(n\pi x'/L)}{(n\pi c/L)^2 - \omega^2}.\tag{18.239}$$

Now construct the homogeneous solutions:

$$(K - \omega^2 \mu) y_1 = 0, \quad y_1(0) = 0 \quad \Rightarrow \quad y_1(x) = \sin\left(\frac{\omega x}{c}\right)\tag{18.240}$$

$$(K - \omega^2 \mu) y_2 = 0, \quad y_2(L) = 0 \quad \Rightarrow \quad y_2(x) = \sin\left(\frac{\omega(L-x)}{c}\right).\tag{18.241}$$

The Wronskian is

$$\mathcal{W} = y_1 y'_2 - y_2 y'_1 = -\frac{\omega}{c} \sin\left(\frac{\omega L}{c}\right).\tag{18.242}$$

Therefore, the Green's function is

$$G_\omega(x, x') = \frac{\sin(\omega x_</c) \sin(\omega(L-x_>)/c)}{(\omega \tau/c) \sin(\omega L/c)}.\tag{18.243}$$

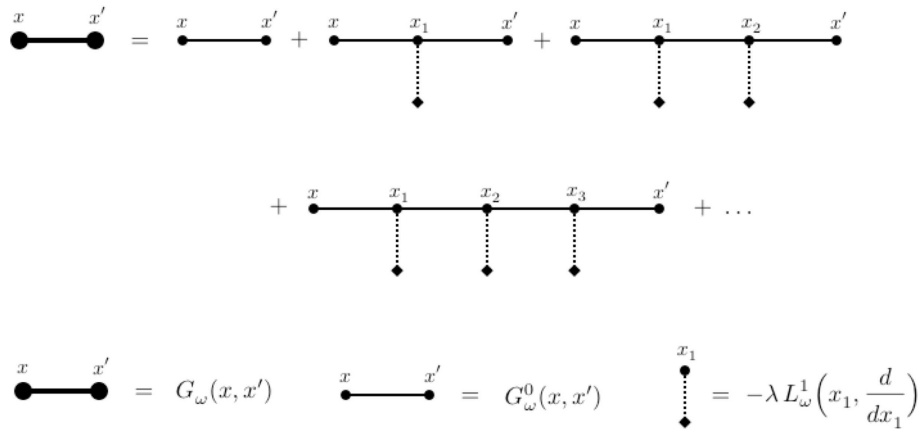


Figure 18.11: Diagrammatic representation of the perturbation expansion in eqn. 18.247.

18.7.2 Perturbation theory

Suppose we have solved for the Green's function for the linear operator K_0 and mass density $\mu_0(x)$. *I.e.* we have

$$(K_0 - \omega^2 \mu_0(x)) G_\omega^0(x, x') = \delta(x - x') . \quad (18.244)$$

We now imagine perturbing $\tau_0 \rightarrow \tau_0 + \lambda \tau_1$, $v_0 \rightarrow v_0 + \lambda v_2$, $\mu_0 \rightarrow \mu_0 + \lambda \mu_1$. What is the new Green's function $G_\omega(x, x')$? We must solve

$$(L_0 + \lambda L_1) G_\omega(x, x') = \delta(x - x') , \quad (18.245)$$

where

$$L_\omega^0 \equiv K_0 - \omega^2 \mu_0 \quad , \quad L_\omega^1 \equiv K_1 - \omega^2 \mu_1 . \quad (18.246)$$

Dropping the ω subscript for simplicity, the full Green's function is then given by

$$\begin{aligned} G_\omega &= [L_\omega^0 + \lambda L_\omega^1]^{-1} = [(G_\omega^0)^{-1} + \lambda L_\omega^1]^{-1} = [1 + \lambda G_\omega^0 L_\omega^1]^{-1} G_\omega^0 \\ &= G_\omega^0 - \lambda G_\omega^0 L_\omega^1 G_\omega^0 + \lambda^2 G_\omega^0 L_\omega^1 G_\omega^0 L_\omega^1 G_\omega^0 + \dots . \end{aligned} \quad (18.247)$$

The ‘matrix multiplication’ is of course a convolution, *i.e.*

$$G_\omega(x, x') = G_\omega^0(x, x') - \lambda \int_{x_a}^{x_b} dx_1 G_\omega^0(x, x_1) L_\omega^1(x_1, \frac{d}{dx_1}) G_\omega^0(x_1, x') + \dots . \quad (18.248)$$

Each term in the perturbation expansion of eqn. 18.247 may be represented by a diagram, as depicted in Fig. 18.11.

As an example, consider a string with $x_a = 0$ and $x_b = L$ with a mass point m affixed at the point $x = d$. Thus, $\mu_1(x) = m \delta(x - d)$, and $L_\omega^1 = -m\omega^2 \delta(x - d)$, with $\lambda = 1$. The perturbation expansion gives

$$\begin{aligned} G_\omega(x, x') &= G_\omega^0(x, x') + m\omega^2 G_\omega^0(x, d) G_\omega^0(d, x') + m^2\omega^4 G_\omega^0(x, d) G_\omega^0(d, d) G_\omega^0(d, x') + \dots \\ &= G_\omega^0(x, x') + \frac{m\omega^2 G_\omega^0(x, d) G_\omega^0(d, x')}{1 - m\omega^2 G_\omega^0(d, d)} . \end{aligned} \quad (18.249)$$

Note that the eigenfunction expansion,

$$G_\omega(x, x') = \sum_n \frac{\psi_n(x) \psi_n(x')}{\omega_n^2 - \omega^2} , \quad (18.250)$$

says that the exact eigenfrequencies are poles of $G_\omega(x, x')$, and furthermore the residue at each pole is

$$\text{Res}_{\omega=\omega_n} G_\omega(x, x') = -\frac{1}{2\omega_n} \psi_n(x) \psi_n(x') . \quad (18.251)$$

According to eqn. 18.249, the poles of $G_\omega(x, x')$ are located at solutions to⁴

$$m\omega^2 G_\omega^0(d, d) = 1 . \quad (18.252)$$

For simplicity let us set $d = \frac{1}{2}L$, so the mass point is in the middle of the string. Then according to eqn. 18.243,

$$G_\omega^0\left(\frac{1}{2}L, \frac{1}{2}L\right) = \frac{\sin^2(\omega L/2c)}{(\omega\tau/c) \sin(\omega L/c)} = \frac{c}{2\omega\tau} \tan\left(\frac{\omega L}{2c}\right) . \quad (18.253)$$

The eigenvalue equation is therefore

$$\tan\left(\frac{\omega L}{2c}\right) = \frac{2\tau}{m\omega c} , \quad (18.254)$$

which can be manipulated to yield

$$\frac{m}{M} \lambda = \operatorname{ctn} \lambda , \quad (18.255)$$

where $\lambda = \omega L/2c$ and $M = \mu L$ is the total mass of the string. When $m = 0$, the LHS vanishes, and the roots lie at $\lambda = (n + \frac{1}{2})\pi$, which gives $\omega = \omega_{2n+1}$. Why don't we see the poles at the even mode eigenfrequencies ω_{2n} ? The answer is that these poles are present in the Green's function. They do not cancel for $d = \frac{1}{2}L$ because the perturbation does not couple to the even modes, which all have $\psi_{2n}(\frac{1}{2}L) = 0$. The case of general d may be instructive in this regard. One finds the eigenvalue equation

$$\frac{\sin(2\lambda)}{2\lambda \sin(2\epsilon\lambda) \sin(2(1-\epsilon)\lambda)} = \frac{m}{M} , \quad (18.256)$$

where $\epsilon = d/L$. Now setting $m = 0$ we recover $2\lambda = n\pi$, which says $\omega = \omega_n$, and all the modes are recovered.

18.7.3 Perturbation theory for eigenvalues and eigenfunctions

We wish to solve

$$(K_0 + \lambda K_1) \psi = \omega^2 (\mu_0 + \lambda \mu_1) \psi , \quad (18.257)$$

which is equivalent to

$$L_\omega^0 \psi = -\lambda L_\omega^1 \psi . \quad (18.258)$$

⁴Note in particular that there is no longer any divergence at the location of the original poles of $G_\omega^0(x, x')$. These poles are cancelled.

Multiplying by $(L_\omega^0)^{-1} = G_\omega^0$ on the left, we have

$$\begin{aligned}\psi(x) &= -\lambda \int_{x_a}^{x_b} dx' G_\omega(x, x') L_\omega^1 \psi(x') \\ &= \lambda \sum_{m=1}^{\infty} \frac{\psi_m(x)}{\omega^2 - \omega_m^2} \int_{x_a}^{x_b} dx' \psi_m(x') L_\omega^1 \psi(x') .\end{aligned}\tag{18.259}$$

We are free to choose any normalization we like for $\psi(x)$. We choose

$$\langle \psi | \psi_n \rangle = \int_{x_a}^{x_b} dx \mu_0(x) \psi_n(x) \psi(x) = 1 ,\tag{18.260}$$

which entails

$$\omega^2 - \omega_n^2 = \lambda \int_{x_a}^{x_b} dx \psi_n(x) L_\omega^1 \psi(x)\tag{18.261}$$

as well as

$$\psi(x) = \psi_n(x) + \lambda \sum_{k \neq n} \frac{\psi_k(x)}{\omega^2 - \omega_k^2} \int_{x_a}^{x_b} dx' \psi_k(x') L_\omega^1 \psi(x') .\tag{18.262}$$

By expanding ψ and ω^2 in powers of λ , we can develop an order by order perturbation series.

To lowest order, we have

$$\omega^2 = \omega_n^2 + \lambda \int_{x_a}^{x_b} dx \psi_n(x) L_{\omega_n}^1 \psi_n(x) .\tag{18.263}$$

For the case $L_\omega^1 = -m \omega^2 \delta(x - d)$, we have

$$\frac{\delta \omega_n}{\omega_n} = -\frac{1}{2} m [\psi_n(d)]^2 = -\frac{m}{M} \sin^2\left(\frac{n\pi d}{L}\right) .\tag{18.264}$$

For $d = \frac{1}{2}L$, only the odd n modes are affected, as the even n modes have a node at $x = \frac{1}{2}L$.

Carried out to second order, one obtains for the eigenvalues,

$$\begin{aligned}\omega^2 &= \omega_n^2 + \lambda \int_{x_a}^{x_b} dx \psi_n(x) L_{\omega_n}^1 \psi_n(x) + \lambda^2 \sum_{k \neq n} \frac{\left| \int_{x_a}^{x_b} dx \psi_k(x) L_{\omega_n}^1 \psi_n(x) \right|^2}{\omega_n^2 - \omega_k^2} \\ &\quad - \lambda^2 \int_{x_a}^{x_b} dx \psi_n(x) L_{\omega_n}^1 \psi_n(x) \cdot \int_{x_a}^{x_b} dx' \mu_1(x') [\psi_n(x')]^2 + \mathcal{O}(\lambda^3) .\end{aligned}\tag{18.265}$$

Chapter 19

Special Relativity

For an extraordinarily lucid, if characteristically brief, discussion, see chs. 1 and 2 of L. D. Landau and E. M. Lifshitz, *The Classical Theory of Fields (Course of Theoretical Physics, vol. 2)*.

19.1 Introduction

All distances are relative in physics. They are measured with respect to a fixed *frame of reference*. Frames of reference in which free particles move with constant velocity are called *inertial frames*. The *principle of relativity* states that the laws of Nature are identical in all inertial frames.

19.1.1 Michelson-Morley experiment

We learned how sound waves in a fluid, such as air, obey the Helmholtz equation. Let us restrict our attention for the moment to solutions of the form $\phi(x, t)$ which do not depend on y or z . We then have a one-dimensional wave equation,

$$\frac{\partial^2 \phi}{\partial x^2} = \frac{1}{c^2} \frac{\partial^2 \phi}{\partial t^2}. \quad (19.1)$$

The fluid in which the sound propagates is assumed to be at rest. But suppose the fluid is not at rest. We can investigate this by shifting to a moving frame, defining $x' = x - ut$, with $y' = y$, $z' = z$ and of course $t' = t$. This is a Galilean transformation. In terms of the new variables, we have

$$\frac{\partial}{\partial x} = \frac{\partial}{\partial x'} \quad , \quad \frac{\partial}{\partial t} = -u \frac{\partial}{\partial x'} + \frac{\partial}{\partial t'} . \quad (19.2)$$

The wave equation is then

$$\left(1 - \frac{u^2}{c^2}\right) \frac{\partial^2 \phi}{\partial x'^2} = \frac{1}{c^2} \frac{\partial^2 \phi}{\partial t'^2} - \frac{2u}{c^2} \frac{\partial^2 \phi}{\partial x' \partial t'} . \quad (19.3)$$

Clearly the wave equation acquires a different form when expressed in the new variables (x', t') , *i.e.* in a frame in which the fluid is not at rest. The general solution is then of the modified d'Alembert form,

$$\phi(x', t') = f(x' - c_R t') + g(x' + c_L t') , \quad (19.4)$$

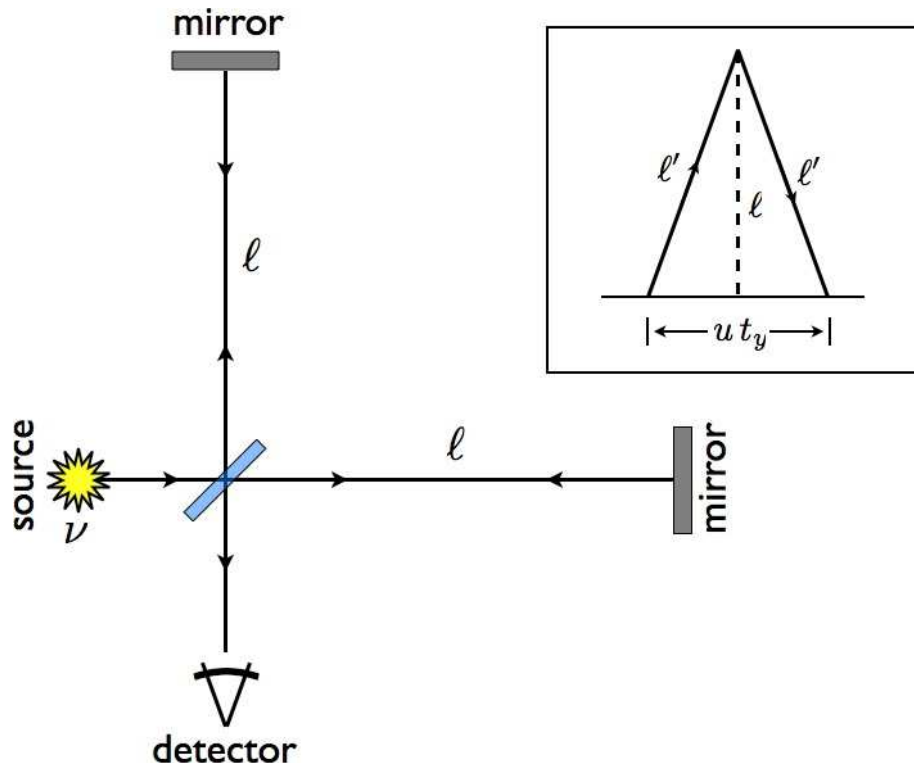


Figure 19.1: The Michelson-Morley experiment (1887) used an interferometer to effectively measure the time difference for light to travel along two different paths. Inset: analysis for the y -directed path.

where $c_R = c - u$ and $c_L = c + u$ are the speeds of rightward and leftward propagating disturbances, respectively. Thus, there is a *preferred frame of reference* – the frame in which the fluid is at rest. In the rest frame of the fluid, sound waves travel with velocity c in either direction.

Light, as we know, is a wave phenomenon in classical physics. The propagation of light is described by Maxwell's equations,

$$\nabla \cdot \mathbf{E} = 4\pi\rho \quad \nabla \times \mathbf{E} = -\frac{1}{c} \frac{\partial \mathbf{B}}{\partial t} \quad (19.5)$$

$$\nabla \cdot \mathbf{B} = 0 \quad \nabla \times \mathbf{B} = \frac{4\pi}{c} \mathbf{j} + \frac{1}{c} \frac{\partial \mathbf{E}}{\partial t}, \quad (19.6)$$

where ρ and \mathbf{j} are the local charge and current density, respectively. Taking the curl of Faraday's law, and restricting to free space where $\rho = \mathbf{j} = 0$, we once again have (using a Cartesian system for the fields) the wave equation,

$$\nabla^2 \mathbf{E} = \frac{1}{c^2} \frac{\partial^2 \mathbf{E}}{\partial t^2}. \quad (19.7)$$

(We shall discuss below, in section 19.8, the beautiful properties of Maxwell's equations under general coordinate transformations.)

In analogy with the theory of sound, it was assumed prior to Einstein that there was in fact a preferred reference frame for electromagnetic radiation – one in which the medium which was excited during the

EM wave propagation was at rest. This notional medium was called the *lumineferous ether*. Indeed, it was generally assumed during the 19th century that light, electricity, magnetism, and heat (which was not understood until Boltzmann's work in the late 19th century) all had separate ethers. It was Maxwell who realized that light, electricity, and magnetism were all unified phenomena, and accordingly he proposed a single ether for electromagnetism. It was believed at the time that the earth's motion through the ether would result in a drag on the earth.

In 1887, Michelson and Morley set out to measure the changes in the speed of light on earth due to the earth's movement through the ether (which was generally assumed to be at rest in the frame of the Sun). The Michelson interferometer is shown in fig. 19.1, and works as follows. Suppose the apparatus is moving with velocity $u \hat{x}$ through the ether. Then the time it takes a light ray to travel from the half-silvered mirror to the mirror on the right and back again is

$$t_x = \frac{\ell}{c+u} + \frac{\ell}{c-u} = \frac{2\ell c}{c^2 - u^2} . \quad (19.8)$$

For motion along the other arm of the interferometer, the geometry in the inset of fig. 19.1 shows $\ell' = \sqrt{\ell^2 + \frac{1}{4}u^2 t_y^2}$, hence

$$t_y = \frac{2\ell'}{c} = \frac{2}{c} \sqrt{\ell^2 + \frac{1}{4}u^2 t_y^2} \quad \Rightarrow \quad t_y = \frac{2\ell}{\sqrt{c^2 - u^2}} . \quad (19.9)$$

Thus, the difference in times along these two paths is

$$\Delta t = t_x - t_y = \frac{2\ell c}{c^2} - \frac{2\ell}{\sqrt{c^2 - u^2}} \approx \frac{\ell}{c} \cdot \frac{u^2}{c^2} . \quad (19.10)$$

Thus, the difference in phase between the two paths is

$$\frac{\Delta\phi}{2\pi} = \nu \Delta t \approx \frac{\ell}{\lambda} \cdot \frac{u^2}{c^2} , \quad (19.11)$$

where λ is the wavelength of the light. We take $u \approx 30$ km/s, which is the earth's orbital velocity, and $\lambda \approx 5000$ Å. From this we find that $\Delta\phi \approx 0.02 \times 2\pi$ if $\ell = 1$ m. Michelson and Morley found that the observed fringe shift $\Delta\phi/2\pi$ was approximately 0.02 times the expected value. The inescapable conclusion was that the speed of light did not depend on the motion of the source. This was very counterintuitive!

The history of the development of special relativity is quite interesting, but we shall not have time to dwell here on the many streams of scientific thought during those exciting times. Suffice it to say that the Michelson-Morley experiment, while a landmark result, was not the last word. It had been proposed that the ether could be dragged, either entirely or partially, by moving bodies. If the earth dragged the ether along with it, then there would be no ground-level 'ether wind' for the MM experiment to detect. Other experiments, however, such as stellar aberration, in which the apparent position of a distant star varies due to the earth's orbital velocity, rendered the "ether drag" theory untenable – the notional 'ether bubble' dragged by the earth could not reasonably be expected to extend to the distant stars.

A more recent test of the effect of a moving source on the speed of light was performed by T. Alvåger *et al.*, *Phys. Lett.* **12**, 260 (1964), who measured the velocity of γ -rays (photons) emitted from the decay of highly energetic neutral pions (π^0). The pion energies were in excess of 6 GeV, which translates to a

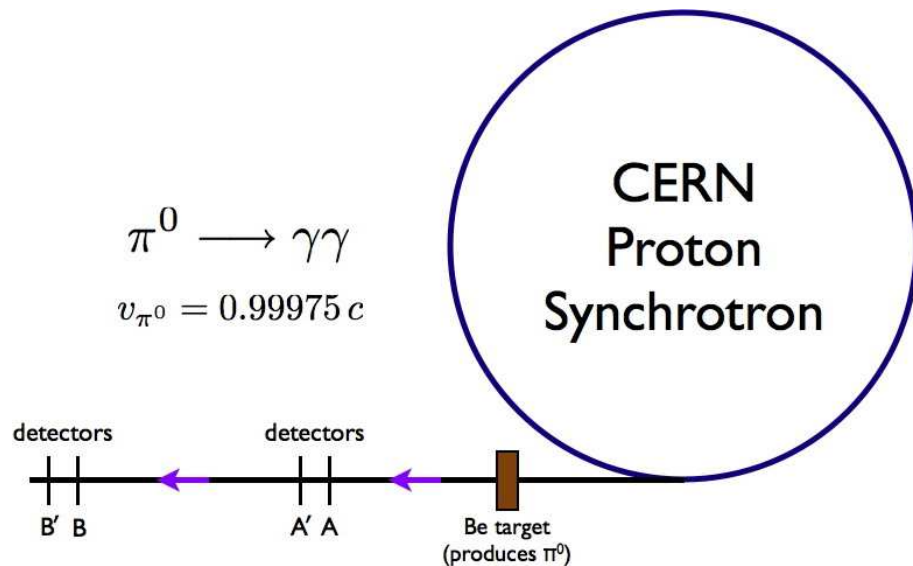


Figure 19.2: Experimental setup of Alvager *et al.* (1964), who used the decay of high energy neutral pions to test the source velocity dependence of the speed of light.

velocity of $v = 0.99975 c$, according to special relativity. Thus, photons emitted in the direction of the pions should be traveling at close to $2c$, if the source and photon velocities were to add. Instead, the velocity of the photons was found to be $c = 2.9977 \pm 0.0004 \times 10^{10} \text{ cm/s}$, which is within experimental error of the best accepted value.

19.1.2 Einsteinian and Galilean relativity

The *Principle of Relativity* states that the laws of nature are the same when expressed in any inertial frame. This principle can further be refined into two classes, depending on whether one takes the velocity of the propagation of interactions to be finite or infinite.

The interaction of matter in classical mechanics is described by a potential function $U(\mathbf{r}_1, \dots, \mathbf{r}_N)$. Typically, one has two-body interactions in which case one writes $U = \sum_{i < j} U(\mathbf{r}_i, \mathbf{r}_j)$. These interactions are thus assumed to be instantaneous, which is unphysical. The interaction of particles is mediated by the exchange of gauge bosons, such as the photon (for electromagnetic interactions), gluons (for the strong interaction, at least on scales much smaller than the ‘confinement length’), or the graviton (for gravity). Their velocity of propagation, according to the principle of relativity, is the same in all reference frames, and is given by the speed of light, $c = 2.998 \times 10^8 \text{ m/s}$.

Since c is so large in comparison with terrestrial velocities, and since d/c is much shorter than all other relevant time scales for typical interparticle separations d , the assumption of an instantaneous interaction is usually quite accurate. The combination of the principle of relativity with finiteness of c is known as

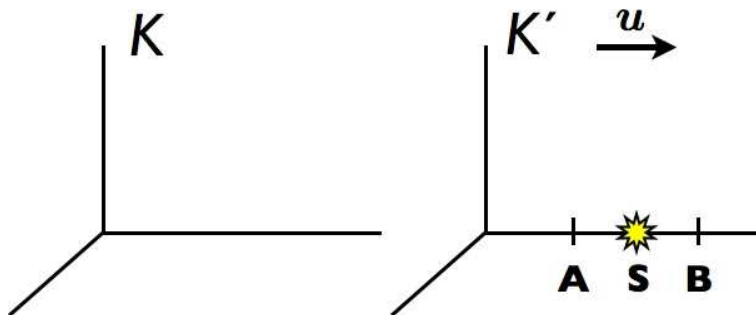


Figure 19.3: Two reference frames.

Einsteinian relativity. When $c = \infty$, the combination comprises Galilean relativity:

$$\begin{aligned} c < \infty & : \text{ Einsteinian relativity} \\ c = \infty & : \text{ Galilean relativity .} \end{aligned}$$

Consider a train moving at speed u . In the rest frame of the train track, the speed of the light beam emanating from the train's headlight is $c + u$. This would contradict the principle of relativity. This leads to some very peculiar consequences, foremost among them being the fact that events which are simultaneous in one inertial frame will not in general be simultaneous in another. In Newtonian mechanics, on the other hand, time is absolute, and is independent of the frame of reference. If two events are simultaneous in one frame then they are simultaneous in all frames. This is not the case in Einsteinian relativity!

We can begin to apprehend this curious feature of simultaneity by the following *Gedankenexperiment* (a long German word meaning “thought experiment”)¹. Consider the case in fig. 19.3 in which frame K' moves with velocity $u \hat{x}$ with respect to frame K . Let a source at S emit a signal (a light pulse) at $t = 0$. In the frame K' the signal’s arrival at equidistant locations A and B is simultaneous. In frame K , however, A moves toward left-propagating emitted wavefront, and B moves away from the right-propagating wavefront. For classical sound, the speed of the left-moving and right-moving wavefronts is $c \mp u$, taking into account the motion of the source, and thus the relative velocities of the signal and the detectors remain at c . But according to the principle of relativity, the speed of light is c in all frames, and is so in frame K for both the left-propagating and right-propagating signals. Therefore, the relative velocity of A and the left-moving signal is $c + u$ and the relative velocity of B and the right-moving signal is $c - u$. Therefore, A ‘closes in’ on the signal and receives it before B , which is moving away from the signal. We might expect the arrival times to be $t_A^* = d/(c + u)$ and $t_B^* = d/(c - u)$, where d is the distance between the source S and either detector A or B in the K' frame. Later on we shall analyze this problem and show that

$$t_A^* = \sqrt{\frac{c-u}{c+u}} \cdot \frac{d}{c} \quad , \quad t_B^* = \sqrt{\frac{c+u}{c-u}} \cdot \frac{d}{c} . \quad (19.12)$$

Our naïve analysis has omitted an important detail – the *Lorentz contraction* of the distance d as seen by an observer in the K frame.

¹Unfortunately, many important physicists were German and we have to put up with a legacy of long German words like *Gedankenexperiment*, *Zitterbewegung*, *Brehmsstrahlung*, *Stosszahlansatz*, *Kartoffelsalat*, etc.

19.2 Intervals

Now let us express mathematically the constancy of c in all frames. An *event* is specified by the time and place where it occurs. Thus, an event is specified by *four* coordinates, (t, x, y, z) . The four-dimensional space spanned by these coordinates is called *spacetime*. The *interval* between two events in spacetime at (t_1, x_1, y_1, z_1) and (t_2, x_2, y_2, z_2) is defined to be

$$s_{12} = \sqrt{c^2(t_1 - t_2)^2 - (x_1 - x_2)^2 - (y_1 - y_2)^2 - (z_1 - z_2)^2}. \quad (19.13)$$

For two events separated by an infinitesimal amount, the interval ds is infinitesimal, with

$$ds^2 = c^2 dt^2 - dx^2 - dy^2 - dz^2. \quad (19.14)$$

Now when the two events denote the emission and reception of an electromagnetic signal, we have $ds^2 = 0$. This must be true in any frame, owing to the invariance of c , hence since ds and ds' are differentials of the same order, we must have $ds'^2 = ds^2$. This last result requires homogeneity and isotropy of space as well. Finally, if infinitesimal intervals are invariant, then integrating we obtain $s = s'$, and we conclude that *the interval between two space-time events is the same in all inertial frames*.

When $s_{12}^2 > 0$, the interval is said to be *time-like*. For timelike intervals, we can always find a reference frame in which the two events occur at the same *locations*. As an example, consider a passenger sitting on a train. Event #1 is the passenger yawning at time t_1 . Event #2 is the passenger yawning again at some later time t_2 . To an observer sitting in the train station, the two events take place at different locations, but in the frame of the passenger, they occur at the same location.

When $s_{12}^2 < 0$, the interval is said to be *space-like*. Note that $s_{12} = \sqrt{s_{12}^2} \in i\mathbb{R}$ is pure imaginary, so one says that imaginary intervals are spacelike. As an example, at this moment, in the frame of the reader, the North and South poles of the earth are separated by a space-like interval. If the interval between two events is space-like, a reference frame can always be found in which the events are simultaneous.

An interval with $s_{12} = 0$ is said to be *light-like*.

This leads to the concept of the *light cone*, depicted in fig. 19.4. Consider an event E. In the frame of an inertial observer, all events with $s^2 > 0$ and $\Delta t > 0$ are in E's *forward light cone* and are part of his *absolute future*. Events with $s^2 > 0$ and $\Delta t < 0$ lie in E's *backward light cone* and are part of his *absolute past*. Events with spacelike separations $s^2 < 0$ are *causally disconnected* from E. Two events which are causally disconnected can not possibly influence each other. Uniform rectilinear motion is represented by a line $t = x/v$ with constant slope. If $v < c$, this line is contained within E's light cone. E is potentially influenced by all events in its backward light cone, *i.e.* its absolute past. It is impossible to find a frame of reference which will transform past into future, or spacelike into timelike intervals.

19.2.1 Proper time

Proper time is the time read on a clock traveling with a moving observer. Consider two observers, one at rest and one in motion. If dt is the differential time elapsed in the rest frame, then

$$\begin{aligned} ds^2 &= c^2 dt^2 - dx^2 - dy^2 - dz^2 \\ &= c^2 dt'^2, \end{aligned} \quad (19.15)$$

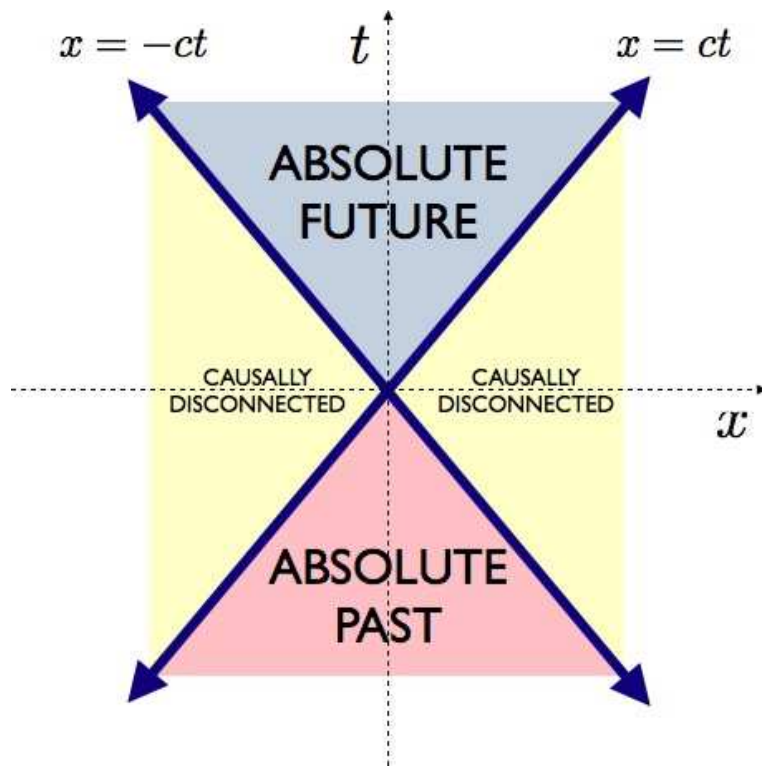


Figure 19.4: A $(1+1)$ -dimensional light cone. The forward light cone consists of timelike events with $\Delta t > 0$. The backward light cone consists of timelike events with $\Delta t < 0$. The causally disconnected regions are time-like, and intervals connecting the origin to any point on the light cone itself are light-like.

where dt' is the differential time elapsed on the moving clock. Thus,

$$dt' = dt \sqrt{1 - \frac{\mathbf{v}^2}{c^2}}, \quad (19.16)$$

and the time elapsed on the moving observer's clock is

$$t'_2 - t'_1 = \int_{t_1}^{t_2} dt \sqrt{1 - \frac{\mathbf{v}^2(t)}{c^2}}. \quad (19.17)$$

Thus, *moving clocks run slower*. This is an essential feature which is key to understanding many important aspects of particle physics. A particle with a brief lifetime can, by moving at speeds close to c , appear to an observer in our frame to be long-lived. It is customary to define two dimensionless measures of a particle's velocity:

$$\beta \equiv \frac{\mathbf{v}}{c}, \quad \gamma \equiv \frac{1}{\sqrt{1 - \beta^2}}. \quad (19.18)$$

As $v \rightarrow c$, we have $\beta \rightarrow 1$ and $\gamma \rightarrow \infty$.

Suppose we wish to compare the elapsed time on two clocks. We keep one clock at rest in an inertial frame, while the other executes a closed path in space, returning to its initial location after some interval

of time. When the clocks are compared, the moving clock will show a smaller elapsed time. This is often stated as the “twin paradox.” The total elapsed time on a moving clock is given by

$$\tau = \frac{1}{c} \int_a^b ds , \quad (19.19)$$

where the integral is taken over the *world line* of the moving clock. The elapsed time τ takes on a minimum value when the path from a to b is a straight line. To see this, one can express $\tau[\mathbf{x}(t)]$ as a functional of the path $\mathbf{x}(t)$ and extremize. This results in $\ddot{\mathbf{x}} = 0$.

19.2.2 Irreverent problem from Spring 2002 final exam

Flowers for Algernon – Bob’s beloved hamster, Algernon, is very ill. He has only three hours to live. The veterinarian tells Bob that Algernon can be saved only through a gallbladder transplant. A suitable donor gallbladder is available from a hamster recently pronounced brain dead after a blender accident in New York (miraculously, the gallbladder was unscathed), but it will take Life Flight five hours to bring the precious rodent organ to San Diego.

Bob embarks on a bold plan to save Algernon’s life. He places him in a cage, ties the cage to the end of a strong meter-long rope, and whirls the cage above his head while the Life Flight team is *en route*. Bob reasons that *if he can make time pass more slowly for Algernon*, the gallbladder will arrive in time to save his life.

- (a) At how many revolutions per second must Bob rotate the cage in order that the gallbladder arrive in time for the life-saving surgery? What is Algernon’s speed v_0 ?

Solution : We have $\beta(t) = \omega_0 R/c$ is constant, therefore, from eqn. 19.17,

$$\Delta t = \gamma \Delta t' . \quad (19.20)$$

Setting $\Delta t' = 3 \text{ hr}$ and $\Delta t = 5 \text{ hr}$, we have $\gamma = \frac{5}{3}$, which entails $\beta = \sqrt{1 - \gamma^{-2}} = \frac{4}{5}$. Thus, $v_0 = \frac{4}{5} c$, which requires a rotation frequency of $\omega_0/2\pi = 38.2 \text{ MHz}$.

- (b) Bob finds that he cannot keep up the pace! Assume Algernon’s speed is given by

$$v(t) = v_0 \sqrt{1 - \frac{t}{T}} \quad (19.21)$$

where v_0 is the speed from part (a), and $T = 5 \text{ h}$. As the plane lands at the pet hospital’s emergency runway, Bob peers into the cage to discover that Algernon is dead! In order to fill out his death report, the veterinarian needs to know: *when did Algernon die?* Assuming he died after his own hamster watch registered three hours, derive an expression for the elapsed time on the veterinarian’s clock at the moment of Algernon’s death.

Solution : (Sniffle). We have $\beta(t) = \frac{4}{5} (1 - \frac{t}{T})^{1/2}$. We set

$$T' = \int_0^{T^*} dt \sqrt{1 - \beta^2(t)} \quad (19.22)$$

where $T' = 3 \text{ hr}$ and T^* is the time of death in Bob's frame. We write $\beta_0 = \frac{4}{5}$ and $\gamma_0 = (1 - \beta_0^2)^{-1/2} = \frac{5}{3}$. Note that $T'/T = \sqrt{1 - \beta_0^2} = \gamma_0^{-1}$.

Rescaling by writing $\zeta = t/T$, we have

$$\begin{aligned}\frac{T'}{T} &= \gamma_0^{-1} = \int_0^{T^*/T} d\zeta \sqrt{1 - \beta_0^2 + \beta_0^2 \zeta} \\ &= \frac{2}{3\beta_0^2} \left[\left(1 - \beta_0^2 + \beta_0^2 \frac{T^*}{T} \right)^{3/2} - (1 - \beta_0^2)^{3/2} \right] \\ &= \frac{2}{3\gamma_0} \cdot \frac{1}{\gamma_0^2 - 1} \left[\left(1 + (\gamma_0^2 - 1) \frac{T^*}{T} \right)^{3/2} - 1 \right].\end{aligned}\quad (19.23)$$

Solving for T^*/T we have

$$\frac{T^*}{T} = \frac{\left(\frac{3}{2}\gamma_0^2 - \frac{1}{2}\right)^{2/3} - 1}{\gamma_0^2 - 1}. \quad (19.24)$$

With $\gamma_0 = \frac{5}{3}$ we obtain

$$\frac{T^*}{T} = \frac{9}{16} \left[\left(\frac{11}{3}\right)^{2/3} - 1 \right] = 0.77502\dots \quad (19.25)$$

Thus, $T^* = 3.875 \text{ hr} = 3 \text{ hr } 52 \text{ min } 50.5 \text{ sec}$ after Bob starts swinging.

(c) Identify at least three practical problems with Bob's scheme.

Solution : As you can imagine, student responses to this part were varied and generally sarcastic. *E.g.* “the atmosphere would ignite,” or “Bob’s arm would fall off,” or “Algernon’s remains would be found on the inside of the far wall of the cage, squashed flatter than a coat of semi-gloss paint,” *etc.*

19.3 Four-Vectors and Lorentz Transformations

We have spoken thus far about different reference frames. So how precisely do the coordinates (t, x, y, z) transform between frames K and K' ? In classical mechanics, we have $t = t'$ and $\mathbf{x} = \mathbf{x}' + \mathbf{u}t$, according to fig. 19.3. This yields the *Galilean transformation*,

$$\begin{pmatrix} t \\ x \\ y \\ z \end{pmatrix} = \begin{pmatrix} 1 & 0 & 0 & 0 \\ u_x & 1 & 0 & 0 \\ u_y & 0 & 1 & 0 \\ u_z & 0 & 0 & 1 \end{pmatrix} \begin{pmatrix} t' \\ x' \\ y' \\ z' \end{pmatrix}. \quad (19.26)$$

Such a transformation does not leave intervals invariant.

Let us define the *four-vector* x^μ as

$$x^\mu = \begin{pmatrix} ct \\ x \\ y \\ z \end{pmatrix} \equiv \begin{pmatrix} ct \\ \mathbf{x} \end{pmatrix}. \quad (19.27)$$

Thus, $x^0 = ct$, $x^1 = x$, $x^2 = y$, and $x^3 = z$. In order for intervals to be invariant, the transformation between x^μ in frame K and x'^μ in frame K' must be linear:

$$x^\mu = L_\nu^\mu x'^\nu , \quad (19.28)$$

where we are using the Einstein convention of summing over repeated indices. We define the *Minkowski metric tensor* $g_{\mu\nu}$ as follows:

$$g_{\mu\nu} = g^{\mu\nu} = \begin{pmatrix} 1 & 0 & 0 & 0 \\ 0 & -1 & 0 & 0 \\ 0 & 0 & -1 & 0 \\ 0 & 0 & 0 & -1 \end{pmatrix} . \quad (19.29)$$

Clearly $g = g^t$ is a symmetric matrix.

Note that the matrix L_β^α has one raised index and one lowered index. For the notation we are about to develop, it is very important to distinguish raised from lowered indices. To raise or lower an index, we use the metric tensor. For example,

$$x_\mu = g_{\mu\nu} x^\nu = \begin{pmatrix} ct \\ -x \\ -y \\ -z \end{pmatrix} . \quad (19.30)$$

The act of summing over an identical raised and lowered index is called *index contraction*. Note that

$$g_\nu^\mu = g^{\mu\rho} g_{\rho\nu} = \delta_\nu^\mu = \begin{pmatrix} 1 & 0 & 0 & 0 \\ 0 & 1 & 0 & 0 \\ 0 & 0 & 1 & 0 \\ 0 & 0 & 0 & 1 \end{pmatrix} . \quad (19.31)$$

Now let's investigate the invariance of the interval. We must have $x'^\mu x'_\mu = x^\mu x_\mu$. Note that

$$\begin{aligned} x^\mu x_\mu &= L_\alpha^\mu x'^\alpha L_\mu^\beta x'_\beta \\ &= (L_\alpha^\mu g_{\mu\nu} L_\beta^\nu) x'^\alpha x'^\beta , \end{aligned} \quad (19.32)$$

from which we conclude

$$L_\alpha^\mu g_{\mu\nu} L_\beta^\nu = g_{\alpha\beta} . \quad (19.33)$$

This result also may be written in other ways:

$$L^{\mu\alpha} g_{\mu\nu} L^{\nu\beta} = g^{\alpha\beta} , \quad L_\alpha^\mu g_{\mu\nu} L_\beta^\nu = g_{\alpha\beta} \quad (19.34)$$

Another way to write this equation is $L^t g L = g$. A rank-4 matrix which satisfies this constraint, with $g = \text{diag}(+, -, -, -)$ is an element of the group $O(3, 1)$, known as the *Lorentz group*.

Let us now count the freedoms in L . As a 4×4 real matrix, it contains 16 elements. The matrix $L^t g L$ is a symmetric 4×4 matrix, which contains 10 independent elements: 4 along the diagonal and 6 above the diagonal. Thus, there are 10 constraints on 16 elements of L , and we conclude that the group $O(3, 1)$ is 6-dimensional. This is also the dimension of the four-dimensional orthogonal group $O(4)$, by the way.

Three of these six parameters may be taken to be the Euler angles. That is, the group $O(3)$ constitutes a three-dimensional *subgroup* of the Lorentz group $O(3, 1)$, with elements

$$L^\mu{}_\nu = \begin{pmatrix} 1 & 0 & 0 & 0 \\ 0 & R_{11} & R_{12} & R_{13} \\ 0 & R_{21} & R_{22} & R_{23} \\ 0 & R_{31} & R_{32} & R_{33} \end{pmatrix}, \quad (19.35)$$

where $R^t R = MI$, *i.e.* $R \in O(3)$ is a rank-3 orthogonal matrix, parameterized by the three Euler angles (ϕ, θ, ψ) . The remaining three parameters form a vector $\beta = (\beta_x, \beta_y, \beta_z)$ and define a second class of Lorentz transformations, called boosts:²

$$L^\mu{}_\nu = \begin{pmatrix} \gamma & \gamma \beta_x & \gamma \beta_y & \gamma \beta_z \\ \gamma \beta_x & 1 + (\gamma - 1) \hat{\beta}_x \hat{\beta}_x & (\gamma - 1) \hat{\beta}_x \hat{\beta}_y & (\gamma - 1) \hat{\beta}_x \hat{\beta}_z \\ \gamma \beta_y & (\gamma - 1) \hat{\beta}_x \hat{\beta}_y & 1 + (\gamma - 1) \hat{\beta}_y \hat{\beta}_y & (\gamma - 1) \hat{\beta}_y \hat{\beta}_z \\ \gamma \beta_z & (\gamma - 1) \hat{\beta}_x \hat{\beta}_z & (\gamma - 1) \hat{\beta}_y \hat{\beta}_z & 1 + (\gamma - 1) \hat{\beta}_z \hat{\beta}_z \end{pmatrix}, \quad (19.36)$$

where

$$\hat{\beta} = \frac{\beta}{|\beta|}, \quad \gamma = (1 - \beta^2)^{-1/2}. \quad (19.37)$$

IMPORTANT : Since the components of β are not the spatial components of a four vector, we will only write these components with a lowered index, as β_i , with $i = 1, 2, 3$. We will not write β^i with a raised index, but if we did, we'd mean the same thing, *i.e.* $\beta^i = \beta_i$. Note that for the spatial components of a 4-vector like x^μ , we have $x_i = -x^i$.

Let's look at a simple example, where $\beta_x = \beta$ and $\beta_y = \beta_z = 0$. Then

$$L^\mu{}_\nu = \begin{pmatrix} \gamma & \gamma \beta & 0 & 0 \\ \gamma \beta & \gamma & 0 & 0 \\ 0 & 0 & 1 & 0 \\ 0 & 0 & 0 & 1 \end{pmatrix}. \quad (19.38)$$

The effect of this Lorentz transformation $x^\mu = L^\mu{}_\nu x'^\nu$ is thus

$$\begin{aligned} ct &= \gamma ct' + \gamma \beta x' \\ x &= \gamma \beta ct' + \gamma x'. \end{aligned} \quad (19.39)$$

How fast is the origin of K' moving in the K frame? We have $dx' = 0$ and thus

$$\frac{1}{c} \frac{dx}{dt} = \frac{\gamma \beta c dt'}{\gamma c dt'} = \beta. \quad (19.40)$$

Thus, $u = \beta c$, *i.e.* $\beta = u/c$.

It is convenient to take advantage of the fact that $P_{ij}^\beta \equiv \hat{\beta}_i \hat{\beta}_j$ is a *projection operator*, which satisfies $(P^\beta)^2 = P^\beta$. The action of P_{ij}^β on any vector ξ is to project that vector onto the $\hat{\beta}$ direction:

$$P^\beta \xi = (\hat{\beta} \cdot \xi) \hat{\beta}. \quad (19.41)$$

²Unlike rotations, the boosts do not themselves define a subgroup of $O(3, 1)$.

We may now write the general Lorentz boost, with $\beta = \mathbf{u}/c$, as

$$L = \begin{pmatrix} \gamma & \gamma\beta^t \\ \gamma\beta & I + (\gamma - 1)P^\beta \end{pmatrix}, \quad (19.42)$$

where I is the 3×3 unit matrix, and where we write column and row vectors

$$\beta = \begin{pmatrix} \beta_x \\ \beta_y \\ \beta_z \end{pmatrix}, \quad \beta^t = \begin{pmatrix} \beta_x & \beta_y & \beta_z \end{pmatrix} \quad (19.43)$$

as a mnemonic to help with matrix multiplications. We now have

$$\begin{pmatrix} ct \\ \mathbf{x} \end{pmatrix} = \begin{pmatrix} \gamma & \gamma\beta^t \\ \gamma\beta & I + (\gamma - 1)P^\beta \end{pmatrix} \begin{pmatrix} ct' \\ \mathbf{x}' \end{pmatrix} = \begin{pmatrix} \gamma ct' + \gamma\beta \cdot \mathbf{x}' \\ \gamma\beta ct' + \mathbf{x}' + (\gamma - 1)P^\beta \mathbf{x}' \end{pmatrix}. \quad (19.44)$$

Thus,

$$\begin{aligned} ct &= \gamma ct' + \gamma\beta \cdot \mathbf{x}' \\ \mathbf{x} &= \gamma\beta ct' + \mathbf{x}' + (\gamma - 1)(\hat{\beta} \cdot \mathbf{x}') \hat{\beta}. \end{aligned} \quad (19.45)$$

If we resolve \mathbf{x} and \mathbf{x}' into components parallel and perpendicular to β , writing

$$x_{\parallel} = \hat{\beta} \cdot \mathbf{x}, \quad x_{\perp} = \mathbf{x} - (\hat{\beta} \cdot \mathbf{x}) \hat{\beta}, \quad (19.46)$$

with corresponding definitions for x'_{\parallel} and x'_{\perp} , the general Lorentz boost may be written as

$$\begin{aligned} ct &= \gamma ct' + \gamma\beta x'_{\parallel} \\ x_{\parallel} &= \gamma\beta ct' + \gamma x'_{\parallel} \\ \mathbf{x}_{\perp} &= \mathbf{x}'_{\perp}. \end{aligned} \quad (19.47)$$

Thus, the components of \mathbf{x} and \mathbf{x}' which are parallel to β enter into a one-dimensional Lorentz boost along with t and t' , as described by eqn. 19.39. The components of \mathbf{x} and \mathbf{x}' which are perpendicular to β are unaffected by the boost.

Finally, the Lorentz group $O(3, 1)$ is a group under multiplication, which means that if L_a and L_b are elements, then so is the product $L_a L_b$. Explicitly, we have

$$(L_a L_b)^t g L_a L_b = L_b^t (L_a^t g L_a) L_b = L_b^t g L_b = g. \quad (19.48)$$

19.3.1 Covariance and contravariance

Note that

$$\begin{aligned} L_{\alpha}^{t\mu} g_{\mu\nu} L_{\beta}^{\nu} &= \begin{pmatrix} \gamma & \gamma\beta & 0 & 0 \\ \gamma\beta & \gamma & 0 & 0 \\ 0 & 0 & 1 & 0 \\ 0 & 0 & 0 & 1 \end{pmatrix} \begin{pmatrix} 1 & 0 & 0 & 0 \\ 0 & -1 & 0 & 0 \\ 0 & 0 & -1 & 0 \\ 0 & 0 & 0 & -1 \end{pmatrix} \begin{pmatrix} \gamma & \gamma\beta & 0 & 0 \\ \gamma\beta & \gamma & 0 & 0 \\ 0 & 0 & 1 & 0 \\ 0 & 0 & 0 & 1 \end{pmatrix} \\ &= \begin{pmatrix} 1 & 0 & 0 & 0 \\ 0 & -1 & 0 & 0 \\ 0 & 0 & -1 & 0 \\ 0 & 0 & 0 & -1 \end{pmatrix} = g_{\alpha\beta}, \end{aligned} \quad (19.49)$$

since $\gamma^2(1-\beta^2) = 1$. This is in fact the general way that tensors transform under a Lorentz transformation:

$$\begin{aligned} \text{covariant vectors : } x^{\mu} &= L_{\nu}^{\mu} x'^{\nu} \\ \text{covariant tensors : } F^{\mu\nu} &= L_{\alpha}^{\mu} L_{\beta}^{\nu} F'^{\alpha\beta} = L_{\alpha}^{\mu} F'^{\alpha\beta} L_{\beta}^{t\nu} \end{aligned} \quad (19.50)$$

Note how index contractions always involve one raised index and one lowered index. Raised indices are called *contravariant indices* and lowered indices are called *covariant indices*. The transformation rules for contravariant vectors and tensors are

$$\begin{aligned} \text{contravariant vectors : } x_{\mu} &= L_{\mu}^{\nu} x'_{\nu} \\ \text{contravariant tensors : } F_{\mu\nu} &= L_{\mu}^{\alpha} L_{\nu}^{\beta} F'_{\alpha\beta} = L_{\mu}^{\alpha} F'_{\alpha\beta} L_{\beta}^{t\nu} \end{aligned} \quad (19.51)$$

A *Lorentz scalar* has no indices at all. For example,

$$ds^2 = g_{\mu\nu} dx^{\mu} dx^{\nu}, \quad (19.52)$$

is a Lorentz scalar. In this case, we have contracted a tensor with two four-vectors. The dot product of two four-vectors is also a Lorentz scalar:

$$\begin{aligned} \mathbf{a} \cdot \mathbf{b} &\equiv a^{\mu} b_{\mu} = g_{\mu\nu} a^{\mu} b^{\nu} \\ &= a^0 b^0 - a^1 b^1 - a^2 b^2 - a^3 b^3 \\ &= a^0 b^0 - \mathbf{a} \cdot \mathbf{b}. \end{aligned} \quad (19.53)$$

Note that the dot product $a \cdot b$ of four-vectors is invariant under a simultaneous Lorentz transformation of both a^{μ} and b^{μ} , i.e. $a \cdot b = a' \cdot b'$. Indeed, this invariance is the very definition of what it means for something to be a Lorentz scalar. Derivatives with respect to covariant vectors yield contravariant vectors:

$$\frac{\partial f}{\partial x^{\mu}} \equiv \partial_{\mu} f \quad , \quad \frac{\partial A^{\mu}}{\partial x^{\nu}} = \partial_{\nu} A^{\mu} \equiv B^{\mu}_{\nu} \quad , \quad \frac{\partial B^{\mu}_{\nu}}{\partial x^{\lambda}} = \partial_{\lambda} B^{\mu}_{\nu} \equiv C^{\mu}_{\nu\lambda} \quad (19.54)$$

et cetera. Note that differentiation with respect to the covariant vector x^{μ} is expressed by the *contravariant differential operator* ∂_{μ} :

$$\begin{aligned} \frac{\partial}{\partial x^{\mu}} &\equiv \partial_{\mu} = \left(\frac{1}{c} \frac{\partial}{\partial t}, \frac{\partial}{\partial x}, \frac{\partial}{\partial y}, \frac{\partial}{\partial z} \right) \\ \frac{\partial}{\partial x_{\mu}} &\equiv \partial^{\mu} = \left(\frac{1}{c} \frac{\partial}{\partial t}, -\frac{\partial}{\partial x}, -\frac{\partial}{\partial y}, -\frac{\partial}{\partial z} \right). \end{aligned} \quad (19.55)$$

The contraction $\square \equiv \partial^\mu \partial_\mu$ is a Lorentz scalar differential operator, called the *D'Alembertian*:

$$\square = \frac{1}{c^2} \frac{\partial^2}{\partial t^2} - \frac{\partial^2}{\partial x^2} - \frac{\partial^2}{\partial y^2} - \frac{\partial^2}{\partial z^2}. \quad (19.56)$$

The Helmholtz equation for scalar waves propagating with speed c can thus be written in compact form as $\square \phi = 0$.

19.3.2 What to do if you hate raised and lowered indices

Admittedly, this covariant and contravariant business takes some getting used to. Ultimately, it helps to keep straight which indices transform according to L (covariantly) and which transform according to L^t (contravariantly). If you find all this irksome, the raising and lowering can be safely ignored. We define the position four-vector as before, but with no difference between raised and lowered indices. In fact, we can just represent all vectors and tensors with lowered indices exclusively, writing *e.g.* $x_\mu = (ct, x, y, z)$. The metric tensor is $g = \text{diag}(+, -, -, -)$ as before. The dot product of two four-vectors is

$$\mathbf{x} \cdot \mathbf{y} = g_{\mu\nu} x_\mu y_\nu. \quad (19.57)$$

The Lorentz transformation is

$$x_\mu = L_{\mu\nu} x'_\nu. \quad (19.58)$$

Since this preserves intervals, we must have

$$\begin{aligned} g_{\mu\nu} x_\mu y_\nu &= g_{\mu\nu} L_{\mu\alpha} x'_\alpha L_{\nu\beta} y'_\beta \\ &= (L_{\alpha\mu}^t g_{\mu\nu} L_{\nu\beta}) x'_\alpha y'_\beta, \end{aligned} \quad (19.59)$$

which entails

$$L_{\alpha\mu}^t g_{\mu\nu} L_{\nu\beta} = g_{\alpha\beta}. \quad (19.60)$$

In terms of the quantity L_ν^μ defined above, we have $L_{\mu\nu} = L_\nu^\mu$. In this convention, we could completely avoid raised indices, or we could simply make no distinction, taking $x^\mu = x_\mu$ and $L_{\mu\nu} = L^\mu_\nu = L^{\mu\nu}$, *etc.*

19.3.3 Comparing frames

Suppose in the K frame we have a measuring rod which is at rest. What is its length as measured in the K' frame? Recall K' moves with velocity $\mathbf{u} = u \hat{x}$ with respect to K . From the Lorentz transformation in eqn. 19.39, we have

$$\begin{aligned} x_1 &= \gamma(x'_1 + \beta c t'_1) \\ x_2 &= \gamma(x'_2 + \beta c t'_2), \end{aligned} \quad (19.61)$$

where $x_{1,2}$ are the positions of the ends of the rod in frame K . The rod's length in any frame is the instantaneous spatial separation of its ends. Thus, we set $t'_1 = t'_2$ and compute the separation $\Delta x' = x'_2 - x'_1$:

$$\Delta x = \gamma \Delta x' \quad \implies \quad \Delta x' = \gamma^{-1} \Delta x = (1 - \beta^2)^{1/2} \Delta x. \quad (19.62)$$

The *proper length* ℓ_0 of a rod is its instantaneous end-to-end separation in its rest frame. We see that

$$\ell(\beta) = (1 - \beta^2)^{1/2} \ell_0 , \quad (19.63)$$

so the length is always greatest in the rest frame. This is an example of a *Lorentz-Fitzgerald contraction*. Note that the *transverse* dimensions do not contract:

$$\Delta y' = \Delta y \quad , \quad \Delta z' = \Delta z . \quad (19.64)$$

Thus, the *volume contraction* of a bulk object is given by its length contraction: $\mathcal{V}' = \gamma^{-1} \mathcal{V}$.

A striking example of relativistic issues of length, time, and simultaneity is the famous ‘pole and the barn’ paradox, described in the Appendix (section 19.9). Here we illustrate some essential features via two examples.

19.3.4 Example I

Next, let’s analyze the situation depicted in fig. 19.3. In the K' frame, we’ll denote the following spacetime points:

$$A' = \begin{pmatrix} ct' \\ -d \end{pmatrix} \quad , \quad B' = \begin{pmatrix} ct' \\ +d \end{pmatrix} \quad , \quad S'_- = \begin{pmatrix} ct' \\ -ct' \end{pmatrix} \quad , \quad S'_+ = \begin{pmatrix} ct' \\ +ct' \end{pmatrix} . \quad (19.65)$$

Note that the origin in K' is given by $O' = (ct', 0)$. Here we are setting $y = y' = z = z' = 0$ and dealing only with one spatial dimension. The points S'_\pm denote the left-moving (S'_-) and right-moving (S'_+) wavefronts. We see that the arrival of the signal S'_1 at A' requires $S'_1 = A'$, hence $ct' = d$. The same result holds when we set $S'_2 = B'$ for the arrival of the right-moving wavefront at B' .

We now use the Lorentz transformation

$$L^\mu_\nu = \begin{pmatrix} \gamma & \gamma\beta \\ \gamma\beta & \gamma \end{pmatrix} \quad (19.66)$$

to transform to the K frame. Thus,

$$\begin{aligned} A &= \begin{pmatrix} ct_A^* \\ x_A^* \end{pmatrix} = LA' = \gamma \begin{pmatrix} 1 & \beta \\ \beta & 1 \end{pmatrix} \begin{pmatrix} d \\ -d \end{pmatrix} = \gamma(1 - \beta)d \begin{pmatrix} 1 \\ -1 \end{pmatrix} \\ B &= \begin{pmatrix} ct_B^* \\ x_B^* \end{pmatrix} = LB' = \gamma \begin{pmatrix} 1 & \beta \\ \beta & 1 \end{pmatrix} \begin{pmatrix} d \\ +d \end{pmatrix} = \gamma(1 + \beta)d \begin{pmatrix} 1 \\ 1 \end{pmatrix} . \end{aligned} \quad (19.67)$$

Thus, $t_A^* = \gamma(1 - \beta)d/c$ and $t_B^* = \gamma(1 + \beta)d/c$. Thus, the two events are *not* simultaneous in K . The arrival at A is first.

19.3.5 Example II

Consider a rod of length ℓ_0 extending from the origin to the point $\ell_0 \hat{x}$ at rest in frame K . In the frame K , the two ends of the rod are located at spacetime coordinates

$$A = \begin{pmatrix} ct \\ 0 \end{pmatrix} \quad \text{and} \quad B = \begin{pmatrix} ct \\ \ell_0 \end{pmatrix} , \quad (19.68)$$

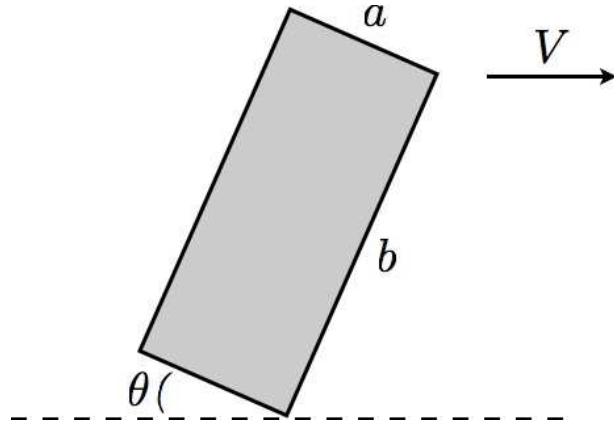


Figure 19.5: A rectangular plate moving at velocity $\mathbf{V} = V \hat{x}$.

respectively. Now consider the origin in frame K' . Its spacetime coordinates are

$$C' = \begin{pmatrix} ct' \\ 0 \end{pmatrix}. \quad (19.69)$$

To an observer in the K frame, we have

$$C = \begin{pmatrix} \gamma & \gamma\beta \\ \gamma\beta & \gamma \end{pmatrix} \begin{pmatrix} ct' \\ 0 \end{pmatrix} = \begin{pmatrix} \gamma ct' \\ \gamma\beta ct' \end{pmatrix}. \quad (19.70)$$

Now consider two events. The first event is the coincidence of A with C , *i.e.* the origin of K' instantaneously coincides with the origin of K . Setting $A = C$ we obtain $t = t' = 0$. The second event is the coincidence of B with C . Setting $B = C$ we obtain $t = l_0/\beta c$ and $t' = l_0/\gamma\beta c$. Note that $t = \ell(\beta)/\beta c$, *i.e.* due to the Lorentz-Fitzgerald contraction of the rod as seen in the K' frame, where $\ell(\beta) = l_0/\gamma$.

19.3.6 Deformation of a rectangular plate

Problem: A rectangular plate of dimensions $a \times b$ moves at relativistic velocity $\mathbf{V} = V \hat{x}$ as shown in fig. 19.5. In the rest frame of the rectangle, the a side makes an angle θ with respect to the \hat{x} axis. Describe in detail and sketch the shape of the plate as measured by an observer in the laboratory frame. Indicate the lengths of all sides and the values of all interior angles. Evaluate your expressions for the case $\theta = \frac{1}{4}\pi$ and $V = \sqrt{\frac{2}{3}}c$.

Solution: An observer in the laboratory frame will measure lengths parallel to \hat{x} to be Lorentz contracted by a factor γ^{-1} , where $\gamma = (1 - \beta^2)^{-1/2}$ and $\beta = V/c$. Lengths perpendicular to \hat{x} remain unaffected. Thus, we have the situation depicted in fig. 19.6. Simple trigonometry then says

$$\tan \phi = \gamma \tan \theta, \quad \tan \tilde{\phi} = \gamma^{-1} \tan \theta, \quad (19.71)$$

as well as

$$\begin{aligned} a' &= a \sqrt{\gamma^{-2} \cos^2 \theta + \sin^2 \theta} = a \sqrt{1 - \beta^2 \cos^2 \theta} \\ b' &= b \sqrt{\gamma^{-2} \sin^2 \theta + \cos^2 \theta} = b \sqrt{1 - \beta^2 \sin^2 \theta}. \end{aligned} \quad (19.72)$$

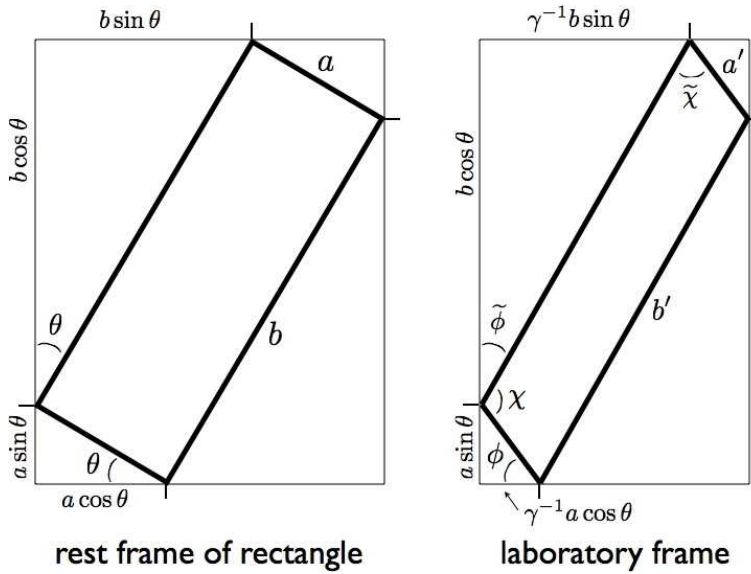


Figure 19.6: Relativistic deformation of the rectangular plate.

The plate deforms to a parallelogram, with internal angles

$$\begin{aligned}\chi &= \frac{1}{2}\pi + \tan^{-1}(\gamma \tan \theta) - \tan^{-1}(\gamma^{-1} \tan \theta) \\ \tilde{\chi} &= \frac{1}{2}\pi - \tan^{-1}(\gamma \tan \theta) + \tan^{-1}(\gamma^{-1} \tan \theta)\end{aligned}\quad (19.73)$$

Note that the area of the plate as measured in the laboratory frame is

$$\begin{aligned}\Omega' &= a' b' \sin \chi = a' b' \cos(\phi - \tilde{\phi}) \\ &= \gamma^{-1} \Omega,\end{aligned}\quad (19.74)$$

where $\Omega = ab$ is the proper area. The area contraction factor is γ^{-1} and not γ^{-2} (or γ^{-3} in a three-dimensional system) because only the parallel dimension gets contracted.

Setting $V = \sqrt{\frac{2}{3}}c$ gives $\gamma = \sqrt{3}$, and with $\theta = \frac{1}{4}\pi$ we have $\phi = \frac{1}{3}\pi$ and $\tilde{\phi} = \frac{1}{6}\pi$. The interior angles are then $\chi = \frac{2}{3}\pi$ and $\tilde{\chi} = \frac{1}{3}\pi$. The side lengths are $a' = \sqrt{\frac{2}{3}}a$ and $b' = \sqrt{\frac{2}{3}}b$.

19.3.7 Transformation of velocities

Let K' move at velocity $\mathbf{u} = c\beta$ relative to K . The transformation from K' to K is given by the Lorentz boost,

$$L^\mu_\nu = \begin{pmatrix} \gamma & \gamma \beta_x & \gamma \beta_y & \gamma \beta_z \\ \gamma \beta_x & 1 + (\gamma - 1) \hat{\beta}_x \hat{\beta}_x & (\gamma - 1) \hat{\beta}_x \hat{\beta}_y & (\gamma - 1) \hat{\beta}_x \hat{\beta}_z \\ \gamma \beta_y & (\gamma - 1) \hat{\beta}_x \hat{\beta}_y & 1 + (\gamma - 1) \hat{\beta}_y \hat{\beta}_y & (\gamma - 1) \hat{\beta}_y \hat{\beta}_z \\ \gamma \beta_z & (\gamma - 1) \hat{\beta}_x \hat{\beta}_z & (\gamma - 1) \hat{\beta}_y \hat{\beta}_z & 1 + (\gamma - 1) \hat{\beta}_z \hat{\beta}_z \end{pmatrix}. \quad (19.75)$$

Applying this, we have

$$dx^\mu = L^\mu_\nu dx'^\nu. \quad (19.76)$$

This yields

$$\begin{aligned} dx^0 &= \gamma dx'^0 + \gamma \beta \cdot d\mathbf{x}' \\ d\mathbf{x} &= \gamma \beta dx'^0 + d\mathbf{x}' + (\gamma - 1) \hat{\beta} \hat{\beta} \cdot d\mathbf{x}' . \end{aligned} \quad (19.77)$$

We then have

$$\begin{aligned} \mathbf{V} = c \frac{d\mathbf{x}}{dx^0} &= \frac{c \gamma \beta dx'^0 + c d\mathbf{x}' + c(\gamma - 1) \hat{\beta} \hat{\beta} \cdot d\mathbf{x}'}{\gamma dx'^0 + \gamma \beta \cdot d\mathbf{x}'} \\ &= \frac{\mathbf{u} + \gamma^{-1} \mathbf{V}' + (1 - \gamma^{-1}) \hat{\mathbf{u}} \hat{\mathbf{u}} \cdot \mathbf{V}'}{1 + \mathbf{u} \cdot \mathbf{V}' / c^2} . \end{aligned} \quad (19.78)$$

The second line is obtained by dividing both numerator and denominator by dx'^0 , and then writing $\mathbf{V}' = d\mathbf{x}' / dx'^0$. There are two special limiting cases:

$$\begin{aligned} \text{velocities parallel } (\hat{\mathbf{u}} \cdot \hat{\mathbf{V}}' = 1) &\implies \mathbf{V} = \frac{(u + V') \hat{\mathbf{u}}}{1 + u V' / c^2} \\ \text{velocities perpendicular } (\hat{\mathbf{u}} \cdot \hat{\mathbf{V}}' = 0) &\implies \mathbf{V} = \mathbf{u} + \gamma^{-1} \mathbf{V}' . \end{aligned} \quad (19.79)$$

Note that if either u or V' is equal to c , the resultant expression has $|\mathbf{V}| = c$ as well. One can't boost the speed of light!

Let's revisit briefly the example in section 19.3.4. For an observer, in the K frame, the relative velocity of S and A is $c + u$, because even though we must boost the velocity $-c \hat{\mathbf{x}}$ of the left-moving light wave by $u \hat{\mathbf{x}}$, the result is still $-c \hat{\mathbf{x}}$, according to our velocity addition formula. The distance between the emission and detection points is $d(\beta) = d/\gamma$. Thus,

$$t_A^* = \frac{d(\beta)}{c + u} = \frac{d}{\gamma} \cdot \frac{1}{c + u} = \frac{d}{\gamma c} \cdot \frac{1 - \beta}{1 - \beta^2} = \gamma(1 - \beta) \frac{d}{c} . \quad (19.80)$$

This result is exactly as found in section 19.3.4 by other means. A corresponding analysis yields $t_B^* = \gamma(1 + \beta) d/c$, again in agreement with the earlier result. Here, it is crucial to account for the Lorentz contraction of the distance between the source S and the observers A and B as measured in the K frame.

19.3.8 Four-velocity and four-acceleration

In nonrelativistic mechanics, the velocity $\mathbf{V} = \frac{d\mathbf{x}}{dt}$ is locally tangent to a particle's trajectory. In relativistic mechanics, one defines the *four-velocity*,

$$u^\alpha \equiv \frac{dx^\alpha}{ds} = \frac{dx^\alpha}{\sqrt{1 - \beta^2} c dt} = \begin{pmatrix} \gamma \\ \gamma \beta \end{pmatrix} , \quad (19.81)$$

which is locally tangent to the world line of a particle. Note that

$$g_{\alpha\beta} u^\alpha u^\beta = 1 . \quad (19.82)$$

The four-acceleration is defined as

$$w^\nu \equiv \frac{du^\nu}{ds} = \frac{d^2x^\nu}{ds^2} . \quad (19.83)$$

Note that $u \cdot w = 0$, so the 4-velocity and 4-acceleration are orthogonal with respect to the Minkowski metric.

19.4 Three Kinds of Relativistic Rockets

19.4.1 Constant acceleration model

Consider a rocket which undergoes constant acceleration along \hat{x} . Clearly the rocket has no rest frame *per se*, because its velocity is changing. However, this poses no serious obstacle to discussing its relativistic motion. We consider a frame K' in which the rocket is *instantaneously* at rest. In such a frame, the rocket's 4-acceleration is $w'^\alpha = (0, a/c^2)$, where we suppress the transverse coordinates y and z . In an inertial frame K , we have

$$w^\alpha = \frac{d}{ds} \begin{pmatrix} \gamma \\ \gamma\beta \\ \gamma \end{pmatrix} = \frac{\gamma}{c} \begin{pmatrix} \dot{\gamma} \\ \gamma\dot{\beta} + \dot{\gamma}\beta \\ \gamma \end{pmatrix} . \quad (19.84)$$

Transforming w'^α into the K frame, we have

$$w^\alpha = \begin{pmatrix} \gamma & \gamma\beta \\ \gamma\beta & \gamma \end{pmatrix} \begin{pmatrix} 0 \\ a/c^2 \end{pmatrix} = \begin{pmatrix} \gamma\beta a/c^2 \\ \gamma a/c^2 \end{pmatrix} . \quad (19.85)$$

Taking the upper component, we obtain the equation

$$\dot{\gamma} = \frac{\beta a}{c} \quad \Rightarrow \quad \frac{d}{dt} \left(\frac{\beta}{\sqrt{1 - \beta^2}} \right) = \frac{a}{c} , \quad (19.86)$$

the solution of which, with $\beta(0) = 0$, is

$$\beta(t) = \frac{at}{\sqrt{c^2 + a^2 t^2}} , \quad \gamma(t) = \sqrt{1 + \left(\frac{at}{c} \right)^2} . \quad (19.87)$$

The proper time for an observer moving with the rocket is thus

$$\tau = \int_0^t \frac{c dt_1}{\sqrt{c^2 + a^2 t_1^2}} = \frac{c}{a} \sinh^{-1} \left(\frac{at}{c} \right) . \quad (19.88)$$

For large times $t \gg c/a$, the proper time grows logarithmically in t , which is parametrically slower. To find the position of the rocket, we integrate $\dot{x} = c\beta$, and obtain, with $x(0) = 0$,

$$x(t) = \int_0^t \frac{a ct_1 dt_1}{\sqrt{c^2 + a^2 t_1^2}} = \frac{c}{a} \left(\sqrt{c^2 + a^2 t^2} - c \right) . \quad (19.89)$$

It is interesting to consider the situation in the frame K' . We then have

$$\beta(\tau) = \tanh(a\tau/c) , \quad \gamma(\tau) = \cosh(a\tau/c) . \quad (19.90)$$

For an observer in the frame K' , the distance he has traveled is $\Delta x'(\tau) = \Delta x(\tau)/\gamma(\tau)$, as we found in eqn. 19.62. Now $x(\tau) = (c^2/a)(\cosh(a\tau/c) - 1)$, hence

$$\Delta x'(\tau) = \frac{c^2}{a} \left(1 - \operatorname{sech}(a\tau/c) \right) . \quad (19.91)$$

For $\tau \ll c/a$, we expand $\operatorname{sech}(a\tau/c) \approx 1 - \frac{1}{2}(a\tau/c)^2$ and find $x'(\tau) = \frac{1}{2}a\tau^2$, which clearly is the nonrelativistic limit. For $\tau \rightarrow \infty$, however, we have $\Delta x'(\tau) \rightarrow c^2/a$ is finite! Thus, while the entire Universe is falling behind the accelerating observer, it all piles up at a *horizon* a distance c^2/a behind it, in the frame of the observer. The light from these receding objects is increasingly red-shifted (see section 19.6 below), until it is no longer visible. Thus, as John Baez describes it, the horizon is “a dark plane that appears to be swallowing the entire Universe!” In the frame of the inertial observer, however, nothing strange appears to be happening at all!

19.4.2 Constant force with decreasing mass

Suppose instead the rocket is subjected to a constant force F_0 in its instantaneous rest frame, and furthermore that the rocket’s mass satisfies $m(\tau) = m_0(1 - \alpha\tau)$, where τ is the proper time for an observer moving with the rocket. Then from eqn. 19.86, we have

$$\begin{aligned} \frac{F_0}{m_0(1 - \alpha\tau)} &= \frac{d(\gamma\beta)}{dt} = \gamma^{-1} \frac{d(\gamma\beta)}{d\tau} \\ &= \frac{1}{1 - \beta^2} \frac{d\beta}{d\tau} = \frac{d}{d\tau} \frac{1}{2} \ln \left(\frac{1 + \beta}{1 - \beta} \right) , \end{aligned} \quad (19.92)$$

after using the chain rule, and with $d\tau/dt = \gamma^{-1}$. Integrating, we find

$$\ln \left(\frac{1 + \beta}{1 - \beta} \right) = \frac{2F_0}{\alpha m_0 c} \ln(1 - \alpha\tau) \implies \beta(\tau) = \frac{1 - (1 - \alpha\tau)^r}{1 + (1 - \alpha\tau)^r} , \quad (19.93)$$

with $r = 2F_0/\alpha m_0 c$. As $\tau \rightarrow \alpha^{-1}$, the rocket loses all its mass, and it asymptotically approaches the speed of light.

It is convenient to write

$$\beta(\tau) = \tanh \left[\frac{r}{2} \ln \left(\frac{1}{1 - \alpha\tau} \right) \right] , \quad (19.94)$$

in which case

$$\begin{aligned} \gamma &= \frac{dt}{d\tau} = \cosh \left[\frac{r}{2} \ln \left(\frac{1}{1 - \alpha\tau} \right) \right] \\ \frac{1}{c} \frac{dx}{d\tau} &= \sinh \left[\frac{r}{2} \ln \left(\frac{1}{1 - \alpha\tau} \right) \right] . \end{aligned} \quad (19.95)$$

Integrating the first of these from $\tau = 0$ to $\tau = \alpha^{-1}$, we find $t^* \equiv t(\tau = \alpha^{-1})$ is

$$t^* = \frac{1}{2\alpha} \int_0^1 d\sigma \left(\sigma^{-r/2} + \sigma^{r/2} \right) = \begin{cases} \left[\alpha^2 - \left(\frac{F_0}{mc} \right)^2 \right]^{-1} \alpha & \text{if } \alpha > \frac{F_0}{mc} \\ \infty & \text{if } \alpha \leq \frac{F_0}{mc} . \end{cases} \quad (19.96)$$

Since $\beta(\tau = \alpha^{-1}) = 1$, this is the time in the K frame when the rocket reaches the speed of light.

19.4.3 Constant *ejecta* velocity

Our third relativistic rocket model is a generalization of what is commonly known as the *rocket equation* in classical physics. The model is one of a rocket which is continually ejecting burnt fuel at a velocity $-u$ in the instantaneous rest frame of the rocket. The nonrelativistic rocket equation follows from overall momentum conservation:

$$dp_{\text{rocket}} + dp_{\text{fuel}} = d(mv) + (v - u)(-dm) = 0 , \quad (19.97)$$

since if $dm < 0$ is the differential change in rocket mass, the differential *ejecta* mass is $-dm$. This immediately gives

$$m dv + u dm = 0 \implies v = u \ln \left(\frac{m_0}{m} \right) , \quad (19.98)$$

where the rocket is assumed to begin at rest, and where m_0 is the initial mass of the rocket. Note that as $m \rightarrow 0$ the rocket's speed increases without bound, which of course violates special relativity.

In relativistic mechanics, as we shall see in section 19.5, the rocket's momentum, as described by an inertial observer, is $p = \gamma mv$, and its energy is γmc^2 . We now write two equations for overall conservation of momentum and energy:

$$\begin{aligned} d(\gamma mv) + \gamma_e v_e dm_e &= 0 \\ d(\gamma mc^2) + \gamma_e (dm_e c^2) &= 0 , \end{aligned} \quad (19.99)$$

where v_e is the velocity of the *ejecta* in the inertial frame, dm_e is the differential mass of the *ejecta*, and $\gamma_e = (1 - \frac{v_e^2}{c^2})^{-1/2}$. From the second of these equations, we have

$$\gamma_e dm_e = -d(\gamma m) , \quad (19.100)$$

which we can plug into the first equation to obtain

$$(v - v_e) d(\gamma m) + \gamma m dv = 0 . \quad (19.101)$$

Before solving this, we remark that eqn. 19.100 implies that $dm_e < |dm|$ – the differential mass of the *ejecta* is less than the mass lost by the rocket! This is Einstein's famous equation $E = mc^2$ at work – more on this later.

To proceed, we need to use the parallel velocity addition formula of eqn. 19.79 to find v_e :

$$v_e = \frac{v - u}{1 - \frac{uv}{c^2}} \implies v - v_e = \frac{u(1 - \frac{v^2}{c^2})}{(1 - \frac{uv}{c^2})} . \quad (19.102)$$

We now define $\beta_u = u/c$, in which case eqn, 19.101 becomes

$$\beta_u (1 - \beta^2) d(\gamma m) + (1 - \beta \beta_u) \gamma m d\beta = 0 . \quad (19.103)$$

Using $d\gamma = \gamma^3 \beta d\beta$, we observe a felicitous cancellation of terms, leaving

$$\beta_u \frac{dm}{m} + \frac{d\beta}{1 - \beta^2} = 0 . \quad (19.104)$$

Integrating, we obtain

$$\beta = \tanh \left(\beta_u \ln \frac{m_0}{m} \right) . \quad (19.105)$$

Note that this agrees with the result of eqn. 19.94, if we take $\beta_u = F_0/\alpha mc$.

19.5 Relativistic Mechanics

Relativistic particle dynamics follows from an appropriately extended version of Hamilton's principle $\delta S = 0$. The action S must be a Lorentz scalar. The action for a free particle is

$$S[\mathbf{x}(t)] = -mc \int_a^b ds = -mc^2 \int_{t_a}^{t_b} dt \sqrt{1 - \frac{\mathbf{v}^2}{c^2}} . \quad (19.106)$$

Thus, the free particle Lagrangian is

$$L = -mc^2 \sqrt{1 - \frac{\mathbf{v}^2}{c^2}} = -mc^2 + \frac{1}{2} m \mathbf{v}^2 + \frac{1}{8} m c^2 \left(\frac{\mathbf{v}^2}{c^2} \right)^2 + \dots . \quad (19.107)$$

Thus, L can be written as an expansion in powers of \mathbf{v}^2/c^2 . Note that $L(\mathbf{v} = 0) = -mc^2$. We interpret this as $-U_0$, where $U_0 = mc^2$ is the *rest energy* of the particle. As a constant, it has no consequence for the equations of motion. The next term in L is the familiar nonrelativistic kinetic energy, $\frac{1}{2} m \mathbf{v}^2$. Higher order terms are smaller by increasing factors of $\beta^2 = v^2/c^2$.

We can add a potential $U(\mathbf{x}, t)$ to obtain

$$L(\mathbf{x}, \dot{\mathbf{x}}, t) = -mc^2 \sqrt{1 - \frac{\dot{\mathbf{x}}^2}{c^2}} - U(\mathbf{x}, t) . \quad (19.108)$$

The momentum of the particle is

$$\mathbf{p} = \frac{\partial L}{\partial \dot{\mathbf{x}}} = \gamma m \dot{\mathbf{x}} . \quad (19.109)$$

The force is $\mathbf{F} = -\nabla U$ as usual, and Newton's Second Law still reads $\dot{\mathbf{p}} = \mathbf{F}$. Note that

$$\dot{\mathbf{p}} = \gamma m \left(\dot{\mathbf{v}} + \frac{v\dot{v}}{c^2} \gamma^2 \mathbf{v} \right). \quad (19.110)$$

Thus, the force \mathbf{F} is not necessarily in the direction of the acceleration $\mathbf{a} = \dot{\mathbf{v}}$. The Hamiltonian, recall, is a function of coordinates and momenta, and is given by

$$H = \mathbf{p} \cdot \dot{\mathbf{x}} - L = \sqrt{m^2 c^4 + \mathbf{p}^2 c^2} + U(\mathbf{x}, t). \quad (19.111)$$

Since $\partial L/\partial t = 0$ for our case, H is conserved by the motion of the particle. There are two limits of note:

$$\begin{aligned} |\mathbf{p}| \ll mc & \text{ (non-relativistic)} & : & H = mc^2 + \frac{\mathbf{p}^2}{2m} + U + \mathcal{O}(p^4/m^4 c^4) \\ |\mathbf{p}| \gg mc & \text{ (ultra-relativistic)} & : & H = c|\mathbf{p}| + U + \mathcal{O}(mc/p). \end{aligned} \quad (19.112)$$

Expressed in terms of the coordinates and velocities, we have $H = E$, the total energy, with

$$E = \gamma mc^2 + U. \quad (19.113)$$

In particle physics applications, one often defines the kinetic energy T as

$$T = E - U - mc^2 = (\gamma - 1)mc^2. \quad (19.114)$$

When electromagnetic fields are included,

$$\begin{aligned} L(\mathbf{x}, \dot{\mathbf{x}}, t) &= -mc^2 \sqrt{1 - \frac{\dot{\mathbf{x}}^2}{c^2}} - q\phi + \frac{q}{c} \mathbf{A} \cdot \dot{\mathbf{x}} \\ &= -\gamma mc^2 - \frac{q}{c} A_\mu \frac{dx^\mu}{dt}, \end{aligned} \quad (19.115)$$

where the electromagnetic 4-potential is $A^\mu = (\phi, \mathbf{A})$. Recall $A_\mu = g_{\mu\nu} A^\nu$ has the sign of its spatial components reversed. One then has

$$\mathbf{p} = \frac{\partial L}{\partial \dot{\mathbf{x}}} = \gamma m \dot{\mathbf{x}} + \frac{q}{c} \mathbf{A}, \quad (19.116)$$

and the Hamiltonian is

$$H = \sqrt{m^2 c^4 + \left(\mathbf{p} - \frac{q}{c} \mathbf{A} \right)^2} + q\phi. \quad (19.117)$$

19.5.1 Relativistic harmonic oscillator

From $E = \gamma mc^2 + U$, we have

$$\dot{x}^2 = c^2 \left[1 - \left(\frac{mc^2}{E - U(x)} \right)^2 \right]. \quad (19.118)$$

Consider the one-dimensional harmonic oscillator potential $U(x) = \frac{1}{2}kx^2$. We define the turning points as $x = \pm b$, satisfying

$$E - mc^2 = U(\pm b) = \frac{1}{2}kb^2. \quad (19.119)$$

Now define the angle θ via $x \equiv b \cos \theta$, and further define the dimensionless parameter $\epsilon = kb^2/4mc^2$. Then, after some manipulations, one obtains

$$\dot{\theta} = \omega_0 \frac{\sqrt{1 + \epsilon \sin^2 \theta}}{1 + 2\epsilon \sin^2 \theta}, \quad (19.120)$$

with $\omega_0 = \sqrt{k/m}$ as in the nonrelativistic case. Hence, the problem is reduced to quadratures (a quaint way of saying ‘doing an integral’):

$$t(\theta) - t_0 = \omega_0^{-1} \int_{\theta_0}^{\theta} d\vartheta \frac{1 + 2\epsilon \sin^2 \vartheta}{\sqrt{1 + \epsilon \sin^2 \vartheta}}. \quad (19.121)$$

While the result can be expressed in terms of elliptic integrals, such an expression is not particularly illuminating. Here we will content ourselves with computing the period $T(\epsilon)$:

$$\begin{aligned} T(\epsilon) &= \frac{4}{\omega_0} \int_0^{\frac{\pi}{2}} d\vartheta \frac{1 + 2\epsilon \sin^2 \vartheta}{\sqrt{1 + \epsilon \sin^2 \vartheta}} \\ &= \frac{4}{\omega_0} \int_0^{\frac{\pi}{2}} d\vartheta \left(1 + \frac{3}{2}\epsilon \sin^2 \vartheta - \frac{5}{8}\epsilon^2 \sin^4 \vartheta + \dots \right) \\ &= \frac{2\pi}{\omega_0} \cdot \left\{ 1 + \frac{3}{4}\epsilon - \frac{15}{64}\epsilon^2 + \dots \right\}. \end{aligned} \quad (19.122)$$

Thus, for the relativistic harmonic oscillator, the period does depend on the amplitude, unlike the non-relativistic case.

19.5.2 Energy-momentum 4-vector

Let’s focus on the case where $U(\mathbf{x}) = 0$. This is in fact a realistic assumption for subatomic particles, which propagate freely between collision events.

The differential proper time for a particle is given by

$$d\tau = \frac{ds}{c} = \gamma^{-1} dt, \quad (19.123)$$

where $x^\mu = (ct, \mathbf{x})$ are coordinates for the particle in an inertial frame. Thus,

$$\mathbf{p} = \gamma m \dot{\mathbf{x}} = m \frac{d\mathbf{x}}{d\tau}, \quad \frac{E}{c} = mc\gamma = m \frac{dx^0}{d\tau}, \quad (19.124)$$

with $x^0 = ct$. Thus, we can write the *energy-momentum 4-vector* as

$$p^\mu = m \frac{dx^\mu}{d\tau} = \begin{pmatrix} E/c \\ p^x \\ p^y \\ p^z \end{pmatrix}. \quad (19.125)$$

Note that $p^\nu = mcu^\nu$, where u^ν is the 4-velocity of eqn. 19.81. The four-momentum satisfies the relation

$$p^\mu p_\mu = \frac{E^2}{c^2} - \mathbf{p}^2 = m^2 c^2 . \quad (19.126)$$

The relativistic generalization of force is

$$f^\mu = \frac{dp^\mu}{d\tau} = (\gamma \mathbf{F} \cdot \mathbf{v}/c, \gamma \mathbf{F}) , \quad (19.127)$$

where $\mathbf{F} = d\mathbf{p}/dt$ as usual.

The energy-momentum four-vector transforms covariantly under a Lorentz transformation. This means

$$p^\mu = L_\nu^\mu p'^\nu . \quad (19.128)$$

If frame K' moves with velocity $\mathbf{u} = c\beta \hat{\mathbf{x}}$ relative to frame K , then

$$\frac{E}{c} = \frac{c^{-1}E' + \beta p'^x}{\sqrt{1 - \beta^2}} , \quad p^x = \frac{p'^x + \beta c^{-1}E'}{\sqrt{1 - \beta^2}} , \quad p^y = p'^y , \quad p^z = p'^z . \quad (19.129)$$

In general, from eqns. 19.47, we have

$$\begin{aligned} \frac{E}{c} &= \gamma \frac{E'}{c} + \gamma \beta p'_\parallel \\ p_\parallel &= \gamma \beta \frac{E}{c} + \gamma p'_\parallel \\ \mathbf{p}_\perp &= \mathbf{p}'_\perp \end{aligned} \quad (19.130)$$

where $p_\parallel = \hat{\beta} \cdot \mathbf{p}$ and $\mathbf{p}_\perp = \mathbf{p} - (\hat{\beta} \cdot \mathbf{p}) \hat{\beta}$.

19.5.3 4-momentum for massless particles

For a massless particle, such as a photon, we have $p^\mu p_\mu = 0$, which means $E^2 = \mathbf{p}^2 c^2$. The 4-momentum may then be written $p^\mu = (|p|, \mathbf{p})$. We define the 4-wavevector k^μ by the relation $p^\mu = \hbar k^\mu$, where $\hbar = h/2\pi$ and h is Planck's constant. We also write $\omega = ck$, with $E = \hbar\omega$.

19.6 Relativistic Doppler Effect

The 4-wavevector $k^\mu = (\omega/c, \mathbf{k})$ for electromagnetic radiation satisfies $k^\mu k_\mu = 0$. The energy-momentum 4-vector is $p^\mu = \hbar k^\mu$. The phase $\phi(x^\mu) = -k_\mu x^\mu = \mathbf{k} \cdot \mathbf{x} - \omega t$ of a plane wave is a Lorentz scalar. This means that the total number of wave crests (*i.e.* $\phi = 2\pi n$) emitted by a source will be the total number observed by a detector.

Suppose a moving source emits radiation of angular frequency ω' in its rest frame. Then

$$\begin{aligned} k'^\mu &= L_\nu^\mu(-\beta) k^\nu \\ &= \begin{pmatrix} \gamma & -\gamma\beta_x & -\gamma\beta_y & -\gamma\beta_z \\ -\gamma\beta_x & 1 + (\gamma - 1)\hat{\beta}_x\hat{\beta}_x & (\gamma - 1)\hat{\beta}_x\hat{\beta}_y & (\gamma - 1)\hat{\beta}_x\hat{\beta}_z \\ -\gamma\beta_y & (\gamma - 1)\hat{\beta}_x\hat{\beta}_y & 1 + (\gamma - 1)\hat{\beta}_y\hat{\beta}_y & (\gamma - 1)\hat{\beta}_y\hat{\beta}_z \\ -\gamma\beta_z & (\gamma - 1)\hat{\beta}_x\hat{\beta}_z & (\gamma - 1)\hat{\beta}_y\hat{\beta}_z & 1 + (\gamma - 1)\hat{\beta}_z\hat{\beta}_z \end{pmatrix} \begin{pmatrix} \omega/c \\ k^x \\ k^y \\ k^z \end{pmatrix}. \end{aligned} \quad (19.131)$$

This gives

$$\frac{\omega'}{c} = \gamma \frac{\omega}{c} - \gamma \beta \cdot \mathbf{k} = \gamma \frac{\omega}{c} (1 - \beta \cos \theta), \quad (19.132)$$

where $\theta = \cos^{-1}(\hat{\beta} \cdot \hat{\mathbf{k}})$ is the angle measured in K between $\hat{\beta}$ and $\hat{\mathbf{k}}$. Solving for ω , we have

$$\omega = \frac{\sqrt{1 - \beta^2}}{1 - \beta \cos \theta} \omega_0, \quad (19.133)$$

where $\omega_0 = \omega'$ is the angular frequency in the rest frame of the moving source. Thus,

$$\begin{aligned} \theta = 0 &\Rightarrow \text{source approaching} \Rightarrow \omega = \sqrt{\frac{1 + \beta}{1 - \beta}} \omega_0 \\ \theta = \frac{1}{2}\pi &\Rightarrow \text{source perpendicular} \Rightarrow \omega = \sqrt{1 - \beta^2} \omega_0 \\ \theta = \pi &\Rightarrow \text{source receding} \Rightarrow \omega = \sqrt{\frac{1 - \beta}{1 + \beta}} \omega_0. \end{aligned} \quad (19.134)$$

Recall the non-relativistic Doppler effect:

$$\omega = \frac{\omega_0}{1 - (V/c) \cos \theta}. \quad (19.135)$$

We see that approaching sources have their frequencies shifted higher; this is called the *blue shift*, since blue light is on the high frequency (short wavelength) end of the optical spectrum. By the same token, receding sources are *red-shifted* to lower frequencies.

19.6.1 Romantic example

Alice and Bob have a “May-December” thang going on. Bob is May and Alice December, if you get my drift. The social stigma is too much to bear! To rectify this, they decide that Alice should take a ride in a space ship. Alice’s itinerary takes her along a sector of a circle of radius R and angular span of $\Theta = 1$ radian, as depicted in fig. 19.7. Define $O \equiv (r = 0)$, $P \equiv (r = R, \phi = -\frac{1}{2}\Theta)$, and $Q \equiv (r = R, \phi = \frac{1}{2}\Theta)$. Alice’s speed along the first leg (straight from O to P) is $v_a = \frac{3}{5}c$. Her speed along the second leg (an arc from P to Q) is $v_b = \frac{12}{13}c$. The final leg (straight from Q to O) she travels at speed $v_c = \frac{4}{5}c$. Remember that the length of an circular arc of radius R and angular spread α (radians) is $\ell = \alpha R$.

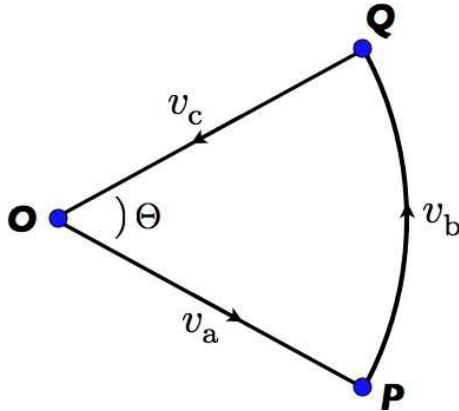


Figure 19.7: Alice's big adventure.

- (a) Alice and Bob synchronize watches at the moment of Alice's departure. What is the elapsed time on Bob's watch when Alice returns? What is the elapsed time on Alice's watch? What must R be in order for them to erase their initial 30 year age difference?

Solution : In Bob's frame, Alice's trip takes a time

$$\begin{aligned}\Delta t &= \frac{R}{c\beta_a} + \frac{R\Theta}{c\beta_b} + \frac{R}{c\beta_c} \\ &= \frac{R}{c} \left(\frac{5}{3} + \frac{13}{12} + \frac{5}{4} \right) = \frac{4R}{c}.\end{aligned}\tag{19.136}$$

The elapsed time on Alice's watch is

$$\begin{aligned}\Delta t' &= \frac{R}{c\gamma_a\beta_a} + \frac{R\Theta}{c\gamma_b\beta_b} + \frac{R}{c\gamma_c\beta_c} \\ &= \frac{R}{c} \left(\frac{5}{3} \cdot \frac{4}{5} + \frac{13}{12} \cdot \frac{5}{13} + \frac{5}{4} \cdot \frac{3}{5} \right) = \frac{5R}{2c}.\end{aligned}\tag{19.137}$$

Thus, $\Delta T = \Delta t - \Delta t' = 3R/2c$ and setting $\Delta T = 30$ yr, we find $R = 20$ ly. So Bob will have aged 80 years and Alice 50 years upon her return. (Maybe this isn't such a good plan after all.)

- (b) As a signal of her undying love for Bob, Alice continually shines a beacon throughout her trip. The beacon produces monochromatic light at wavelength $\lambda_0 = 6000$ Å (frequency $f_0 = c/\lambda_0 = 5 \times 10^{14}$ Hz). Every night, Bob peers into the sky (with a radiotelescope), hopefully looking for Alice's signal. What frequencies f_a , f_b , and f_c does Bob see?

Solution : Using the relativistic Doppler formula, we have

$$\begin{aligned}f_a &= \sqrt{\frac{1 - \beta_a}{1 + \beta_a}} \times f_0 = \frac{1}{2}f_0 \\ f_b &= \sqrt{1 - \beta_b^2} \times f_0 = \frac{5}{13}f_0 \\ f_c &= \sqrt{\frac{1 + \beta_c}{1 - \beta_c}} \times f_0 = 3f_0.\end{aligned}\tag{19.138}$$

(c) Show that the total number of wave crests counted by Bob is the same as the number emitted by Alice, over the entire trip.

Solution : Consider first the O–P leg of Alice’s trip. The proper time elapsed on Alice’s watch during this leg is $\Delta t'_a = R/c\gamma_a\beta_a$, hence she emits $N'_a = Rf_0/c\gamma_a\beta_a$ wavefronts during this leg. Similar considerations hold for the P–Q and Q–O legs, so $N'_b = R\Theta f_0/c\gamma_b\beta_b$ and $N'_c = Rf_0/c\gamma_c\beta_c$.

Although the duration of the O–P segment of Alice’s trip takes a time $\Delta t_a = R/c\beta_a$ in Bob’s frame, he keeps receiving the signal at the Doppler-shifted frequency f_a until the wavefront emitted when Alice arrives at P makes its way back to Bob. That takes an extra time R/c , hence the number of crests emitted for Alice’s O–P leg is

$$N_a = \left(\frac{R}{c\beta_a} + \frac{R}{c} \right) \sqrt{\frac{1 - \beta_a}{1 + \beta_a}} \times f_0 = \frac{Rf_0}{c\gamma_a\beta_a} = N'_a , \quad (19.139)$$

since the source is receding from the observer.

During the P–Q leg, we have $\theta = \frac{1}{2}\pi$, and Alice’s velocity is orthogonal to the wavevector \mathbf{k} , which is directed radially inward. Bob’s first signal at frequency f_b arrives a time R/c after Alice passes P, and his last signal at this frequency arrives a time R/c after Alice passes Q. Thus, the total time during which Bob receives the signal at the Doppler-shifted frequency f_b is $\Delta t_b = R\Theta/c$, and

$$N_b = \frac{R\Theta}{c\beta_b} \cdot \sqrt{1 - \beta_b^2} \times f_0 = \frac{R\Theta f_0}{c\gamma_b\beta_b} = N'_b . \quad (19.140)$$

Finally, during the Q–O home stretch, Bob first starts to receive the signal at the Doppler-shifted frequency f_c a time R/c after Alice passes Q, and he continues to receive the signal until the moment Alice rushes into his open and very flabby old arms when she makes it back to O. Thus, Bob receives the frequency f_c signal for a duration $\Delta t_c - R/c$, where $\Delta t_c = R/c\beta_c$. Thus,

$$N_c = \left(\frac{R}{c\beta_c} - \frac{R}{c} \right) \sqrt{\frac{1 + \beta_c}{1 - \beta_c}} \times f_0 = \frac{Rf_0}{c\gamma_c\beta_c} = N'_c , \quad (19.141)$$

since the source is approaching.

Therefore, the number of wavelengths emitted by Alice will be precisely equal to the number received by Bob – none of the waves gets lost.

19.7 Relativistic Kinematics of Particle Collisions

As should be expected, special relativity is essential toward the understanding of subatomic particle collisions, where the particles themselves are moving at close to the speed of light. In our analysis of the kinematics of collisions, we shall find it convenient to adopt the standard convention on units, where we set $c \equiv 1$. Energies will typically be given in GeV, where $1 \text{ GeV} = 10^9 \text{ eV} = 1.602 \times 10^{-10} \text{ J}$. Momenta will then be in units of GeV/c , and masses in units of GeV/c^2 . With $c \equiv 1$, it is then customary to

quote masses in energy units. For example, the mass of the proton in these units is $m_p = 938 \text{ MeV}$, and $m_{\pi^-} = 140 \text{ MeV}$.

For a particle of mass M , its 4-momentum satisfies $P_\mu P^\mu = M^2$ (remember $c = 1$). Consider now an observer with 4-velocity U^μ . The energy of the particle, in the rest frame of the observer is $E = P^\mu U_\mu$. For example, if $P^\mu = (M, 0, 0, 0)$ is its rest frame, and $U^\mu = (\gamma, \gamma\beta)$, then $E = \gamma M$, as we have already seen.

Consider next the emission of a photon of 4-momentum $P^\mu = (\hbar\omega/c, \hbar\mathbf{k})$ from an object with 4-velocity V^μ , and detected in a frame with 4-velocity U^μ . In the frame of the detector, the photon energy is $E = P^\mu U_\mu$, while in the frame of the emitter its energy is $E' = P^\mu V_\mu$. If $U^\mu = (1, 0, 0, 0)$ and $V^\mu = (\gamma, \gamma\beta)$, then $E = \hbar\omega$ and $E' = \hbar\omega' = \gamma\hbar(\omega - \beta \cdot \mathbf{k}) = \gamma\hbar\omega(1 - \beta \cos\theta)$, where $\theta = \cos^{-1}(\hat{\beta} \cdot \hat{\mathbf{k}})$. Thus, $\omega = \gamma^{-1}\omega'/(1 - \beta \cos\theta)$. This recapitulates our earlier derivation in eqn. 19.132.

Consider next the interaction of several particles. If in a given frame the 4-momenta of the reactants are P_i^μ , where n labels the reactant ‘species’, and the 4-momenta of the products are Q_j^μ , then if the collision is elastic, we have that total 4-momentum is conserved, *i.e.*

$$\sum_{i=1}^N P_i^\mu = \sum_{j=1}^{\bar{N}} Q_j^\mu , \quad (19.142)$$

where there are N reactants and \bar{N} products. For massive particles, we can write

$$P_i^\mu = \gamma_i m_i (1, \mathbf{v}_i) , \quad Q_j^\mu = \bar{\gamma}_j \bar{m}_j (1, \bar{\mathbf{v}}_j) , \quad (19.143)$$

while for massless particles,

$$P_i^\mu = \hbar k_i (1, \hat{\mathbf{k}}) , \quad Q_j^\mu = \hbar \bar{k}_j (1, \hat{\bar{\mathbf{k}}}) . \quad (19.144)$$

19.7.1 Spontaneous particle decay into two products

Consider first the decay of a particle of mass M into two particles. We have $P^\mu = Q_1^\mu + Q_2^\mu$, hence in the rest frame of the (sole) reactant, which is also called the ‘center of mass’ (CM) frame since the total 3-momentum vanishes therein, we have $M = E_1 + E_2$. Since $E_i^{\text{CM}} = \gamma^{\text{CM}} m_i$, and $\gamma_i \geq 1$, clearly we must have $M > m_1 + m_2$, or else the decay cannot possibly conserve energy. To analyze further, write $P^\mu - Q_1^\mu = Q_2^\mu$. Squaring, we obtain

$$M^2 + m_1^2 - 2P_\mu Q_1^\mu = m_2^2 . \quad (19.145)$$

The dot-product $P \cdot Q_1$ is a Lorentz scalar, and hence may be evaluated in any frame.

Let us first consider the CM frame, where $P^\mu = M(1, 0, 0, 0)$, and $P_\mu Q_1^\mu = M E_1^{\text{CM}}$, where E_1^{CM} is the energy of $n = 1$ product in the rest frame of the reactant. Thus,

$$E_1^{\text{CM}} = \frac{M^2 + m_1^2 - m_2^2}{2M} , \quad E_2^{\text{CM}} = \frac{M^2 + m_2^2 - m_1^2}{2M} , \quad (19.146)$$

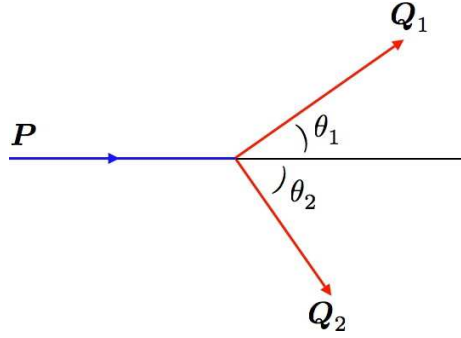


Figure 19.8: Spontaneous decay of a single reactant into two products.

where the second result follows merely from switching the product labels. We may now write $Q_1^\mu = (E_1^{\text{CM}}, \mathbf{p}^{\text{CM}})$ and $Q_2^\mu = (E_2^{\text{CM}}, -\mathbf{p}^{\text{CM}})$, with

$$\begin{aligned} (\mathbf{p}^{\text{CM}})^2 &= (E_1^{\text{CM}})^2 - m_1^2 = (E_2^{\text{CM}})^2 - m_2^2 \\ &= \left(\frac{M^2 - m_1^2 - m_2^2}{2M} \right)^2 - \left(\frac{m_1 m_2}{M} \right)^2. \end{aligned} \quad (19.147)$$

In the laboratory frame, we have $P^\mu = \gamma M(1, \mathbf{V})$ and $Q_i^\mu = \gamma_i m_i(1, \mathbf{V}_i)$. Energy and momentum conservation then provide four equations for the six unknowns \mathbf{V}_1 and \mathbf{V}_2 . Thus, there is a two-parameter family of solutions, assuming we regard the reactant velocity \mathbf{V}^K as fixed, corresponding to the freedom to choose $\hat{\mathbf{p}}^{\text{CM}}$ in the CM frame solution above. Clearly the three vectors \mathbf{V} , \mathbf{V}_1 , and \mathbf{V}_2 must lie in the same plane, and with \mathbf{V} fixed, only one additional parameter is required to fix this plane. The other free parameter may be taken to be the relative angle $\theta_1 = \cos^{-1}(\hat{\mathbf{V}} \cdot \hat{\mathbf{V}}_1)$ (see fig. 19.8). The angle θ_2 as well as the speed V_2 are then completely determined. We can use eqn. 19.145 to relate θ_1 and V_1 :

$$M^2 + m_1^2 - m_2^2 = 2Mm_1\gamma\gamma_1(1 - VV_1 \cos\theta_1). \quad (19.148)$$

It is convenient to express both γ_1 and V_1 in terms of the energy E_1 :

$$\gamma_1 = \frac{E_1}{m_1}, \quad V_1 = \sqrt{1 - \gamma_1^{-2}} = \sqrt{1 - \frac{m_1^2}{E_1^2}}. \quad (19.149)$$

This results in a quadratic equation for E_1 , which may be expressed as

$$(1 - V^2 \cos^2\theta_1)E_1^2 - 2\sqrt{1 - V^2} E_1^{\text{CM}} E_1 + (1 - V^2)(E_1^{\text{CM}})^2 + m_1^2 V^2 \cos^2\theta_1 = 0, \quad (19.150)$$

the solutions of which are

$$E_1 = \frac{\sqrt{1 - V^2} E_1^{\text{CM}} \pm V \cos\theta_1 \sqrt{(1 - V^2)(E_1^{\text{CM}})^2 - (1 - V^2 \cos^2\theta_1)m_1^2}}{1 - V^2 \cos^2\theta_1}. \quad (19.151)$$

The discriminant is positive provided

$$\left(\frac{E_1^{\text{CM}}}{m_1} \right)^2 > \frac{1 - V^2 \cos^2\theta_1}{1 - V^2}, \quad (19.152)$$

which means

$$\sin^2\theta_1 < \frac{V^{-2} - 1}{(V_1^{\text{CM}})^{-2} - 1} \equiv \sin^2\theta_1^*, \quad (19.153)$$

where

$$V_1^{\text{CM}} = \sqrt{1 - \left(\frac{m_1}{E_1^{\text{CM}}}\right)^2} \quad (19.154)$$

is the speed of product 1 in the CM frame. Thus, for $V < V_1^{\text{CM}} < 1$, the scattering angle θ_1 may take on any value, while for larger reactant speeds $V_1^{\text{CM}} < V < 1$ the quantity $\sin^2\theta_1$ cannot exceed a critical value.

19.7.2 Miscellaneous examples of particle decays

Let us now consider some applications of the formulae in eqn. 19.146:

- Consider the decay $\pi^0 \rightarrow \gamma\gamma$, for which $m_1 = m_2 = 0$. We then have $E_1^{\text{CM}} = E_2^{\text{CM}} = \frac{1}{2}M$. Thus, with $M = m_{\pi^0} = 135 \text{ MeV}$, we have $E_1^{\text{CM}} = E_2^{\text{CM}} = 67.5 \text{ MeV}$ for the photon energies in the CM frame.
- For the reaction $K^+ \rightarrow \mu^+ + \nu_\mu$ we have $M = m_{K^+} = 494 \text{ MeV}$ and $m_1 = m_{\mu^-} = 106 \text{ MeV}$. The neutrino mass is $m_2 \approx 0$, hence $E_2^{\text{CM}} = 236 \text{ MeV}$ is the emitted neutrino's energy in the CM frame.
- A Λ^0 hyperon with a mass $M = m_{\Lambda^0} = 1116 \text{ MeV}$ decays into a proton ($m_1 = m_p = 938 \text{ MeV}$) and a pion $m_2 = m_{\pi^-} = 140 \text{ MeV}$). The CM energy of the emitted proton is $E_1^{\text{CM}} = 943 \text{ MeV}$ and that of the emitted pion is $E_2^{\text{CM}} = 173 \text{ MeV}$.

19.7.3 Threshold particle production with a stationary target

Consider now a particle of mass M_1 moving with velocity $\mathbf{V}_1 = V_1 \hat{\mathbf{x}}$, incident upon a stationary target particle of mass M_2 , as indicated in fig. 19.9. Let the product masses be $m_1, m_2, \dots, m_{N'}$. The 4-momenta of the reactants and products are

$$P_1^\mu = (E_1, \mathbf{P}_1) , \quad P_2^\mu = M_2 (1, 0) , \quad Q_j^\mu = (\varepsilon_j, \mathbf{p}_j) . \quad (19.155)$$

Note that $E_1^2 - \mathbf{P}_1^2 = M_1^2$ and $\varepsilon_j^2 - \mathbf{p}_j^2 = m_j^2$, with $j \in \{1, 2, \dots, N'\}$.

Conservation of momentum means that

$$P_1^\mu + P_2^\mu = \sum_{j=1}^{N'} Q_j^\mu . \quad (19.156)$$

In particular, taking the $\mu = 0$ component, we have

$$E_1 + M_2 = \sum_{j=1}^{N'} \varepsilon_j , \quad (19.157)$$

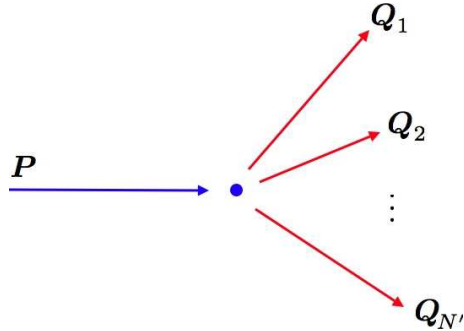


Figure 19.9: A two-particle initial state, with a stationary target in the LAB frame, and an N' -particle final state.

which certainly entails

$$E_1 \geq \sum_{j=1}^{N'} m_j - M_2 \quad (19.158)$$

since $\varepsilon_j = \gamma_j m_j \geq m_j$. But can the equality ever be achieved? This would only be the case if $\gamma_j = 1$ for all j , i.e. the final velocities are all zero. But this itself is quite impossible, since the initial state momentum is P .

To determine the threshold energy E_1^{thr} , we compare the length of the total momentum vector in the LAB and CM frames:

$$\begin{aligned} (P_1 + P_2)^2 &= M_1^2 + M_2^2 + 2E_1 M_2 \quad (\text{LAB}) \\ &= \left(\sum_{j=1}^{N'} \varepsilon_j^{\text{CM}} \right)^2 \quad (\text{CM}) . \end{aligned} \quad (19.159)$$

Thus,

$$E_1 = \frac{\left(\sum_{j=1}^{N'} \varepsilon_j^{\text{CM}} \right)^2 - M_1^2 - M_2^2}{2M_2} \quad (19.160)$$

and we conclude

$$E_1 \geq E_1^{\text{THR}} = \frac{\left(\sum_{j=1}^{N'} m_j \right)^2 - M_1^2 - M_2^2}{2M_2} . \quad (19.161)$$

Note that in the CM frame it *is* possible for each $\varepsilon_j^{\text{CM}} = m_j$.

Finally, we must have $E_1^{\text{THR}} \geq \sum_{j=1}^{N'} m_j - M_2$. This then requires

$$M_1 + M_2 \leq \sum_{j=1}^{N'} m_j . \quad (19.162)$$

19.7.4 Transformation between frames

Consider a particle with 4-velocity u^μ in frame K and consider a Lorentz transformation between this frame and a frame K' moving relative to K with velocity \mathbf{V} . We may write

$$u^\mu = (\gamma, \gamma v \cos \theta, \gamma v \sin \theta \hat{\mathbf{n}}_\perp) , \quad u'^\mu = (\gamma', \gamma' v' \cos \theta', \gamma' v' \sin \theta' \hat{\mathbf{n}}'_\perp) . \quad (19.163)$$

According to the general transformation rules of eqns. 19.47, we may write

$$\begin{aligned} \gamma &= \Gamma \gamma' + \Gamma V \gamma' v' \cos \theta' \\ \gamma v \cos \theta &= \Gamma V \gamma' + \Gamma \gamma' v' \cos \theta' \\ \gamma v \sin \theta &= \gamma' v' \sin \theta' \\ \hat{\mathbf{n}}_\perp &= \hat{\mathbf{n}}'_\perp , \end{aligned} \quad (19.164)$$

where the \hat{x} axis is taken to be $\hat{\mathbf{V}}$, and where $\Gamma \equiv (1 - V^2)^{-1/2}$. Note that the last two of these equations may be written as a single vector equation for the transverse components.

Dividing the third and second of eqns. 19.164, we obtain the result

$$\tan \theta = \frac{\sin \theta'}{\Gamma \left(\frac{V}{v'} + \cos \theta' \right)} . \quad (19.165)$$

We can then use the first of eqns. 19.164 to relate v' and $\cos \theta'$:

$$\gamma'^{-1} = \sqrt{1 - v'^2} = \frac{\Gamma}{\gamma} (1 + V v' \cos \theta') . \quad (19.166)$$

Squaring both sides, we obtain a quadratic equation whose roots are

$$v' = \frac{-\Gamma^2 V \cos \theta' \pm \sqrt{\gamma^4 - \Gamma^2 \gamma^2 (1 - V^2 \cos^2 \theta')}}{\gamma^2 + \Gamma^2 V^2 \cos^2 \theta'} . \quad (19.167)$$

CM frame mass and velocity

To find the velocity of the CM frame, simply write

$$\begin{aligned} P_{\text{tot}}^\mu &= \sum_{i=1}^N P_i^\mu = \left(\sum_{i=1}^N \gamma_i m_i, \sum_{i=1}^N \gamma_i m_i \mathbf{v}_i \right) \\ &\equiv \Gamma M (1, \mathbf{V}) . \end{aligned} \quad (19.168)$$

Then

$$M^2 = \left(\sum_{i=1}^N \gamma_i m_i \right)^2 - \left(\sum_{i=1}^N \gamma_i m_i \mathbf{v}_i \right)^2 \quad (19.169)$$

and

$$\mathbf{V} = \frac{\sum_{i=1}^N \gamma_i m_i \mathbf{v}_i}{\sum_{i=1}^N \gamma_i m_i} . \quad (19.170)$$

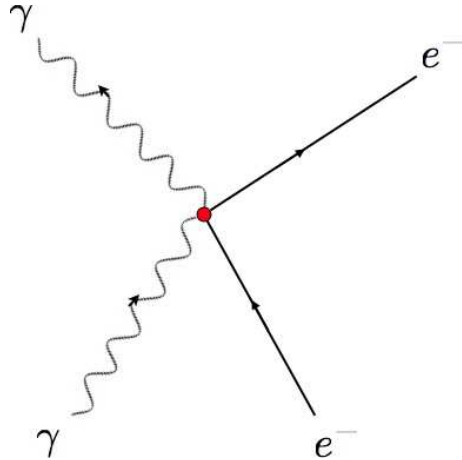


Figure 19.10: Compton scattering of a photon and an electron.

19.7.5 Compton scattering

An extremely important example of relativistic scattering occurs when a photon scatters off an electron: $e^- + \gamma \rightarrow e^- + \gamma$ (see fig. 19.10). Let us work in the rest frame of the reactant electron. Then we have

$$P_e^\mu = m_e(1, 0) \quad , \quad \tilde{P}_e^\mu = m_e(\gamma, \gamma\mathbf{V}) \quad (19.171)$$

for the initial and final 4-momenta of the electron. For the photon, we have

$$P_\gamma^\mu = (\omega, \mathbf{k}) \quad , \quad \tilde{P}_\gamma^\mu = (\tilde{\omega}, \tilde{\mathbf{k}}) \quad , \quad (19.172)$$

where we've set $\hbar = 1$ as well. Conservation of 4-momentum entails

$$P_\gamma^\mu - \tilde{P}_\gamma^\mu = \tilde{P}_e^\mu - P_e^\mu . \quad (19.173)$$

Thus,

$$(\omega - \tilde{\omega}, \mathbf{k} - \tilde{\mathbf{k}}) = m_e(\gamma - 1, \gamma\mathbf{V}) . \quad (19.174)$$

Squaring each side, we obtain

$$\begin{aligned} (\omega - \tilde{\omega})^2 - (\mathbf{k} - \tilde{\mathbf{k}})^2 &= 2\omega\tilde{\omega}(\cos\theta - 1) \\ &= m_e^2((\gamma - 1)^2 - \gamma^2\mathbf{V}^2) \\ &= 2m_e^2(1 - \gamma) \\ &= 2m_e(\tilde{\omega} - \omega) . \end{aligned} \quad (19.175)$$

Here we have used $|\mathbf{k}| = \omega$ for photons, and also $(\gamma - 1)m_e = \omega - \tilde{\omega}$, from eqn. 19.174.

Restoring the units \hbar and c , we find the Compton formula

$$\frac{1}{\tilde{\omega}} - \frac{1}{\omega} = \frac{\hbar}{m_e c^2} (1 - \cos\theta) . \quad (19.176)$$

This is often expressed in terms of the photon wavelengths, as

$$\tilde{\lambda} - \lambda = \frac{4\pi\hbar}{m_e c} \sin^2\left(\frac{1}{2}\theta\right), \quad (19.177)$$

showing that the wavelength of the scattered light increases with the scattering angle in the rest frame of the target electron.

19.8 Covariant Electrodynamics

We begin with the following expression for the Lagrangian density of charged particles coupled to an electromagnetic field, and then show that the Euler-Lagrange equations recapitulate Maxwell's equations. The Lagrangian density is

$$\mathcal{L} = -\frac{1}{16\pi} F_{\mu\nu} F^{\mu\nu} - \frac{1}{c} j_\mu A^\mu. \quad (19.178)$$

Here, $A^\mu = (\phi, \mathbf{A})$ is the *electromagnetic 4-potential*, which combines the scalar field ϕ and the vector field \mathbf{A} into a single 4-vector. The quantity $F_{\mu\nu}$ is the *electromagnetic field strength tensor* and is given by

$$F_{\mu\nu} = \partial_\mu A_\nu - \partial_\nu A_\mu. \quad (19.179)$$

Note that as defined $F_{\mu\nu} = -F_{\nu\mu}$ is antisymmetric. Note that, if $i = 1, 2, 3$ is a spatial index, then

$$\begin{aligned} F_{0i} &= -\frac{1}{c} \frac{\partial A^i}{\partial t} - \frac{\partial A^0}{\partial x^i} = E_i \\ F_{ij} &= \frac{\partial A^i}{\partial x^j} - \frac{\partial A^j}{\partial x^i} = -\epsilon_{ijk} B_k. \end{aligned} \quad (19.180)$$

Here we have used $A^\mu = (A^0, \mathbf{A})$ and $A_\mu = (A^0, -\mathbf{A})$, as well as $\partial_\mu = (c^{-1}\partial_t, \nabla)$.

IMPORTANT : Since the electric and magnetic fields \mathbf{E} and \mathbf{B} are not part of a 4-vector, we do not use covariant / contravariant notation for their components. Thus, E_i is the i^{th} component of the vector \mathbf{E} . We will not write E^i with a raised index, but if we did, we'd mean the same thing: $E^i = E_i$. By contrast, for the spatial components of a four-vector like A^μ , we have $A_i = -A^i$.

Explicitly, then, we have

$$F_{\mu\nu} = \begin{pmatrix} 0 & E_x & E_y & E_z \\ -E_x & 0 & -B_z & B_y \\ -E_y & B_z & 0 & -B_x \\ -E_z & -B_y & B_x & 0 \end{pmatrix}, \quad F^{\mu\nu} = \begin{pmatrix} 0 & -E_x & -E_y & -E_z \\ E_x & 0 & -B_z & B_y \\ E_y & B_z & 0 & -B_x \\ E_z & -B_y & B_x & 0 \end{pmatrix}, \quad (19.181)$$

where $F^{\mu\nu} = g^{\mu\alpha} g^{\nu\beta} F_{\alpha\beta}$. Note that when comparing $F^{\mu\nu}$ and $F_{\mu\nu}$, the components with one space and one time index differ by a minus sign. Thus,

$$-\frac{1}{16\pi} F_{\mu\nu} F^{\mu\nu} = \frac{\mathbf{E}^2 - \mathbf{B}^2}{8\pi}, \quad (19.182)$$

which is the electromagnetic Lagrangian density. The $j \cdot A$ term accounts for the interaction between matter and electromagnetic degrees of freedom. We have

$$\frac{1}{c} j_\mu A^\mu = \varrho \phi - \frac{1}{c} \mathbf{j} \cdot \mathbf{A} , \quad (19.183)$$

where

$$j^\mu = \begin{pmatrix} c\varrho \\ \mathbf{j} \end{pmatrix} , \quad A^\mu = \begin{pmatrix} \phi \\ \mathbf{A} \end{pmatrix} , \quad (19.184)$$

where ϱ is the charge density and \mathbf{j} is the current density. Charge conservation requires

$$\partial_\mu j^\mu = \frac{\partial \varrho}{\partial t} + \nabla \cdot \mathbf{j} = 0 . \quad (19.185)$$

We shall have more to say about this further on below.

Let us now derive the Euler-Lagrange equations for the action functional,

$$S = -c^{-1} \int d^4x \left(\frac{1}{16\pi} F_{\mu\nu} F^{\mu\nu} + c^{-1} j_\mu A^\mu \right) . \quad (19.186)$$

We first vary with respect to A_μ . Clearly

$$\delta F_{\mu\nu} = \partial_\mu \delta A_\nu - \partial_\nu \delta A_\mu . \quad (19.187)$$

We then have

$$\delta \mathcal{L} = \left(\frac{1}{4\pi} \partial_\mu F^{\mu\nu} - c^{-1} j^\nu \right) \delta A_\nu - \partial_\mu \left(\frac{1}{4\pi} F^{\mu\nu} \delta A_\nu \right) . \quad (19.188)$$

Ignoring the boundary term, we obtain Maxwell's equations,

$$\partial_\mu F^{\mu\nu} = 4\pi c^{-1} j^\nu \quad (19.189)$$

The $\nu = k$ component of these equations yields

$$\partial_0 F^{0k} + \partial_i F^{jk} = -\partial_0 E_k - \epsilon_{jkl} \partial_j B_l = 4\pi c^{-1} j^k , \quad (19.190)$$

which is the k component of the Maxwell-Ampère law,

$$\nabla \times \mathbf{B} = \frac{4\pi}{c} \mathbf{j} + \frac{1}{c} \frac{\partial \mathbf{E}}{\partial t} . \quad (19.191)$$

The $\nu = 0$ component reads

$$\partial_i F^{i0} = \frac{4\pi}{c} j^0 \Rightarrow \nabla \cdot \mathbf{E} = 4\pi \varrho , \quad (19.192)$$

which is Gauss's law. The remaining two Maxwell equations come 'for free' from the very definitions of \mathbf{E} and \mathbf{B} :

$$\begin{aligned} \mathbf{E} &= -\nabla A^0 - \frac{1}{c} \frac{\partial \mathbf{A}}{\partial t} \\ \mathbf{B} &= \nabla \times \mathbf{A} , \end{aligned} \quad (19.193)$$

which imply

$$\begin{aligned} \nabla \times \mathbf{E} &= -\frac{1}{c} \frac{\partial \mathbf{B}}{\partial t} \\ \nabla \cdot \mathbf{B} &= 0 . \end{aligned} \quad (19.194)$$

19.8.1 Lorentz force law

This has already been worked out in chapter 7. Here we reiterate our earlier derivation. The 4-current may be written as

$$j^\mu(\mathbf{x}, t) = c \sum_n q_n \int d\tau \frac{dX_n^\mu}{d\tau} \delta^{(4)}(\mathbf{x} - \mathbf{X}) . \quad (19.195)$$

Thus, writing $X_n^\mu = (ct, \mathbf{X}_n(t))$, we have

$$\begin{aligned} j^0(\mathbf{x}, t) &= \sum_n q_n c \delta(\mathbf{x} - \mathbf{X}_n(t)) \\ \mathbf{j}(\mathbf{x}, t) &= \sum_n q_n \dot{\mathbf{X}}_n(t) \delta(\mathbf{x} - \mathbf{X}_n(t)) . \end{aligned} \quad (19.196)$$

The Lagrangian for the matter-field interaction term is then

$$\begin{aligned} L &= -c^{-1} \int d^3x (j^0 A^0 - \mathbf{j} \cdot \mathbf{A}) \\ &= - \sum_n \left[q_n \phi(\mathbf{X}_n, t) - \frac{q_n}{c} \mathbf{A}(\mathbf{X}_n, t) \cdot \dot{\mathbf{X}}_n \right] , \end{aligned} \quad (19.197)$$

where $\phi = A^0$. For each charge q_n , this is equivalent to a particle with velocity-dependent potential energy

$$U(\mathbf{x}, t) = q \phi(\mathbf{x}, t) - \frac{q}{c} \mathbf{A}(\mathbf{r}, t) \cdot \dot{\mathbf{x}} , \quad (19.198)$$

where $\mathbf{x} = \mathbf{X}_n$.

Let's work out the equations of motion. We assume a kinetic energy $T = \frac{1}{2}m\dot{\mathbf{x}}^2$ for the charge. We then have

$$\frac{d}{dt} \left(\frac{\partial L}{\partial \dot{\mathbf{x}}} \right) = \frac{\partial L}{\partial \mathbf{x}} \quad (19.199)$$

with $L = T - U$, which gives

$$m \ddot{\mathbf{x}} + \frac{q}{c} \frac{d\mathbf{A}}{dt} = -q \nabla \phi + \frac{q}{c} \nabla(\mathbf{A} \cdot \dot{\mathbf{x}}) , \quad (19.200)$$

or, in component notation,

$$m \ddot{x}^i + \frac{q}{c} \frac{\partial A^i}{\partial x^j} \dot{x}^j + \frac{q}{c} \frac{\partial A^i}{\partial t} = -q \frac{\partial \phi}{\partial x^i} + \frac{q}{c} \frac{\partial A^j}{\partial x^i} \dot{x}^j , \quad (19.201)$$

which is to say

$$m \ddot{x}^i = -q \frac{\partial \phi}{\partial x^i} - \frac{q}{c} \frac{\partial A^i}{\partial t} + \frac{q}{c} \left(\frac{\partial A^j}{\partial x^i} - \frac{\partial A^i}{\partial x^j} \right) \dot{x}^j . \quad (19.202)$$

It is convenient to express the cross product in terms of the completely antisymmetric tensor of rank three, ϵ_{ijk} :

$$B_i = \epsilon_{ijk} \frac{\partial A^k}{\partial x^j} , \quad (19.203)$$

and using the result

$$\epsilon_{ijk} \epsilon_{imn} = \delta_{jm} \delta_{kn} - \delta_{jn} \delta_{km} , \quad (19.204)$$

we have $\epsilon_{ijk} B_i = \partial^j A^k - \partial^k A^j$, and

$$m \ddot{x}^i = -q \frac{\partial \phi}{\partial x^i} - \frac{q}{c} \frac{\partial A^i}{\partial t} + \frac{q}{c} \epsilon_{ijk} \dot{x}^j B_k , \quad (19.205)$$

or, in vector notation,

$$\begin{aligned} m \ddot{\mathbf{x}} &= -q \nabla \phi - \frac{q}{c} \frac{\partial \mathbf{A}}{\partial t} + \frac{q}{c} \dot{\mathbf{x}} \times (\nabla \times \mathbf{A}) \\ &= q \mathbf{E} + \frac{q}{c} \dot{\mathbf{x}} \times \mathbf{B} , \end{aligned} \quad (19.206)$$

which is, of course, the Lorentz force law.

19.8.2 Gauge invariance

The action $S = c^{-1} \int d^4x \mathcal{L}$ admits a *gauge invariance*. Let $A^\mu \rightarrow A^\mu + \partial^\mu \Lambda$, where $\Lambda(\mathbf{x}, t)$ is an arbitrary scalar function of spacetime coordinates. Clearly

$$F_{\mu\nu} \rightarrow F_{\mu\nu} + (\partial_\mu \partial_\nu \Lambda - \partial_\nu \partial_\mu \Lambda) = F_{\mu\nu} , \quad (19.207)$$

and hence the fields \mathbf{E} and \mathbf{B} remain *invariant* under the gauge transformation, even though the 4-potential itself changes. What about the matter term? Clearly

$$\begin{aligned} -c^{-1} j^\mu A_\mu &\rightarrow -c^{-1} j^\mu A_\mu - c^{-1} j^\mu \partial_\mu \Lambda \\ &= -c^{-1} j^\mu A_\mu + c^{-1} \Lambda \partial_\mu j^\mu - \partial_\mu (c^{-1} \Lambda j^\mu) . \end{aligned} \quad (19.208)$$

Once again we ignore the boundary term. We may now invoke charge conservation to write $\partial_\mu j^\mu = 0$, and we conclude that the action is invariant! Woo hoo! Note also the very deep connection

$$\text{gauge invariance} \longleftrightarrow \text{charge conservation} . \quad (19.209)$$

19.8.3 Transformations of fields

One last detail remains, and that is to exhibit explicitly the Lorentz transformation properties of the electromagnetic field. For the case of vectors like A^μ , we have

$$A^\mu = L_\nu^\mu A'^\nu . \quad (19.210)$$

The \mathbf{E} and \mathbf{B} fields, however, appear as elements in the field strength tensor $F^{\mu\nu}$. Clearly this must transform as a tensor:

$$F^{\mu\nu} = L_\alpha^\mu L_\beta^\nu F'^{\alpha\beta} = L_\alpha^\mu F'^{\alpha\beta} L_\beta^\nu . \quad (19.211)$$



Figure 19.11: Homer celebrates the manifest gauge invariance of classical electromagnetic theory.

We can write a general Lorentz transformation as a product of a rotation L_{rot} and a boost L_{boost} . Let's first see how rotations act on the field strength tensor. We take

$$L = L_{\text{rot}} = \begin{pmatrix} 1_{1 \times 1} & 0_{1 \times 3} \\ 0_{3 \times 1} & R_{3 \times 3} \end{pmatrix}, \quad (19.212)$$

where $R^t R = \mathbb{I}$, i.e. $R \in O(3)$ is an orthogonal matrix. We must compute

$$\begin{aligned} L^\mu_\alpha F'^{\alpha\beta} L^\nu_\beta &= \begin{pmatrix} 1 & 0 \\ 0 & R_{ij} \end{pmatrix} \begin{pmatrix} 0 & -E'_k \\ E'_j & -\epsilon_{jkm} B'_m \end{pmatrix} \begin{pmatrix} 1 & 0 \\ 0 & R^t_{kl} \end{pmatrix} \\ &= \begin{pmatrix} 0 & -E'_k R^t_{kl} \\ R_{ij} E'_j & -\epsilon_{jkm} R_{ij} R_{lk} B'_m \end{pmatrix}. \end{aligned} \quad (19.213)$$

Thus, we conclude

$$\begin{aligned} E_l &= R_{lk} E'_k \\ \epsilon_{iln} B_n &= \epsilon_{jkm} R_{ij} R_{lk} B'_m. \end{aligned} \quad (19.214)$$

Now for any 3×3 matrix R we have

$$\epsilon_{jks} R_{ij} R_{lk} R_{rs} = \det(R) \epsilon_{ilr}, \quad (19.215)$$

and therefore

$$\begin{aligned} \epsilon_{jkm} R_{ij} R_{lk} B'_m &= \epsilon_{jkm} R_{ij} R_{lk} R_{nm} R_{ns} B'_s \\ &= \det(R) \epsilon_{iln} R_{ns} B'_s, \end{aligned} \quad (19.216)$$

Therefore,

$$E_i = R_{ij} E'_j, \quad B_i = \det(R) \cdot R_{ij} B'_j. \quad (19.217)$$

For any orthogonal matrix, $R^t R = \mathbb{I}$ gives that $\det(R) = \pm 1$. The extra factor of $\det(R)$ in the transformation properties of \mathbf{B} is due to the fact that the electric field transforms as a *vector*, while the magnetic field transforms as a *pseudovector*. Under space inversion, for example, where $R = -\mathbb{I}$, the electric field is *odd* under this transformation ($\mathbf{E} \rightarrow -\mathbf{E}$) while the magnetic field is *even* ($\mathbf{B} \rightarrow +\mathbf{B}$). Similar considerations hold in particle mechanics for the linear momentum, \mathbf{p} (a vector) and the angular momentum $\mathbf{L} = \mathbf{r} \times \mathbf{p}$ (a pseudovector). The analogy is not complete, however, because while both \mathbf{p} and \mathbf{L} are odd under the operation of time-reversal, \mathbf{E} is even while \mathbf{B} is odd.

OK, so how about boosts? We can write the general boost, from eqn. 19.36, as

$$L = \begin{pmatrix} \gamma & \gamma \hat{\beta} \\ \gamma \hat{\beta} & I + (\gamma - 1)P^\beta \end{pmatrix} \quad (19.218)$$

where $P_{ij}^\beta = \hat{\beta}_i \hat{\beta}_j$ is the projector onto the direction of β . We now compute

$$L_\alpha^\mu F'^{\alpha\beta} L_\beta^{\nu} = \begin{pmatrix} \gamma & \gamma \beta^t \\ \gamma \beta & I + (\gamma - 1)P \end{pmatrix} \begin{pmatrix} 0 & -\mathbf{E}'^t \\ \mathbf{E}' & -\epsilon_{jkm} B'_m \end{pmatrix} \begin{pmatrix} \gamma & \gamma \beta^t \\ \gamma \beta & I + (\gamma - 1)P \end{pmatrix}. \quad (19.219)$$

Carrying out the matrix multiplications, we obtain

$$\begin{aligned} \mathbf{E} &= \gamma(\mathbf{E}' - \beta \times \mathbf{B}') - (\gamma - 1)(\hat{\beta} \cdot \mathbf{E}') \hat{\beta} \\ \mathbf{B} &= \gamma(\mathbf{B}' + \beta \times \mathbf{E}') - (\gamma - 1)(\hat{\beta} \cdot \mathbf{B}') \hat{\beta}. \end{aligned} \quad (19.220)$$

Expressed in terms of the components E_{\parallel} , \mathbf{E}_{\perp} , B_{\parallel} , and \mathbf{B}_{\perp} , one has

$$\begin{aligned} E_{\parallel} &= E'_{\parallel} & , & \mathbf{E}_{\perp} = \gamma(\mathbf{E}'_{\perp} - \beta \times \mathbf{B}'_{\perp}) \\ B_{\parallel} &= B'_{\parallel} & , & \mathbf{B}_{\perp} = \gamma(\mathbf{B}'_{\perp} + \beta \times \mathbf{E}'_{\perp}). \end{aligned} \quad (19.221)$$

Recall that for any vector ξ , we write

$$\begin{aligned} \xi_{\parallel} &= \hat{\beta} \cdot \xi \\ \xi_{\perp} &= \xi - (\hat{\beta} \cdot \xi) \hat{\beta}, \end{aligned} \quad (19.222)$$

so that $\hat{\beta} \cdot \xi_{\perp} = 0$.

19.8.4 Invariance versus covariance

We saw that the laws of electromagnetism were *gauge invariant*. That is, the solutions to the field equations did not change under a gauge transformation $A^\mu \rightarrow A^\mu + \partial^\mu \Lambda$. With respect to Lorentz transformations, however, the theory is *Lorentz covariant*. This means that Maxwell's equations in different inertial frames take the exact same form, $\partial_\mu F^{\mu\nu} = 4\pi c^{-1} j^\nu$, but that both the fields and the sources transform appropriately under a change in reference frames. The sources are described by the

current 4-vector $j^\mu = (c\varrho, \mathbf{j})$ and transform as

$$\begin{aligned} c\varrho &= \gamma c\varrho' + \gamma\beta j'_\parallel \\ j'_\parallel &= \gamma\beta c\varrho' + \gamma j'_\parallel \\ \mathbf{j}_\perp &= \mathbf{j}'_\perp . \end{aligned} \tag{19.223}$$

The fields transform according to eqns. 19.221.

Consider, for example, a static point charge q located at the origin in the frame K' , which moves with velocity $u\hat{\mathbf{x}}$ with respect to K . An observer in K' measures a charge density $\varrho'(\mathbf{x}', t') = q\delta(\mathbf{x}')$. The electric and magnetic fields in the K' frame are then $\mathbf{E}' = q\hat{\mathbf{r}}'/r'^2$ and $\mathbf{B}' = 0$. For an observer in the K frame, the coordinates transform as

$$\begin{aligned} ct &= \gamma ct' + \gamma\beta x' & ct' &= \gamma ct - \gamma\beta x \\ x &= \gamma\beta ct' + \gamma x' & x' &= -\gamma\beta ct + \gamma x , \end{aligned} \tag{19.224}$$

as well as $y = y'$ and $z = z'$. The observer in the K frame sees instead a charge at $x^\mu = (ct, ut, 0, 0)$ and both a charge density as well as a current density:

$$\begin{aligned} \varrho(\mathbf{x}, t) &= \gamma\varrho(\mathbf{x}', t') = q\delta(x - ut)\delta(y)\delta(z) \\ \mathbf{j}(\mathbf{x}, t) &= \gamma\beta c\varrho(\mathbf{x}', t')\hat{\mathbf{x}} = uq\delta(x - ut)\delta(y)\delta(z)\hat{\mathbf{x}} . \end{aligned} \tag{19.225}$$

OK, so much for the sources. How about the fields? Expressed in terms of Cartesian coordinates, the electric field in K' is given by

$$\mathbf{E}'(\mathbf{x}', t') = q \frac{x'\hat{\mathbf{x}} + y'\hat{\mathbf{y}} + z'\hat{\mathbf{z}}}{(x'^2 + y'^2 + z'^2)^{3/2}} . \tag{19.226}$$

From eqns. 19.221, we have $E_x = E'_x$ and $B_x = B'_x = 0$. Furthermore, we have $E_y = \gamma E'_y$, $E_z = \gamma E'_z$, $B_y = -\gamma\beta E'_z$, and $B_z = \gamma\beta E'_y$. Thus,

$$\begin{aligned} \mathbf{E}(\mathbf{x}, t) &= \gamma q \frac{(x - ut)\hat{\mathbf{x}} + y\hat{\mathbf{y}} + z\hat{\mathbf{z}}}{[\gamma^2(x - ut)^2 + y^2 + z^2]^{3/2}} \\ \mathbf{B}(\mathbf{x}, t) &= \frac{\gamma u}{c} q \frac{y\hat{\mathbf{z}} - z\hat{\mathbf{y}}}{[\gamma^2(x - ut)^2 + y^2 + z^2]^{3/2}} . \end{aligned} \tag{19.227}$$

Let us define

$$\mathbf{R}(t) = (x - ut)\hat{\mathbf{x}} + y\hat{\mathbf{y}} + z\hat{\mathbf{z}} . \tag{19.228}$$

We further define the angle $\theta \equiv \cos^{-1}(\hat{\beta} \cdot \hat{\mathbf{R}})$. We may then write

$$\begin{aligned} \mathbf{E}(x, t) &= \frac{q\mathbf{R}}{R^3} \cdot \frac{1 - \beta^2}{(1 - \beta^2 \sin^2 \theta)^{3/2}} \\ \mathbf{B}(x, t) &= \frac{q\hat{\beta} \times \mathbf{R}}{R^3} \cdot \frac{1 - \beta^2}{(1 - \beta^2 \sin^2 \theta)^{3/2}} . \end{aligned} \tag{19.229}$$

The fields are therefore enhanced in the transverse directions: $E_\perp/E_\parallel = \gamma^3$.

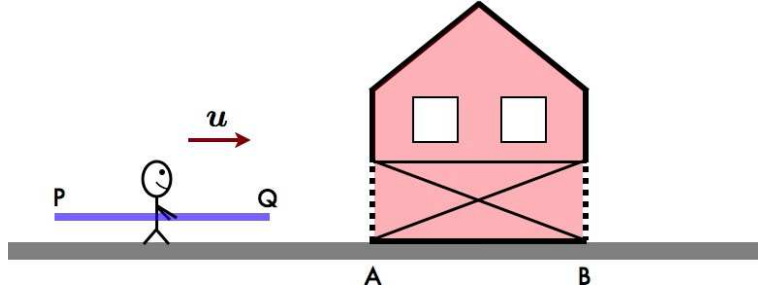


Figure 19.12: A relativistic runner carries a pole of proper length ℓ into a barn of proper length ℓ .

19.9 Appendix I : The Pole, the Barn, and *Rashoman*

Akira Kurosawa's 1950 cinematic masterpiece, *Rashoman*, describes a rape, murder, and battle from four different and often contradictory points of view. It poses deep questions regarding the nature of truth. Psychologists sometimes refer to problems of subjective perception as the *Rashoman effect*. In literature, William Faulkner's 1929 novel, *The Sound and the Fury*, which describes the tormented incestuous life of a Mississippi family, also is told from four points of view. Perhaps Faulkner would be a more apt comparison with Einstein, since time plays an essential role in his novel. For example, Quentin's watch, given to him by his father, represents time and the sweep of life's arc ("Quentin, *I give you the mausoleum of all hope and desire...*"). By breaking the watch, Quentin symbolically attempts to escape time and fate. One could draw an analogy to Einstein, inheriting a watch from those who came before him, which he too broke – and refashioned. Did Faulkner know of Einstein? But I digress.

Consider a relativistic runner carrying a pole of proper length ℓ , as depicted in fig. 19.12. He runs toward a barn of proper length ℓ at velocity $u = c\beta$. Let the frame of the barn be K and the frame of the runner be K' . Recall that the Lorentz transformations between frames K and K' are given by

$$\begin{aligned} ct &= \gamma ct' + \gamma\beta x' & ct' &= \gamma ct - \gamma\beta x \\ x &= \gamma\beta ct' + \gamma x' & x' &= -\gamma\beta ct + \gamma x . \end{aligned} \tag{19.230}$$

We define the following points. Let A denote the left door of the barn and B the right door. Furthermore, let P denote the left end of the pole and Q its right end. The spacetime coordinates for these points in the two frames are clearly .

$$\begin{aligned} A &= (ct, 0) & P' &= (ct', 0) \\ B &= (ct, \ell) & Q' &= (ct', \ell) \end{aligned} \tag{19.231}$$

We now compute A' and B' in frame K' , as well as P and Q in frame K :

$$\begin{aligned} A' &= (\gamma ct, -\gamma\beta ct) & B' &= (\gamma ct - \gamma\beta\ell, -\gamma\beta ct + \gamma\ell) \\ &\equiv (ct', -\beta ct') & &\equiv (ct', -\beta ct + \gamma^{-1}\ell) . \end{aligned} \tag{19.232}$$

Similarly,

$$\begin{aligned} P &= (\gamma ct', \gamma\beta ct') & Q &= (\gamma ct' + \gamma\beta\ell, \gamma\beta ct' + \gamma\ell) \\ &\equiv (ct, \beta ct) & &\equiv (ct, \beta ct + \gamma^{-1}\ell) . \end{aligned} \tag{19.233}$$

We now define four events, by the coincidences of A and B with P and Q :

- Event I : The right end of the pole enters the left door of the barn. This is described by $Q = A$ in frame K and by $Q' = A'$ in frame K' .
- Event II : The right end of the pole exits the right door of the barn. This is described by $Q = B$ in frame K and by $Q' = B'$ in frame K' .
- Event III : The left end of the pole enters the left door of the barn. This is described by $P = A$ in frame K and by $P' = A'$ in frame K' .
- Event IV : The left end of the pole exits the right door of the barn. This is described by $P = B$ in frame K and by $P' = B'$ in frame K' .

Mathematically, we have in frame K that

$$\begin{aligned} \text{I : } Q = A &\Rightarrow t_{\text{I}} = -\frac{\ell}{\gamma u} \\ \text{II : } Q = B &\Rightarrow t_{\text{II}} = (\gamma - 1) \frac{\ell}{\gamma u} \\ \text{III : } P = A &\Rightarrow t_{\text{III}} = 0 \\ \text{IV : } P = B &\Rightarrow t_{\text{IV}} = \frac{\ell}{u} \end{aligned} \tag{19.234}$$

In frame K' , however

$$\begin{aligned} \text{I : } Q' = A' &\Rightarrow t'_{\text{I}} = -\frac{\ell}{u} \\ \text{II : } Q' = B' &\Rightarrow t'_{\text{II}} = -(\gamma - 1) \frac{\ell}{\gamma u} \\ \text{III : } P' = A' &\Rightarrow t'_{\text{III}} = 0 \\ \text{IV : } P' = B' &\Rightarrow t'_{\text{IV}} = \frac{\ell}{\gamma u} \end{aligned} \tag{19.235}$$

Thus, to an observer in frame K , the order of events is I, III, II, and IV, because

$$t_{\text{I}} < t_{\text{III}} < t_{\text{II}} < t_{\text{IV}}. \tag{19.236}$$

For $t_{\text{III}} < t < t_{\text{II}}$, he observes that *the pole is entirely in the barn*. Indeed, the right door can start shut and the left door open, and sensors can automatically and, for the purposes of argument, instantaneously trigger the closing of the left door immediately following event III and the opening of the right door immediately prior to event II. So the pole can be inside the barn with both doors shut!

But now for the *Rashoman effect*: according to the runner, the order of events is I, II, III, and IV, because

$$t'_{\text{I}} < t'_{\text{II}} < t'_{\text{III}} < t'_{\text{IV}}. \tag{19.237}$$

At no time does the runner observe the pole to be entirely within the barn. Indeed, for $t'_{\text{II}} < t' < t'_{\text{III}}$, both ends of the pole are sticking outside of the barn!

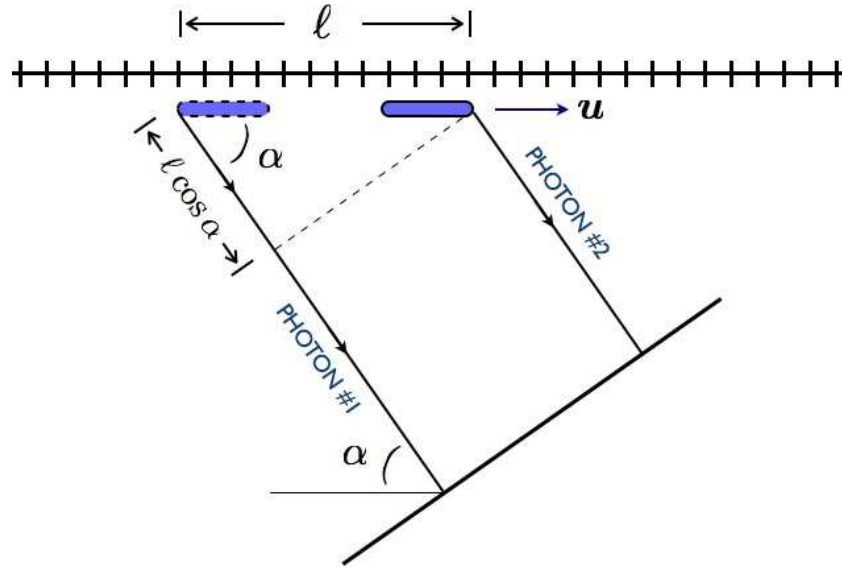


Figure 19.13: An object of proper length ℓ and moving with velocity \mathbf{u} , when photographed from an angle α , appears to have a length $\tilde{\ell}$.

19.10 Appendix II : Photographing a Moving Pole

What is the length ℓ of a moving pole of proper length ℓ_0 as measured by an observer at rest? The answer would appear to be $\gamma^{-1}\ell_0$, as we computed in eqn. 19.63. However, we should be more precise when we speak of ‘length’. The relation $\ell(\beta) = \gamma^{-1}\ell_0$ tells us the *instantaneous end-to-end distance as measured in the observer’s rest frame K*. But an actual experiment might not measure this quantity.

For example, suppose a relativistic runner carrying a pole of proper length ℓ_0 runs past a measuring rod which is at rest in the rest frame K of an observer. The observer *takes a photograph* of the moving pole as it passes by. Suppose further that the angle between the observer’s line of sight and the velocity \mathbf{u} of the pole is α , as shown in fig. 19.13. What is the apparent length $\ell(\alpha, u)$ of the pole as observed in the photograph? (*I.e.* the pole will appear to cover a portion of the measuring rod which is of length ℓ .)

The point here is that the shutter of the camera is very fast (otherwise the image will appear blurry). In our analysis we will assume the shutter opens and closes instantaneously. Let’s define two events:

- Event 1 : photon γ_1 is emitted by the rear end of the pole.
- Event 2 : photon γ_2 is emitted by the front end of the pole.

Both photons must arrive at the camera’s lens simultaneously. Since, as shown in the figure, the path of photon #1 is longer by a distance $\ell \cos \alpha$, where ℓ is the apparent length of the pole, γ_2 must be emitted a time $\Delta t = c^{-1}\ell \cos \alpha$ after γ_1 . Now if we Lorentz transform from frame K to frame K' , we have

$$\Delta x' = \gamma \Delta x - \gamma \beta \Delta t . \quad (19.238)$$

But $\Delta x' = \ell_0$ is the proper length of the pole, and $\Delta x = \ell$ is the apparent length. With $c\Delta t = \ell \cos \alpha$, then, we have

$$\ell = \frac{\gamma^{-1} \ell_0}{1 - \beta \cos \alpha}. \quad (19.239)$$

When $\alpha = 90^\circ$, we recover the familiar Lorentz-Fitzgerald contraction $\ell(\beta) = \gamma^{-1} \ell_0$. This is because the photons γ_1 and γ_2 are then emitted simultaneously, and the photograph measures the instantaneous end-to-end distance of the pole as measured in the observer's rest frame K . When $\cos \alpha \neq 0$, however, the two photons are not emitted simultaneously, and the apparent length is given by eqn. 19.239.